

THE MEASUREMENT OF SOIL-WATER RETENTION CURVES USING THE TENSIOMETER METHOD

P.F. le Roux

THE MEASUREMENT OF SOIL-WATER RETENTION CURVES USING THE TENSIOMETER METHOD

Paul Francois le Roux

A dissertation submitted in partial fulfilment of the requirements for the degree of

MASTER OF ENGINEERING (GEOTECHNICAL ENGINEERING)

in the

**FACULTY OF ENGINEERING, BUILT-ENVIRONMENT AND INFORMATION
TECHNOLOGY**

University of Pretoria

December 2019

DISSERTATION SUMMARY

THE MEASUREMENT OF SOIL-WATER RETENTION CURVES USING THE TENSIO METER METHOD

P.F. LE ROUX

Supervisor: Professor S.W. Jacobsz
Department: Civil Engineering
University: University of Pretoria
Degree: Master of Engineering (Geotechnical Engineering)

The soil-water retention curve (SWRC) is an essential tool in geotechnical engineering and agriculture used in the analysis of unsaturated soil conditions such as those found in tailings dams and the water retention capacity of agricultural lands. The SWRC describes the relationship between the soil matric suction and the water content of an unsaturated soil. The SWRC can be used as a basis to model various unsaturated soil parameters, such as the hydraulic conductivity and shear-strength functions. It is, therefore, vital that an accurate characterisation of the SWRC of a soil be made.

Until recently, the methods used to obtain the SWRC have involved obtaining point measurements along the SWRC and fitting an empirically derived curve through these points. These procedures can take weeks to complete and usually rely on indirect methods of measuring soil suction. These factors have limited the widespread use of the SWRC, and therefore, the adoption of unsaturated soil mechanics into modern geotechnical engineering practice.

The development of high-capacity tensiometers (HCTs), the only devices capable of directly measuring high soil suctions, has enabled researchers to significantly expand the study into unsaturated soils and the determination of SWRCs. Toker *et al.* (2004) introduced a rapid method for determining continuous SWRCs using an HCT and a digital laboratory balance by continuously monitoring the mass and suction generated in a drying a soil sample.

This method was investigated by first developing a new low-cost tensiometer capable of measuring suctions up to 1150 kPa. Simple procedures were developed to reliably saturate and calibrate the tensiometer without the need for specialised equipment.

The SWRCs of five different soil types were determined using the continuous drying method and then compared to the SWRCs determined from point measurements by the filter paper method. A novel way of volume change measurement was also incorporated into the method to produce SWRCs for soils that undergo shrinkage during drying. Excellent agreement between the methods was found for both the granular soils and fine-grained clayey soils tested. The method reduced the time taken to determine SWRCs from weeks to mere hours.

DECLARATION

I, the undersigned, hereby declare that:

I understand what plagiarism is and I am aware of the University's policy in this regard;

The work contained in this project report is my own original work;

I did not refer to work of current or previous students, lecture notes, handbooks or any other study material without proper referencing;

I have not allowed anyone to copy any part of my project report;

I have not previously in its entirety or in part submitted this project report at any university for a degree.

Paul Francois le Roux

10339648

16 January 2020

ACKNOWLEDGEMENTS

The following persons deserve praise and acknowledgement for their role in supporting me and this research:

- a) I would like to thank my supervisor, Prof. S.W. Jacobsz, for much-needed guidance, continued encouragement and support. Most of all, he inspired me to pursue the field of geotechnical engineering and a spirit of continuous learning.
- b) I am grateful for the constructive advice and enthusiasm of Prof. E. Kearsley, without whom I would not have been able to complete this research.
- c) I am thankful for the financial support of the Department of Civil Engineering of the University of Pretoria, facilitated by Prof. E. Kearsley after Prof. S.W. Jacobsz's recommendation.
- d) I would like to thank my close friend and colleague, M.S. Smit, for her unwavering support and belief in my abilities.
- e) A massive amount of respect goes out to T.A.V. Gaspar for endeavouring to advance this research beyond what I thought was capable and for 'holding the fort' in my absence.
- f) Lastly, I would like to thank my family. I love you all. Thank you for putting up with me.

TABLE OF CONTENTS

	PAGE
TABLE OF CONTENTS	1-1
LIST OF APPENDICES	1-3
LIST OF TABLES	1-3
LIST OF FIGURES	1-3
1 INTRODUCTION	1-1
1.1 Background	1-1
1.2 Study Objectives	1-2
1.3 Scope of Study	1-2
1.4 Methodology	1-2
1.5 Organisation of Report	1-3
2 LITERATURE REVIEW	2-1
2.1 Saturated and Unsaturated Soils	2-1
2.1.1 Unsaturated soil phases	2-1
2.1.2 Surface tension	2-2
2.1.3 Cavitation	2-3
2.2 Soil Suction	2-4
2.2.1 Components of soil suction	2-5
2.2.2 Effects of soil suction components	2-6
2.2.3 Soil Suction and Soil-Water Content	2-7
2.3 Measurement of Soil Suction	2-13
2.3.1 Indirect methods of soil suction measurement	2-14
2.3.2 Direct methods of soil suction measurement	2-17
2.4 High-Capacity Tensiometers	2-20
2.4.1 High air-entry materials	2-21
2.4.2 Operating principle	2-22
2.4.3 Cavitation	2-22
2.4.4 Tensiometer saturation	2-23
2.5 Development of High-Capacity Tensiometers	2-25
2.5.1 Tensiometer saturation	2-28
2.5.2 Tensiometer calibration	2-29
2.6 Determination of Soil-Water Retention Curves by Experimental Methods	2-29
2.6.1 Conventional methods	2-30
2.6.2 Continuous drying methods	2-30
3 TENSIO METER DEVELOPMENT	3-1
3.1 Tensiometer Development	3-1
3.1.1 Tensiometer design	3-1
3.1.2 Tensiometer assembly	3-10
3.2 Procedures for Tensiometer Use	3-15
3.2.1 Experimental saturation and calibration set-up	3-15
3.2.2 Saturation procedure	3-19
3.2.3 Calibration procedure	3-19
3.3 Evaluation of Tensiometer Performance	3-20
3.3.1 Calibration results	3-20

3.3.2	Instrument performance	3-37
4	DETERMINATION OF SOIL-WATER RETENTION CURVES	4-1
4.1	Materials	4-1
4.2	Experimental Test Set-up for Continuous Drying Tests	4-4
4.2.1	Continuous drying with hanger set-up	4-4
4.2.2	Continuous drying with laboratory balance and environmental enclosure set-up	4-5
4.3	Comparison of Results	4-14
4.3.1	The filter paper method	4-14
5	EXPERIMENTAL RESULTS AND DISCUSSION	5-1
5.1	Soil-Water Retention Curves of Granular Soils	5-1
5.1.1	Testing program for granular soils	5-1
5.1.2	Sample FS001: Fine sand – tensiometer method	5-2
5.1.3	Sample GT001: Gold mine tailings – tensiometer method	5-7
5.2	Comparison of the Tensiometer and Filter Paper Methods for Determining SWRCs of Granular Soils	5-11
5.2.1	Granular soils - filter paper method	5-11
5.2.2	Sample FS001: Fine sand – tensiometer vs filter paper methods	5-15
5.2.3	Sample GT001: Gold mine tailings – tensiometer vs filter paper methods	5-17
5.3	Soil-Water Retention Curves of Fine-Grained Soils Undergoing Volume Change	5-18
5.3.1	Testing program for fine-grained soils	5-19
5.3.2	Sample TP148: Clayey sand – tensiometer method	5-19
5.3.3	Sample TP149: Lean clay – tensiometer method	5-23
5.3.4	Sample TP016: Clay – tensiometer method	5-26
5.4	Comparison of the Tensiometer and Filter Paper Methods for Determining SWRCs of Fine-Grained Soils	5-29
5.4.1	Fine-grained soils – filter paper method	5-29
5.4.2	Sample TP148: Clayey sand – tensiometer vs filter paper methods	5-31
5.4.3	Sample TP149: Lean clay – tensiometer vs filter paper methods	5-32
5.4.4	Sample TP016: Clay – tensiometer vs filter paper methods	5-33
6	CONCLUSIONS	6-1
6.1	Conclusions	6-1
6.2	Recommendations	6-2
7	REFERENCES	7-1
8	APPENDICES	8-1

LIST OF APPENDICES

	PAGE
APPENDIX A: DETAILED PROCEDURES	A-1
A.1 Detailed saturation procedure	A-1
A.1.1 Initial saturation	A-1
A.1.2 Saturation (pre-pressurisation)	A-2
A.2 Detailed calibration procedure	A-2
A.2.1 Response time	A-2
A.2.2 Calibration	A-3
A.3 Data processing	A-3
A.3.1 Data processing and calculations	A-3
A.3.2 Volume determination	A-5
APPENDIX B: ADDITIONAL FIGURES	B-1
APPENDIX C: TECHNICAL DATA	C-1

LIST OF TABLES

	PAGE
Table 2-1 Soil suction measurement techniques	2-13
Table 3-1 Properties of HAE ceramics	3-5
Table 3-2 Results of positive pressure calibration	3-23
Table 3-3 Results of positive pressure calibration in over-range	3-24
Table 3-4 Calibration constants	3-25
Table 3-5 Results of negative pressure calibration (isotropic unloading tests)	3-35
Table 3-6 Results of temperature calibration	3-39
Table 4-1 Properties of soils tested	4-2
Table 5-1 Filter paper SWRC properties and curve-fitting parameters	5-13
Table 5-2 Shrinkage curve-fitting parameters for sample TP148	5-21
Table 5-3 Shrinkage curve-fitting parameters for sample TP149	5-24
Table 5-4 Shrinkage curve-fitting parameters for sample TP016	5-27

LIST OF FIGURES

	PAGE
Figure 2-1 Saturated vs unsaturated soil mechanics	2-1
Figure 2-2 Surface tension at the air-water interface	2-2
Figure 2-3 Idealised thermodynamic phase diagram	2-4

Figure 2-4 A conceptual model of soil suction regimes	2-6
Figure 2-5 General features of SWRCs	2-8
Figure 2-6 Stages of soil desaturation and the SWRC	2-9
Figure 2-7 SWRCs of different soils	2-9
Figure 2-8 Calibration curves for <i>Whatman</i> No. 42 filter paper	2-15
Figure 2-9 Calibration curve variability for <i>Whatman</i> No. 42 filter paper	2-17
Figure 2-10 Simple tensiometer device	2-18
Figure 2-11 Conventional tensiometers	2-19
Figure 2-12 Simple pressure plate device	2-20
Figure 2-13 Simple high-capacity tensiometer	2-21
Figure 2-14 High-suction tensiometers	2-26
Figure 2-15 Test set-up for the MIT technique	2-31
Figure 2-16 MIT tensiometer	2-32
Figure 3-1 Design of the new tensiometer	3-2
Figure 3-2 Alternative configuration of the new tensiometer	3-2
Figure 3-3 “MS54XX” range miniature pressure sensors	3-3
Figure 3-4 Detail of “MS54XX” range miniature pressure sensor	3-4
Figure 3-5 High air-entry ceramic plate	3-5
Figure 3-6 Structural epoxy samples for water absorption test	3-7
Figure 3-7 Water absorption of structural epoxies	3-9
Figure 3-8 Electrical connection cable	3-10
Figure 3-9 Coring of ceramic filter	3-11
Figure 3-10 Surface texture of 5 bar HAE ceramic plate	3-12
Figure 3-11 Preparation of ceramic filter surfaces	3-13
Figure 3-12 Assembly of tensiometer	3-14
Figure 3-13 Standard triaxial cell for low-pressure saturation (< 700 kPa)	3-16
Figure 3-14 Modified high triaxial cell for high-pressure saturation (> 700 kPa)	3-17
Figure 3-15 Diagram of saturation and calibration set-up	3-18
Figure 3-16 Response times	3-19
Figure 3-17 Typical calibration cycle	3-20
Figure 3-18 Positive pressure calibration 0 – 2000 kPa range	3-22
Figure 3-19 Positive pressure calibration curves	3-24
Figure 3-20 Positive pressure calibration 0 – 700 kPa range	3-27
Figure 3-21 Isotropic unloading configuration in the modified high triaxial cell	3-28
Figure 3-22 Tensiometer response to isotropic unloading, Test #1	3-30
Figure 3-23 Isotropic unloading Test #2	3-31
Figure 3-24 Tensiometer response to consolidation, Test #2	3-32

Figure 3-25 Tensiometer response to isotropic unloading, Test #2	3-33
Figure 3-26 Negative pressure calibration	3-36
Figure 3-27 Temperature calibration cycles	3-38
Figure 3-28 Temperature calibration curves	3-40
Figure 3-29 Tensiometer air-entry	3-41
Figure 4-1 Particle size distributions	4-3
Figure 4-2 Cumulative particle size distributions	4-3
Figure 4-3 Test set-up on strain-gauged hangers	4-4
Figure 4-4 Complete continuous drying test set-up on strain-gauged hangers	4-5
Figure 4-5 Continuous drying test set-up diagram	4-6
Figure 4-6 Continuous drying test set-up inside environmental enclosure	4-6
Figure 4-7 Essential continuous drying test set-up	4-7
Figure 4-8 Continuous drying test set-up during testing	4-7
Figure 4-9 Equipment for placement of soil specimen	4-9
Figure 4-10 Equipment for mixing of soil specimen	4-10
Figure 4-11 Test specimen placement	4-11
Figure 4-12 Continuous drying test set-up in the enclosure	4-12
Figure 4-13 Processing of specimen after test	4-13
Figure 4-14 <i>Whatman</i> No. 42 filter paper	4-14
Figure 4-15 Filter paper specimen	4-15
Figure 4-16 <i>Mettler</i> B5 single-pan precision balance	4-16
Figure 4-17 Filter paper specimens after oven-drying	4-17
Figure 5-1 Tensiometer desaturation in sample FS001	5-2
Figure 5-2 Zero-pressure offset confirmation	5-3
Figure 5-3 Matric suction vs filter desaturation	5-4
Figure 5-4 Evaporation of pore water in sample FS001	5-5
Figure 5-5 Tensiometer SWRCs (ψ_m-w) for sample FS001	5-6
Figure 5-6 Tensiometer SWRCs (ψ_m-S) for sample FS001	5-7
Figure 5-7 Tensiometer desaturation in sample GT001	5-8
Figure 5-8 Evaporation of pore water in sample GT001	5-9
Figure 5-9 Tensiometer SWRCs (ψ_m-w) for sample GT001	5-10
Figure 5-10 Tensiometer SWRCs (ψ_m-S) for sample GT001	5-10
Figure 5-11 Filter paper suctions for granular soil samples	5-12
Figure 5-12 Initial graphical construction of SWRC (ψ_m-w) for sample FS001	5-14
Figure 5-13 Final SWRC curve fit (ψ_m-w) for sample FS001	5-14
Figure 5-14 Initial graphical construction of SWRC (ψ_m-w) for sample GT001	5-15
Figure 5-15 Final SWRC curve fit (ψ_m-w) for sample GT001	5-15

Figure 5-16 Tensiometer vs filter paper SWRCs (ψ_m-w) for sample FS001	5-16
Figure 5-17 Tensiometer vs filter paper SWRCs (ψ_m-S) for sample FS001	5-17
Figure 5-18 Tensiometer vs filter paper SWRCs (ψ_m-w) for sample GT001	5-18
Figure 5-19 Tensiometer vs filter paper SWRCs (ψ_m-S) for sample GT001	5-18
Figure 5-20 Tensiometer desaturation in sample TP148	5-20
Figure 5-21 Tensiometer SWRCs (ψ_m-w) for sample TP148	5-21
Figure 5-22 Shrinkage curves ($e-w$) for sample TP148	5-22
Figure 5-23 Tensiometer SWRCs (ψ_m-S) for sample TP148	5-22
Figure 5-24 Tensiometer desaturation in sample TP149	5-23
Figure 5-25 Tensiometer SWRCs (ψ_m-w) for sample TP149	5-24
Figure 5-26 Shrinkage curves ($e-w$) for sample TP149	5-25
Figure 5-27 Tensiometer SWRCs (ψ_m-S) for sample TP149	5-25
Figure 5-28 Tensiometer desaturation in sample TP016	5-26
Figure 5-29 Tensiometer SWRCs (ψ_m-w) for sample TP016	5-27
Figure 5-30 Shrinkage curves ($e-w$) for sample TP016	5-28
Figure 5-31 Tensiometer SWRCs (ψ_m-S) for sample TP016	5-28
Figure 5-32 Final SWRC curve fits (ψ_m-w) for fine-grained soil samples	5-30
Figure 5-33 Tensiometer vs filter paper SWRCs (ψ_m-w) for sample TP148	5-31
Figure 5-34 Tensiometer vs filter paper SWRCs (ψ_m-S) for sample TP148	5-32
Figure 5-35 Tensiometer vs filter paper SWRCs (ψ_m-w) for sample TP149	5-33
Figure 5-36 Tensiometer vs filter paper SWRCs (ψ_m-S) for sample TP149	5-33
Figure 5-37 Tensiometer vs filter paper SWRCs (ψ_m-w) for sample TP016	5-34
Figure 5-38 Compacted vs initially slurried SWRCs (ψ_m-w) for sample TP016	5-35
Figure 5-39 Tensiometer vs filter paper SWRCs (ψ_m-S) for sample TP016	5-35
Figure 8-1 Data processing flow chart	A-4
Figure 8-2 Latex membrane seal dimensions	B-1
Figure 8-3 Custom triaxial cell top dimensions	B-2
Figure 8-4 Additional particle size distributions	B-3
Figure 8-5 Additional cumulative particle size distributions	B-3
Figure 8-6 MS54XX Miniature SMD Pressure Sensor	C-1

LIST OF SYMBOLS

Symbol	Description	Units
G_s	specific gravity	
T_s	surface tension	N/m
u_a	pore-air pressure, air pressure	kPa
u_g	cavitation pressure	kPa
u_v	partial vapour pressure	kPa
u_w	pore-water pressure, water pressure	kPa
θ_r	residual volumetric water content	%
θ_s	saturated volumetric water content	%
ρ_d	dry density	g/cm ³
ψ_{aev}	air-entry value, air-entry pressure	kPa
ψ_b	air-entry (bubbling) pressure	kPa
ψ_m	matric suction	kPa
ψ_o	osmotic suction	kPa
ψ_r	residual suction	kPa
ψ_t	total suction	kPa
AEV	air-entry value	kPa
HAE	high air-entry	
HCT	high-capacity tensiometer	
PDC	primary drying curve	
PWC	primary wetting curve	
RH	relative humidity	%
SWCC	soil-water characteristic curve	
SWRC	soil-water retention curve	
TSF	tailings storage facility	
D	dimension - diameter	mm
H	Henry's constant	
H	dimension - height	mm
M	mass	g
P	pressure	kPa
R	the universal gas constant	J/(mol·K)
S	degree of saturation	

T	absolute temperature	K
V	volume	cm^3
e	void ratio	
k	hydraulic conductivity	m/s
w	gravimetric water content	%
θ	volumetric water content	%
ν	specific volume	m^3/kg
ψ	suction pressure	kPa
ω	molecular mass	g/mol

1 INTRODUCTION

This study aims to examine the determination of soil-water retention curves for various soils using the tensiometer method first introduced by Toker *et al.* (2004). The development of a new high-capacity tensiometer for use in the geotechnical laboratory is also examined for this purpose. This chapter provides a brief background to the problem and outlines the objectives, scope and methodology of the study.

1.1 BACKGROUND

The principles of classical saturated soil mechanics have been well established and used in geotechnical engineering solutions. These principles often serve as conservative estimates for regions where mostly unsaturated soil conditions are encountered, such as in Southern Africa. The field of unsaturated soil mechanics can often be disregarded due to its apparent complexity.

Fundamental to the understanding of unsaturated soil mechanics is the concept of soil suction which adds strength to unsaturated soils and alters their volumetric and hydraulic behaviours. A key stumbling block limiting the advancement and implementation of these concepts is the lack of accessible methods of measuring soil suction. An increased interest in the use of ‘high-capacity tensiometers’ or ‘HCTs’, devices capable of measuring high values of soil suctions directly, has inspired more studies into and confidence in the use of unsaturated soil mechanics around several parts of the world.

An invaluable tool used in unsaturated soil mechanics is called the ‘soil-water retention curve’ or ‘SWRC’ which describes the relationship between the soil matric suction and the water content of an unsaturated soil. The SWRC can be used as a basis to model various unsaturated soil parameters, such as the hydraulic conductivity and shear-strength functions. It is, therefore, vital that an accurate characterisation of the SWRC of a soil be made.

If the complexities involved with the accurate measurement of soil suction and the determination of the SWRC could be solved, a new stage of development for unsaturated soil mechanics could be unlocked. It is, therefore, the focus of this study to investigate suction measurement through a new high-capacity tensiometer and a simplified method for determining the SWRCs for various soils.

1.2 STUDY OBJECTIVES

This study aims to determine the effectiveness of a proposed method for rapidly determining continuous soil-water retention curves (SWRCs) of various soils with the use of a low-cost tensiometer developed as a part of the research methodology.

The main objectives of the study are to;

- manufacture, test and implement a low-cost tensiometer for the use in a geotechnical laboratory environment,
- develop a procedure for determining SWRCs for different granular soils using the tensiometer method,
- compare the results with the conventional method for determining SWRCs via the filter paper method, and
- investigate the incorporation of dimensional change measurement to the procedure to determine SWRCs for different fine-grained or clayey soils.

1.3 SCOPE OF STUDY

The study was limited in the following ways:

- Five types of soil were tested, consisting of two granular soils and three fine-grained or clayey soils.
- Verification of the results was achieved using only one other method, the filter paper method.
- The temperature and humidity of the test environment were not controlled or measured.

1.4 METHODOLOGY

The following methodology was implemented to investigate the effectiveness of a proposed method for rapidly determining soil-water retention curves (SWRCs) of various soils with the use of a low-cost tensiometer:

- A literature study was conducted to establish a basic knowledge of unsaturated soil mechanics and how it relates to soil suctions, the current state of non-commercial tensiometers and methods for determining soil-water retention curves.
- A framework of experimental procedures was established for determining SWRCs using the tensiometer method:

- In the first part of the investigation, a new prototype tensiometer was developed and tested. Procedures were developed to reliably saturate and calibrate the tensiometer to enable its use in the geotechnical laboratory.
- In the second part of the investigation, two different soils were tested to determine SWRCs for each using the proposed tensiometer method and then compared to the filter paper method.
- Three additional soils were then tested, incorporating dimensional change measurement to the procedure, and determining SWRCs for each, again using both methods.
- The results of the procedures were then analysed and presented to evaluate the efficacy of both the tensiometer and the tensiometer method for determining SWRCs for various soils.

1.5 ORGANISATION OF REPORT

This dissertation document comprises several chapters consisting of:

- Chapter 1 serves as an introduction to the study.
- Chapter 2 investigates, records and critically reviews the findings from the currently available literature.
- Chapter 3 describes the development of a prototype tensiometer and the experimental procedures that were used for its implementation.
- Chapter 4 describes the experimental procedures that were used throughout the study to determine soil-water retention curves of various soils.
- Chapter 5 reports analysis and discussion of the results from the experimental procedures.
- Chapter 6 reports the conclusions drawn from the study and offers recommendations for future research and applications of the study.
- Chapter 7 lists the references pertaining to the study.
- Appendices A to C contain additional materials referenced in the report.

2 LITERATURE REVIEW

This chapter presents an overview of the literature that relates to the work presented in the study. After an initial overview of the concepts concerning unsaturated soils and soil suction, a more detailed look at high-capacity tensiometers (HCTs), their development and recent developments on the topic of direct suction measurement is provided. An overview of the relationship between soil suction and soil-water content and methods for determining the soil-water retention curve (SWRC) is then discussed. Lastly, this chapter reviews the seminal contributions made by authors who have studied the use of recently advanced HCTs for determining the SWRC.

2.1 SATURATED AND UNSATURATED SOILS

A *saturated* soil consists of two incompressible phases, namely liquid pore water and solid soil particles. An *unsaturated* soil consists of three phases: liquid pore water, solid soil particles, gaseous pore air. The presence of a third phase, namely the pore air, indicates that the degree of saturation of unsaturated soil is less than unity. The qualifier ‘unsaturated’ therefore bears the same meaning as ‘partially saturated.’ Figure 2-1 illustrates the difference between the soil phase and stresses taken into consideration in saturated and unsaturated soil mechanics, respectively.

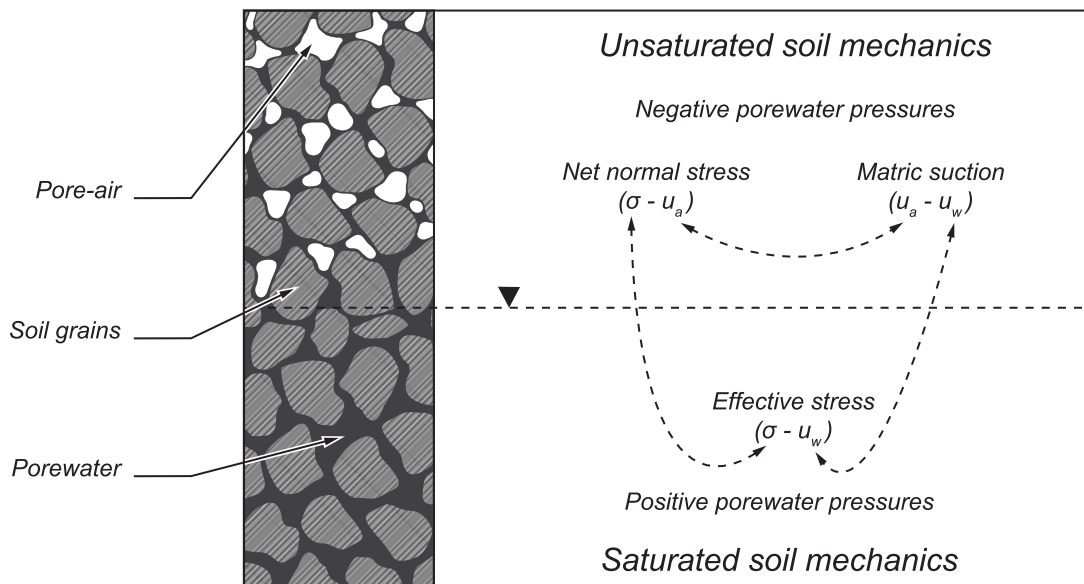


Figure 2-1 Saturated vs unsaturated soil mechanics (Lu & Likos, 2004)

2.1.1 Unsaturated soil phases

An unsaturated soil is generally considered physically as a three-phase system consisting of solids, water and air. The interface between pore air and pore water also plays a significant role

in the physical mechanisms controlling unsaturated soils. The air-water interface (or ‘contractile skin’) should be viewed as an additional phase when considering specific physical mechanisms (Fredlund & Morgenstern, 1977). The viewing of the air-water interface as a separate phase is justified by it having specific properties that differ from its surrounding material, specifically in its ability to exert a tensile pull (surface tension) that mechanically influences soil particles. The air-water interface has definitive bounding surfaces, and its thickness is only in the order of a few molecular layers. It is therefore excluded from the summation of masses and volumes in soil phases without significant error (Lu & Likos, 2004).

2.1.2 Surface tension

The air-water interface possesses a property known as surface tension. Surface tension is produced by an imbalance in the intermolecular forces acting on water molecules in the air-water interface. Water molecules located in the interior of the water experience an equal cohesive force in all directions. Water molecules located in the interface, however, experience an imbalanced force towards the interior of the water due to the break of continuity. A tensile pull is generated along the interface to maintain equilibrium. This property of the air-water interface to exert a tensile pull is known as surface tension (Figure 2-2). Surface tension acts tangentially to the air-water interface surface.

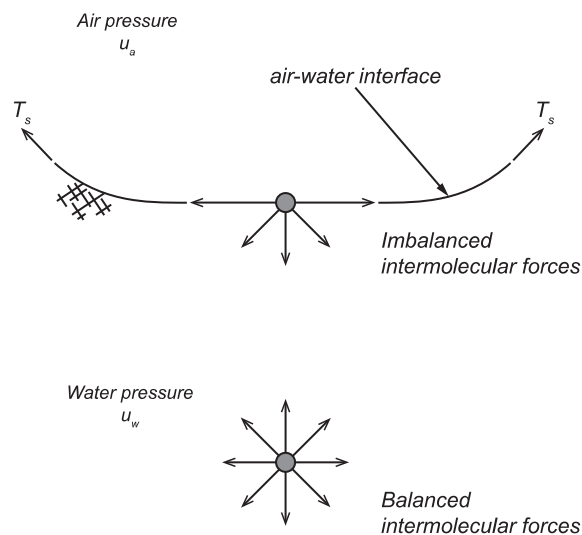


Figure 2-2 Surface tension at the air-water interface, after Fredlund & Rahardjo (1993).

Surface tension causes the air-water interface to behave like an elastic membrane. A difference in pressure across any flexible membrane must be accompanied by a change in curvature of the surface geometry, concave towards the higher pressure, to maintain equilibrium. The pressure difference across the curved surface is related to the surface tension (T_s) and the radius of curvature (R_s). It can be shown that for a system subjected to air pressure (u_a) higher than the

water pressure (u_w) the curvature of the air-water interface caused by the pressure difference ($u_a - u_w$) is following Kelvin's capillary model equation (Equation 2.1) (Fredlund *et al.*, 2012).

$$(u_a - u_w) = \frac{2T_s}{R_s} \quad 2.1$$

The curved air-water interface is often called a meniscus. For a pressure difference of zero, the radius of curvature tends to infinity, implying a flat air-water interface. As the pressure difference increases, the radius of curvature decreases. Surface tension is temperature-dependent and decreases as temperature increases. The radius of curvature (R_s) of the air-water interface and the pressure difference ($u_a - u_w$) are analogous to the pore radius and maximum sustainable negative pore-water pressure of an unsaturated soil, respectively. (Fredlund *et al.*, 2012)

2.1.3 Cavitation

The phenomenon of cavitation is a crucial consideration in this study. Cavitation is the formation of cavities (gas or vapour filled bubbles) in a liquid. Cavitation may refer to either the creation of a new cavity ('*nucleation*') or the expansion of a pre-existing cavity. These cavities may be suspended in the body of the liquid, trapped in minute crevices in the liquid's boundary surface or solid particles suspended in the liquid. The expansion of minute cavities to a size where they have observable macroscopic effects ('cavity growth' or 'bubble growth') is related to a reduction in pressure of a liquid to its vapour pressure. These cavities may contain gas or vapour, or a mixture of gas and vapour. A gas-containing cavity may expand due to the diffusion of dissolved gasses from the liquid into the cavity, by a pressure reduction, or by a temperature increase. Explosive vaporisation into a vapour-containing cavity due to a sufficient decrease in pressure is termed '*cavitation*'. The continuous growth of a vapour-containing cavity due to a sufficient increase in temperature is known as '*boiling*' (Ng & Menzies, 2007). Young (1989) reports four mechanisms that may induce cavity growth:

- *gaseous cavitation* by pressure decrease or temperature increase,
- *degassing* by diffusion of dissolved gasses,
- *vaporous cavitation* by pressure decrease, and
- *boiling* by temperature increase.

In theory, a liquid will vaporise when the absolute pressure falls below its vapour pressure, or the vapour pressure is increased with temperature. Ideal paths of cavitation (a-b) and boiling

(a-c) are shown on a thermodynamic phase diagram for a simple substance (e.g. pure water) (Figure 2-3). It indicates that ‘explosive’ cavitation or boiling do not occur until a threshold is reached, i.e. crossing the vaporisation curve. In practice, the pressure at which cavitation initiates is dependent on the liquid’s physical state. Crossing the vaporisation curve does not assure cavity nucleation. Instead, the liquid enters a metastable phase at which the liquid is under tension. Vaporisation occurs if and when the tensile strength of the liquid is reached (Lu & Likos, 2004).

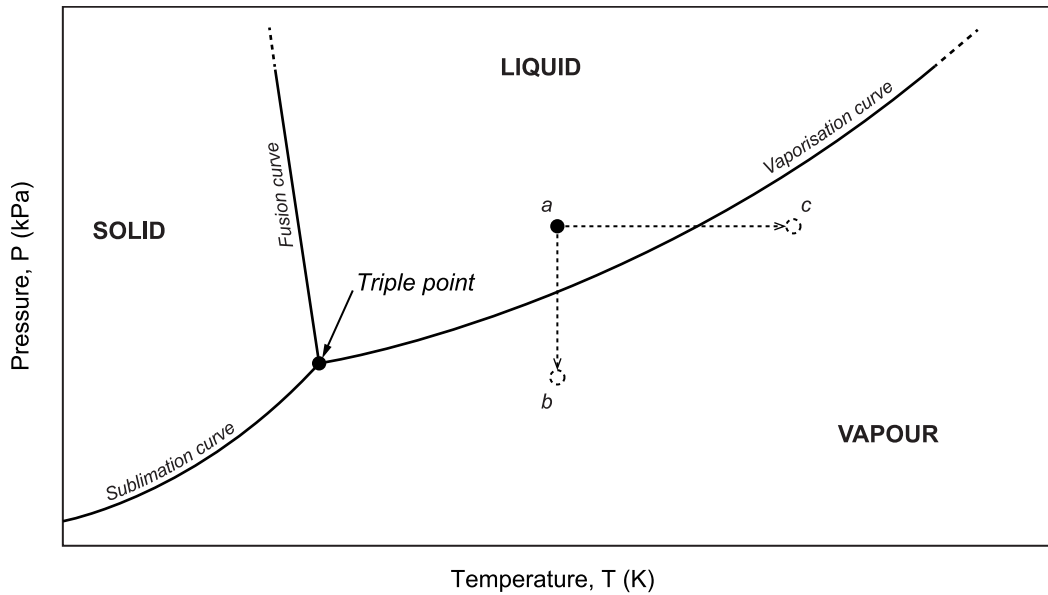


Figure 2-3 Idealised thermodynamic phase diagram (Lu & Likos, 2004)

2.2 SOIL SUCTION

Soil suction or ‘total soil suction’ (ψ_t) refers to the free energy state of soil pore water measured in terms of its partial vapour pressure (Ng & Menzies, 2007). It is the amount of energy required to remove a unit volume of water from an unsaturated soil. From thermodynamics, total suction can be described by Kelvin’s equation (Equation 2.2).

$$\psi_t = -\frac{RT}{v_{w0}\omega_v} \ln\left(\frac{u_v}{u_{v0}}\right) \tag{2.2}$$

where:

- ψ_t = total suction,
- R = the universal gas constant,
- T = absolute temperature,
- v_{w0} = specific volume of water,
- ω_v = molecular mass of water vapour,
- u_v = partial pressure of pore water vapour, and
- u_{v0} = saturation pressure of water vapour over pure free water

Total suction is derived from the measurement of the partial vapour pressure of pore water (u_v) relative to the saturation pressure of water vapour (u_{v0}) over pure free water at the same temperature. Free water refers to water containing no dissolved solutes with a flat air-water interface and having no external forces acting on it other than gravity (Lu & Likos, 2004). The term (u_v/u_{v0}) is called relative humidity (RH). A change in total suction is caused by a change of RH (Ng & Menzies, 2007).

2.2.1 Components of soil suction

2.2.1.1 Total suction

Total soil suction is composed of two components, namely *matric* and *osmotic* suction and is expressed as the algebraic sum of these terms (Ng & Menzies, 2007) (Equation 2.3).

$$\psi_t = \psi_m + \psi_o \quad 2.3$$

2.2.1.2 Matric and osmotic suction

Matric suction

Matric suction (ψ_m) is related to the combined effects of capillarity and short-range adsorption effects of fine-grained soil particles. It can be considered as the physical component of total suction. Matric suction is algebraically equal to the difference between the pore-air pressure (u_a) and the pore-water pressure (u_w) (Equation 2.4). The pore-air pressure is equal to the local air pressure and is generally atmospheric ($u_a =$ zero gauge pressure).

$$\psi_m = u_a - u_w \quad 2.4$$

The difference between the pore-air pressure and pore-water pressure produces a curved air-water interface where the radius of curvature is inversely proportional to the pressure difference (Equation 2.1). The pore water has a negative pressure relative to the pore-air pressure. The pressure difference is compensated for by surface tension at the air-water interface. It is this surface tension property of water that enables suction to be sustained in the pores of a soil. The presence of a curved air-water interface can reduce the RH, resulting in soil suction.

At relatively high degrees of saturation, capillarity effects in the small pores of soil take the primary relevance. Soil pores with small radii act similar to capillary tubes, drawing pore water above the water table. Pore water is then held in menisci between soil particles known as the capillary effect in soils.

At relatively low degrees of saturation, adsorbed pore water is primarily in the form of thin films coating the soil particle surfaces and isolated menisci. The short-range adsorption effects arising from electrical and van der Waals force fields in the vicinity of the soil-pore water interface take the primary relevance (Krahn & Fredlund, 1972).

A conceptual model for the suction regimes at different relative degrees of saturation is illustrated in Figure 2-4.

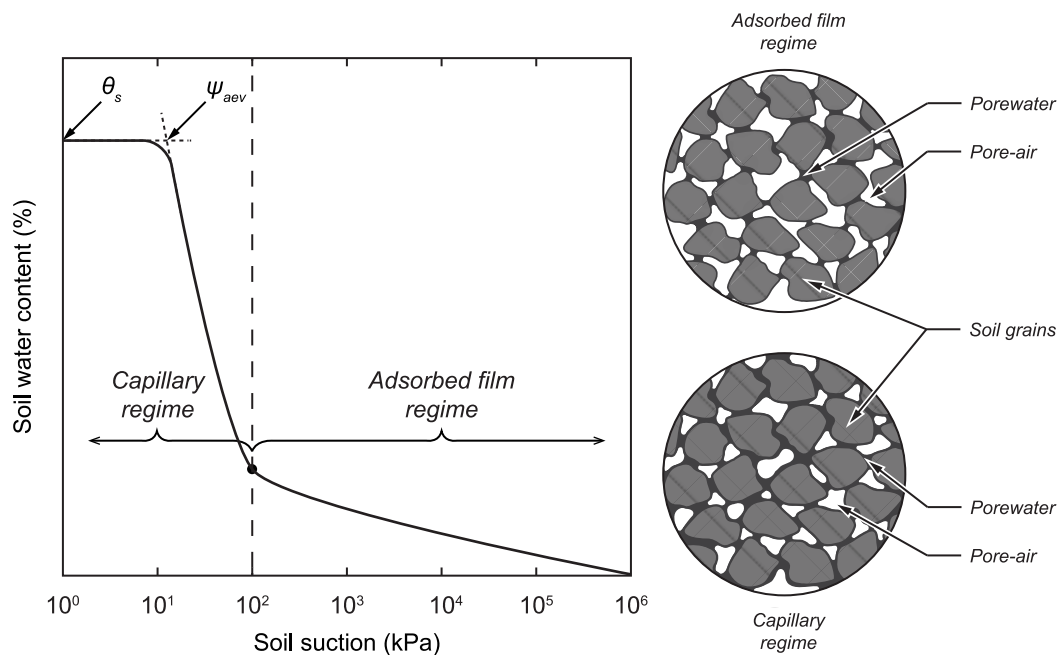


Figure 2-4 A conceptual model of soil suction regimes (Lu & Likos, 2004).

Osmotic suction

Osmotic suction (ψ_{mo}) is a function of the concentration of dissolved solutes (salts and contaminants) in pore water expressed in terms of pressure (Ng & Menzies, 2007). It can be considered as the chemical component of total suction. Fundamentally, a differential pressure is created between two concentrations of dissolved solutes if the flow of water between them is restricted. The potential for pore water to flow created by this differential pressure inside the soil pore matrix is known as the *osmotic suction* component of total suction. The presence of dissolved solutes in pore water can reduce the RH, producing suction (Peck & Rabbige, 1969).

2.2.2 Effects of soil suction components

Environmental changes affecting the condition of unsaturated soil, such as wetting or drying (through evaporation-transpiration and infiltration), primarily influence the matric component of soil suction. The majority of relationships of unsaturated soil parameters are also derived from the changes in soil suction and thus changes in matric soil suction. The measurement of

matric suction is commonly the primary focus of research and geotechnical problems related to soil suction. At high suctions (greater than about 1500 kPa), the matric and total soil suction can generally be assumed to be equivalent (Fredlund & Xing, 1994).

It must be noted that osmotic suction may, in some instances, be the dominant component of total suction. Although the concentration of dissolved solutes may change with the degree of saturation, osmotic suction remains constant as long as the relative concentration of dissolved solutes remains unchanged (Lu & Likos, 2004). It is accepted that a concentration gradient must exist between two points over which the movement of solutes is restricted for osmotic suction to be generated.

2.2.3 Soil Suction and Soil-Water Content

The magnitude of soil suction developed in an unsaturated soil depends on the water content of the soil, water and air system. As previously discussed, at relatively high degrees of saturation, the dominant pore water retention mechanism is capillarity, governed primarily by the particle structure, pore structure, and pore size distribution. Relatively high degrees of saturation have corresponding low values of suction. At relatively low degrees of saturation, pore water is primarily in the form of thin films on the particle surfaces where the dominant mechanism contributing to suction is the relatively short-range adsorption effects governed by the surface properties of the soil particles (Lu & Likos, 2004). Relatively low degrees of saturation have corresponding high values of suction.

As the soil-water content decreases, the magnitude of the soil suction developed increases. The relationship between soil suction and soil-water content is fundamental to the understanding of the behaviour of unsaturated soils. The soil-water retention curve describes this relationship and is a valuable tool for the study of unsaturated soil mechanics.

2.2.3.1 Soil-water retention curves

The soil-water retention curve (SWRC) for a soil is defined as the relationship between the soil-water content and suction of the soil. It expresses the variation of soil suction with the water storage capacity within the pores of an unsaturated soil.

Features of the soil-water retention curve

The SWRC is most commonly graphed on a semi-logarithmic scale with the gravimetric water content (w) volumetric water content (θ) or degree of saturation (S) against soil suction (ψ) on a logarithmic scale. Figure 2-5 shows the typical features of idealised SWRCs for a silty soil.

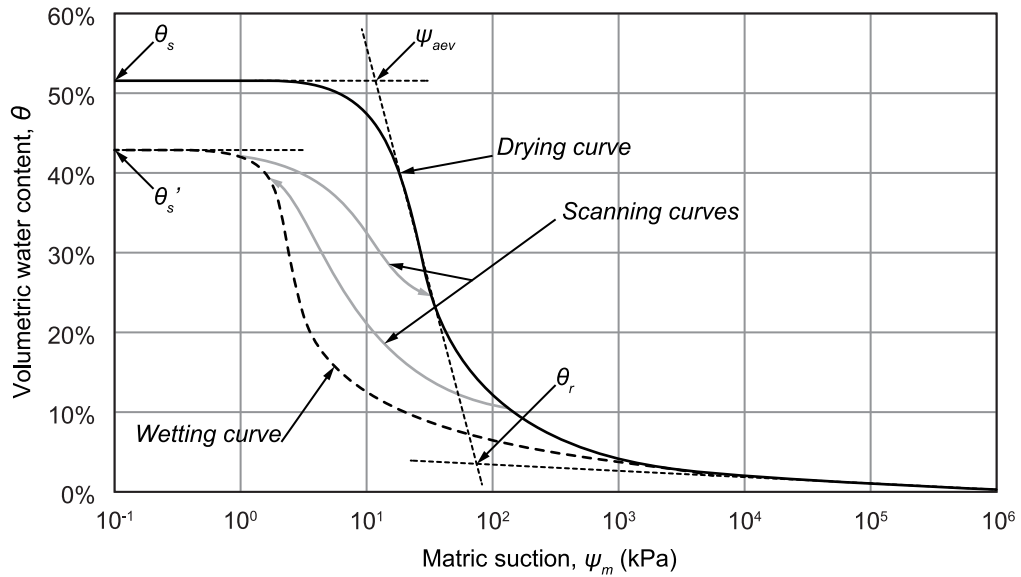


Figure 2-5 General features of SWRCs (Fredlund & Xing, 1994)

Two branches of the SWRC, the drying (desorption or desaturation) and wetting (adsorption or saturation) curves are depicted. Non-uniformity in pore size distribution, void passage irregularities and changing advancing and receding meniscus contact angles can all explain the significant hysteresis between the drying and wetting curves (Pham *et al.*, 2001). Scanning curves describe the states between the drying and wetting curves. The saturated volumetric water content (θ_s) corresponds to the water content before drying at which all the pores in the soil are completely saturated. The saturated water content corresponds to the porosity and ultimately, the water storage capacity of a soil. At any given value of soil suction, the soil-water content during drying and rewetting is not the same (Fredlund & Rahardjo, 1993). Furthermore, at the end of the wetting curve, the volumetric water content (θ'_s) may differ from the water content at the start of the drying curve as a result of air entrapment in the soil pores (Fredlund & Xing, 1994). The air-entry value (ψ_{aev}) describes the suction on the drying curve at which air first starts to enter the largest pores of the soil and signifies the starting point of desaturation. The residual volumetric water content (θ_r) is thought to describe the condition at which pore water is in the form of isolated menisci surrounding the interparticle interfaces (Figure 2-6). It indicates the transition of the mechanism holding soil-water from capillarity to adsorption effects (Sillers, 1997). Substantial changes in suction would be necessary to further desaturate the soil beyond the residual water content. The residual water content lacks a formal definition and is usually determined by a graphical construction method using tangent lines (Figure 2-5). The theoretical maximum value of suction corresponding to a completely dry soil (e.g. oven dry), regardless of soil type, is experimentally reported as just below 1000000 kPa. This value is also supported by thermodynamic considerations (Fredlund & Xing, 1994).

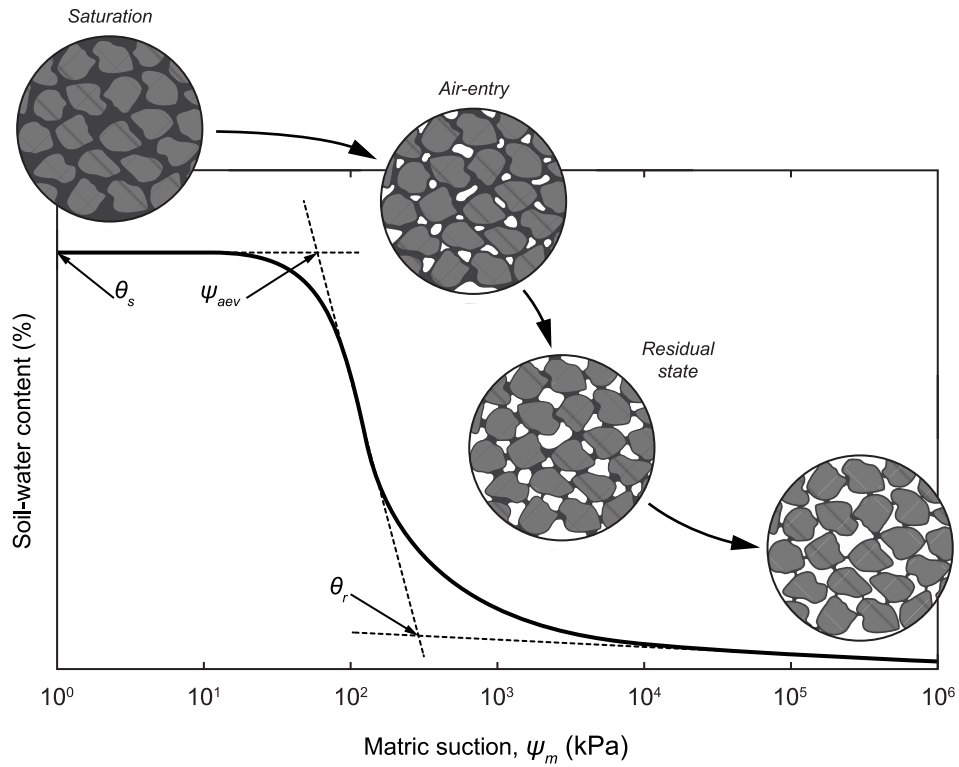


Figure 2-6 Stages of soil desaturation and the SWRC

SWRCs of different soils may differ based on their dissimilar grain sizes and composition. Figure 2-7 shows the typical features of desorption SWRCs for different soils (Fredlund & Xing, 1994). In general, the saturated water content, residual state water content and air-entry value increase as the grain size of the soil decreases (or the plasticity increases).

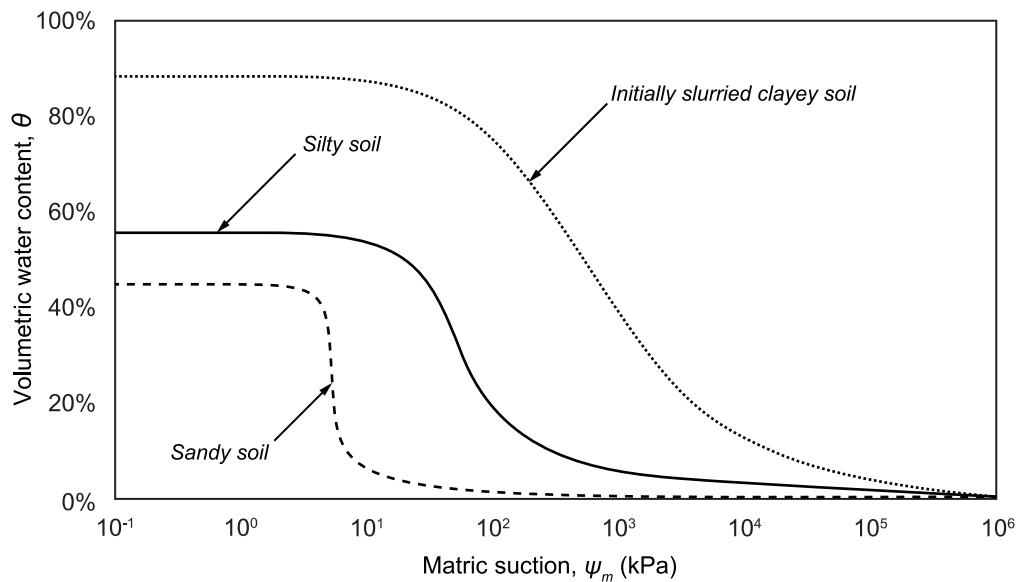


Figure 2-7 SWRCs of different soils (Fredlund & Xing, 1994)

Nomenclature

The most common terms for describing the relationship between the amount of water in a soil and soil suction found in the literature are all synonymous and are:

- soil-water characteristic curve (SWCC),
- soil-water retention curve (SWRC),
- soil-water curve,
- soil moisture curve (SMC),
- soil moisture retention curve (SMRC), and
- water retention curves.

The term “soil-water characteristic curve” or “SWCC” is the most commonly found term throughout literature relating to unsaturated soil mechanics. The term “soil-water” is preferred to indicate that it is the pore-water content that is being considered when defining this relationship. The term “characteristic” indicates that the curve describes the behaviour of the soil and should not be misinterpreted as having the same meaning as “unique” since any particular soil may have many characteristic curves, influenced primarily by the volumetric state of the soil (Toll, 2012). A case can be made to do away with the misnomer and refer to the relationship as the “soil-water retention curve” instead. Traditionally, the term “retention” was related more to the water-retaining ability of a soil and was reserved for use in agricultural and soil sciences (Fredlund *et al.*, 2001). However, for the remainder of this study, the term “soil-water retention curve” or “SWRC” will be used for the reasons presented, and it is recommended that it be used in geotechnical engineering applications. It is also suggested that the term “soil-water retention curve” is used to represent the relationship between volumetric water content and matric suction specifically (Fredlund & Xing, 1994).

SWRCs can be further categorised as:

- desorption, desaturation, or drying curves,
- saturation, adsorption, or wetting curves, and
- scanning curves in between the above (refer to Figure 2-5).

Parameters influencing the soil-water retention curve

General models for the SWRC have been determined experimentally. Soils composed of different materials will have different SWRC's due to changes in the many parameters that set them apart. Therefore, a given material may have different SWRC curves corresponding to a change in each parameter. The term ‘characteristic’ in soil-water characteristic curve implies that for a single given soil, there exists a unique curve describing the relationship between the water content and suction of the soil. However, many parameters influence the uniqueness of

the SWRC. A critical review of these parameters is contained in Malaya & Sreedeeep (2012). Apart from the mineralogy and particle size distribution, the most influential parameter affecting the form of the SWRC is the initial density of the soil being tested.

It is widely accepted that unsaturated soil behaviour is governed by two independent stress state variables, i.e. net normal stress and matric suction. The SWRC is typically determined by suction measurements using the pressure plate in which no external pressure is applied, and the volume change of the soil is assumed to be zero (Ng & Menzies, 2007). However, all the parameters controlling the behaviour of an unsaturated soil must be collected to establish accurate relationships for the SWRC that suit the intended application, which may include the stress state variables.

Uses for the soil-water retention curve

It is proposed that the SWRC can be used to estimate various unsaturated soil parameters. For example, it is proposed that there exists a significant correlation between the soil-water content, and therefore soil suction, and the shear strength of an unsaturated soil (Vanapalli *et al.*, 1998). The SWRC is used as the basis for prediction of other unsaturated soil parameters, such as the hydraulic conductivity (permeability) and shear-strength functions. It is, therefore, vital that an accurate characterisation of the SWRC be made (Fredlund & Xing, 1994). It is an essential tool in geotechnical engineering and agriculture used for the analysis of unsaturated soil conditions such as found in tailings dams and the water retention capacity of agricultural lands (Lu & Likos, 2004). Traditionally the focus of most studies is on the drying curve, however more and more interest is being expressed in the direct measurement and monitoring of soils that undergo changes in water content and volume.

2.2.3.2 Interpretation of soil-water retention curves

The interpretation of SWRCs is an involved topic, one that this study aims to expand by enabling further investigations. A comprehensive paper on the interpretation of SWRCs was published by Fredlund *et al.* (2001). The meaning and relevance of the residual state of soils are discussed critically in Vanapalli *et al.* (1998). Fredlund & Houston (2013) delve into the topic of SWRCs, where volume change occurs as soil suction is changed. Lastly, a recommended guide to the SWRCs for different soils is contained in Mercer *et al.* (2019).

2.2.3.3 Determination of soil-water retention curves by empirical methods

SWRCs can be estimated indirectly from particle size distributions or statistical analysis of other soil parameter functions (Van Genuchten, 1980). Empirical equations are applied to produce the SWRC in a recognisable form (Fredlund *et al.*, 1997). The most common set of empirical equations is discussed here.

Soil-water retention curve equations

General empirical equations have been proposed to describe the SWRC. Each equation (or set of equations) has its limitations or computational advantages. Fredlund & Xing (1994) have proposed a single general equation for the SWRC that fit the entire range of soil suction. The equation is based on the pore-size distribution of a soil which may be either determined or predicted. A graphical construction is used to estimate the residual suction (and air-entry value) from SWRC data (as shown in Figure 2-5). A computational technique employs non-linear least-squares error minimisation to determine best-fit curve-fitting parameters for the general equation in the form of Equation 2.5.

The Fredlund & Xing (1994) best-fit gravimetric water content SWRC is given in Equation 2.5. The equation contains a shape correction factor (Equation 2.6) to force the form of the curve to fit over the entire range of soil suction (0 – 1000000 kPa).

$$w(\psi) = \frac{w_s C_r(\psi_r)}{\left[\ln \left(e + \left(\frac{\psi}{a_f} \right)^{n_f} \right) \right]^{m_f}} \quad 2.5$$

$$C_r(\psi_r) = \left[1 - \frac{\ln \left(1 + \frac{\psi}{\psi_r} \right)}{\ln \left(1 + \frac{10^6}{\psi_r} \right)} \right] \quad 2.6$$

where:

- $w(\psi)$ = gravimetric water content at any specified suction, ψ (kPa),
- w_s = saturated gravimetric water content,
- ψ_r = residual soil suction (kPa),
- a_f = fitting parameter related to the air-entry value,
- m_f = fitting parameter related to the residual water content,
- n_f = fitting parameter related to the slope at the inflection point, and
- $C_r(\psi_r)$ = shape correction factor.

The Fredlund *et al.* (2002) best-fit shrinkage curve for the principal shrinkage path is given in Equation 2.7. The ratio $\frac{a_{sh}}{b_{sh}} = \frac{G_s}{S}$ is constant for a specific soil where G_s = specific gravity and S = degree of saturation.

$$e(w) = a_{sh} \left[\frac{w^{c_{sh}}}{b_{sh}^{c_{sh}}} + 1 \right]^{\left(\frac{1}{c_{sh}} \right)} \quad 2.7$$

where:

- $e(w)$ = void ratio at any specified gravimetric water content, w
- a_{sh} = minimum void ratio,

- b_{sh} = slope of the line of tangency (saturation line) when dried from saturated conditions, and
 c_{sh} = fitting parameter relating to the curvature of shrinkage curve,

The combination of these equations enables a full description of the SWRC, even when volume change occurs as suctions are generated.

2.3 MEASUREMENT OF SOIL SUCTION

Soil suction takes different measurable forms: total soil suction or of one of its components, either matric or osmotic suction. Osmotic suction remains constant in the majority of geotechnical problems related to soil suction. Although its influence cannot be neglected, the change in the stress state of unsaturated soil, the primary focus of most studies, is governed by the change in the matric suction component rather than the total suction or osmotic suction component (Fredlund, 2006). Exceptions to this generalisation can be present in coastal and tidal regions.

Techniques for measuring soil suction can be categorised as either direct or indirect. The differences are discussed in further detail in sections 2.3.1 and 2.3.2. Techniques can be further categorised by their applicability in field or laboratory uses. Table 2-1 summarises commonly used techniques for determining matric and total suction, although the list is not exhaustive.

Table 2-1 Soil suction measurement techniques (as presented in Lu & Likos (2004))

Component	Technique/Instrument	Suction range (kPa)	Direct/Indirect	Use case
Matric suction	Tensiometers	0 - 100	Direct	Laboratory and field
	High-capacity tensiometers	0 - 1500	Direct	Laboratory and field
	Axis translation	0 - 1500	Direct	Laboratory
	Conductivity sensors	0 - 400	Indirect	Laboratory and field
	Contact filter paper method	Entire range	Indirect	Laboratory and field
Total suction	Psychrometers	100 - 8000	Indirect	Laboratory and field
	Chilled mirror techniques	1000 - 450000	Indirect	Laboratory
	Resistance/capacitance sensors	Entire range	Indirect	Laboratory
	Humidity control techniques	4000 - 600000	Indirect	Laboratory
	Noncontact filter paper method	1000 - 500000	Indirect	Laboratory and field

The measurement of the osmotic suction component is challenging to accomplish, although methods have been proposed to measure osmotic suction directly (refer to Bocking & Fredlund (1979), Ridley & Wray (1995) and Tang *et al.* (2010)). These researchers indicate that, although it is known that the osmotic suction component may significantly influence the behaviour of unsaturated soils and methods exist to quantify it, the major limitation in furthering research is

the lack of practical and accessible methods for controlling or measuring osmotic suction in soils. Generally, osmotic suction is determined indirectly by the difference in total and matric suction, both of which can be measured by the methods listed above.

2.3.1 Indirect methods of soil suction measurement

Indirect methods of soil suction measurement are termed ‘indirect’ because they relate the magnitude of soil suction to some physical property of the unsaturated soil that is also related to the soil suction, rather than measure it directly. They rely on the calibration between a more measurable property and the amount of soil suction. The property may be:

- relative humidity (psychrometer, non-contact filter paper method),
- absorption (contact filter paper method), or
- electrical resistance or thermal conductivity (gypsum or thermal block) (Ridley & Burland, 1993).

These methods will not be looked at in detail here. Bulut & Leong (2008) offer a critical review of these methods and conclude that accurate suction measurement remains challenging with the current technology, particularly in the low suction range which is often of interest to studies on unsaturated soils. They also offer that the filter paper method remains the most convenient indirect suction measurement method.

2.3.1.1 The filter paper method

The filter paper method is one of the most commonly used indirect methods for measuring soil suction (Suits *et al.*, 2012). It has seen widespread implementation since its first appearance in agricultural applications (Gardener, 1937). Filter paper has also been extensively used to evaluate and verify the results of other measurement techniques (Muñoz-Castelblanco *et al.*, 2012). Most researches will point to Hamblin (1981) or Greacen *et al.* (1987) and the use of *Whatman* No. 42 filter paper in their research. It is also currently the standard test method for the measurement of soil suction (ASTM, 2003).

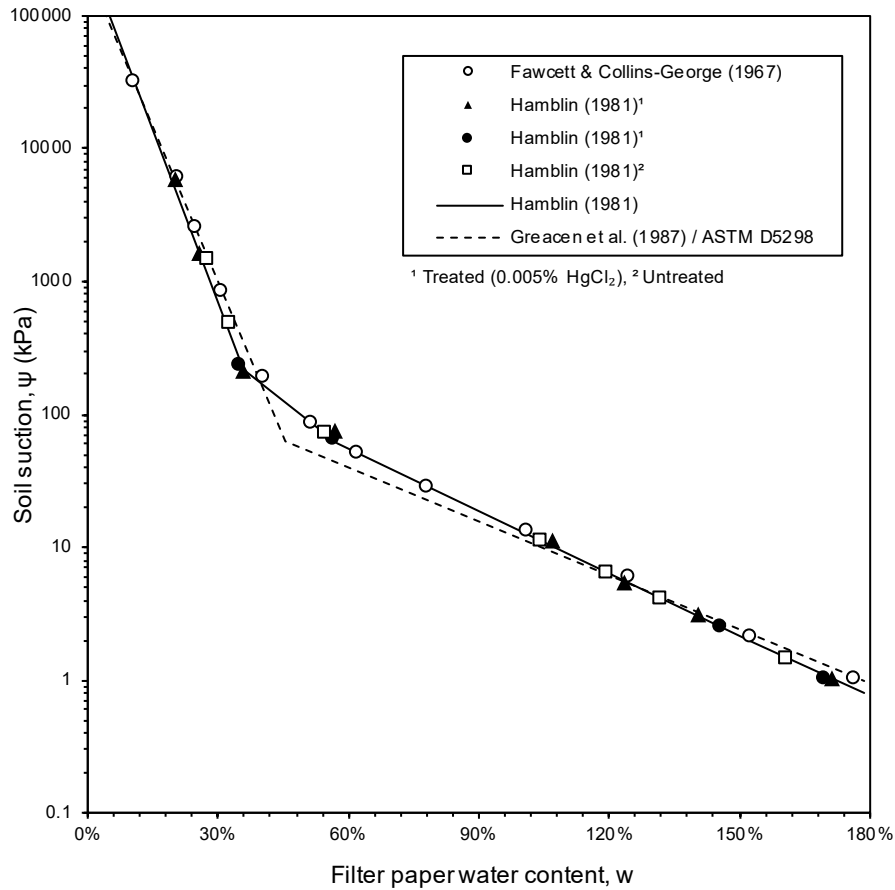


Figure 2-8 Calibration curves for *Whatman* No. 42 filter paper (after Fawcett & Collins-George (1967), Hamblin (1981) and Greacen *et al.* (1987))

The Hamblin (1981) piecewise-defined calibration curve is given in Equation 2.8.

$$\log \psi(w) = \begin{cases} 5.4327 - 8.6729(w) & \text{if } w \leq 35.70\% \\ 3.2390 - 2.5276(w) & \text{if } 35.70\% < w \leq 57.53\% \\ 2.6843 - 1.5635(w) & \text{if } 57.53\% < w \leq 153.6\% \\ 2.5975 - 1.5070(w) & \text{if } 153.6\% < w \end{cases} \quad 2.8$$

where:

* ψ = soil suction (kPa), and
 w = filter paper water content

* $\psi = \psi_m$ for contact filter paper method and $\psi = \psi_t$ for non-contact filter paper method

The Greacen *et al.* (1987) piecewise-defined calibration curve adapted from the current standard (ASTM, 2003) is given in Equation 2.9.

$$\log \psi(w) = \begin{cases} 5.3270 - 7.7900(w) & \text{if } w \leq 45.26\% \\ 3.2390 - 2.5276(w) & \text{if } 45.26\% < w \end{cases} \quad 2.9$$

Bicalho *et al.* (2010) provide a detailed review of the independent filter paper calibrations of different researchers for *Whatman* No. 42 filter paper listed below in the adapted form:

(Fawcett & Collins-George, 1967):

$$\log \psi(w) = \begin{cases} 4.7770 - 6.0000(w) & \text{if } w \leq 47.49\% \\ 2.6401 - 1.5000(w) & \text{if } 47.49\% < w \end{cases} \quad 2.10$$

(Chandler *et al.*, 1992):

$$\log \psi(w) = \begin{cases} 4.8400 - 6.2200(w) & \text{if } w \leq 46.97\% \\ 1.0500 - 2.5 \log(w) & \text{if } 46.97\% < w \end{cases} \quad 2.11$$

(Leong *et al.*, 2002):

$$\log \psi(w) = \begin{cases} 4.9500 - 6.7300(w) & \text{if } w \leq 47.10\% \\ 2.9100 - 2.2900(w) & \text{if } 47.10\% < w \end{cases} \quad 2.12$$

(Marinho & Oliveira, 2006):

$$\log \psi(w) = \begin{cases} 4.8300 - 8.3900(w) & \text{if } w \leq 33.00\% \\ 2.5700 - 1.5400(w) & \text{if } 33.00\% < w \end{cases} \quad 2.13$$

(Bicalho *et al.*, 2010):

$$\log \psi(w) = \begin{cases} 4.7500 - 4.8000(w) & \text{if } w \leq 50.00\% \\ 3.3650 - 2.7000(w) & \text{if } 50.00\% < w \end{cases} \quad 2.14$$

where:

ψ = soil suction (kPa), and

w = filter paper water content

All of the different calibration curves offered in literature are seldom compared. This comparison is made in Figure 2-9. The shaded region showed the variability in the independent calibrations on the same *Whatman* No. 42 filter paper of different batches. It is clear why it is recommended in D 5298-92 (ASTM, 2003) that independent calibration is undertaken, but the question of the accuracy of these calibrations is debated since usually indirect methods are used.

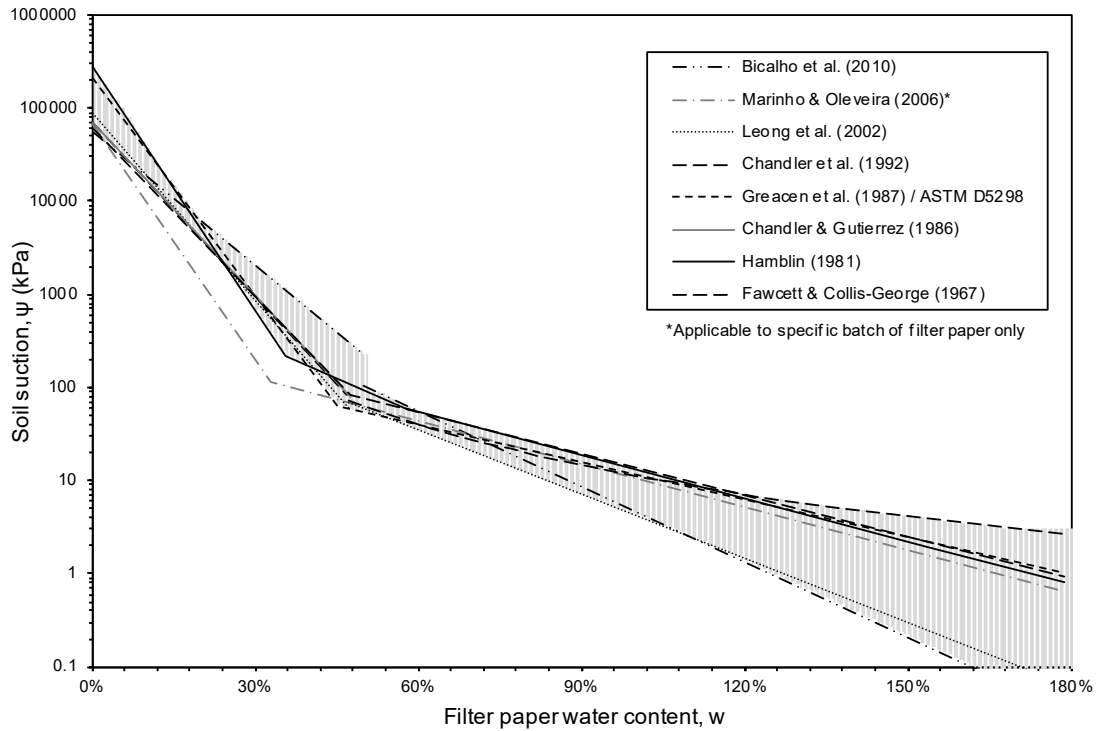


Figure 2-9 Calibration curve variability for *Whatman* No. 42 filter paper

2.3.2 Direct methods of soil suction measurement

Direct methods of soil suction measurement are termed such because they directly measure negative pore-water pressure. These instruments measure soil suction by the direct exchange of water between the instrument and the soil. Techniques like the tensiometer and pressure plate rely on the unique properties of high air-entry ceramic discs for the direct measurement of negative pore-water pressure (See section 2.4.1 on high air-entry materials). Direct measurement is preferred over indirect measurement since the measured suction is reflected more rapidly (Meilani *et al.*, 2002). Direct methods also hold the advantage of being able to measure both positive and negative pore-water pressures (Take & Bolton, 2002).

2.3.2.1 Tensiometers

Tensiometers are the simplest and most common instruments for measuring soil suction directly. In general, a tensiometer consists of a porous HAE ceramic connected to a pressure sensor through a small water reservoir. The ceramic is placed in contact with the soil where pore-water pressures need to be measured and is used to create a connection between the soil pore water, a water-filled reservoir and the pressure sensor (schematically shown in Figure 2-10). Pore-water pressures can be directly measured through the exchange of water between the pores of the soil and the pressure sensor (Lu & Likos, 2004). Pore water in tension will create equal tensile stress in the water of the reservoir that is measurable by the pressure sensor. The pressure sensor can be any device capable of reflecting the change in negative pressure.

Each device has its limitations and is restricted by its range. Tensiometers are applicable for use in the field and laboratory.

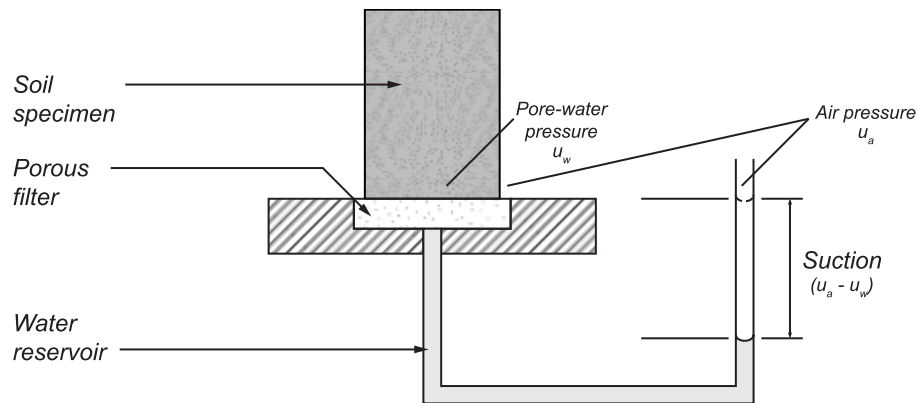


Figure 2-10 Simple tensiometer device (Ridley & Burland, 1993)

Standard tensiometers, commonly used in Agriculture, consist of a sensing probe containing the HAE ceramic connected through a plastic tube to the measurement device, usually a pressure gauge. The probe is placed in the soil where suction measurements are required, usually at depth, while the measurement system is located at the surface (Figure 2-11 (a)). The effect of gravitational potential must be compensated for in the suction reading, i.e. the difference in height between the point at which suction measurements are made and the pressure sensor.

These, along with other types of tensiometers such as the small-tip laboratory tensiometer (Figure 2-11 (b)), have a limited practical range of measurement in the order of 70 to 85 kPa of suction. The low range is due to the relatively low pressure at which cavitation occurs in water (about -1 atm or -100 kPa gauge pressure for pure free water at sea level). The presence of impurities in the pore water and concentrated in the minute crevices on the walls of the sensor body may act as air bubble nucleation sites, further lowering the cavitation pressure (Lu & Likos, 2004).

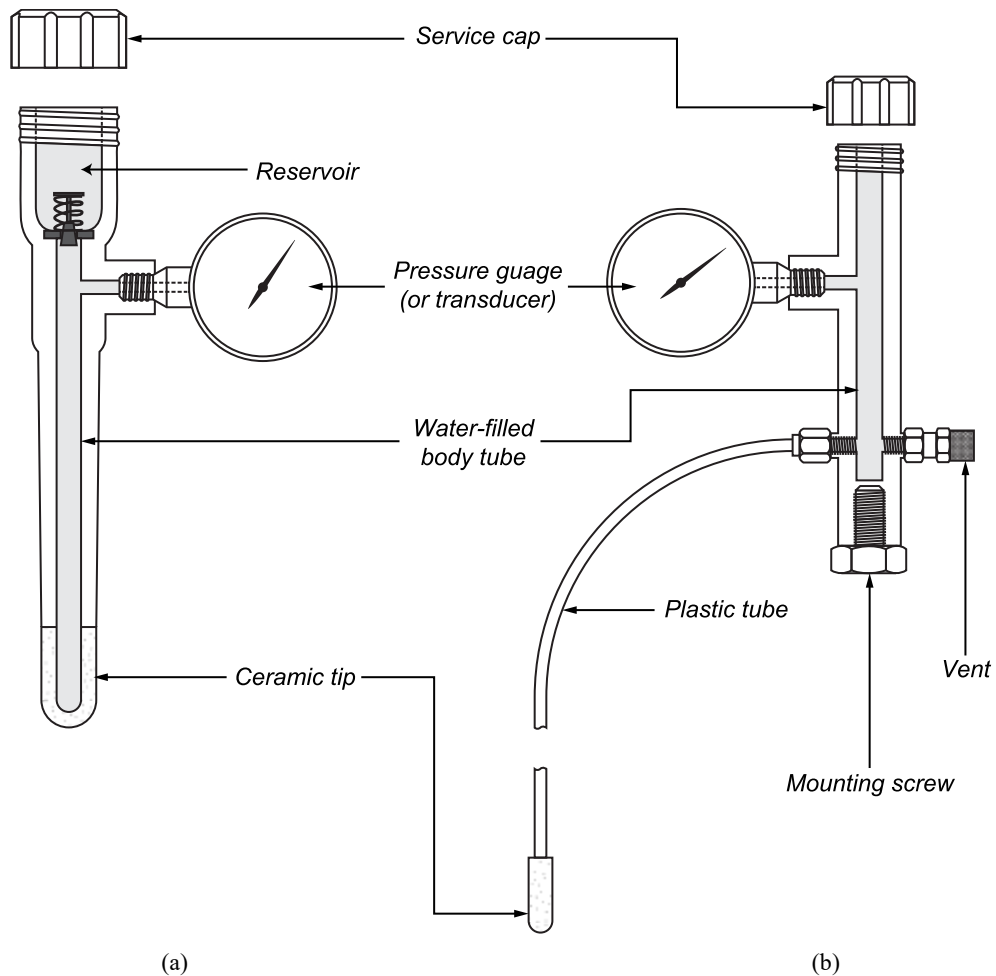


Figure 2-11 Conventional tensiometers:(a) Standard tensiometer; (b) small-tip laboratory tensiometer

The direct measurement of significantly higher soil suction (over 100 kPa) requires practically dealing with the cavitation phenomenon. Cavitation causes the expansion of air bubbles nucleated inside the measurement device, rendering it incapable of measuring further suctions accurately. Cavitation occurs when water reaches its vapour pressure in absolute tension (see section 2.1.3 on Cavitation).

2.3.2.2 Pressure plates

Pressure plates address the problem of cavitation by the axis translation technique, ensuring that pore water never reaches its vapour pressure in absolute tension by applying a high air pressure around the soil sample. The pore-water pressure is raised by the same amount as the applied air pressure and is thus always in the positive range, and measurable (Standing, 2012).

A pressure plate consists of a porous HAE ceramic disc contained in a pressure vessel. A soil sample is placed inside in contact with the ceramic. The air pressure inside the vessel can be regulated, and the suction is calculated with reference to the raised air pressure (schematically shown in Figure 2-12). Pressure plates are not applicable for use in the field owing to the

requirement of a contained raised air pressure. They also suffer from slow response times, and their accuracy is low in low suction range (100 – 1000 kPa) (Ridley & Burland, 1993).

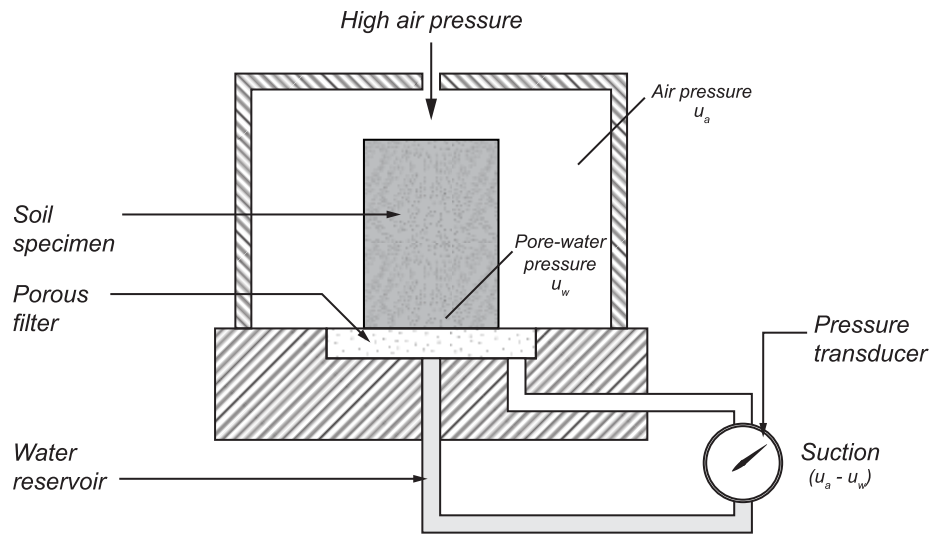


Figure 2-12 Simple pressure plate device (Ridley & Burland, 1993)

2.4 HIGH-CAPACITY TENSIO METERS

Alternative types of tensiometers, namely ‘high-capacity’ tensiometers (HCTs), have been the focus of more recent studies. These devices operate by reducing the potential for cavitation to occur in the measurement system and realise the full tensile strength of water. This is achieved by considerably reducing the dimensions of the water reservoir and the use of very high air-entry pressure ceramics (Lu & Likos, 2004). Devices such as the Imperial College (IC) tensiometer (Ridley & Burland, 1995), the University of Saskatchewan (SASK) tensiometer (Guan & Fredlund, 1997) and the Trento (TN) tensiometer (Tarantino & Mongiovì, 2003) have been developed and improved in reliability. These tensiometers have been specially developed for the advancement in the study of unsaturated soil behaviour.

The term ‘high-capacity tensiometer’ has the same meaning as ‘suction probe’ or ‘high suction tensiometer.’ Tensiometers of this type are often referred to as ‘suction probes’ because of their small size. Though the term ‘probe’ suggests the insertion of the device into a sample, they are also suitable for ‘contact’ or ‘on-sample’ suction measurement provided good contact can be maintained (Lourenço *et al.*, 2006).

Ridley and Burland (1993) showed that measuring substantially high suctions (up to 1500 kPa) using a commercial pressure transducer (*Entran Ltd EPX*), a high air-entry ceramic (15 bar AEV) and a small reservoir size (3 mm³) (Figure 2-13) is relatively easily achievable for a limited time. The response time for the instrument is reported to be a few minutes.

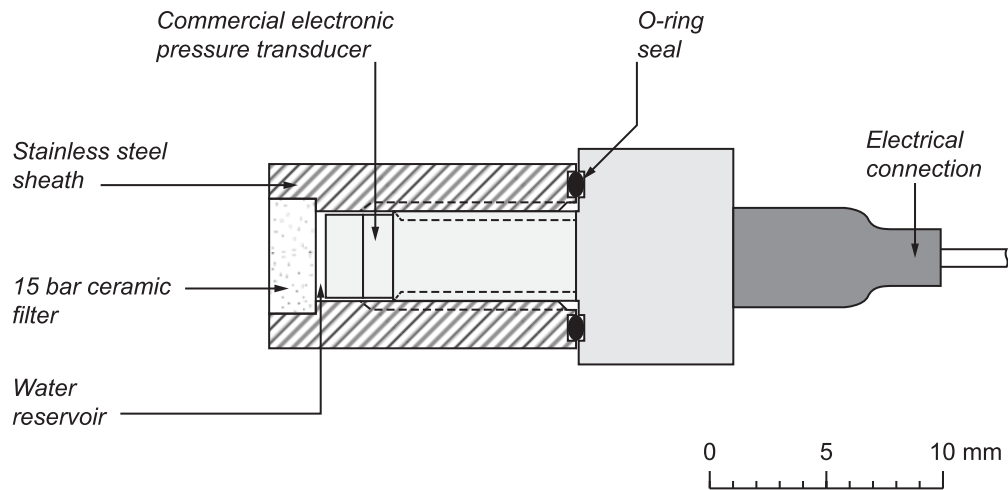


Figure 2-13 Simple high-capacity tensiometer (Ridley & Burland, 1993)

The advantages of HCTs are clear. They are exceptionally suited for use in geotechnical laboratories due to their small size, higher measurement range and rapid response times. Electronic signalling makes them suited for use in geotechnical centrifuge modelling and limits the need for operator intervention and sample disturbance. Long-term monitoring in field applications extends their use beyond laboratory studies.

2.4.1 High air-entry materials

High air-entry (HAE) materials are typically ceramics or special cellulose membranes which have microscopic pores of relatively uniform size and size distribution. HAE materials are unique in their ability to allow the free movement of water while restricting the movement of air through their pores if the pores are saturated with water (Lu & Likos, 2004). Once an HAE material is saturated with water, air cannot pass through it due to the surface tension maintained at the air-water interfaces in the material's pores resisting the flow of air. HAE materials can sustain a pressure difference between air and water on either side with the pressure difference being compensated by surface tension at the air-water interfaces. Surface tension then acts as a physical membrane separating air and water. This surface tension property of water makes the direct measurement of negative water pressures a possibility. The maximum pressure difference that can be maintained across the surface of the material is called the *air-entry value* (AEV) and is dependent on the connectivity and size of the largest pores (Fredlund & Rahardjo, 1993). The term 'high air-entry' refers to the requirement of a relatively high pressure necessary to break the surface tension maintained in the material's pores and for air to be forced through the material.

2.4.2 Operating principle

If the ceramic tip of a tensiometer (either standard or high-capacity) is held in good contact with the soil pores-space, the saturated pores of the ceramic provide a hydraulic connection between pore water and the measurement system (consisting of the saturated ceramic, water reservoir and pressure sensor). Water can flow to and from the measurement system, into or out of the soil pores, to achieve equilibrium. At equilibrium, the pressures in the measurement system and the pore water are equal. During drying of the soil, first capillary forces (or adsorption effects as suction increases) exert a tensile pull on the pore water and water in the saturated pores of the ceramic tip that draws water from the reservoir. The tensile stress of the reservoir water deforms the transducer's pressure sensing element. In this way, negative pressures can be measured. Inversely, during subsequent wetting of the soil, pore water is drawn from the soil into the measurement system until a new equilibrium is reached at a new pressure. The difference between the pore-air pressure and the water pressure across the porous ceramic tip is defined as the matric suction (Equation 2.4).

Tensiometers can measure suction provided the water in the reservoir of the measurement system remains connected to the pore water and free of air bubbles. It is therefore required that volume of the reservoir and the pores of the ceramic filter be completely filled with water. The range of matric suction that can be measured by a tensiometer is thus limited by the air-entry value of the porous ceramic tip, and the limit of negative pressure water can sustain without cavitation occurring.

Air bubbles may enter the measurement system by air diffusion, air-entry, or the cavitation occurrence. The diffusion of dissolved air through the pores of the ceramic tip may occur over time, concentrating air bubbles within the measurement system. At the air-entry pressure of the ceramic, air may be drawn into the measurement device. At very high negative pressures approaching the vapour pressure of water, minute air bubbles in either the water reservoir or the pores of the ceramic tip may cavitate and expand. The effect of cavitation in suction measurement systems is explained below.

2.4.3 Cavitation

The cavitation of water is a practical concern during the measurement of soil suction, particularly with the use of tensiometers. An understanding of the principles of cavitation is required for the provision of practical solutions to combat the occurrence.

2.4.3.1 Cavitation pressure

Under increasingly negative water pressure, cavitation may occur, breaking the continuity in the liquid phase between the measurement system and the pore water. After cavitation, measurement becomes unreliable due to the compressibility of air. Any further increase in negative pressure will cause the pore air of the ceramic or air bubbles formed in the water reservoir to expand making measurement problematic (Take & Bolton, 2003). Cavitation can occur when water pressure (u_w) approaches its vapour pressure (u_v). Measurement devices, such as tensiometers, measure pore-water pressures as a deficit with reference to the local atmospheric pressure or as the *negative gauge pressure*. The *cavitation pressure* for negative gauge instruments (u_g) is therefore the difference between the local atmospheric pressure (u_a) and the water vapour pressure (Equation 2.15) (Lu & Likos, 2004).

$$u_g = u_a - u_v \quad 2.15$$

Cavitation occurring in the measurement system is detected as a sudden increase in pressure, generally to the local atmospheric pressure.

Factors that can lower the cavitation pressure include elevation above sea level, temperature variations in the atmosphere and impurities in the water or on the ceramic and the walls of the tensiometer measurement system. Atmospheric pressure changes with elevation – at sea level hydrostatic atmospheric pressure will be the highest and lowers with an increase in elevation. Temperature variations alter the local vapour pressure (Figure 2-3). Impurities in the reservoir water and small crevices on the walls of the device create nucleation sites where vapour bubbles can form.

2.4.4 Tensiometer saturation

For a tensiometer to be able to measure suction, a continuous link between the pressure sensor and pore water is required. Therefore, the water reservoir must be completely filled with water, and the ceramic filter must be saturated to a high degree. The removal of all air in the measurement system also inhibits the expansion of cavitation nuclei and extends the measurable suction range. Tensiometer saturation is achieved by submerging dry filter elements in de-aired water and applying high positive water pressures.

2.4.4.1 Theoretical background

Take & Bolton (2003) have described the saturation of a porous ceramic using Boyle's Law and Henry's law of solubility in terms of absolute pressures (Equation 2.16).

$$\Delta P = P_i \frac{(S - S_i)(1 - H)}{1 - (1 - H)} \quad 2.16$$

or

$$\Delta P_{100} = 49P_i(1 - S_i) \quad 2.17$$

where:

- H = Henry's constant (approximately 0.02 ml air/ml water at 25 °C),
- ΔP = applied pressure increment,
- P_i = initial absolute pressure,
- S = degree of filter saturation, and
- S_i = initial degree of filter saturation

If the conditions of saturation are known (or controlled), the theoretical pressure required to saturate a ceramic filter fully can be predicted. A completely dry ceramic at atmospheric pressure (1 atm or 100 kPa absolute pressure) submerged in water would require subsequent theoretical pressurisation of 4.9 MPa to become fully saturated (Equation 2.17). From initial vacuum, however, full saturation of a completely dry ceramic may simply require recovery to atmospheric pressure after submergence. The required vacuum would then be only 2 kPa absolute (-98 kPa gauge pressure).

This revelation justifies the use of a two-stage saturation routine consisting of initial pressurisation under high vacuum and pre-pressurisation under high positive water pressure (Take & Bolton, 2003).

2.4.4.2 Practical tensiometer saturation

The theoretical prediction of the pressure required for achieving full saturation falls short in some ways. The influence of having a ceramic that is not initially dry ($S_i > 0$) is not reflected in Equation 2.17. For example, a prediction of half the pre-pressurisation pressure is made for ceramics with $S_i = 0.50$. In reality, it is some orders of magnitude more difficult to saturate a filter that is not completely dry initially. The theoretical explanation is that menisci in a partially saturated porous media may trap air bubbles within the pore space. This suggests that higher saturation pressure is required to account for the need to break surface tension effects (Take & Bolton, 2003).

The time required to achieve full saturation is also not reflected. The permeability of an HAE ceramic disc is extremely low, and the use of a combination of high vacuum, high positive pressure and cyclic positive and negative pressure applications may be required to reduce saturation time.

2.5 DEVELOPMENT OF HIGH-CAPACITY TENSIOMETERS

HCTs have been proven capable of measuring negative pore-water pressures below 100 kPa, but only briefly after a rigorous saturation programme and when unloading from high positive pressures. The first successful HCT was introduced by Ridley & Burland (1993) (Figure 2-13) who continued to advance the technology and was able to raise the range of matric suction measurement to about 1500 kPa. Since then the research area has advanced to produce the IC tensiometer (Figure 2-14 (a)) (Ridley & Burland, 1995), the SASK tensiometer (Figure 2-14 (b)) (Guan & Fredlund, 1997) and the TN tensiometer (Figure 2-14 (b)) (Tarantino & Mongiovi, 2003). These tensiometers were proven capable of measuring suctions in excess of 1500 kPa for more extended periods in a laboratory environment. Another notable tensiometer design includes the École des Ponts ParisTech (CERMES) tensiometer that was used successfully for in-situ suction measurement in France (Cui *et al.*, 2008).

Most of the tensiometers mentioned above use a stain-gauged diaphragm sensing element to register changes in pressure. These type of tensiometers may suffer from plastic deformation of the diaphragm material or hysteretic signal response at high-pressure measurement, non-linear signal response due to diaphragm curvature, loosening of the strain gauge glue with time, reducing the reliability of the instrument and sensitivity to minor temperature and stress effects (Tarantino & Mongiovi, 2003).

Take & Bolton (2002) offers the following desirable characteristics for the design of HCTs:

- the instrument's sensing element needs to be isolated from large deformations associated with high suctions stresses or total applied stresses,
- the pressure sensor needs to be water-tight under working pressure and under considerably higher water pressures used during saturation to prevent electrical interference or malfunction,
- a reliable seal around ceramic filter and sensing element is required to prevent a shortcut for air-entry around the periphery of the device,
- the instrument needs to be physically small to limit disturbance to the specimen or model being tested (for instance in centrifuge modelling or inside triaxial specimens),
- the required volume of water flow required to register suctions needs to be minimised for optimal response time, and
- the instrument should have a changeable filter element.

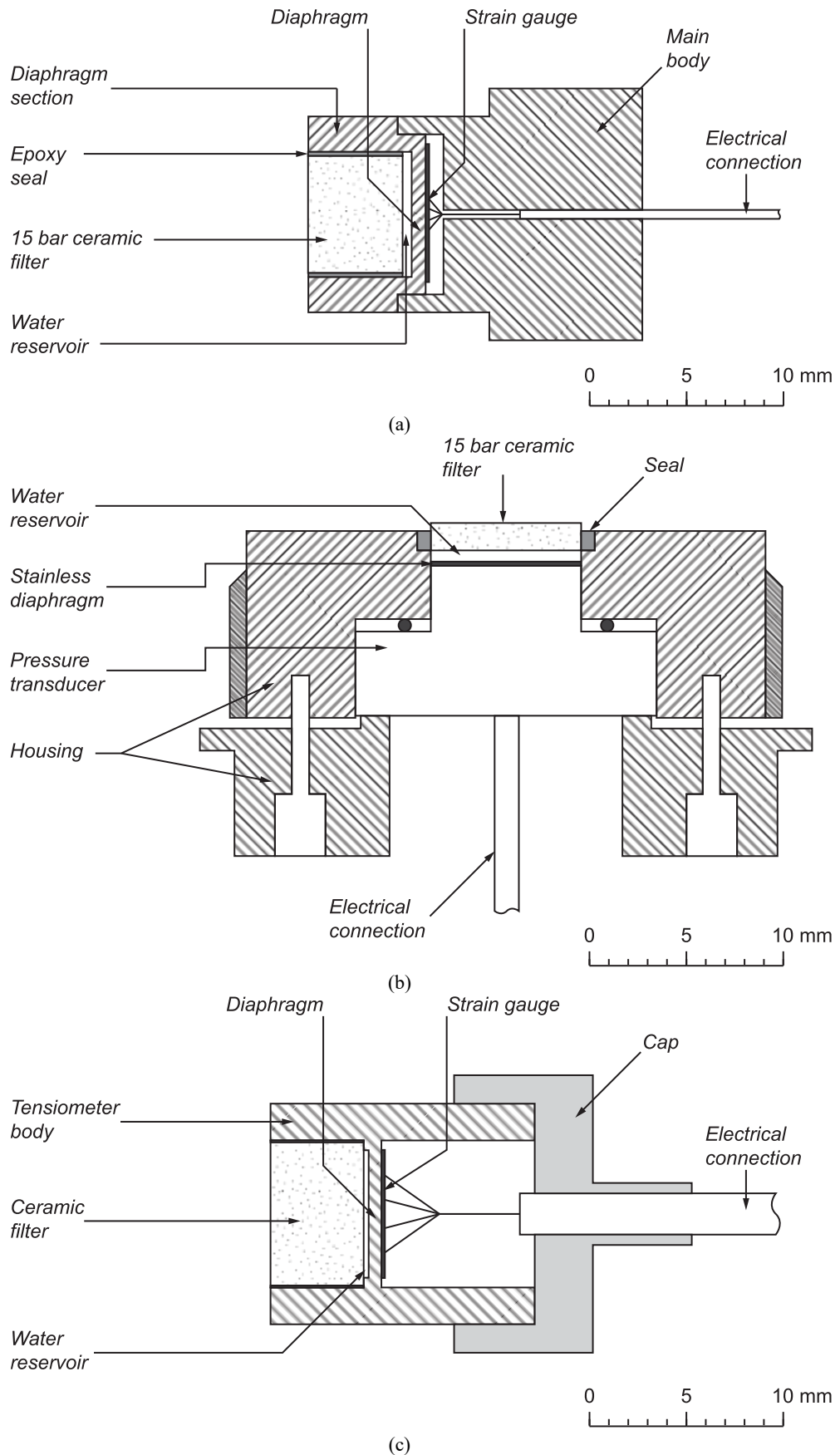


Figure 2-14 High-suction tensiometers: (a) Imperial college (IC) tensiometer; (b) University of Saskatchewan (SASK) tensiometer; (c) Trento (TN) tensiometer

The use of exceptionally small water reservoirs and relatively thick ceramics became commonplace and was proven to provide the best results for reliability and accuracy. A smaller reservoir is statistically less likely to suffer from unpredictable tension breakdowns (Take & Bolton, 2003). A small volume appears to inhibit the formation of air bubbles in the reservoir – thereby increasing the range of negative pressure measurement (Ridley & Burland, 1993). Overall performance of tensiometers has improved in terms of time to achieve de-airing, response time and reliability with the provision of the smallest possible reservoir volumes (Ridley & Burland, 1994).

The provision of an extremely small water reservoir then has clear benefits when considering the cavitation and crevice model. However, a reservoir can be made too small to where the tensiometer is not practically usable. A tensiometer exposed to air will start desaturation from the face of the ceramic filter tip. When the air-entry pressure of the ceramic is reached, cavitation may occur. The current consensus appears to be to strike a balance that suits the needs of the application.

Recent insights into the cavitation mechanisms in high capacity tensiometers have revealed that cavitation only occurs when air reaches the water reservoir through the ceramic filter. Consequently, the size of the water reservoir is not as crucial as the choice of HAE ceramic (Mendes & Buzzi, 2013).

The purpose of the porous filter element of a tensiometer is to enable high water tension to be maintained across its surface. Another vital function is to separate the pore-water pressure from the total stress applied to the face of the filter element (Take & Bolton, 2002). It should, therefore, be well sealed onto the water reservoir. Any shortcut path created on the edge of the ceramic will limit the suction to the air-entry of the gap created. Fredlund *et al.* (1998) suggested the requirements of the HAE ceramic or porous filter to be as follows:

- the pore size should be such that high water tension can be sustained without cavitation,
- it should be sufficiently durable to be handled without cracking or crumbling, and
- it should be robust enough to withstand in situ conditions.

Due to the unpredictability of certain ceramics and the early expense of pressure transducers, it became desirable to reuse elements when a tensiometer became unreliable, thus removable filter elements were introduced to the tensiometer designs. This idea has largely been dispensed with as the reliability of commercially available ceramics improved and parts became less expensive.

Free gas nuclei in water are generally unstable and tend to dissolve. Gas nuclei in the cavities of a contained surface are more stable and may remain undissolved even under high-pressure application (Tarantino & Mongiovi, 2001). Marinho & Chandler summarised the requirements that must be in place to limit cavitation occurrence (in Ridley and Burland (1994)):

- the water and all surfaces of within measurement system must be pure and clean,
- surfaces of the measurement system should be as smooth as possible to avoid or reduce the number and size of crevices as potential nucleation sites,
- the system should be evacuated to remove as much air as possible, and
- pre-pressurisation of the system is required to dissolve all free air.

The potential for cavitation occurring in the measurement system of a tensiometer can be limited by reducing the dimensions of the water reservoir and the use of high air-entry pressure ceramics. The operational procedures introduced by Take & Bolton (2003) may also reduce the potential for cavitation. Methods for dealing with the practical problem of cavitation including the assurance of a high degree of saturation, use of de-aired water, cyclical application of high and low positive pressures to dissolve entrained air bubbles and the application of a high vacuum prior to saturation are discussed in the next section.

2.5.1 Tensiometer saturation

Each of the tensiometer studies introduced proprietary ways of saturating the tensiometers. Ridley & Burland (1993) used an Imperial College high-pressure water pump (6000 kPa) to saturate the IC tensiometer fitted with a 15 bar AEV filter element. Take & Bolton (2002) saturated a 15 bar AEV filter element with 2000 kPa pressure, beyond the air-entry pressure of the ceramic filter. In cases where the solution of applying extremely high pressure to saturate tensiometers is not viable, for instance in smaller laboratories without high-pressure supplies or in field applications, the use of smaller range devices and more advanced saturation techniques become necessary.

Take & Bolton (2003) describe a two-stage saturation process to guarantee a high degree of saturation. The first stage, initial saturation, involves getting a completely dry filter element prior to saturation. They recommend a combination of oven drying at 60 °C and the application of a high vacuum in the absence of water. Both drying and the application of a high vacuum are intended to remove all traces of moisture or air from the ceramic and the water reservoir. The second stage, saturation (or pre-pressurisation), involves the application of high positive water pressure to force entrained air into solution. Pre-pressurisation was considered essential in saturating the IC, SASK and TN tensiometers.

Cyclical application of high and low positive water pressures has been shown to drastically reduce the time necessary to achieve a satisfactory degree of saturation. It is proposed that it helps to dissolve potential cavitation nuclei, although cavitation is not induced (Ridley & Burland, 1994). Guan *et al.* (1998) applied cycles of vacuum and high positive pressure from -85 kPa to pressures ranging from 1000 to 12000 kPa. The number of cycles predominated the saturation procedure and could last between 1 – 30 hours. Others such as Marinho *et al.*, (2008) and Pedrotti *et al.* (2014) have indicated that cyclic pressurisation is theoretically only beneficial if cavitation can be induced by the direct application of negative water pressure and cavities collapsed by subsequent application of extremely high pressure.

The response time of a tensiometer upon positive pressure application was found to be a clear indicator of the degree of saturation achieved (Take & Bolton, 2003). The quicker the response time observed, the higher the degree of saturation achieved.

2.5.2 Tensiometer calibration

If the response time of a tensiometer is satisfactory, calibration can be carried out by the stepwise application of positive water pressure. Ridley & Burland (1993) assumed Hooke's law for the stainless-steel diaphragm of the *Entran* transducer and extrapolated the positive pressure calibration linearly to the negative range. This extrapolation of the positive pressure calibration was shown to be acceptable and confirmed by Ridley & Burland (1993), Tarantino & Mongiovi (2003) and Lourenço *et al.* (2008) independently for diaphragm type tensiometers. This is usually achieved by the isotropic consolidation of clay specimen containing a tensiometer in a triaxial apparatus with controlled cell and backpressure. Releasing the cell pressure under undrained conditions includes a suction instantaneously equal to the effective stress of the specimen before unloading (Ridley & Burland, 1993).

2.6 DETERMINATION OF SOIL-WATER RETENTION CURVES BY EXPERIMENTAL METHODS

As discussed in Section 2.2.3.3, empirical methods can be used to estimate SWRCs indirectly. For greater accuracy, SWRCs can also be determined experimentally using various direct or indirect suction measurement techniques. Familiarity with the various methods for measuring soil suction is required for the explanation of these techniques and is discussed in Section 2.3. This section introduces the experimental approach to determining SWRCs.

2.6.1 Conventional methods

Conventionally, point measurements are taken (discrete sets of water content and soil suction measurements), and the empirical equations are applied to complete the form of the SWRC between these points. Each point on the SWRC is determined by testing different specimens taken from the same sample that are assumed to be identical. The methods for measuring suction are usually indirect methods such as the filter paper method which calculates the suction from relative humidity and does not provide high precision. Errors may be introduced due to the variations between samples and the low precision of suction measurements. Due to their nature, these conventional methods are often lengthy to perform and yield few data points with which to construct the SWRC (Toker *et al.*, 2004).

2.6.2 Continuous drying methods

More recently and due to the advancement of HCTs (Section 2.4), continuous drying methods have been introduced to measure continuous SWRCs with the tensiometer technique directly.

The MIT Technique (Toker *et al.*, 2004)

The MIT technique was introduced by Toker (2002) and Toker *et al.* (2004) as a rapid method for determining continuous SWRCs using a tensiometer and a digital laboratory balance. The technique involves the concurrent measurement of suction via an HCT and the corresponding decrease in mass of a specimen due to the evaporation of pore water under controlled conditions. The gravimetric soil-water content is then back-calculated from the mass measurements to construct the SWRC. The authors were able to theoretically measure suctions up to 1000 kPa with the MIT tensiometer and repeatably determine the SWRCs of various fine sand and uniform glass bead samples between the suction range of 0 – 100 kPa.

The test set-up for the MIT Technique is illustrated in Figure 2-15. It is a conceptually straightforward set-up that may be easily reproduced with the only specialised equipment required being the HCT.

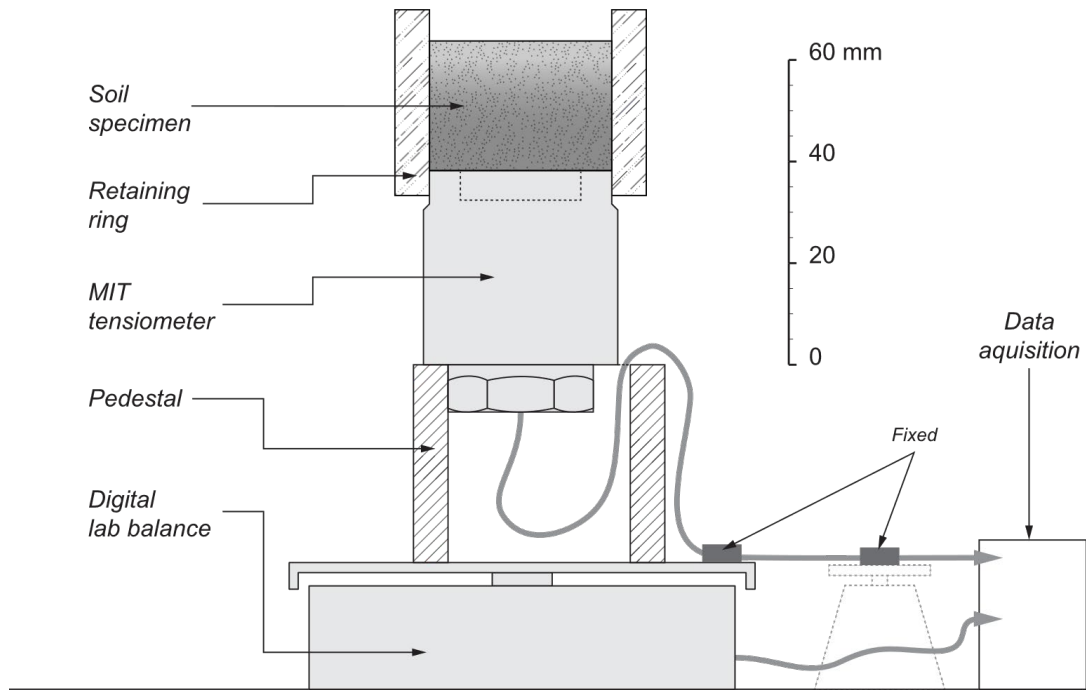


Figure 2-15 Test set-up for the MIT technique (Toker *et al.*, 2004)

The MIT tensiometer

The MIT tensiometer is similar to that of Ridley & Burland (1993) and is shown in Figure 2-16. The design is more substantial than a typical HCT with a diameter equal to the diameter of a standard triaxial test base (38 mm). It has a broad ceramic filter surface that is used as the base for a specimen container that allows for the contact measurement of matric suction.

As with most studies surrounding HCTs, the MIT tensiometer was developed as part of focused research at the university but did not deviate in principle from the first HCT developed by Ridley & Burland (1993). However, the MIT tensiometer used a proprietary ceramic that is not commercially available and prone to fatigue and damage which limited the results.

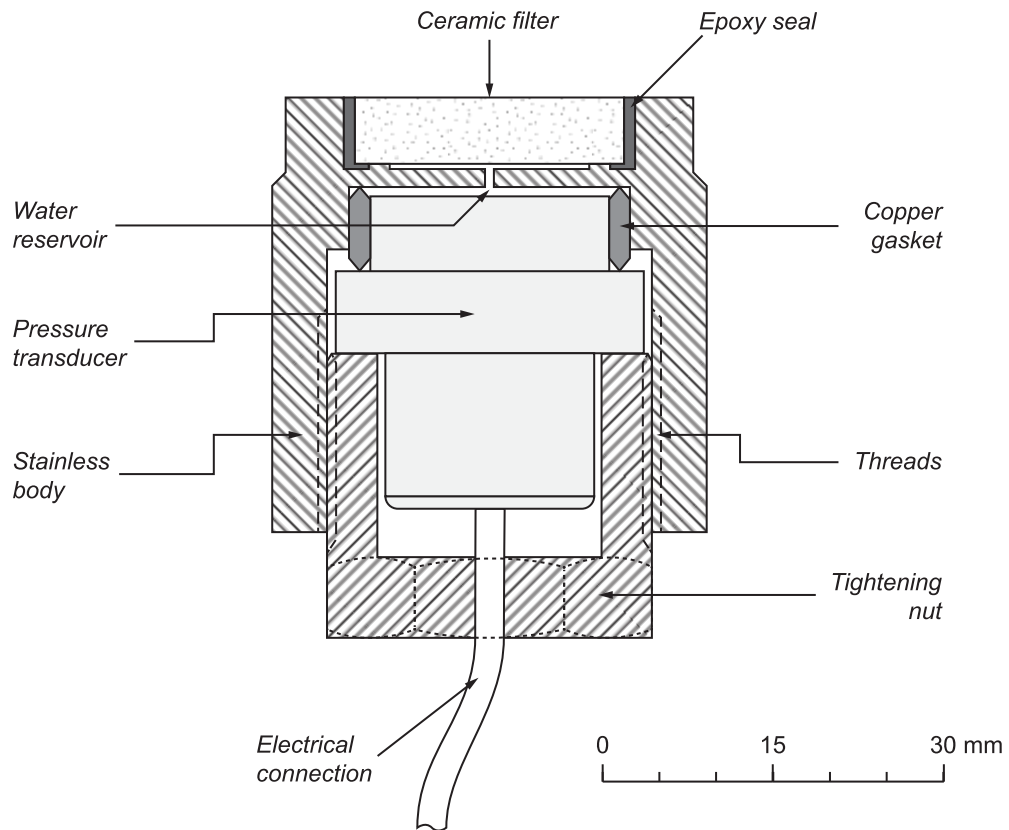


Figure 2-16 MIT tensiometer (Toker, 2002)

Discussion

The MIT technique holds clear advantages over traditional methods of determining SWRCs. The entire SWRC is produced from one specimen, which reduces operator time and variability in measurements due to specimen preparation. Once the test is started, little operator intervention is required. The continuous curves produced by the technique may include features that conventional methods might miss, such as the saturated water content and exact air-entry pressure. The technique also uses a tensiometer, the only device capable of measuring matric soil suction directly. The technique simulates natural soil suction development for the primary drying regime by evaporation. Furthermore and arguably the most significant advantage is that the technique is faster than conventional methods, allowing a nearly complete SWRC to be determined in 3 to 5 days, including specimen preparation, compared to a typical time of 7 days for a single point to be determined conventionally (Toker *et al.*, 2004).

Most of the drawbacks of the technique the authors propose are practical concerns such as the error induced from the mass and flex of the electrical signal cable, the thermal influence of the tensiometer during operation and ensuring good contact between the specimen and the ceramic filter. Another concern is the relatively large sample dimensions calling into question the equal distribution of moisture in the specimen, and thus a possible misreporting of the average suction pressure.

However, the most notable limitation of the study is on the type of soil tested. The ideal samples of fine sand and uniform glass beads do not necessarily represent common problem soils. Specifically, these samples do not exhibit any shrinkage or swelling behaviour. However, the authors suggest that a breakthrough in unsaturated soil mechanics would be reached if dimensional change measurement can be introduced to the technique to provide insight into the relationship between soil suction and swelling and shrinking behaviour (Toker, 2002).

Further studies

Since the introduction of the continuous drying method, other researchers have successfully created their own procedure, usually using their own proprietary tensiometer design. These studies are presented by Lourenço *et al.* (2011), Toll *et al.* (2013) and Qingtian & Standing (2014).

3 TENSIO METER DEVELOPMENT

The experimental procedures undertaken in this study were divided into two focus areas. The first focus area was on the development of a tensiometer for the measurement of soil suction in a typical laboratory environment. In this chapter, the design, construction and operation of a new tensiometer are described. The second focus area was on determining SWRCs using such a tensiometer and is described in Chapter 4.

3.1 TENSIO METER DEVELOPMENT

As discussed in Chapter 2, a typical HCT comprises of three essential elements. A high air-entry porous filter, a pressure transducer and an external housing that forms the assembly of a tensiometer. Each of these three elements combined with an electrical signal connection is present in all modern HCT designs (e.g. Ridley & Burland (1995), Guan & Fredlund (1997) and Tarantino & Mongiovi (2003)).

Take & Bolton (2003) have debated for the need for more sensitive, lower-pressure-range devices that can reliably measure soil suction. However, the majority of previous tensiometer studies place a significant emphasis on the measurement of very high suctions between 1 and 2 MPa, often providing solutions that are expensive or unnecessarily complex for widespread implementation. The design of the tensiometer in this study was therefore focused on reliability, simplicity and cost-effectiveness rather than achieving extremely high suction measurement. As such, the target range of suction measurement was set between 0 and 500 kPa, although the measurement of higher suctions was also attempted.

3.1.1 Tensiometer design

The design of the new HCT tensiometer consisted of an HAE ceramic disc and pre-manufactured pressure sensor adhered together. The gap between the ceramic tip and the pressure sensor formed the water reservoir. A structural epoxy was used to bond the components together, form the external body and seal the instrument from moisture. A flexible multi-core connection cable carried the signal from the pressure sensor to a data acquisition system. Each of these elements is discussed in further detail later. The simple design eliminated the need for a machined external housing while isolating the pressure sensor from externally applied forces. Figure 3-1 shows a cross-section of the design.

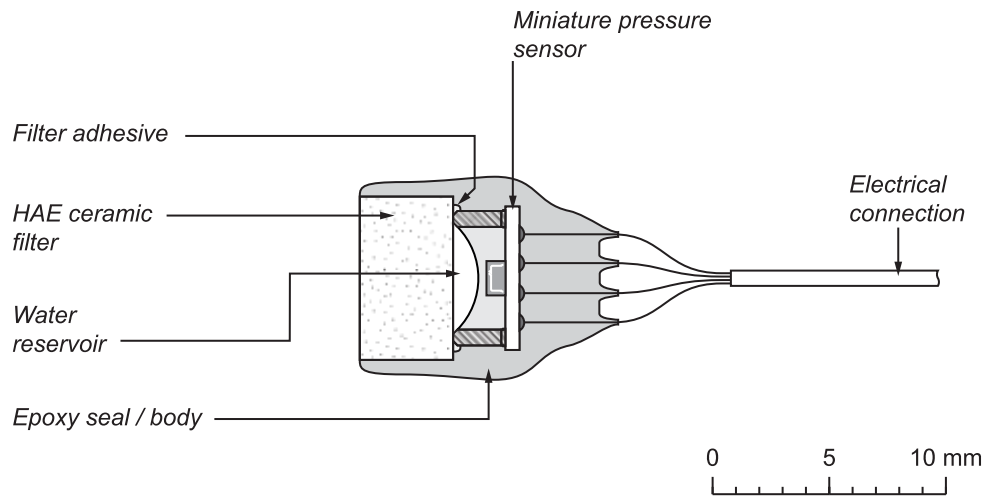


Figure 3-1 Design of the new tensiometer

During the study, many prototype tensiometers were produced and tested in different materials and test set-ups. Two configurations were used for the prototype tensiometers. The filter element was made to be either front-facing or side-facing. The orientation of the tip of the tensiometer depended on how test specimens were prepared, and the choice could help reduce the influence of the electrical connection cables on a sample. The four cores of the cable connection could also be either exposed to provide a flexible connection or shielded for the longevity of the device. Figure 3-2 shows the side-facing tip of the tensiometer with an insulated cable connection.

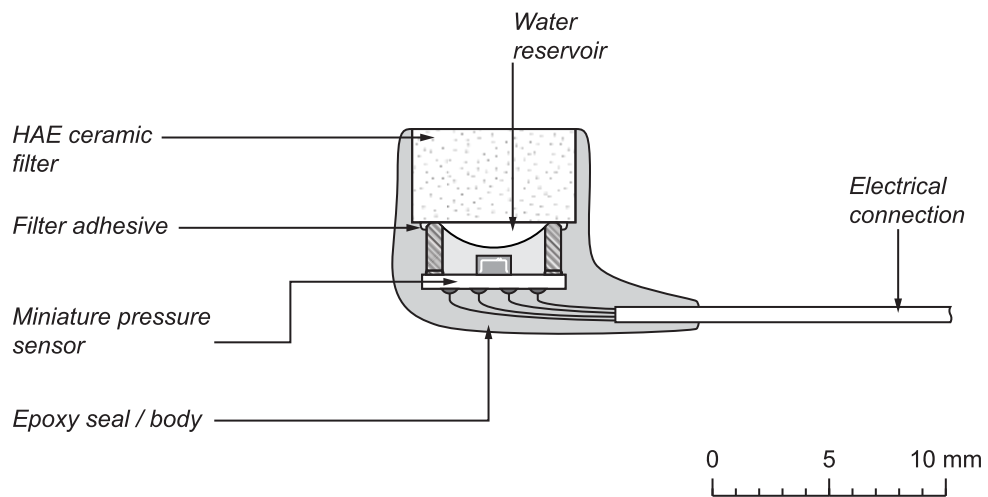


Figure 3-2 Alternative configuration of the new tensiometer

As a summary from Chapter 2, the measurement capacity of any tensiometer device is limited by the following:

- the capacity (full-scale pressure) of the pressure measurement device,
- the air-entry pressure of the filter element, and

- the quality of saturation achieved prior to suction measurement.

The components and methods needed to be appropriately selected or developed for the tensiometer to function effectively. Each of the materials and components of the tensiometer design is discussed in turn below.

3.1.1.1 Pressure sensor

The pressure transducer used in the design of the tensiometer was a miniature pressure sensor from *Measurement Specialties*, which is currently known as *TE Connectivity*. The sensors were readily available commercially and relatively inexpensive. The SMD (surface mounted device) sensor comprises a micromachined piezoresistive silicon sensing element mounted on a ceramic carrier (Figure 3-3). Pre-soldered contact pads provide an electrical connection that forms a Wheatstone bridge electrical circuit. A metal cap protects the sensing element from damage and isolates it from the influence of stresses applied to the body of the sensor. A layer of gel surrounds the sensing element and protects it from environmental contact (Measurement Specialties, 2012), (TE Connectivity, 2018). The details and dimensions of the pressure sensor are shown in Figure 3-4.

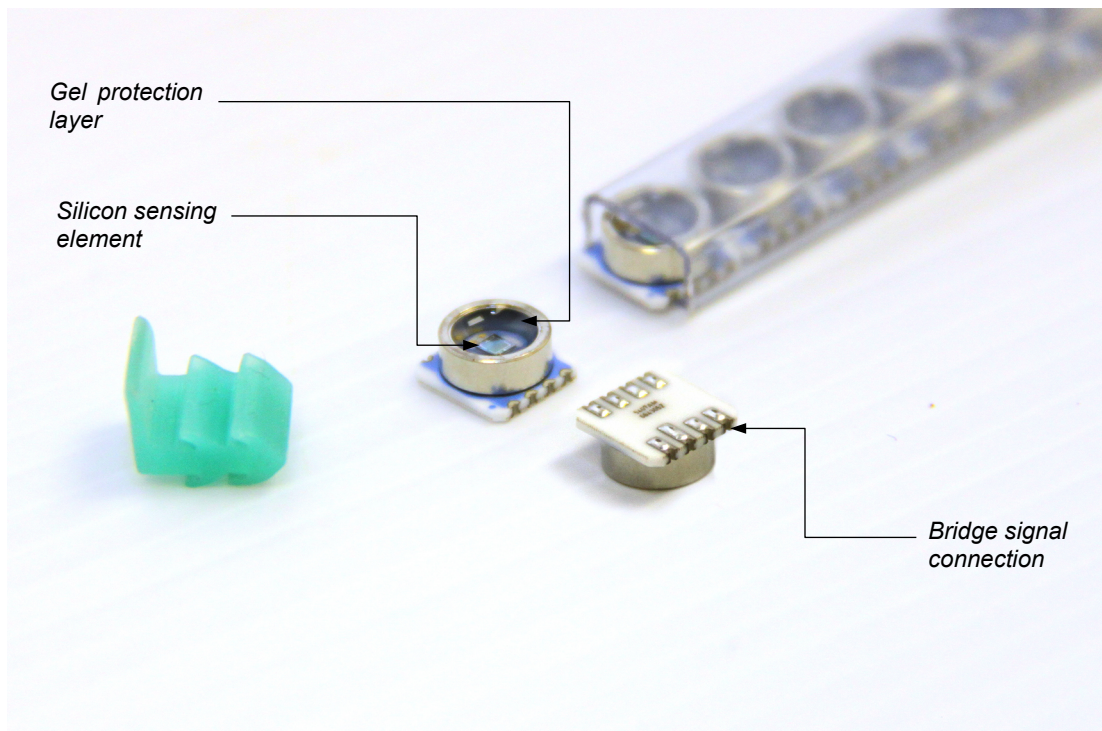


Figure 3-3 “MS4XX” range miniature pressure sensors

Two iterations of the pressure sensor were used. The majority of tensiometers produced incorporated an MS5407-AM ‘high sensitivity’ sensor with a full-scale pressure of 7 bar absolute and a maximum over-range pressure of 21 bar. Additional tensiometers that

incorporated an MS5412-BM ‘high linearity’ sensor with a full-scale pressure of 12 bar and a maximum over-range pressure of 30 bar were used for the measurement of high suctions. Details and dimensions of the pressure sensor are shown in Figure 3-4. Technical specifications for the “MS54XX” range of pressure sensors are provided in Appendix B.

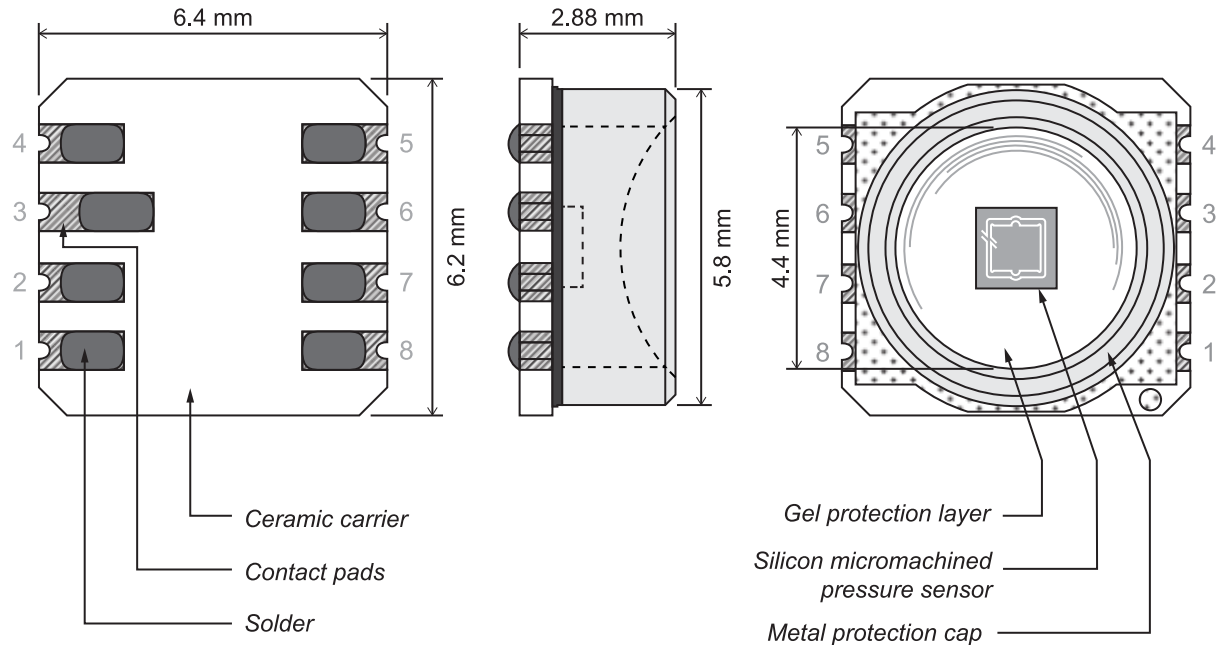


Figure 3-4 Detail of “MS54XX” range miniature pressure sensor

The advantages of the choice of sensors are:

- The sensing element is laser-machined to extremely narrow tolerances, which limits variability between sensors.
- The silicon sensing element also experiences very small strains under pressure, which extends the working life of the sensor.

Therefore, the use of the piezoresistive sensor would appear to be preferable over that of a strain-gauged diaphragm type sensor, which can be prone to fatigue damage.

3.1.1.2 High air-entry porous ceramic

The design of the tensiometer incorporated a small HAE ceramic filter taken from a porous ceramic plate supplied by *Soilmoisture Equipment Corporation*. The ceramic was supplied as 7.14 mm thick plates, either 79.4 mm (3.125 inches) or 104.8 mm (4.125 inches) in diameter (Soilmoisture Equipment Corporation, 2000). Ceramics with nominal AEVs of 0.5, 1, 2, 3, 5 and 15 bar were used. Cores were drilled from a single ceramic plate to make multiple filter elements. Figure 3-5 shows a typical 5 bar AEV ceramic plate.

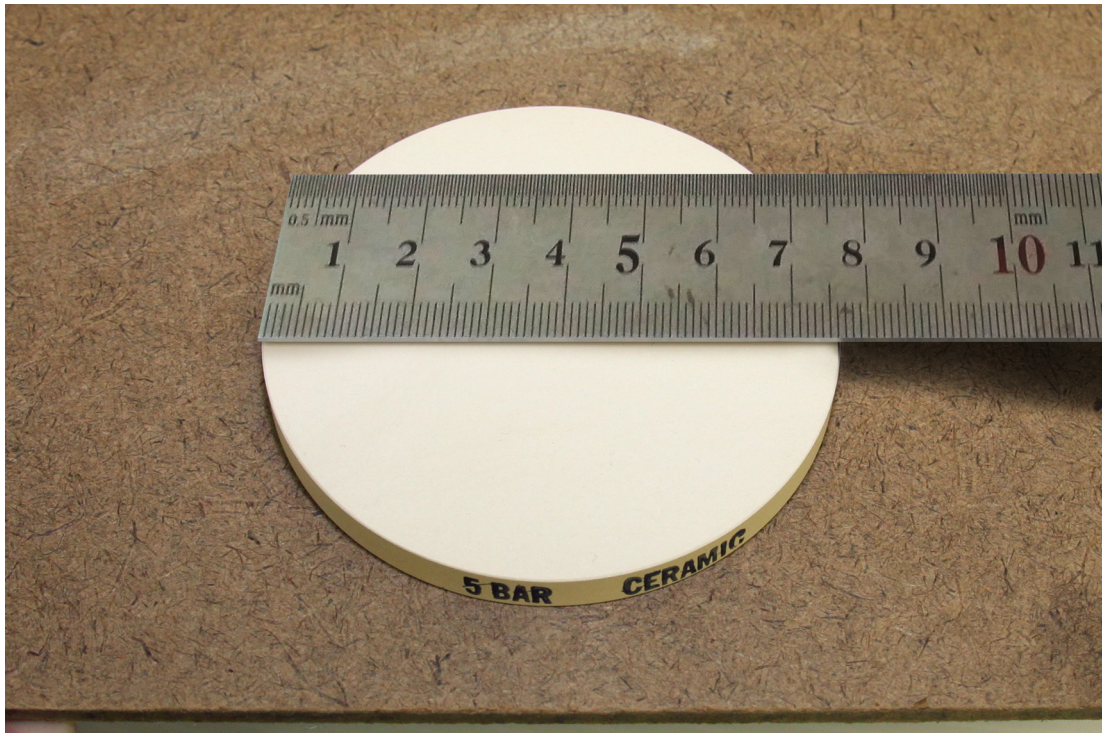


Figure 3-5 High air-entry ceramic plate

Typical properties of the ceramics are provided in Table 3-1. Higher variability in the typical air-entry pressure can be seen in the lower air-entry value ceramics, primarily due to variability in the ceramic manufacturing and firing process. However, the higher air-entry value ceramics perform more predictably. This fact was also experimentally observed when testing the AEVs of the ceramics.

Table 3-1 Properties of HAE ceramics as provided by Soilmoisture Equipment Corporation (Soilmoisture Equipment Corporation, 2000)

Nominal air-entry value (bar)	Typical air-entry pressure			Effective pore size (μm)	Hydraulic conductivity (cm/s)	Approximate porosity (% by vol.)	Typical density (g/cm^3)
	low	average	high				
0.5	83	248	414	6	3.11×10^{-5}	50 %	1.51
1	138	172	207	1.7	7.56×10^{-7}	34 %	1.78
2	262	286	310	1.1	6.30×10^{-7}	32 %	1.66
3	317	400	483	0.7	2.50×10^{-7}	34 %	1.73
5	-	552	-	0.5	1.21×10^{-7}	31 %	1.73
15	-	1517	-	0.16	2.59×10^{-9}	32 %	2.29

3.1.1.3 Water reservoir

The water reservoir of the tensiometer was formed in the space between the ceramic filter and the gel protection layer. As Mendes & Buzzi (2013) have illustrated, the size of the water reservoir does not affect the cavitation pressure or, consequently, the measurement capacity of

an HCT. However, it is desirable to keep the dimensions of the reservoir to a minimum, and in so doing reducing the probability of the occurrence of surface impurities initiating cavitation prematurely (Ridley & Burland (1994), Marinho & Chandler (1995) and Guan *et al.* (1998)). The water reservoir could vary in size depending on the thickness of the gel layer inside the pressure sensor but was estimated to be in the order of 8 mm³ based on the geometry of the device and curvature of a typical gel layer.

3.1.1.4 Structural epoxy

Structural epoxies have been used in HCTs in prior research, both to adhere elements together and to seal components from moisture (Cook & Fredlund (1998), Take & Bolton (2002), Meilani *et al.* (2002), Toker *et al.* (2004), Chui *et al.* (2005) and Beddoe *et al.* (2010)). The new tensiometer design used a structural epoxy to bond the filter element to the pressure sensor, seal the electrical circuit and act as the body of the instrument. The structural epoxy does not influence the measurement capabilities, but rather the durability of the tensiometer. Therefore, the requirements for the structural epoxy were:

- high bond strength,
- high structural strength,
- electrical isolating properties, and
- resistance to water absorption and chemical degradation.

The following candidates were considered:

- *Araldite* Standard two-component epoxy,
- *Loctite Hysol 3450* two-component epoxy,
- *Loctite Hysol 9644* two-component epoxy,
- *Loon Outdoors UV Knot Sense* ultraviolet light-cured epoxy,
- *Pratley Clear Quickset* two-component epoxy, and
- *Pratley Steel Quickset* two-component epoxy.

The final selection of the appropriate epoxy was made based on an experiment evaluating the resistance of the candidate epoxies to water absorption. The epoxy with the lowest water absorption was considered to be the most durable. The procedure is described below.

Water absorption test

The design of the test was formulated to consider the exposed surface area of the epoxy by making each sample to have close to the same surface area. Three small discs of each candidate epoxy were made to have approximately the same surface area (Figure 3-6 shows three

candidate samples). When the epoxies had cured, the initial mass of each disc was determined using a *Mettler* B5 precision balance.



Figure 3-6 Structural epoxy samples for water absorption test

The discs were then placed in a container of water (approximately 75 mm in diameter with a water level of 125 mm) to absorb water over time. After selected intervals of time, the discs were removed from the water, wiped dry with paper towelling, weighed, and placed back in the container.

After a record of the water absorption had been recorded, the discs were placed in an oven at 60 °C for 48 hours to dry. The water absorption was tested once more using the same discs. The water absorption of the epoxy (expressed as a percentage) was then calculated as in Equations 3.1 and 3.2:

$$wa_{i,t} = \frac{m_{i,t} - m_{i,0}}{m_{i,0}} \quad 3.1$$

$$wa_t = \frac{\sum_i^n wa_{t,i}}{n} \quad 3.2$$

where:

- wa_t = water absorption at time, t ,
- $m_{i,t}$ = wet mass after time, t ,
- $m_{i,0}$ = initial dry mass of specimen number i ,
- n = number of specimens, and
- i = 1, 2, ..., n

Results

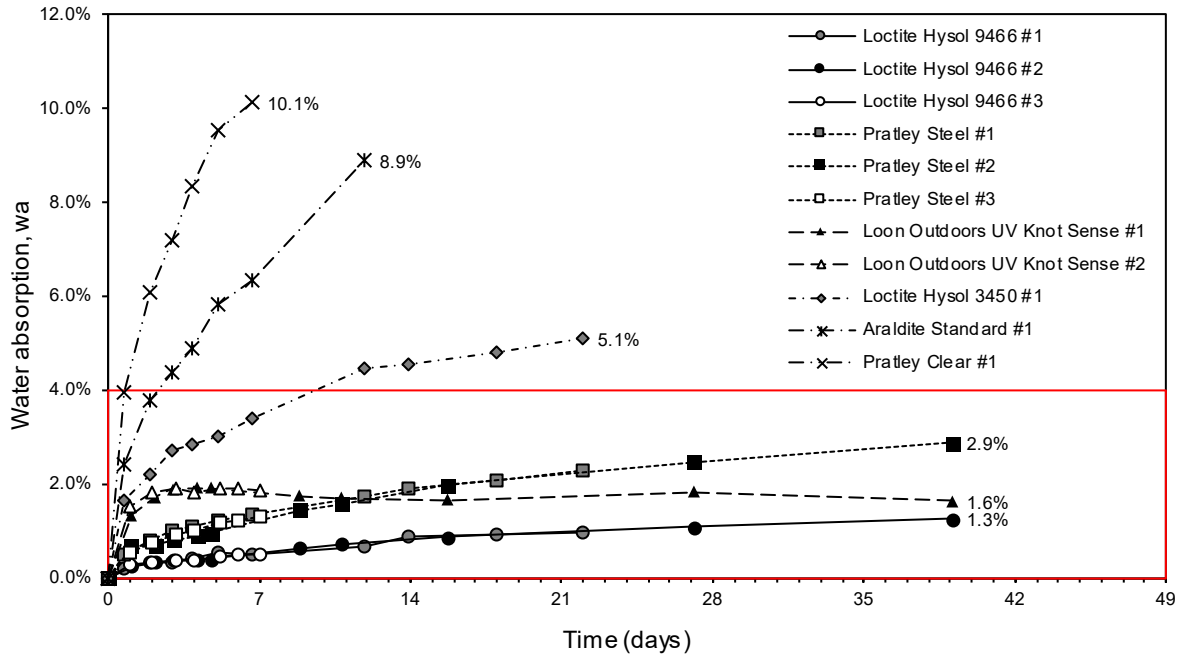
The water absorption of the epoxies is shown below (Figure 3-7 (a)). The three worst performers were excluded from further testing, and the three best performers were tested as described above (Figure 3-7 (b)).

The *Araldite* Standard, *Loctite Hysol 3450* and *Pratley Clear* all showed high levels of water absorption and softening at an early stage and were thus discounted as being viable.

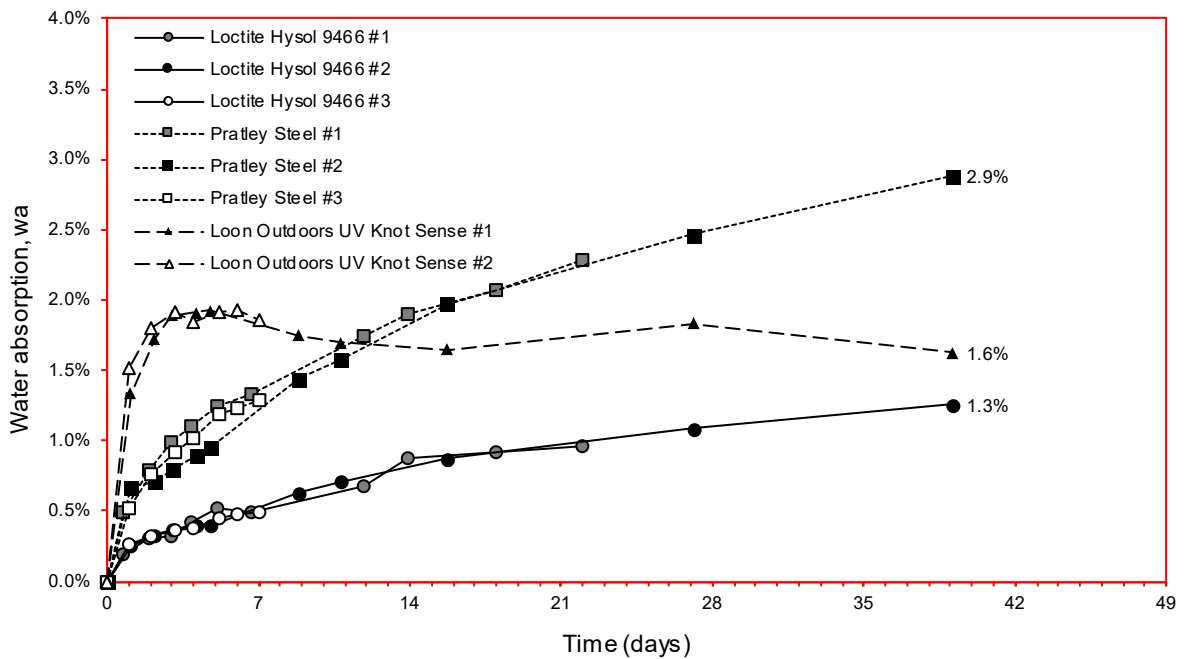
The *Loon Outdoors* UV Knot Sense epoxy appeared to have achieved ultimate saturation at around 1.8 %. However, a physical inspection of the discs showed a significant degree of softening early on and therefore proved to be unsuitable.

The clear choice of epoxy was shown to be the *Loctite Hysol 9466*, having the lowest water absorption in the short and long term. Hysol 9466 is a two-component industrial grade epoxy intended for applications that require extended work-life. Hysol 9466 reportedly provides excellent bond strength, electrical resistance and resistance to chemicals and solvents. It was, however, a relatively expensive option.

Pratley Steel Quickset was a less expensive option and is commonplace in most hardware stores in South Africa. It also performed well and showed no signs of softening, although it had a higher water absorption in the long term, which may indicate degradation over time with prolonged use.



(a)



(b)

Figure 3-7 Water absorption of structural epoxies

3.1.1.5 Electrical connection leads

As with the structural epoxy, the electrical wiring does not influence the measurement capabilities, but rather the durability of the tensiometer. Therefore, the requirements for the electrical cable were:

- to be electrically insulated and shielded,

- low electrical resistance,
- high durability,
- high heat resistance,
- high flexibility, and
- high resistance to shearing.

A four-core insulated computer interface cable was selected based on the properties listed above. The cable carries a voltage rating of 300 V and a temperature resistance up to 80 °C. The four-cores of the cable were also stranded (as opposed to being solid), which provides a more flexible and durable connection. Figure 3-8 shows the cable both shielded (Figure 3-8 (a)) and exposed (Figure 3-8 (c)) as discussed in 3.1.1.

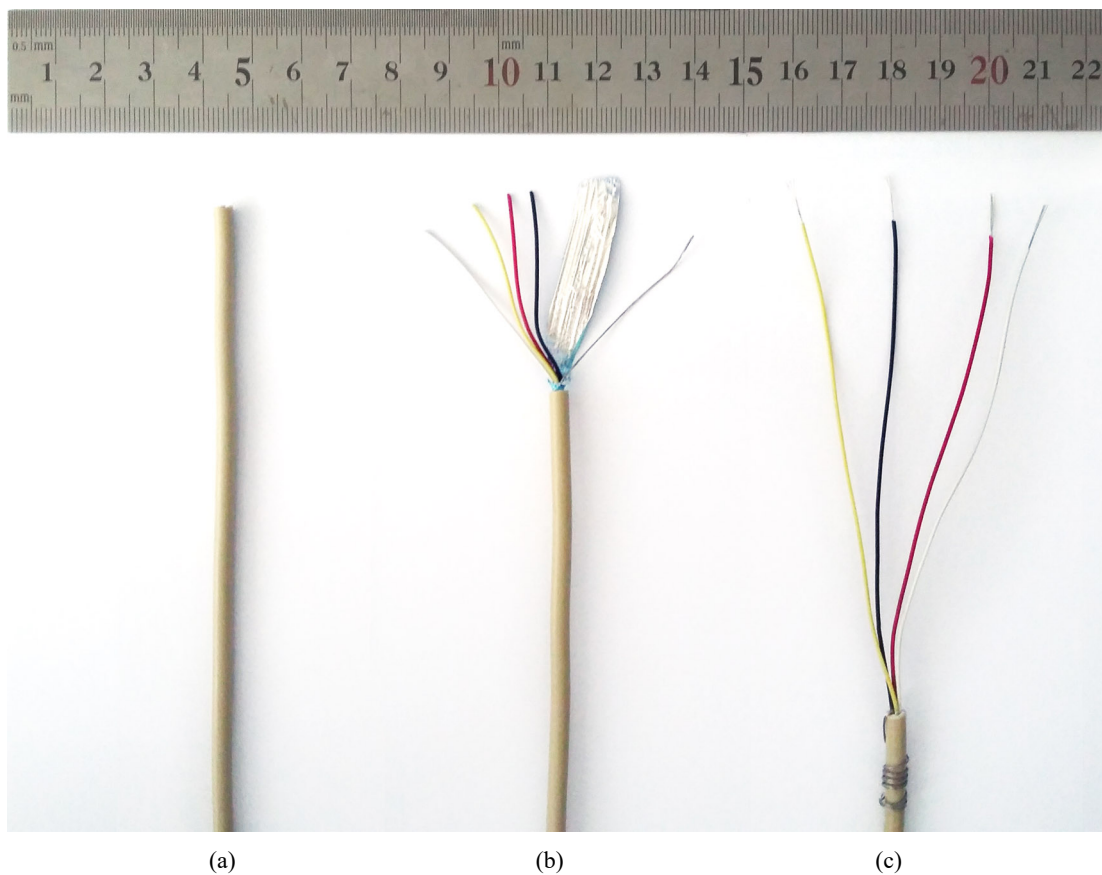


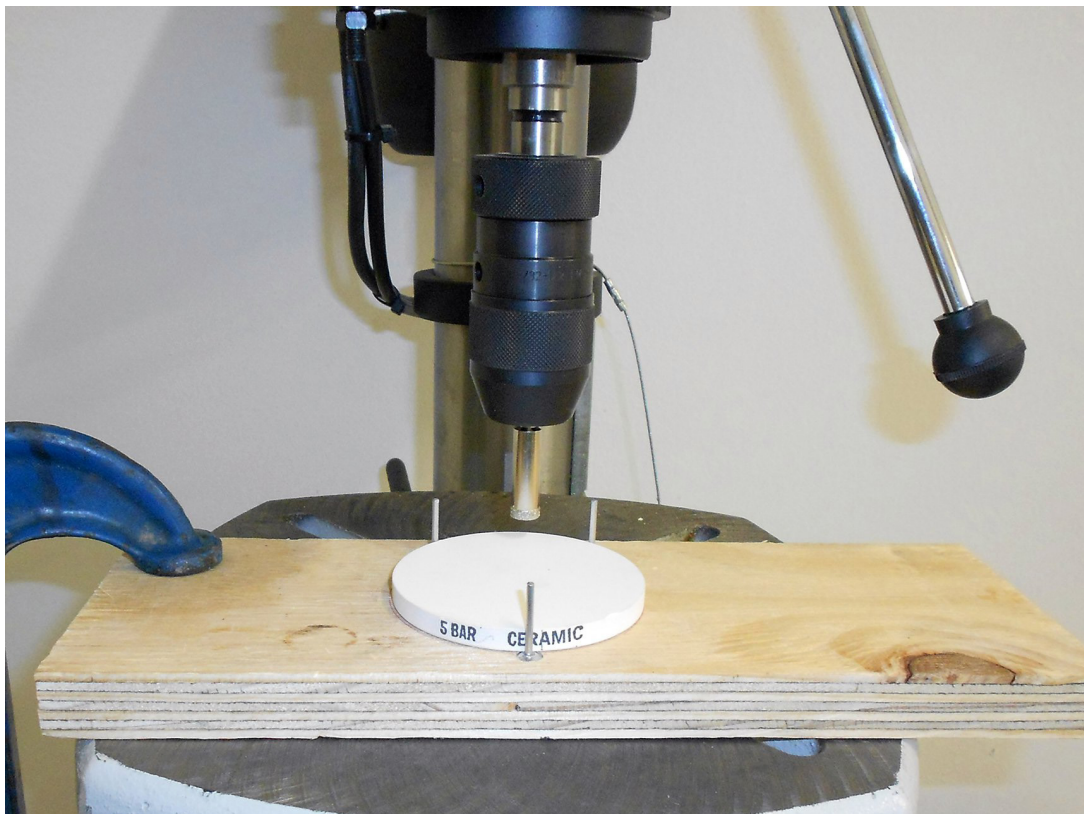
Figure 3-8 Electrical connection cable: (a) shielded; (b) stripped; and (c) exposed

3.1.2 Tensiometer assembly

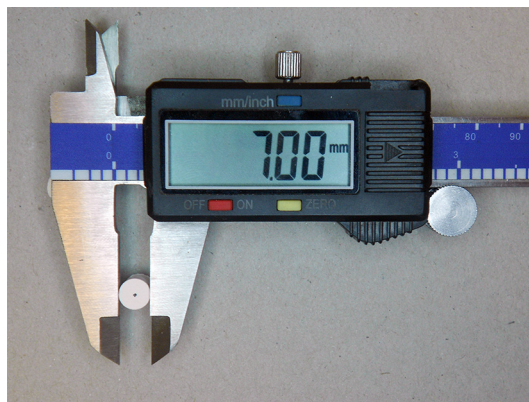
The tensiometers were assembled by hand and required a fair degree of dexterity. However, no complex machining or tooling was required. Through the assembly, steps were taken to minimise the risk of contamination of the surface of the ceramic filter and the protective gel layer of the pressure sensor. The assembly process is described below.

3.1.2.1 Cutting the ceramic filter element

The ceramic filter element was cored from a larger HAE ceramic plate using an 8 mm diamond tip coring bit and a benchtop drill press. The ceramic plate was held steady in a jig with three prongs mounted on a wooden base (Figure 3-9 (a)). The core was produced by slowly advancing the press downward in small increments. Water fed through a pipette was used to cool the coring bit and aid the coring process. Between increments of drilling, water and dust produced by the coring process were wiped or flushed away. The cored ceramic disc had dimensions of 7.00 mm diameter (Figure 3-9 (b)) and 7.14 mm height (Figure 3-9 (c)).



(a)



(b)



(c)

Figure 3-9 Coring of ceramic filter: (a) coring jig; (b) filter diameter; (c) height after coring

The surface texture of a typical 5 bar AEV ceramic plate as supplied by the manufacturer is shown in Figure 3-10. Imperfections from the manufacturing or coring processes on the inner surface of the ceramic (facing the tensiometer reservoir) may act as nucleation sites (crevices) for cavitation. To limit the number of imperfections and attempt to prevent premature cavitation inside the water reservoir, the surface of the ceramic was gradually smoothed and then polished on a sandblasted glass surface before attaching it to the pressure sensor.

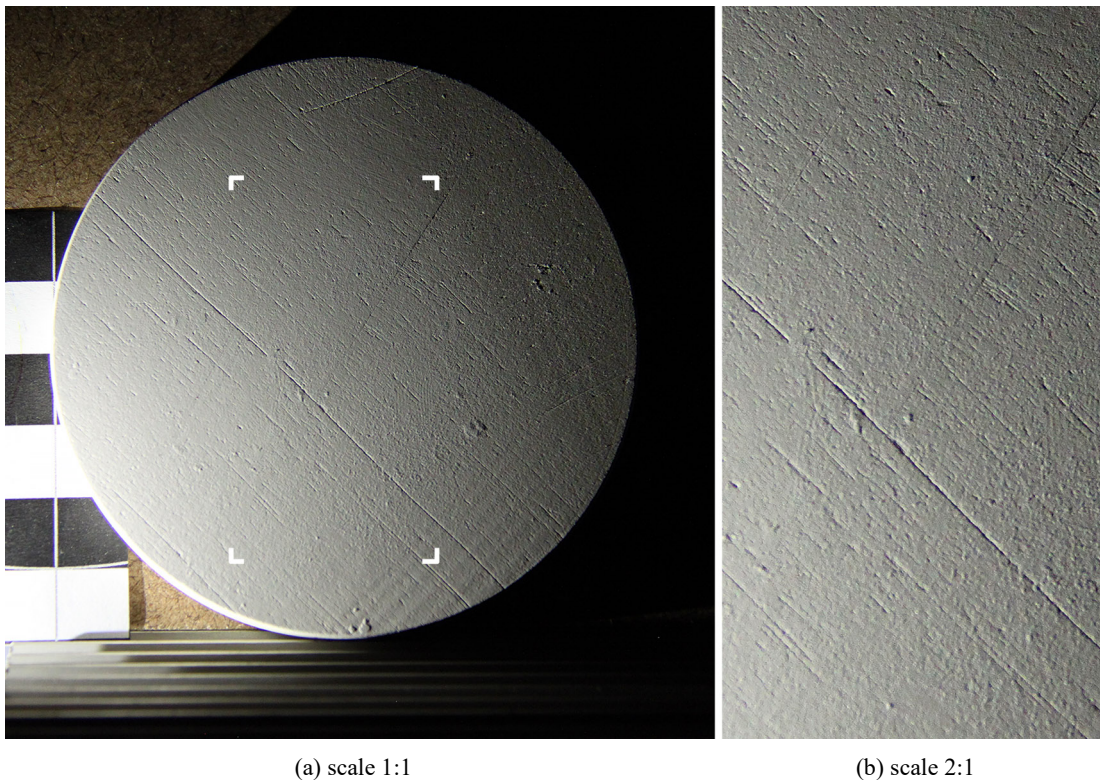


Figure 3-10 Surface texture of 5 bar HAE ceramic plate: (a) full view; (b) enlarged view

One side of the ceramic was selected to act as the inner face of the reservoir. The ceramic was reduced in height using progressively finer metallic files and sanding paper, only taking off material from the opposite side (Figure 3-11 (a)). Both surfaces of the ceramic were then polished on the roughened rim of a flat sandblasted glass plate. The glass plate was taken from a small dry seal vacuum storage container (better known as a desiccator). The face of the ceramic was polished using a circular motion following the perimeter of the plate (Figure 3-11 (b)). The flat glass surface and circular motion ensured that the surface remained planar. When the final height of 4.00 mm had been reached (Figure 3-11 (c)), the ceramic was cleaned with distilled water, ensuring that no dust or other contaminants remained present on its surfaces. The ceramic was then placed on a clean glass surface and dried in a 60 °C oven for at least 2 hours.

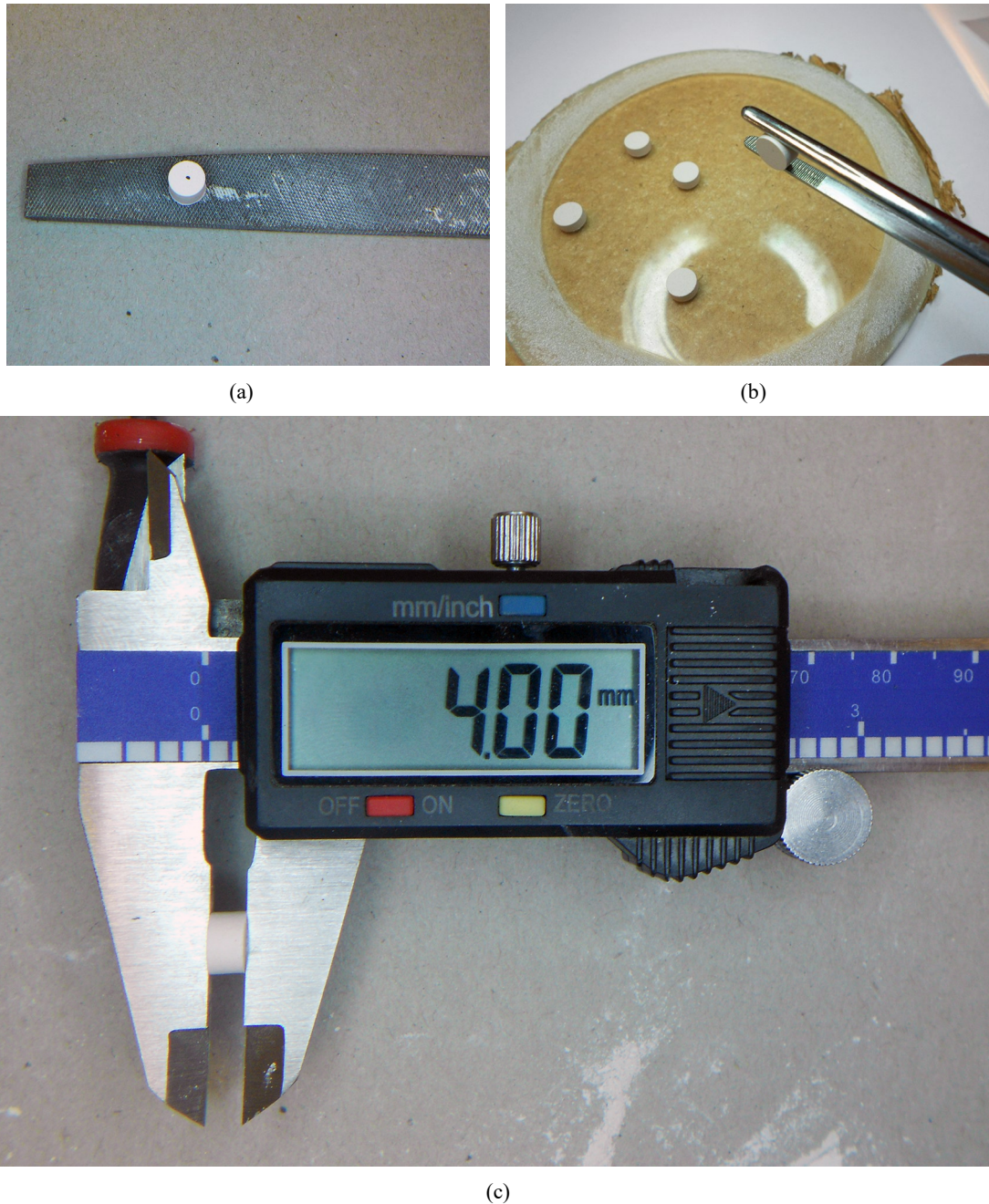


Figure 3-11 Preparation of ceramic filter surfaces: (a) filing down of filter height; (b) polishing of filter faces; (c) final filter height

3.1.2.2 Assembly of tensiometer components

A clean, dry filter element and a single sensor were paired to form the core of the tensiometer (Figure 3-12 (a)). The filter element was placed concentrically on the sensor's metal protection cap, creating a space between the two parts and forming the water reservoir. The filter element and sensor body were pressed tightly together between two fingers. *Loctite* Super Glue (a cyanoacrylate instant adhesive) was then applied to the rim of the metal protection cap and the exposed outer rim of the filter element surface in contact with the sensor. The parts were tightly

pressed together until the adhesive had cured (Figure 3-12 (b)). By applying the adhesive to the outer rim, rather than directly bonding the surfaces together, the risk of contaminating the reservoir with adhesive and creating nucleation sites on the reservoir interior was significantly reduced. The bonded elements could then be handled safely without the risk of contamination, which facilitated the remaining assembly process substantially (Figure 3-12 (c)).

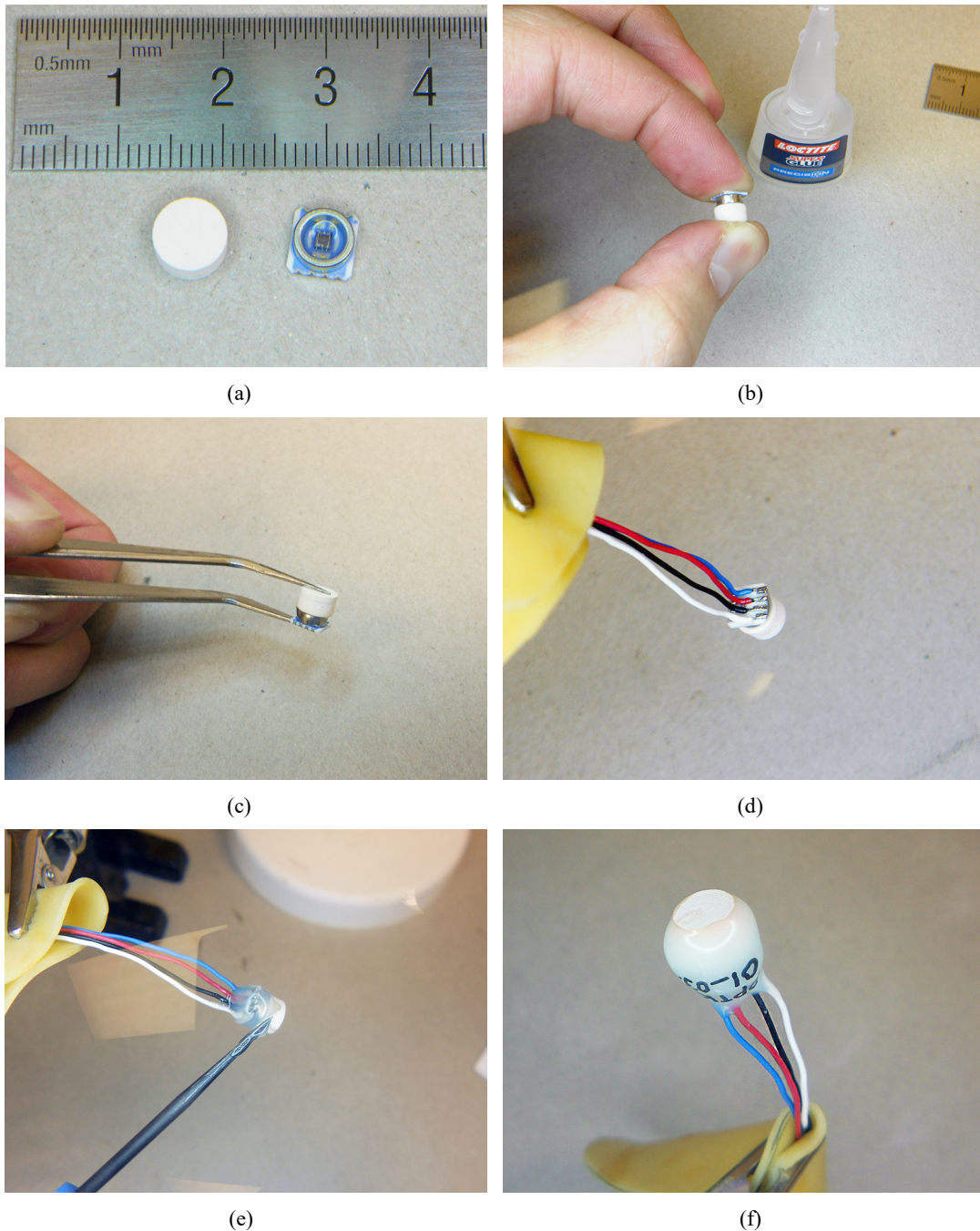


Figure 3-12 Assembly of tensiometer: (a) cleaned ceramic filter and pressure sensor; (b) adhering of ceramic to metal cap of pressure sensor; (c) assembly ready for wire connection; (d) soldering of cables to sensor body; (e) application of epoxy coating; (f) final assembled tensiometer with cured epoxy

The colour-coded wires were soldered to the pressure sensor, leaving as much insulation around the cable as possible (Figure 3-12 (d)). The entire assembly, including the cable connections, was then coated in the structural epoxy. The epoxy was applied in layers to ensure that the cables were encased entirely and insulated from one another (Figure 3-12 (e)). A hot air heat gun or the flame of a small blowtorch could be used to remove any small air bubbles that had formed in the epoxy during mixing of the two components. The epoxy was allowed to cure for 24 hours before the tensiometer was tested. Figure 3-12 (f) shows the completed tensiometer.

Since many prototype tensiometers were constructed during the study using the different sensor types and ceramics available, each tensiometer was labelled with a unique identification number referencing the AEV of the ceramic tip and the pressure range of the sensor.

3.2 PROCEDURES FOR TENSIO METER USE

The tensiometer first had to be saturated and calibrated to enable it to measure suctions. A saturated tensiometer can transfer soil suctions, through the filter element and water reservoir to the pressure sensor by exerting tensile stress on the sensing element. A perfectly saturated tensiometer is one with no entrained or entrapped air in the filter element or in the water contained in the water reservoir. Although every measure was taken to limit variability between each prototype tensiometer during the assembly process, each element had slight variances in their response to a set of applied pressures. Calibration of each individual prototype tensiometer to known values of pressure was therefore also required. The experimental set-up and procedures for saturating and calibrating tensiometers are explained below.

3.2.1 Experimental saturation and calibration set-up

Figure 3-13 shows a standard triaxial cell that was used to saturate and calibrate the tensiometers without modification to the cell. Multiple layers of 1.20 mm thick circular latex membrane were used to seal the signal cable of the tensiometers in compression between the cell top and the acrylic cylinder. This set-up required connection cables that were thin enough for the membrane to conform around creating a seal, but sufficiently flexible and robust to resist shearing under the cell top (as depicted in Figure 3-1). Up to six tensiometers could be placed in the cell at one time by carefully spacing the thin cables (four per tensiometer) around the circular seals. The seals were limited to a maximum pressure of 700 kPa (7 bar), adequate to saturate up to 5 bar AEV ceramics.

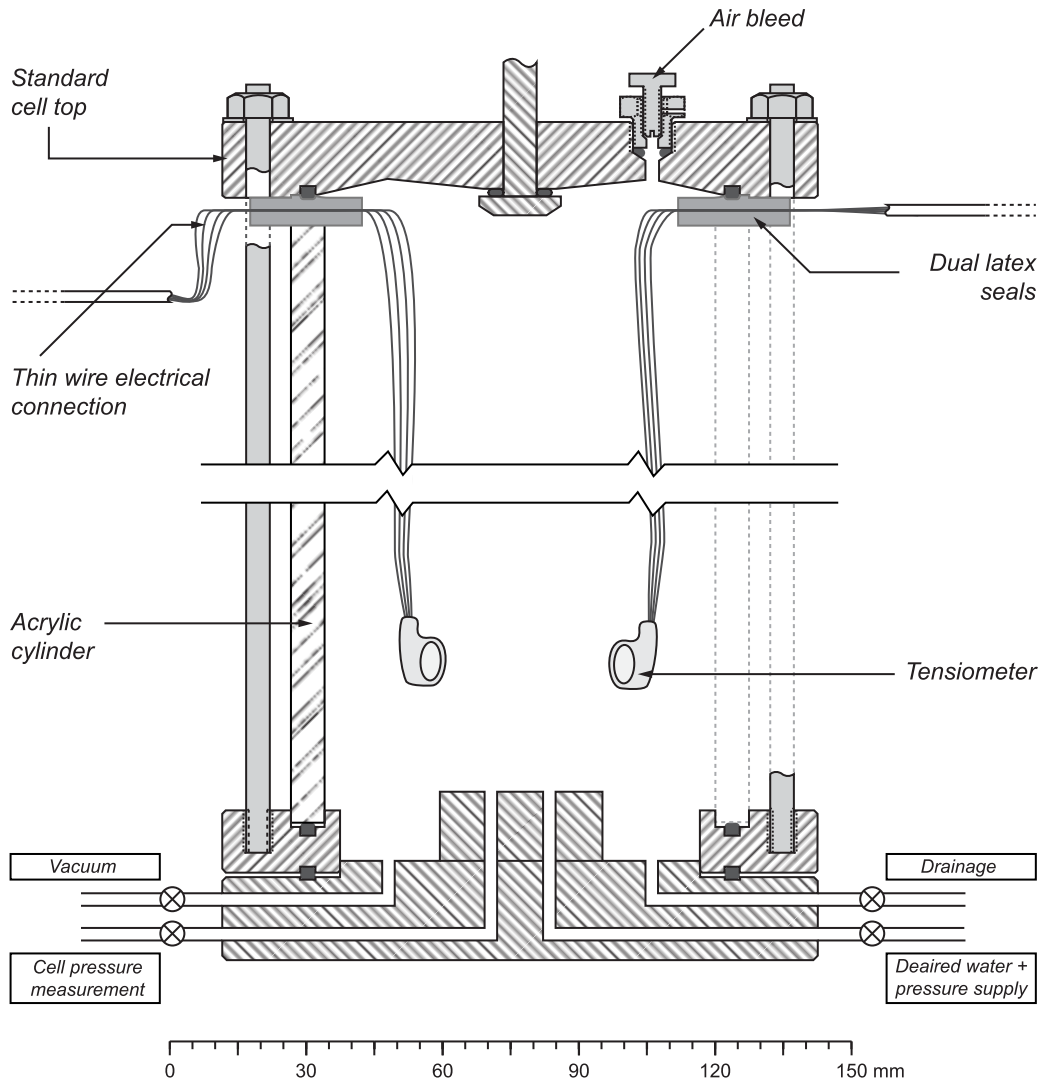


Figure 3-13 Standard triaxial cell for low-pressure saturation (< 700 kPa)

This set-up proved useful for initial tests and illustrated how standard equipment might be used to saturate and calibrate tensiometers. However, the seals were prone to leaks and damage from repeated use and were ultimately abandoned.

A more practical set-up was then devised using a standard triaxial cell with a custom-built cell top. This set-up allowed for the use of more robust electrical connections (as depicted in Figure 3-2). Figure 3-14 shows how the custom cell was used to saturate and calibrate the tensiometers. Threaded fasteners and small O-rings were slipped around the signal cables of the tensiometers and tightened into the cell top. An additional hole and fastener on the cell top allowed a vacuum to be maintained in the cell while being filled as before. Up to six tensiometers could be placed in the cell at one time. The maximum attainable safe cell pressure was increased to 1700 kPa (17 bar) (the limiting element being the acrylic cylinder), adequate to saturate up to 15 bar AEV ceramics.

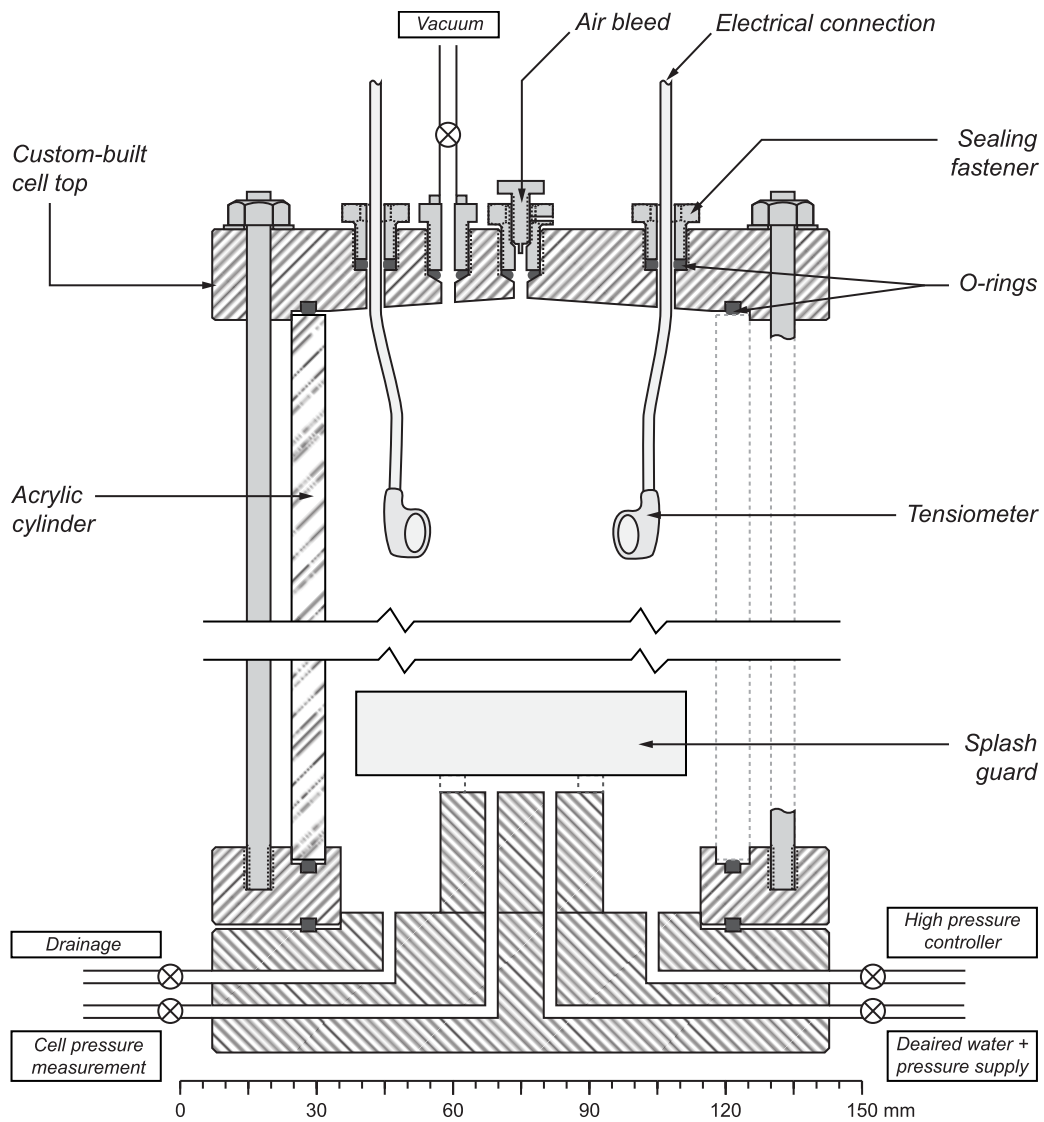


Figure 3-14 Modified high triaxial cell for high-pressure saturation (> 700 kPa)

Detail drawings of the circular seals used in the first set-up and the custom-built cell top in the second set-up are contained in Appendix A (Figure 8-2 and Figure 8-3 respectively).

The essential elements of the full set-up for the saturation and calibration of the tensiometers are similar to that of a typical triaxial testing set-up and are shown numbered in Figure 3-15. These elements are listed below:

- A vacuum agitation/cavitation deaerator (1), with a clean water supply (1.1), a vacuum release valve (1.4), and water flow control valves (1.2 – 1.3),
- a high vacuum pump (2), water/moisture trap (2.4), and vacuum control valves (2.1 – 2.3),
- a pressure control panel (3), air pressure regulators (3.7), and air and pressure control valves (3.2 – 3.6, 3.8),

- an air-water interface (4) with release valve (4.1),
- a modified saturation cell (5) containing tensiometers, a cell pressure transducer (5.6), pressure control valves (5.2 – 5.5), and connections to a central data acquisition system,
- an air compressor (6) supplying low pressure up to 700 kPa, and
- a high-pressure controller (7) supplying high pressure up to 3000 kPa.

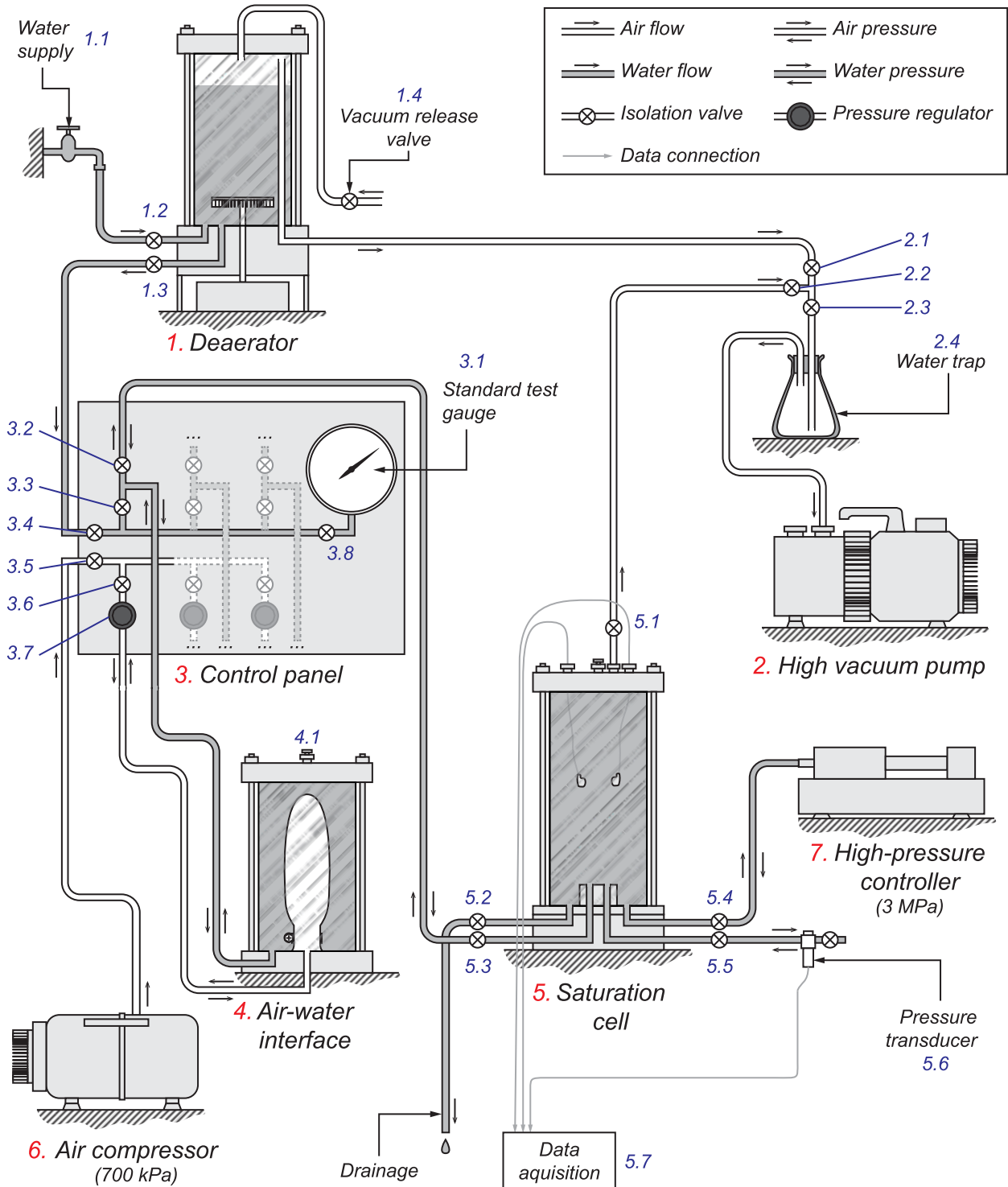


Figure 3-15 Diagram of saturation and calibration set-up

3.2.2 Saturation procedure

The procedure adopted for reliably saturating the tensiometers consisting of initial saturation followed by pre-pressurisation is similar to that proposed by Tarantino & Mongiovi (2003). Initial saturation involved producing a completely dry filter element with all traces of moisture and air removed from the filter element and water reservoir. A combination of oven drying at 60 °C and the application of a high vacuum in the absence of water was used, after Take & Bolton (2003). Pre-pressurisation involved filling the water reservoir and the voids of the filter element with clean, de-aired water and forcing any remaining traces of air into solution through the application of high pressure. These procedures are outlined in detail in Appendix A.

3.2.3 Calibration procedure

The saturation procedure described above was considered completed when the real-time response of the tensiometers to a rapid change in pressure was shown to be sufficient, as in Figure 3-16. When saturation was complete, the tensiometers were calibrated by recording the response of the tensiometers to cycles different applied pressures inside the saturation cell. A typical calibration cycle is shown in Figure 3-17. These procedures are outlined in detail in described Appendix A.

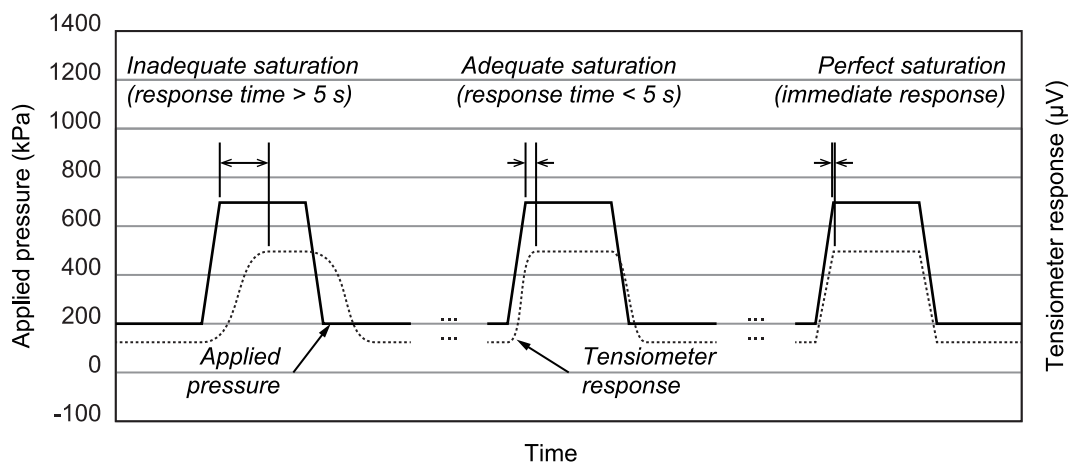


Figure 3-16 Response times

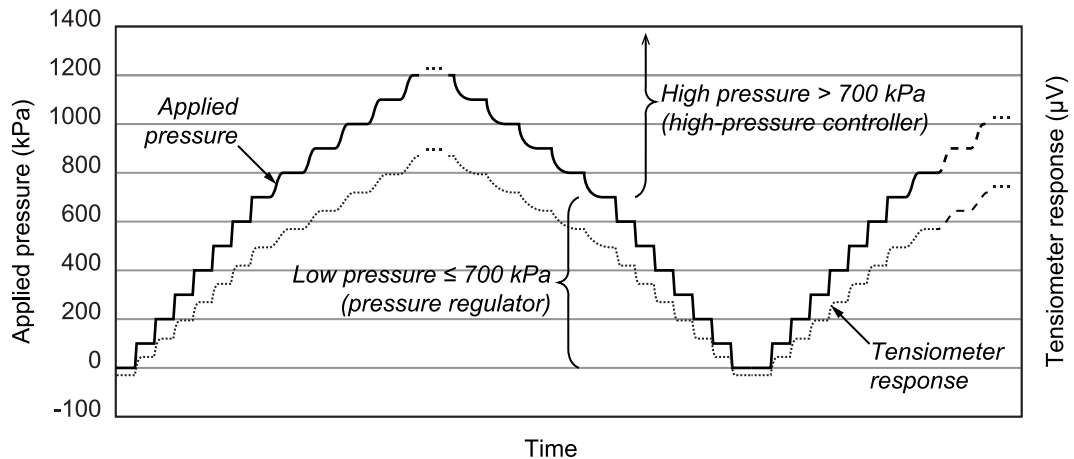


Figure 3-17 Typical calibration cycle

3.2.3.1 Storage

To maintain the saturation of the tensiometers, they were at all times stored in de-aired water and at high pressure if possible:

1. When calibration was complete, the tensiometers were stored in the cell at a high pressure to keep any remaining dissolved air from concentrating over time and reducing the degree of saturation.
2. When required for testing, the tensiometers were taken out of the cell and transferred to a sealed storage container in freshly de-aired water (first depressurising the cell with regulator 3.7 or the high-pressure controller, closing all valves, and draining the cell by opening valve 5.2 and the air release valve in the cell top).

3.3 EVALUATION OF TENSIO METER PERFORMANCE

The tensiometer's suitability as a suction measuring device was evaluated in different ways; through positive pressure calibration, negative pressure calibration and various other tests to quantify the measurement reliability and uncertainty. These are discussed below.

3.3.1 Calibration results

3.3.1.1 Positive pressure calibration

Calibration of HCTs under positive pressure is commonly seen in the literature (see Ridley & Burland (1993), Tarantino & Mongiovi (2003), and Lourenço *et al.* (2008)). Positive pressure calibration is compared to the reading from the standard test gauge (3.1) and further verified by the calibrated pressure sensor of the high-pressure controller (7).

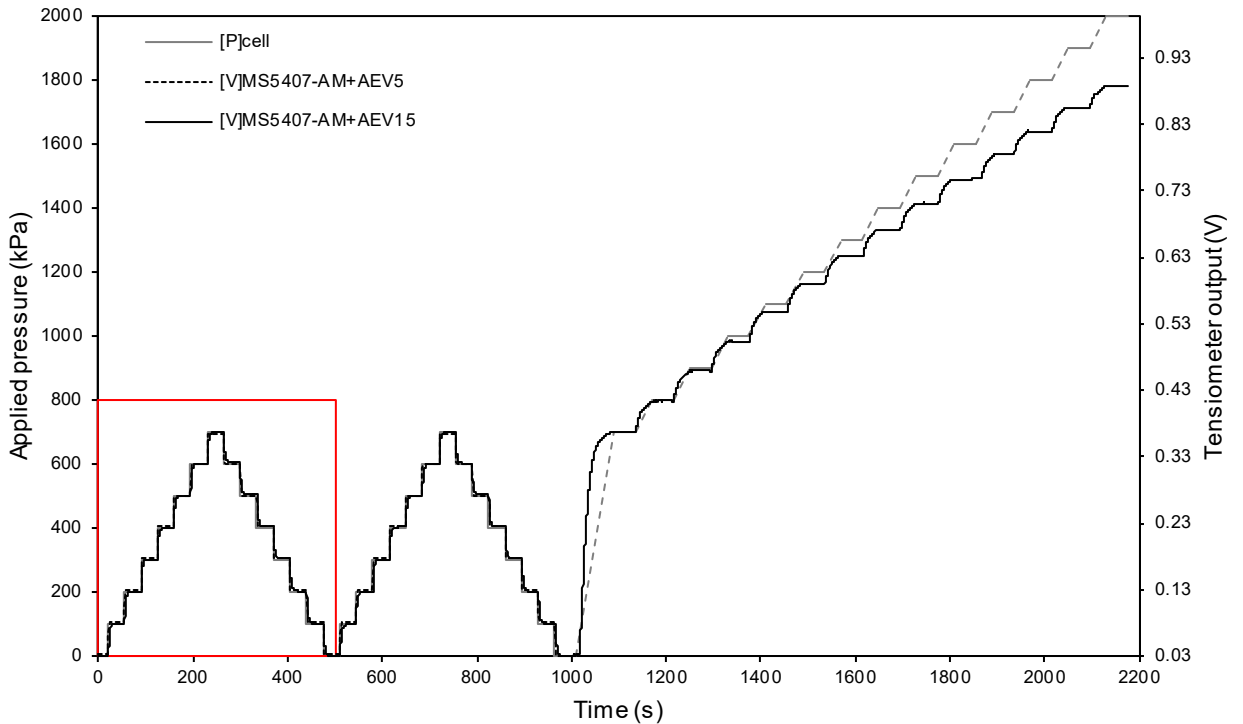
Test set-up

The test set-up was as described in Section 3.2.1 and Figure 3-15. The only change to the regular test set-up was the replacement of the acrylic cylinder with a reinforced stainless-steel cylinder to increase the maximum safe cell pressure from 1700 kPa to 2000 kPa for this test.

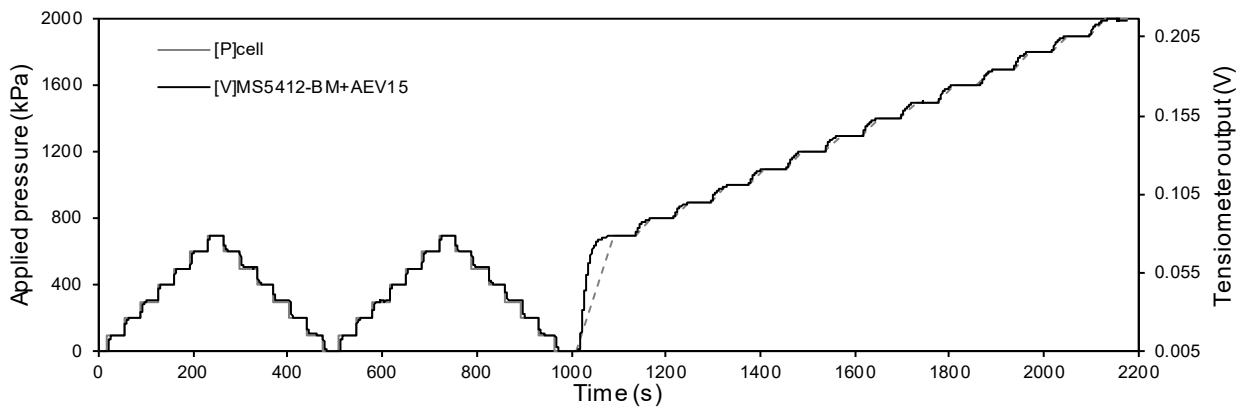
Test procedure

The steps in the calibration procedure were as described in Section A.2.2. Figure 3-18 (a) shows the calibration procedure performed on two saturated tensiometers with 7-bar full-scale MS5407-AM ‘high sensitivity’ pressure sensors fitted with a 5 bar AEV and a 15 bar AEV ceramic, respectively. Figure 3-18 (b) shows the same procedure on a single saturated tensiometer with a 12-bar MS5412-BM ‘high linearity’ pressure sensor fitted with a 15 bar AEV ceramic. The pressure inside the saturation cell was cycled between 0 – 700 kPa using the regulator and standard test gauge in increments of 100 kPa. The pressure was then increased in the same increments up to a maximum applied pressure of 2000 kPa using the high-pressure controller.

The line labelled ‘[P]cell’ does not represent recorded data but rather the cycles of cell pressure application. Each tensiometer output is labelled ‘[V]MS54’ followed by a description of the sensor and AEV of the ceramic (i.e. ‘07-AM’ for 7-bar sensors, ‘12-BM’ for 12-bar sensors, ‘AEV5’ for 5 bar AEV ceramics, and AEV15 for 15 bar AEV ceramics). The 7-bar and 12-bar sensors are graphed separately due to the different sensitivities of the sensors.



(a)



(b)

Figure 3-18 Positive pressure calibration 0 – 2000 kPa range for: (a) 7-bar sensors; (b) 12-bar sensor

Results

Table 3-2 lists the results of the positive pressure calibration test. The tensiometer response (i.e. measured suctions) (Δu_u) to the changes in cell pressure (Δp) is compared in Figure 3-19. The deviation of the measured suction (Δu_u) from the imposed change in cell pressure (Δp) is given by $E = \Delta u_u - \Delta p$. This is the extrapolation error between the measured value and the linear regression of the positive pressure calibration. A maximum deviation of 3.9 kPa was observed at an imposed pressure of 700 kPa.

The extrapolation error, $e = |E|/\Delta p$ can also be expressed as a percentage. A maximum extrapolation error of 0.6 % was observed at an imposed pressure of 700 kPa.

It is also customary to express the measurement error of an instrument as a percentage of the full-scale range of the device. The full-scale pressure of the tensiometer measuring positive pressure was defined as 700 kPa, the same as the 7-bar sensor. The maximum extrapolation error is given by $e' = |E|/|FS|$ and was, therefore, determined to be 0.6 %FS.

The 7-bar sensors thus delivered output closely following the applied cell pressures under 700 kPa, implying a perfectly linear response.

For applied cell pressures over about 1000 kPa, the output of the 7-bar sensor steadily decreased for pressures nearing its maximum over-range pressure (Table 3-3) implying a non-linear response (Figure 3-18 (a) and Figure 3-19). Thus, depending on the accuracy of measurement required, the tensiometer was deemed suitable for measuring positive pressures up to about 1200 kPa with an extrapolation error, e of about 4.1 %.

In contrast, the 12-bar sensor delivered output closely following the applied cell pressure up to 2000 kPa, implying a linear response even into its over-range (Figure 3-18 (b) and Figure 3-19).

Table 3-2 Results of positive pressure calibration

Tensiometer output Δu_u (V)	Imposed change in cell pressure Δp (kPa)	Measured pressure* Δu_u (kPa)	Deviation from linear regression $E = \Delta u_u - \Delta p$ (kPa)	Extrapolation error**	
				$e = \frac{ E }{\Delta u_i}$ (%)	$e' = \frac{ E }{ FS }$ (% FS)
Positive pressure calibration					
0.3614	700	696.1	-3.9	0.6 %	0.6 %
0.3152	600	598.5	-1.5	0.2 %	0.2 %
0.2689	500	500.5	0.5	0.1 %	0.1 %
0.2219	400	401.3	1.3	0.3 %	0.2 %
0.1745	300	301.2	1.2	0.4 %	0.2 %
0.1268	200	200.3	0.3	0.2 %	0.0 %
0.0787	100	98.7	-1.3	1.3 %	0.2 %
0.0306	0	-2.9	-2.9		0.4 %

*The measured value obtained from linear regression of the positive pressure calibration over the range 0 – 700 kPa
 **FS = 700 kPa.

Table 3-3 Results of positive pressure calibration in over-range

Tensiometer output Δu_u (V)	Imposed change in cell pressure Δp (kPa)	Measured pressure* Δu_u (kPa)	Deviation from linear regression $E = \Delta u_u - \Delta p$ (kPa)	Extrapolation error**	
				$e = \frac{ E }{\Delta u_i}$ (%)	$e' = \frac{ E }{ FS }$ (% FS)
Positive pressure calibration					
0.8846	2000	1801.6	-198.4	9.9 %	28.3 %
0.8510	1900	1730.7	-169.3	8.9 %	24.2 %
0.8167	1800	1658.2	-141.8	7.9 %	20.3 %
0.7811	1700	1583.1	-116.9	6.9 %	16.7 %
0.7448	1600	1506.3	-93.7	5.9 %	13.4 %
0.7071	1500	1426.6	-73.4	4.9 %	10.5 %
0.6674	1400	1342.7	-57.3	4.1 %	8.2 %
0.6283	1300	1260.0	-40.0	3.1 %	5.7 %
0.5863	1200	1171.3	-28.7	2.4 %	4.1 %
0.5441	1100	1082.1	-17.9	1.6 %	2.6 %
0.5005	1000	990.0	-10.0	1.0 %	1.4 %
0.4561	900	896.3	-3.7	0.4 %	0.5 %
0.4108	800	800.4	0.4	0.0 %	0.1 %

*The measured value obtained from linear regression of the positive pressure calibration over the range 0 – 700 kPa

**FS = 700 kPa.

Calibration curves

The resulting positive pressure calibration curves for each sensor type are shown in Figure 3-19.

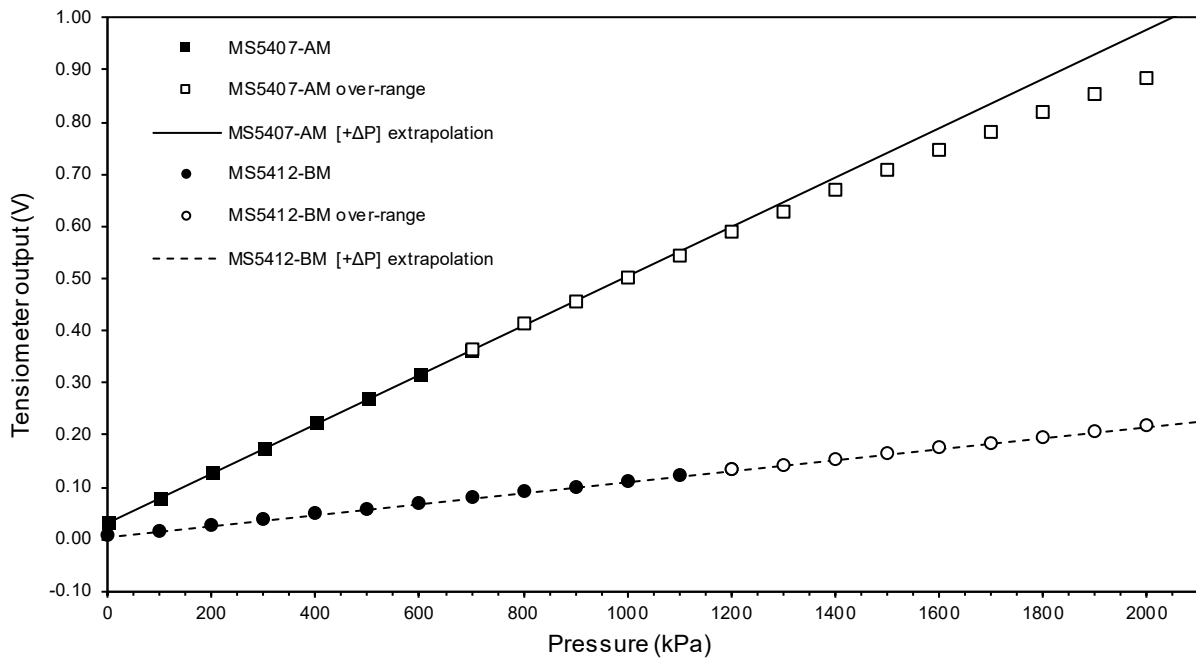


Figure 3-19 Positive pressure calibration curves for 7-bar and 12-bar sensors

The calibration curves labelled ‘[+ΔP] extrapolation’ were obtained from linear regression of the positive pressure calibration over the range 0 – 700 kPa for the 7-bar sensor (or 0 – 1200 kPa for the 12-bar sensor), as only the linear response region was considered.

The calibration curves were defined by the two parameters in Equation 3.3:

$$[P] = \alpha \cdot [V] + \beta \quad 3.3$$

where:

- [P] = pressure (kPa),
- [V] = tensiometer output (V),
- α = slope of the calibration curve (kPa/V),
- β = intercept of the calibration curve (kPa), and

The α -value was unique to each specific sensor (i.e. tensiometer), and thus, calibration of each sensor was required. The value of α remained relatively constant, but the value of B fluctuated between each use due to factors such as temperature, air pressure, and internal resistance of the sensors. It was, therefore, necessary to carefully define the zero-pressure offset prior to each use by taking a measurement at atmospheric pressure (zero-gauge pressure) and applying Equation 3.4.2.9.

$$\beta = -\alpha \cdot [V_0] \quad 3.4$$

where:

- α = slope of the calibration curve (kPa/V),
- β = zero offset (kPa), and
- [V₀] = reference reading at atmospheric pressure (V).

With an excitation voltage of 4.5 V supplied by the data acquisition system, typical values for α and β as were determined by this round of calibration are given in Table 3-4.

Table 3-4 Calibration constants

Sensor	Full-scale pressure (bar)	α (kPa/V)	β (kPa)
MS5407-AM	7	2113.1*	-67.1
MS5412-BM	12	9494.7*	-51.4

*At excitation voltage of 4.5 V

Linearity, sensitivity, resolution and hysteresis

The signal output for the 7-bar sensor was perfectly linear in the 0 – 700 kPa range returning a calibration curve as shown to the left of Figure 3-19. However, for higher pressures reaching

the sensor's over-range capacity, the signal output decreased, resulting in a non-linear calibration curve as shown to the right of Figure 3-19.

The only hysteresis observed was from the slight delay in pressure equilibration (see response time below).

The signal return of the 7-bar sensor was very sensitive to changes in pressure, which was desirable for high-resolution measurement. However, it was not desirable to use the sensor over its full-scale pressure or with a non-linear calibration curve.

Therefore, the measurement of higher pressures required the use of the less sensitive 12-bar sensor, which had a lower signal return but much improved full-scale pressure and linear calibration curve well into its over-range. The calibration curve for the 12-bar sensor is also shown in Figure 3-19.

Response time

It was expected that the higher AEV ceramic would yield slower response times to applied pressures due to its significantly lower hydraulic conductivity restricting flow to and from the water reservoir (1.21×10^{-7} cm/s for the 5 bar AEV vs 2.59×10^{-9} cm/s for the 12 bar AEV, refer to Table 3-1). Inspection of the 0 – 700 kPa range of applied pressure, as shown in Figure 3-20, yielded the typical response times of each ceramic (i.e. tensiometer type). The response times could be determined in this range since the applied pressure could rapidly be changed using the pressure regulator, but not for higher pressures since the high-pressure controller's rate of pressure application was slower than the observed response times of the tensiometers.

The typical response time for equilibration to an applied pressure increase or decrease of 100 kPa was determined to be 2.8 s for the 5 bar AEV ceramic and 16.2 s for the 15 bar AEV ceramic.

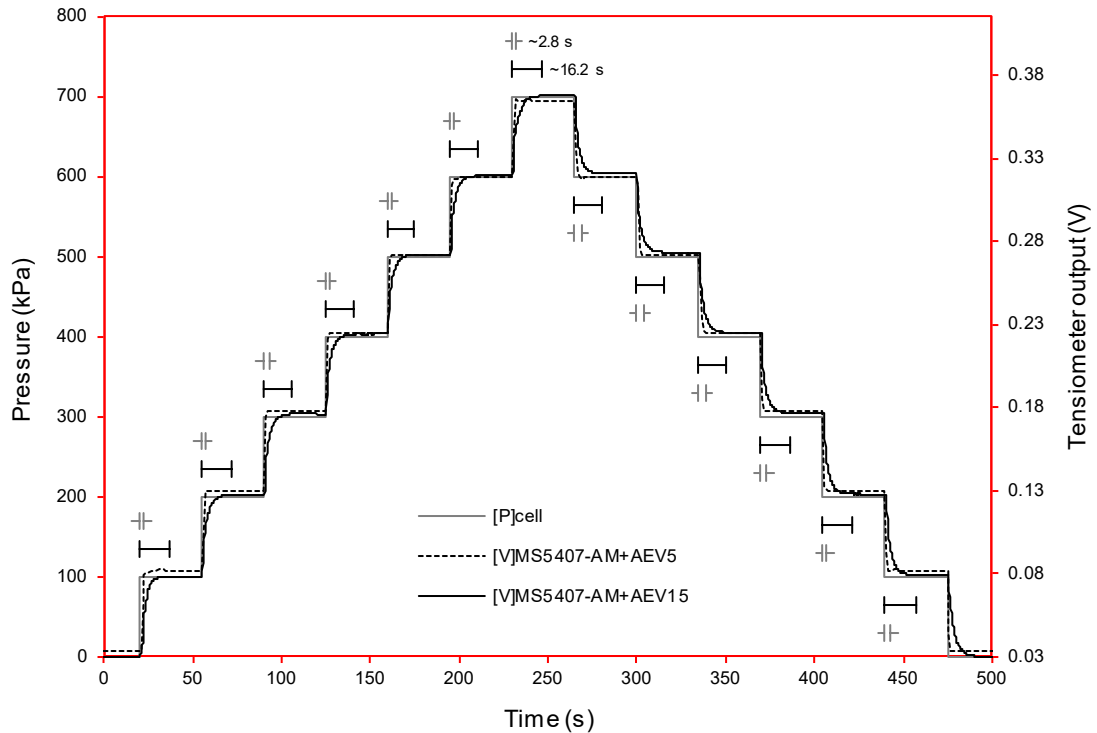


Figure 3-20 Positive pressure calibration 0 – 700 kPa range for 5 bar and 15 bar AEV ceramics

3.3.1.2 Negative pressure calibration

Lourenço *et al.* (2010) postulated that specific designs of pressure transducers may have asymmetrical deflection when subjected to pressures of opposite sign and should be carefully considered when selecting the appropriate transducer in the design of a high-suction tensiometer. Ridley & Burland (1993), Tarantino & Mongiovi (2003) and Lourenço *et al.* (2008) have all independently shown that extrapolation of the positive pressure calibration curve into the negative pressure range is suitable for certain tensiometers using diaphragm-type pressure transducers. The new tensiometer used a sensor with a solid piezoresistive sensing element, rather than a strain gauged diaphragm, to register changes in pressure. Therefore, to evaluate if the same extrapolation would be suitable negative pressure calibration was also performed.

Negative pressure calibration was performed using the isotropic unloading technique described by Ridley & Burland (1993). A saturated clay sample containing a tensiometer was consolidated to known effective stress. A negative pore-water pressure was then imposed by unloading the sample in an undrained manner. The change in effective stress in the sample was thus equal to the change in the pore-water pressure, i.e. the magnitude of the imposed suction. Changes to the procedure were adopted after Lourenço *et al.* (2008), who implemented the use of a zero backpressure and free drainage of the sample, which simplified the procedure.

Test set-up

Figure 3-21 shows the test set-up used for generating negative pore-water pressures in a saturated clay specimen using the modified high triaxial cell. A tensiometer was embedded inside the specimen. The thin cables of the tensiometer were routed between the specimen and latex membrane and sealed to the top cap by tightly compressing the latex membrane and some silicone sealant with a hose clamp. Drainage was provided by way of the top cap.

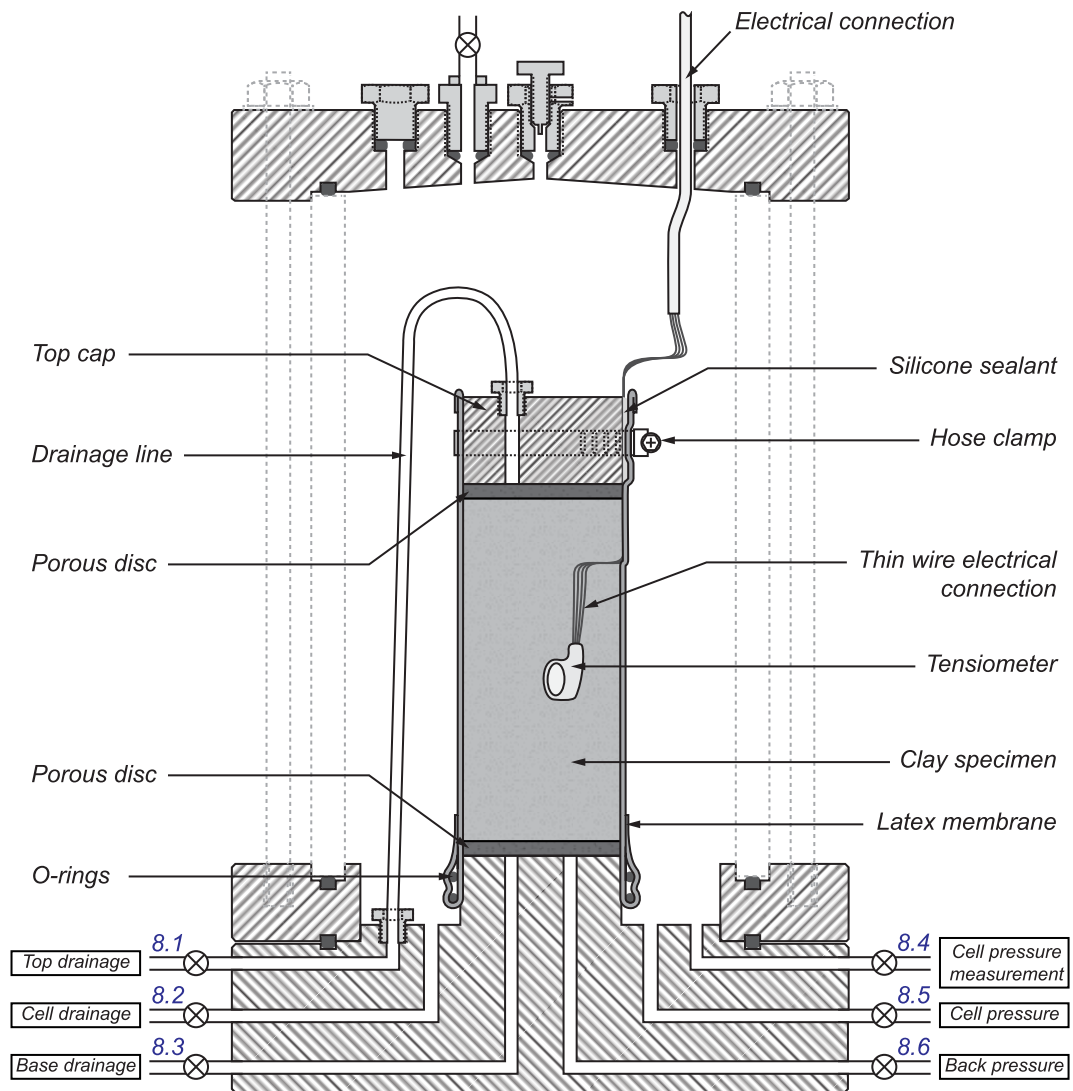


Figure 3-21 Isotropic unloading configuration in the modified high triaxial cell

Test procedure

The procedure for generating suctions in the clay sample, assuming the specimen has been prepared, contains a tensiometer and all control valves were closed, was:

1. The saturated specimen was isotropically consolidated in stages to known values of effective stress (opening valves 8.1, 8.4, and 8.5 and raising the cell pressure with regulator 3.7 and test gauge 3.1).

2. The pore-water pressure of the clay sample (equal to the calibrated tensiometer response) and the cell pressure (8.4) were recorded through the data acquisition system.
3. When equilibrium had been established, as demonstrated by the tensiometer output decreasing to a constant, stable value, the specimen and cell were isolated (closing valves 8.1, 8.2, 8.3, and 8.6).
4. The cell pressure was then abruptly lowered by known increments of pressure (with regulator 3.7 and test gauge 3.1) generating suctions of different magnitudes in the sample.

The set of negative pressure increments was used to generate a negative pressure calibration curve of the tensiometer. The previously defined positive pressure calibration curve (for 0 – 700 kPa range) was linearly extrapolated into the negative pressure range and then compared to that of the negative pressure calibration curve.

Test #1

The first test was performed using a very low permeability red clay sample. The clay was previously sampled from a test pit at an unspecified location and leftover from a previous research project. The clay had an effective particle size (D_{10}) of 0.0026 mm. The particle size distribution for the sample is contained in Appendix B. The specimen was prepared with dimensions equal to that of a standard 50 mm diameter triaxial specimen and containing a tensiometer, as shown in Figure 3-21. Due to the low hydraulic conductivity of the sample and the imperfect improvised seal around the tensiometer cables, achieving good saturation proved to be complicated.

The specimen was consolidated to an effective stress of 300 kPa with the top drainage line open. Immediately prior to the unloading cycle, the cell pressure was rapidly lowered by ± 100 kPa, returned to the consolidation pressure, rapidly raised by ± 100 kPa, and then returned to the consolidation pressure while the valves were isolated. The recorded cell pressure and measured pore-water pressure response was used to determine the specimen's pore pressure parameter, 'B-value' or 'level of saturation'.

After saturation and consolidation of the specimen, a B-value of 0.93 was achieved. This value was lower than the value suggested by most test standards that require a B-value higher than 0.95 (ASTM, 2011). However, by following the procedure described by Lourenço *et al.* (2008), the B-value can be used to adjust the expected pore-pressure response.

The first unloading cycle was applied by briefly dropping the cell pressure to 100 kPa. Upon re-loading, the cell pressure was raised by 100 kPa above the previous consolidation pressure and the specimen allowed to consolidate to an effective stress of to 400 kPa. The unloading

procedure was then repeated, each time increasing the consolidation and unloading pressures by 100 kPa until cavitation in the tensiometer was observed.

Figure 3-22 shows the first isotropic unloading test. The tensiometer output reflects the measured pore-water pressure. The values can be read on the right vertical axis as the signal output of the tensiometer, or on the left vertical axis as the signal output converted to units of pressure using the positive pressure calibration curve linearly extrapolated into the negative range.

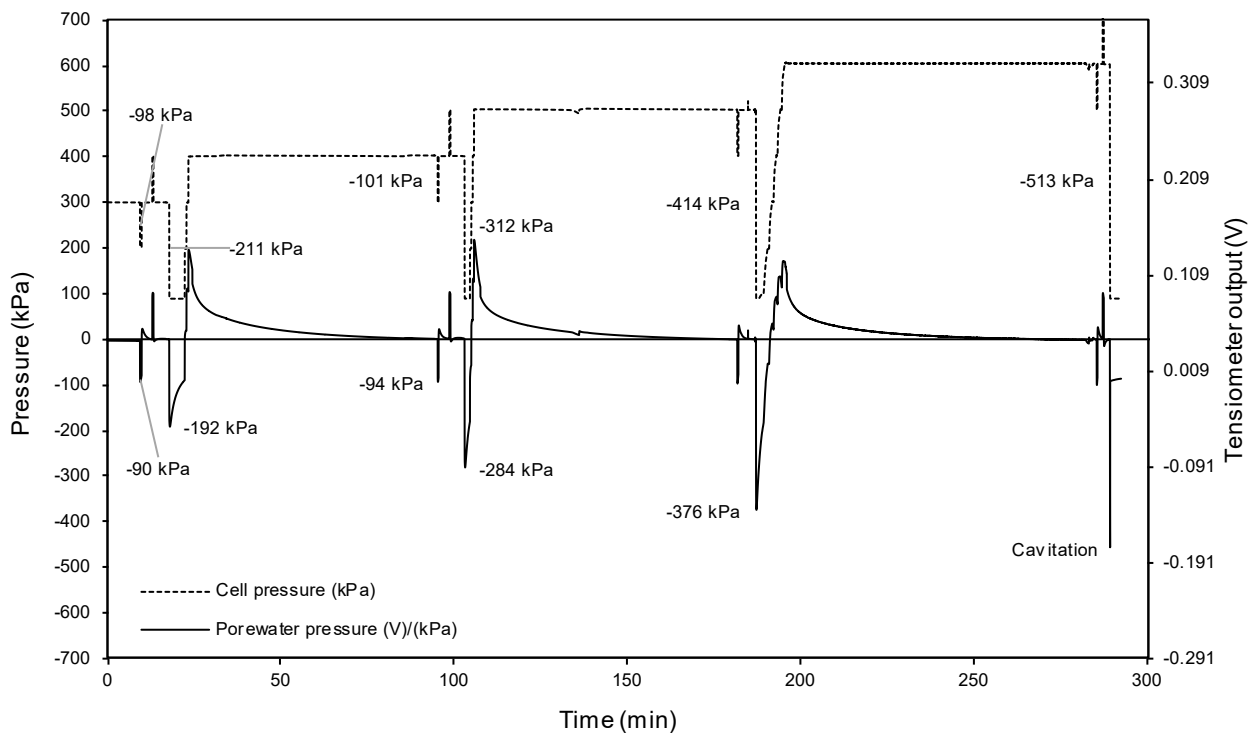


Figure 3-22 Tensiometer response to isotropic unloading, Test #1

After the first unloading cycle of -97.7 kPa, it was observed that cavitation had occurred in the top cap drainage line, where air bubbles could be seen. The presence of the air resulted in delayed pore-water pressure response in the specimen. Thus, the B-value was confirmed prior to each unloading cycle. Upon unloading the cell pressure, the pore-water pressures instantly dropped into the negative range as expected. However, immediately after this drop, the pore-pressures started to dissipate, indicating that the specimen was absorbing water, likely due to an imperfect seal around the tensiometer cables or from the top cap drainage line where the observed air bubbles could expand.

The maximum cell pressure drop of 413.8 kPa was achieved was on the fourth unloading cycle. During the last unloading cycle of -513.4 kPa cavitation in the tensiometer was observed, and this data point was excluded from the results.

Test #2

Due to the issues experienced in the first isotropic unloading test and the limited set of data collected, the test was repeated in an attempt to improve the method and prevent cavitation in the drainage lines. In the second test, a more uniform kaolin clay sample was used. The kaolin clay was supplied from a commercial source in a finely milled powder form having an effective particle size (D_{10}) of 0.0028 mm. The particle size distribution for the sample is contained in Appendix B. The same tensiometer was used so that the calibration curves from the two tests could be directly compared. The calibrated response of a second tensiometer in the cell was used to monitor the cell pressure more precisely and verify the readings from the cell pressure transducer (as shown in Figure 3-23).

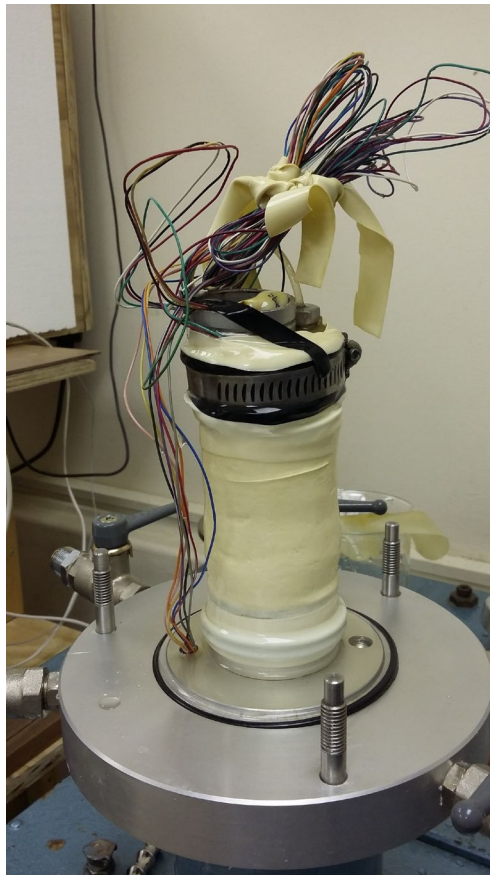


Figure 3-23 Isotropic unloading Test #2

This time, the specimen was consolidated to an effective stress of ± 600 kPa in three stages. Figure 3-24 shows the consolidation procedure for Test #2. The response of the pore pressure was tested by rapidly raising and lowering the cell pressure by ± 100 kPa prior to the isotropic unloading test. The recorded increase in cell pressure and measured pore-water pressure was used to determine the specimen's B -value. After flushing, saturation and consolidation of the specimen, poor saturation with a saturation B -value of only 0.86 was

achieved. However, the tensiometer response was shown to be satisfactorily rapid. Therefore, the test was continued.

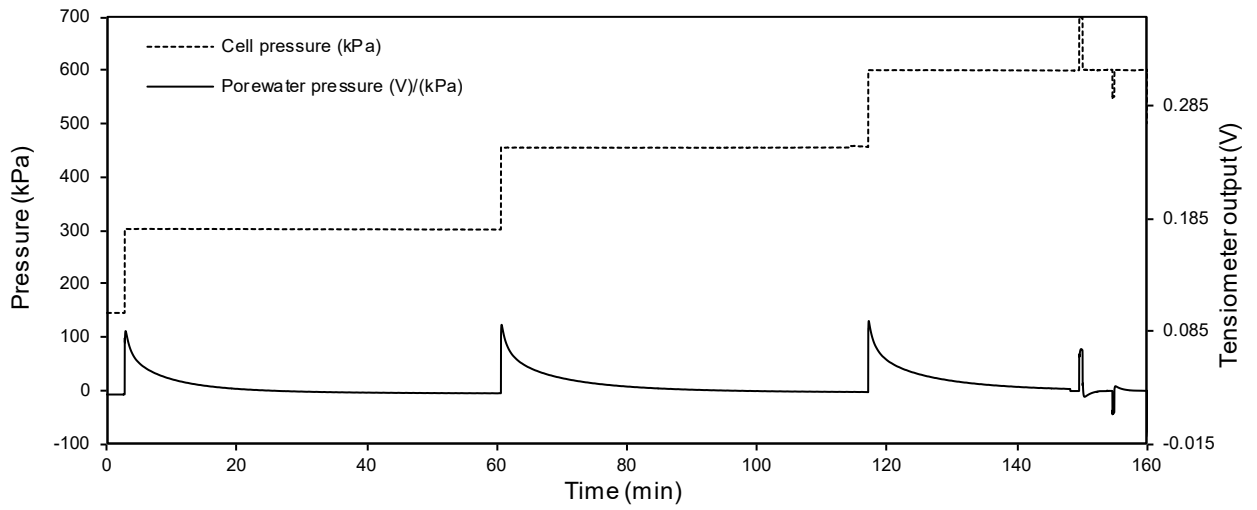


Figure 3-24 Tensiometer response to consolidation, Test #2

Figure 3-25 (a) shows the second isotropic unloading test. As previously, the tensiometer output can be read on the right vertical axis or the left vertical axis.

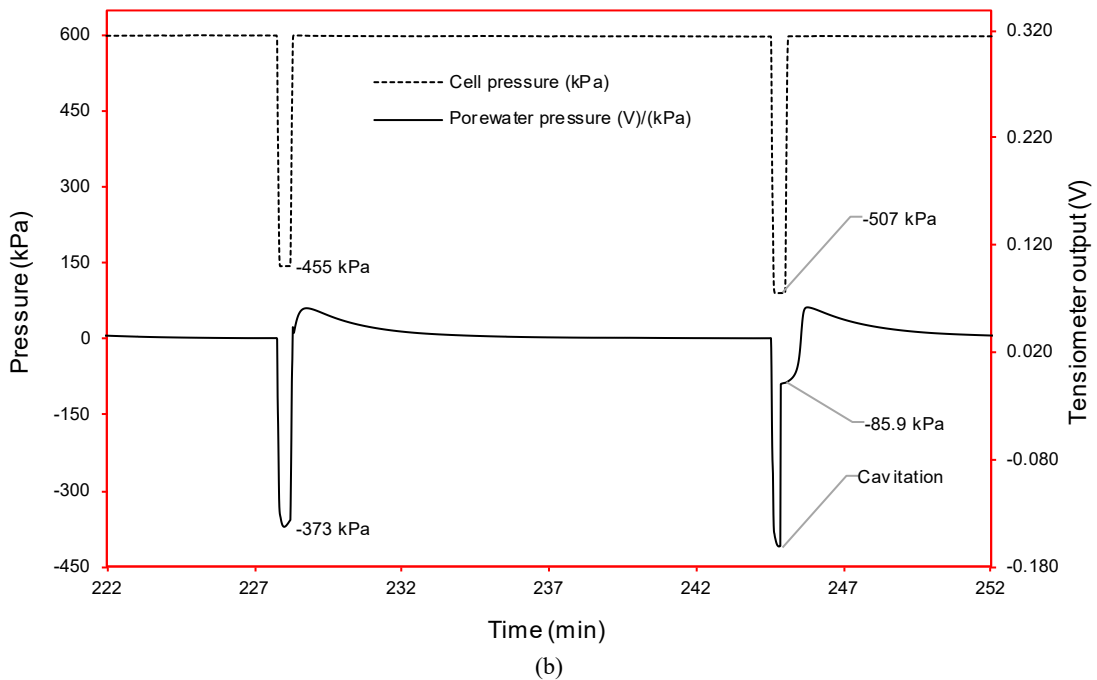
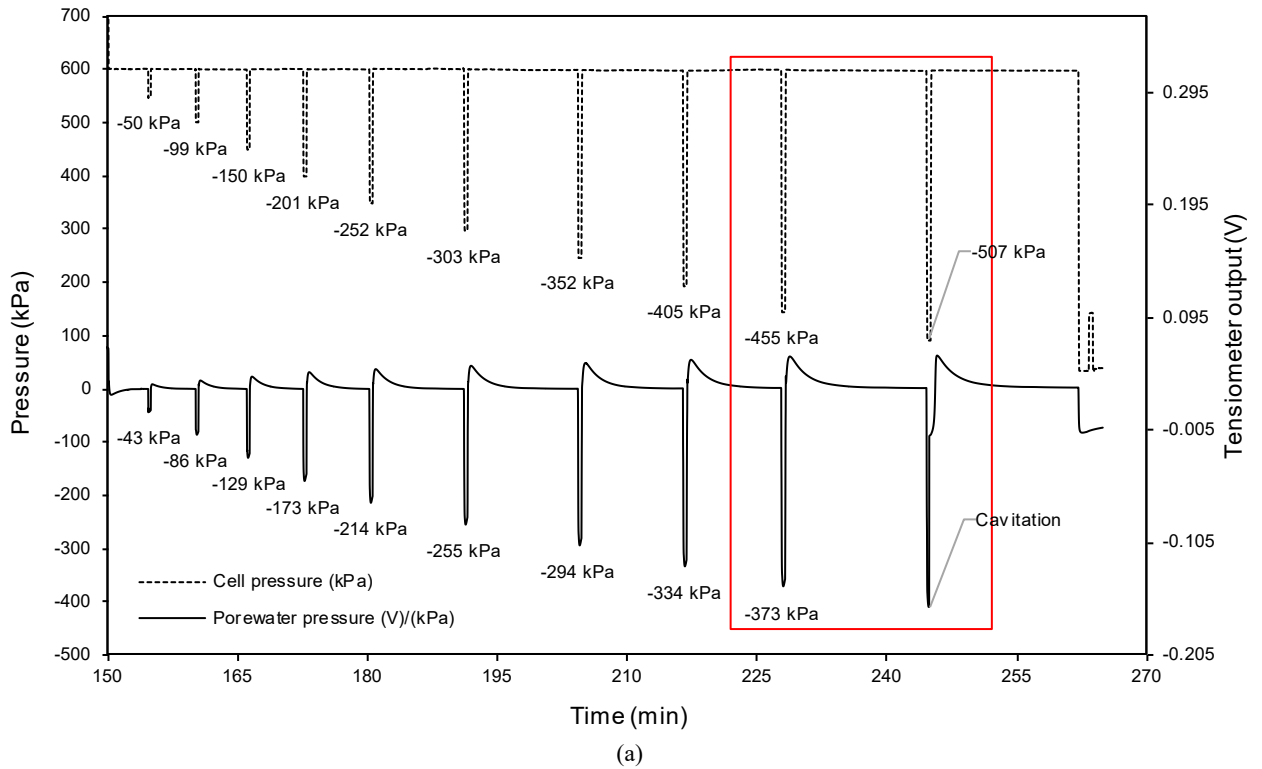


Figure 3-25 Tensiometer response to isotropic unloading, Test #2: (a) full test data; (b) cavitation

At each unloading cycle, starting at -50 kPa, the cell pressure drop was increased by ± 50 kPa and returned to the consolidation pressure of ± 600 kPa. The tensiometer response was seen to drop rapidly with the cell pressure and then return to zero on reapplication of the consolidation pressure. The response time was, however, not immediate and can be explained by the low B -value.

At each unloading cycle, the measured pore pressure rose above 0 kPa and dissipated over time directly after reapplying the consolidation pressure. This behaviour suggests that completely undrained conditions were not achieved. This could be due to a deficient seal around the specimen, or more likely around the tensiometer cables, allowing cell water to be forced into the pores of the specimen. This is also supported by the large volume of water, more than the specimen's pores could contain, that was observed draining from the specimen during consolidation. There might also have been a conformance error due to the exchange of minute amounts of water between the specimen and the tensiometer's reservoir. Therefore, in-between unloading cycles, the top drainage line was opened, and the specimen was allowed to re-consolidate. The pore pressure was monitored until it reached equilibrium at ± 0 kPa before the next unloading cycle was performed.

Nine cycles of unloading were performed to a maximum of -455.0 kPa. On the tenth unloading cycle of -506.8 kPa, the tensiometer response became unreliable, suggesting that cavitation had occurred. Closer inspection of the data, as shown in Figure 3-25 (b), revealed the characteristic behaviour of cavitation having occurred in the tensiometer. In other words, before the cell pressure was increased, the tensiometer measured a very rapid increase of the pressure to the local vapour pressure (± -86 kPa (Jacobsz, 2018)). This was also consistent behaviour for a tensiometer with a 5 bar AEV ceramic to reach cavitation at around -500 kPa. On the last unloading cycle, no further response from the tensiometer was received, confirming that cavitation had occurred.

Results

Table 3-5 lists the results of the positive pressure calibration and the two isotropic unloading tests. The tensiometer response (i.e. measured suctions) (Δu_u) to the changes in cell pressure (Δp) is compared in Figure 3-26 (a). The deviation between these values is a combination of the measurement error and the error due to the pore-water pressure parameter (B).

The suctions imposed by the corresponding changes in cell pressure is given by $\Delta u_i = B \cdot \Delta p$. The deviation of the measured suction (Δu_u) from the imposed negative pore-water pressure (Δu_i) is given by $E = \Delta u_u - \Delta u_i$. This is the extrapolation error between the measured value and the positive pressure calibration line extrapolated into the negative range (Figure 3-26 (b)). A maximum deviation of 17.2 kPa was observed at an imposed suction of 389.9 kPa.

The extrapolation error, $e = |E|/\Delta u_i$ can also be expressed as a percentage. A maximum extrapolation error of 4.4 % was observed at an imposed suction of 389.9 kPa.

It is also customary to express the measurement error of an instrument as a percentage of the full-scale range of the device. The full-scale pressure of the tensiometer was defined as -

500 kPa, the same as the theoretical maximum AEV of the 5-bar AEV ceramic. The maximum extrapolation error is given by $e' = |E|/|FS|$ and was, therefore, determined to be 3.4 %FS.

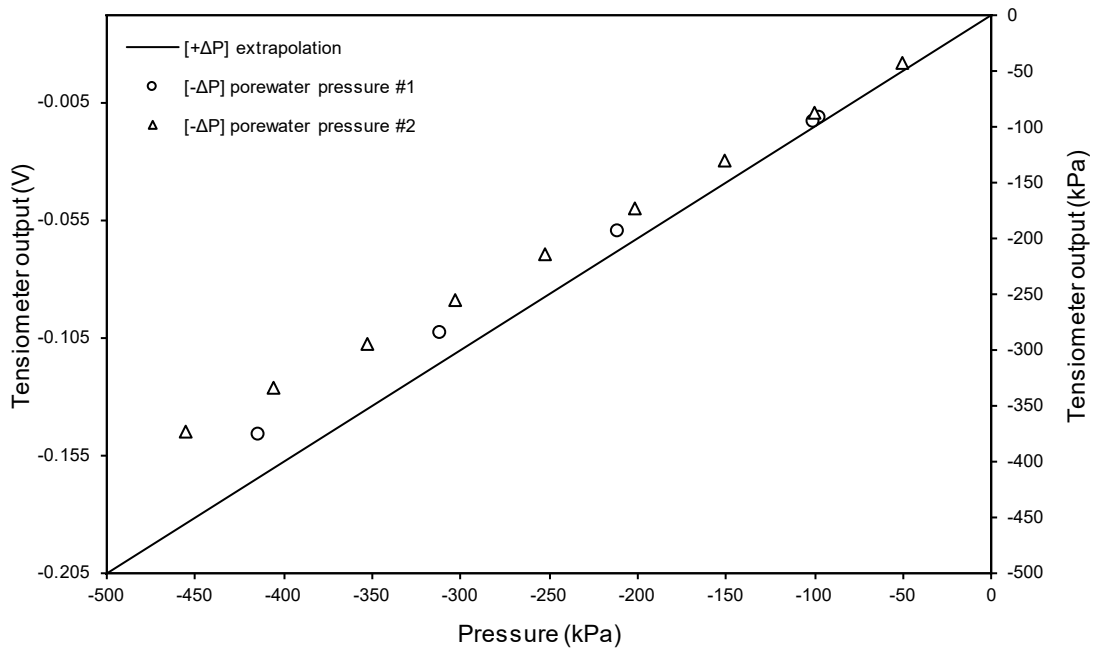
Since the extrapolation error was deemed acceptably low, extrapolation of the positive pressure calibration curve into the negative range could be deemed valid.

Table 3-5 Results of negative pressure calibration (isotropic unloading tests)

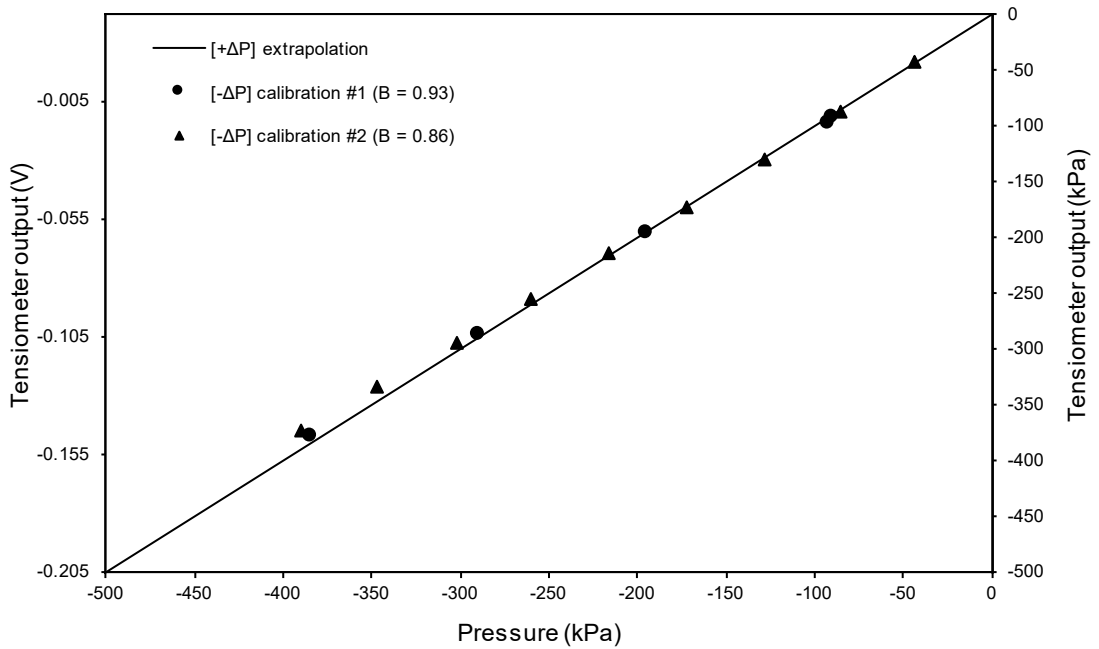
Tensiometer output	Imposed change in cell pressure	Imposed pore-water pressure	Measured pore-water pressure*	Deviation from extrapolation	Extrapolation error**	
Δu_u	Δp	$\Delta u_i = B \cdot \Delta p$	Δu_u	$E = \Delta u_u - \Delta u_i$	$e = \frac{ E }{\Delta u_i}$	$e' = \frac{ E }{ FS }$
(V)	(kPa)	(kPa)	(kPa)	(kPa)	(%)	(% FS)
Positive pressure calibration (B-value = 1.000)						
0.3614	700	-	-	-	-	-
0.3152	600	-	-	-	-	-
0.2689	500	-	-	-	-	-
0.2219	400	-	-	-	-	-
0.1745	300	-	-	-	-	-
0.1268	200	-	-	-	-	-
0.0787	100	-	-	-	-	-
0.0306	0	-	-	-	-	-
Negative pressure calibration 1 (B-value = 0.934)						
-0.0107	-97.7	-91.2	-90.1	1.1	1.2 %	0.2 %
-0.0126	-100.5	-93.8	-94.3	-0.4	0.5 %	0.1 %
-0.0590	-210.9	-196.8	-192.3	4.5	2.3 %	0.9 %
-0.1022	-312.1	-291.3	-283.6	7.7	2.7 %	1.5 %
-0.1457	-413.8	-386.3	-375.6	10.7	2.8 %	2.1 %
-0.1848	-513.4	-	-458.1	-	-	-
Negative pressure calibration 2 (B-value = 0.857)						
0.0118	-50.2	-43.1	-42.6	0.5	1.1 %	0.1 %
-0.0087	-99.2	-85.0	-86.0	-1.0	1.1 %	0.2 %
-0.0293	-150.0	-128.6	-129.4	-0.9	0.7 %	0.2 %
-0.0499	-201.5	-172.7	-173.1	-0.4	0.2 %	0.1 %
-0.0693	-251.7	-215.7	-214.0	1.7	0.8 %	0.3 %
-0.0886	-302.9	-259.6	-254.9	4.7	1.8 %	0.9 %
-0.1073	-351.7	-301.4	-294.3	7.1	2.4 %	1.4 %
-0.1262	-404.9	-347.0	-334.3	12.7	3.6 %	2.5 %
-0.1444	-455.0	-389.9	-372.7	17.2	4.4 %	3.4 %
-0.1626	-506.8	-	-411.3	-	-	-

*The measured value obtained from linear regression of the positive pressure calibration over the range 0 – 700 kPa, extrapolated into the negative range.

**FS = -500 kPa.



(a)



(b)

Figure 3-26 Negative pressure calibration: (a) pore-water pressure response to isotropic unloading; (b) pore-water pressure response to isotropic unloading adjusted with pore pressure parameters

3.3.2 Instrument performance

3.3.2.1 Temperature sensitivity

The sensors used in the assembly of the tensiometer were uncompensated for temperature, and it was expected that temperature would have an effect on the calibration of the device. Therefore, to test the tensiometer's response to temperature, a tensiometer fitted with a 5 bar AEV ceramic was saturated as per usual and held inside the cell along with a calibrated thermistor to monitor the temperature of the cell water.

The temperature of the water was at first increased by opening the cell drainage line and adding hot water to the cell through the air bleed with a large syringe. The temperature of the water was increased to above 50 °C and time was allowed for the water so circulate and distribute the heat to the tensiometers. Some cold water was flushed into the cell to remove air bubbles that were introduced into the cell before pressurising, which brought down the water temperature slightly. When a stable reading of the 41.3 °C was achieved, a simple calibration cycle with 100 kPa increments was performed. The steps were then repeated at 55.4 °C and 57.0 °C.

It was, however, difficult to control the temperature by adding hot water and each time removing excess air through flushing with cold water. Therefore, with the cell remaining sealed, the water temperature was decreased by flushing cold water from the deaerator through the cell with the drainage line open, or merely waiting for the water to dissipate heat into the atmosphere. The calibration cycles were then repeated at 46.0 °C, 36.3 °C, 29.7 °C, 25.3 °C, and 22.5 °C. These calibration cycles are shown in Figure 3-27.

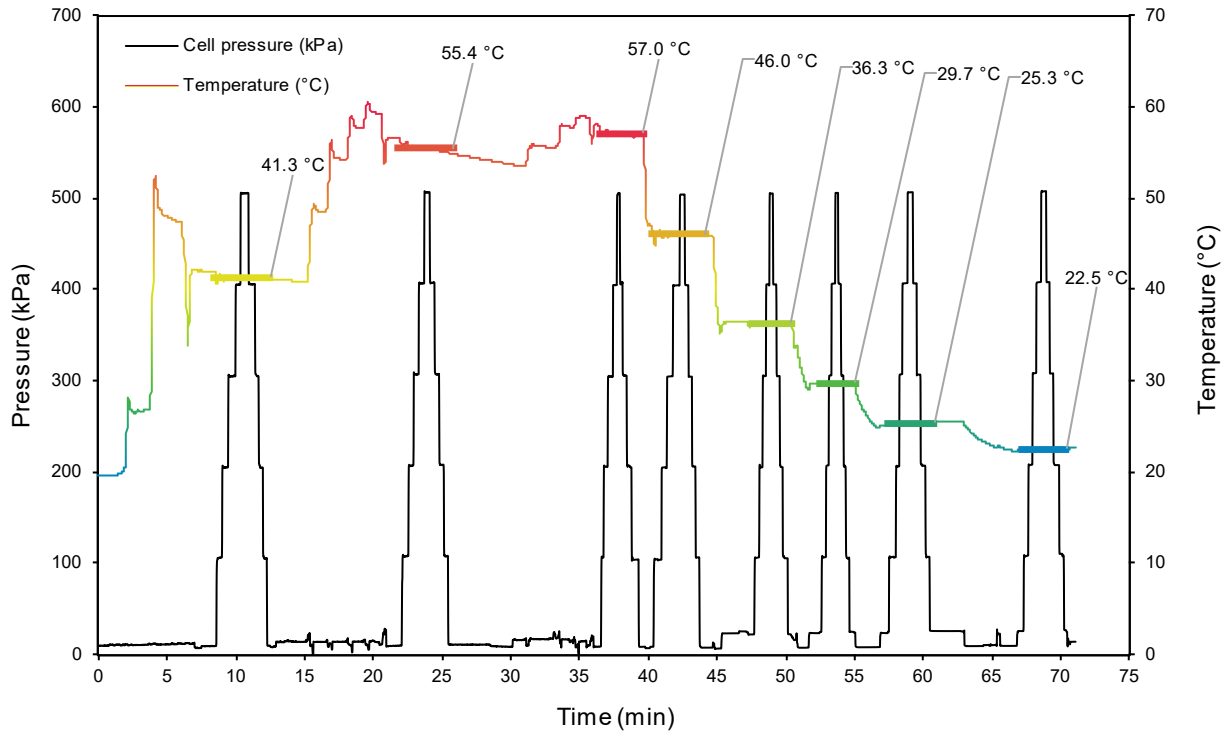


Figure 3-27 Temperature calibration cycles

Results

Table 3-6 presents the results of the temperature calibration procedure. The calibration at 25.3 °C (near room temperature) was taken as the baseline calibration and labelled Δu_0 . Each calibration cycle, $\Delta u_{\Delta T}$ produced a slightly different calibration constant, $\alpha_{\Delta T}$ (i.e. the slope of the calibration curve at temperature, ΔT) when compared to the baseline, α_0 .

As stated before, the measurement error of an instrument can be stated as a percentage of the full-scale range of the device. The full-scale pressure of the tensiometer was defined as -500 kPa, the same as the theoretical maximum AEV of the 5-bar AEV ceramic. The deviation of the pressure indicated by the tensiometer ($\Delta u_{\Delta T}$) to the baseline calibration (Δu_0) is given by $E = (\Delta u_{\Delta T} - \Delta u_0) \cdot \alpha_0$ (in units of pressure). The maximum value of E for each temperature was observed at the full-scale pressure of -500 kPa and is presented in Table 3-6. The maximum deviation observed was +19.6 kPa at 31.7 °C above the baseline.

The temperature sensitivity of the tensiometer can be generalised as $e = E / (FS \cdot \Delta T)$ in units of kPa/(kPa·°C) producing a correction factor that may be applied to the pressure indicated by the tensiometer for temperature-sensitive experiments. When expressed as a percentage, the average temperature sensitivity of the tensiometer was determined to be -0.12 %FS/°C.

Table 3-6 Results of temperature calibration

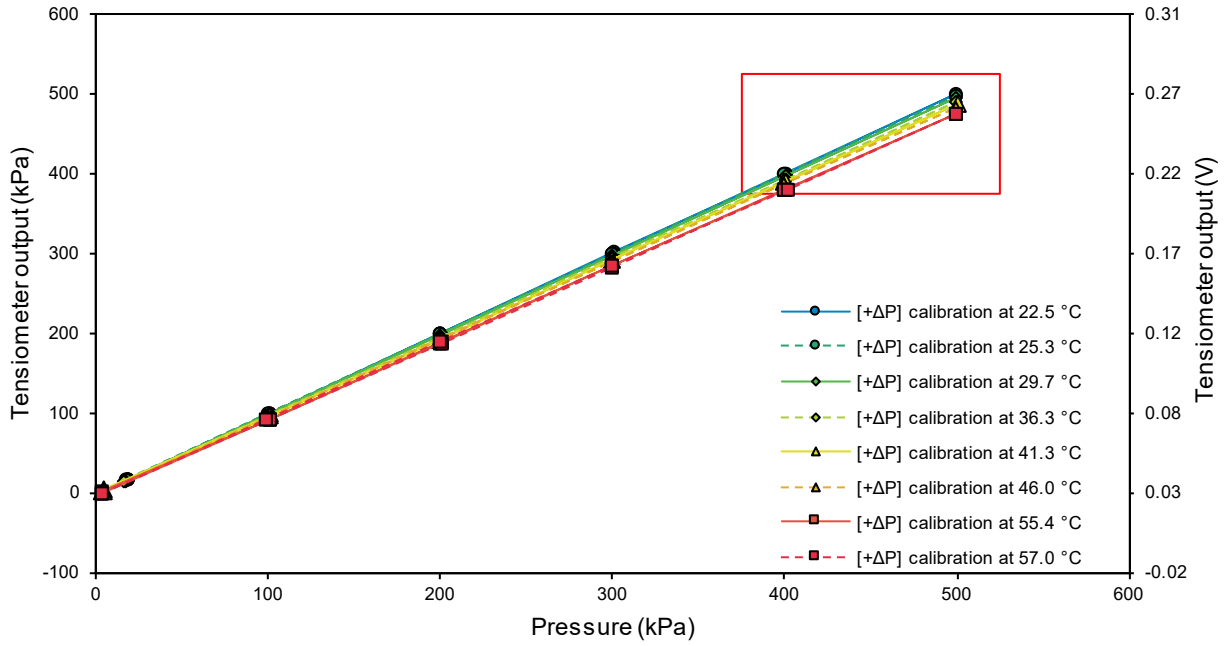
Imposed change in cell pressure Δp (kPa)	Temperature, T							
	22.5 °C	25.3 °C	29.7 °C	36.3 °C	41.3 °C	46.0 °C	55.4 °C	57.0 °C
	Relative temperature, ΔT							
	-2.8 °C	0.0 °C	+4.4 °C	+11.0 °C	+16.0 °C	+20.7 °C	+30.1 °C	+31.7 °C
	Tensiometer output, $\Delta u_{\Delta T}$ (V)							
Positive pressure calibration								
700	0.3624	0.3605	0.3588	0.3556	0.3531	0.3515	0.3459	0.3451
600	0.3147	0.3131	0.3116	0.3088	0.3067	0.3053	0.3004	0.3004
500	0.2671	0.2657	0.2644	0.2621	0.2603	0.2590	0.2549	0.2549
400	0.2194	0.2183	0.2172	0.2153	0.2139	0.2128	0.2095	0.2095
300	0.1718	0.1708	0.1701	0.1685	0.1675	0.1665	0.1640	0.1640
200	0.1241	0.1234	0.1229	0.1217	0.1211	0.1203	0.1185	0.1185
100	0.0764	0.0760	0.0757	0.0749	0.0747	0.0740	0.0730	0.0730
0	0.0288	0.0286	0.0285	0.0281	0.0280	0.0278	0.0276	0.0276
Negative pressure full-scale								
-500	-0.2095	-0.2085	-0.2075	-0.2058	-0.2039	-0.2035	-0.1998	-0.1992
Calibration constants								
$\alpha_{\Delta T}$ (kPa/V)	2098.1	2108.9	2119.0	2137.2	2155.3	2162.2	2199.3	2203.4
$\beta_{\Delta T}$ (kPa)	-60.4	-60.3	-60.3	-60.1	-60.6	-60.1	-60.6	-61.0
Error due to temperature								
	$E = (\Delta u_{\Delta T} - \Delta u_0) \cdot \alpha_0$				$e = E / (FS \cdot \Delta T)$			
E (kPa)	-2.2	-	+2.2	+5.6	+9.8	+10.7	+18.4	+19.6
e (kPa/(kPa·°C))	-0.0016	-	-0.0010	-0.0010	-0.0012	-0.0010	-0.0012	-0.0012
e' (% FS/°C)					-0.12 %			

*FS = -500 kPa

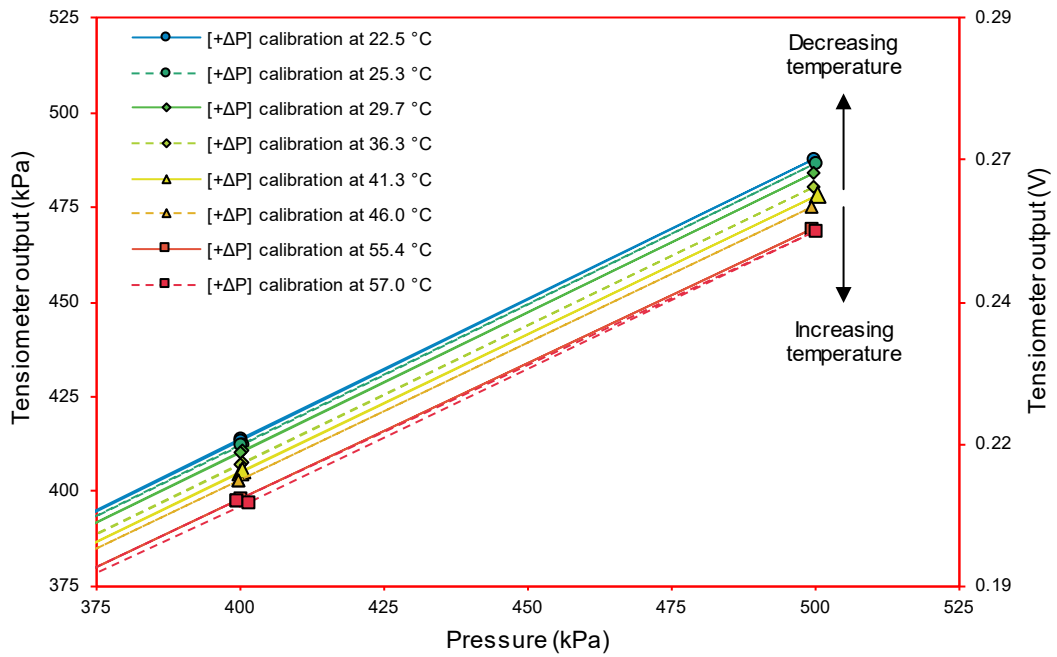
Calibration curves

Figure 3-28 (a) compares the resulting calibration curves in the positive pressure range at temperatures (ΔT). Figure 3-28 (b) shows a closer view of the influence of temperature on the measurements at higher pressures.

In these figures, it is shown that the effect of a tensiometer calibrated at room temperature and used at a higher temperature is an underestimation of the true value being measured. Conversely, the effect of an instrument calibrated at room temperature and used at a lower temperature is an over-estimation of the true value being measured. This holds true for the measurement of suctions and positive pore-water pressures since the slope of the calibration curve ($\alpha_{\Delta T}$) was altered by temperature influence and the intercept of the calibration curve ($\beta_{\Delta T}$) remained relatively constant (Figure 3-28 (a)).



(a)



(b)

Figure 3-28 Temperature calibration curves: (a) Range 0 – 600 kPa; (b) Range 375 – 525 kPa

Discussion

The sensors used in the assembly of the tensiometer were uncompensated for temperature, and it was expected that temperature would have an effect on the calibration of the device. As expected, the temperature did, in fact, influence the tensiometer measurements due to the temperature-uncompensated sensor chosen in its construction (technical specifications for the

“MS54XX” range of pressure sensors are provided in Appendix B). An error of $-0.12\% \text{FS}/^\circ\text{C}$ was deemed to be low enough not to consider its influence on the measured suctions presented in this study and was a scope limitation placed on the study.

The test performed considers only the influence of the sensor calibration due to temperature changes and does not consider factors such as a partially desaturated ceramic or the exchange of pore water between the soil and the water reservoir during suction measurement. Since matric suction is also temperature and relative humidity dependent, consideration of the components of suction being measured and partial vapour pressures are required to fully assess the temperature influence during actual suction measurements in temperature-sensitive experiments.

3.3.2.2 Measurement capacity

The capacity of the tensiometer to measure suctions was measured by allowing a fully saturated tensiometer of each type to dry out in air at room temperature (Figure 3-29).

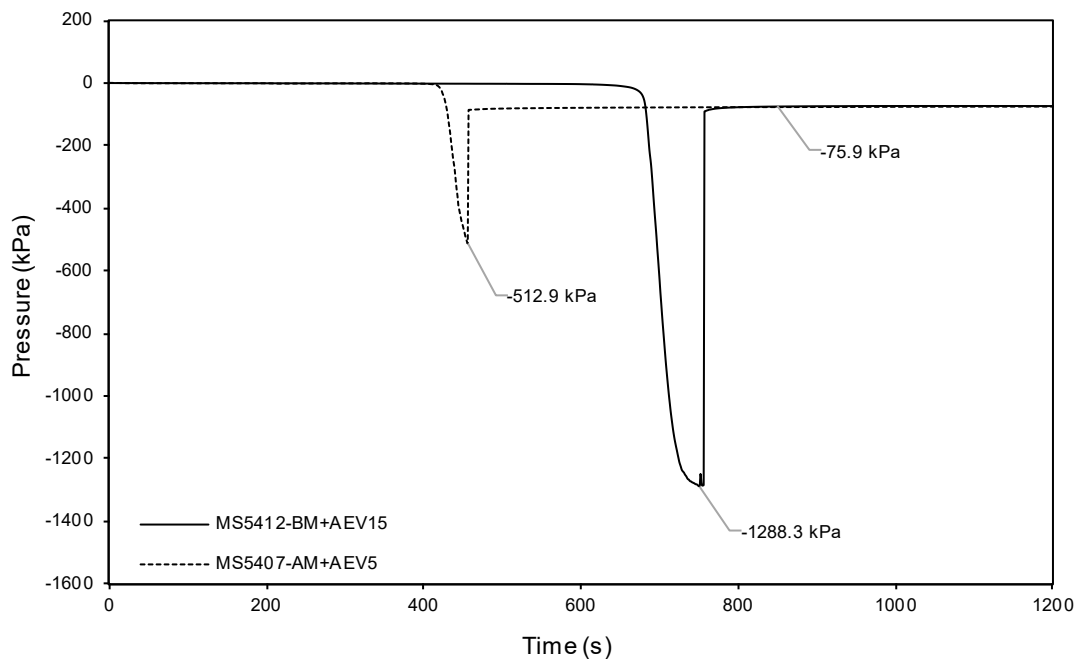


Figure 3-29 Tensiometer air-entry

The MS5407-AM+AEV5 tensiometer reached a maximum suction reading of -512.9 kPa before cavitation occurred. This was consistent for the 5 bar AEV ceramic reaching air-entry at -500 kPa . The MS5412-BM+AEV15, however, reached maximum suction reading of -1288.3 kPa before air-entry initiated followed by cavitation directly after that. This suggests that the typical air-entry pressure of 15 bar ceramic was not achieved. However, the levelling off of pressure prior to cavitation suggests that the air-entry pressure was being approached. It

is possible that the relatively low 1700 kPa pressure used to saturate (pre-pressurise) the tensiometer was not high enough or that the tensiometer should have been left to saturate for longer at that pressure to saturate the ceramic for this test thoroughly. Higher suctions may be attainable using custom saturation equipment that could increase the saturation pressure. However, this was outside the scope of the study and was reserved for future work.

4 DETERMINATION OF SOIL-WATER RETENTION CURVES

The experimental procedures undertaken in this study were divided into two focus areas. The first focus area was on the development of a tensiometer for the measurement of soil suction which was described in Chapter 3. The second focus area was on the determination of SWRCs for granular (non-volume change) soils using such a tensiometer. The intended outcome of the study was to evaluate whether the tensiometer could be used in a simplified, improved or more rapid method for determining SWRCs after the MIT technique (Toker *et al.*, 2004), or other proposed continuous drying techniques (e.g. Lourenço *et al.* (2011), Toll *et al.* (2013), Qingtian & Standing (2014) and Chen *et al.* (2015)).

In this chapter, a method for determining continuous SWRC using the tensiometer is described. The resulting suction measurements and SWRCs were compared with the filter paper method to analyse the effectiveness of the proposed method against known standards, for example, D5298-3 (ASTM, 2003) and D6836-02 (ASTM, 2002). Lastly, the study was expanded to investigate the feasibility of determining SWRCs for soils that undergo volume change during drying by introducing the measurement of dimensional change to the method.

4.1 MATERIALS

To evaluate whether the tensiometer could be used to determine SWRCs, a set of continuous drying tests was performed on different soils. The effective particle size (D_{10}) of a soil, and accordingly, the average pore diameter, is strongly correlated to the magnitude of soil suction (Yang *et al.*, 2004). Four samples were selected from real test pits and chosen to represent different soil textures with decreasing effective particle size. The fifth sample was a calibrated sand used for geotechnical centrifuge modelling (details of which are contained in Archer (2014)). Both non-plastic and plastic soils were tested. Table 4-1 contains the properties of the five sample soils tested.

The five soils tested were:

- Sample FS001 - a poorly graded silica sand (centrifuge modelling sand),
- Sample GT001 - a silty sand (representative gold mine tailings from a TSF),
- Sample TP148 - a clayey sand,
- Sample TP149 - an inorganic lean clay, and
- Sample TP016 - an inorganic highly plastic fat clay.

Table 4-1 Properties of soils tested

	<u>Fine sand</u>	<u>Gold tailings</u>	<u>Clayey sand</u>	<u>Lean clay</u>	<u>Clay</u>
Sample name	FS001	GT001	TP148	TP149	TP016
Unified Soil Classification System, (ASTM, 2017a)	SP Poorly graded sand	SM Silty sand	SC Clayey sand	CL Lean clay	CH Fat clay
Specific gravity, G_s	2.7026	2.6939	2.6746	2.6495	2.5662
Particle-size analysis results:					
Effective size, D_{10} (mm)	0.0797	0.0366	0.0093	0.0026	0.0017
D_{30} (mm)	0.120	0.079	0.039	0.011	0.0046
D_{50} (mm)	0.159	0.110	0.075	0.027	0.010
D_{60} (mm)	0.182	0.127	0.103	0.038	0.014
D_{90} (mm)	0.31	0.22	0.34	0.12	0.06
Coefficient of uniformity, C_u	2.35	3.65	11.60	14.64	8.75
Coefficient of curvature, C_c	0.97	1.36	1.60	1.23	0.90
Gravel (larger than 4.75 mm)	0 %	0 %	0 %	0 %	0 %
Fines (finer than 0.075 mm)	8.1 %	27.1 %	49.8 %	81.2 %	91.3 %
Atterberg limits (on minus 0.425 mm sieve fraction), (ASTM, 2017b):					
Liquid limit, LL	—	—	29	32	53
Plastic limit, PL	NP	NP	21	22	18
Plasticity index, PI	—	—	8	10	35
Linear shrinkage limit, LS	—	—	4.0	4.5	10.5

The specific gravity, G_s of each sample was determined with the *Micromeritics AccuPyc II 1340* gas Pycnometer. The average of three analyses was used to determine the specific gravity very accurately. An accurate value of the specific gravity was essential for determining the mass-volume relationships of each soil during testing.

The particle size distributions and cumulative particle size distributions for the soils tested are shown in Figure 4-1 and Figure 4-2. The distribution was produced from a *Malvern Mastersizer 2000* analysis that uses laser diffraction to calculate the percentage of particle sizes.

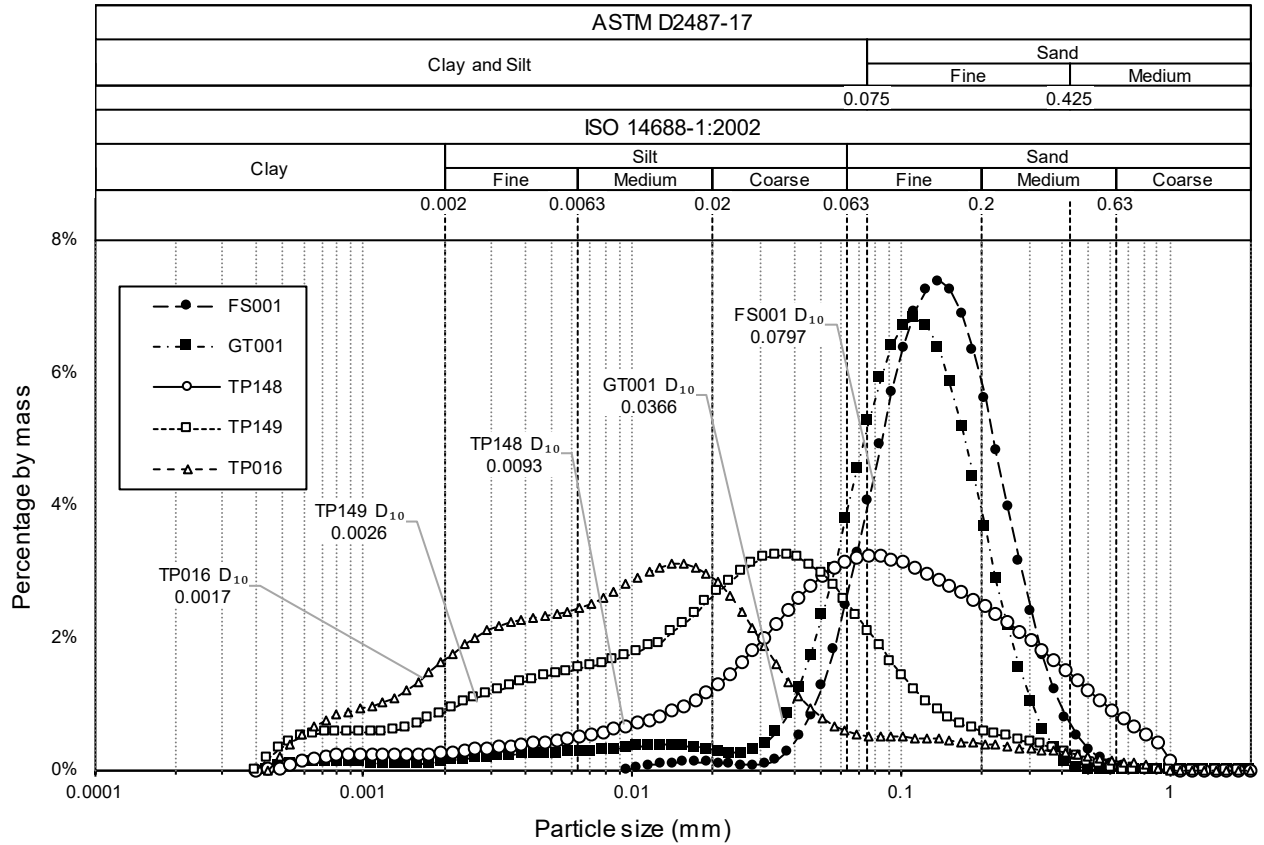


Figure 4-1 Particle size distributions

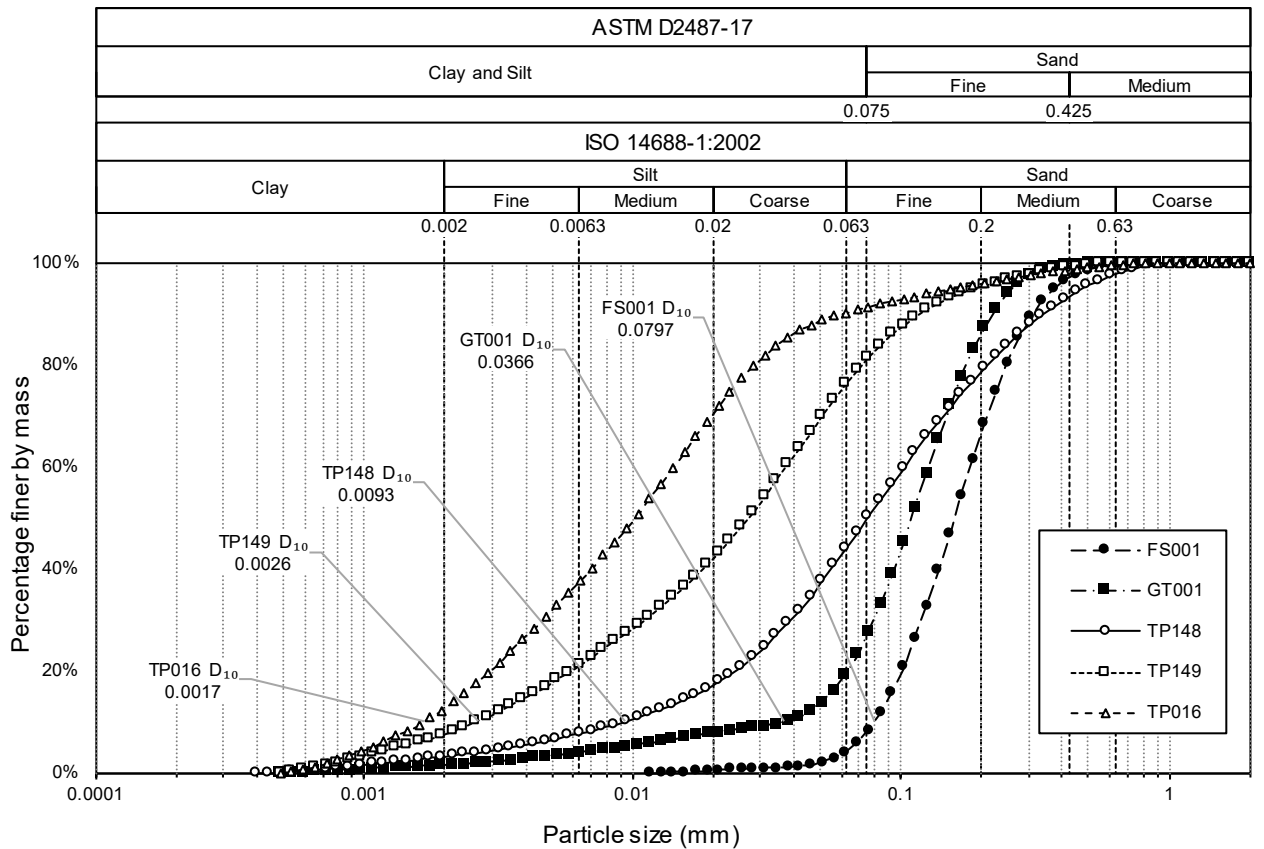


Figure 4-2 Cumulative particle size distributions

4.2 EXPERIMENTAL TEST SET-UP FOR CONTINUOUS DRYING TESTS

In this chapter, a method for determining continuous SWRCs using the tensiometer is described. The resulting suction measurements and SWRCs were validated by the filter paper method to analyse the effectiveness of the proposed method against known standards, for example, D5298-3 (ASTM, 2003) and D6836-02 (ASTM, 2002). Lastly, the study was expanded to investigate the feasibility of determining SWRCs for soils that undergo volume change during drying by introducing the measurement of dimensional change to the method.

4.2.1 Continuous drying with hanger set-up

The validity of the proposed method was first evaluated with a simple set-up for continuously weighing an initially saturated soil specimen containing two tensiometers. It consisted of a steel hanger fitted on one end with four strain gauges forming a Wheatstone bridge electrical circuit. The weight of the specimen placed on the opposite end of the hanger could be registered through the bending of the hanger. Figure 4-3 shows this test set-up.

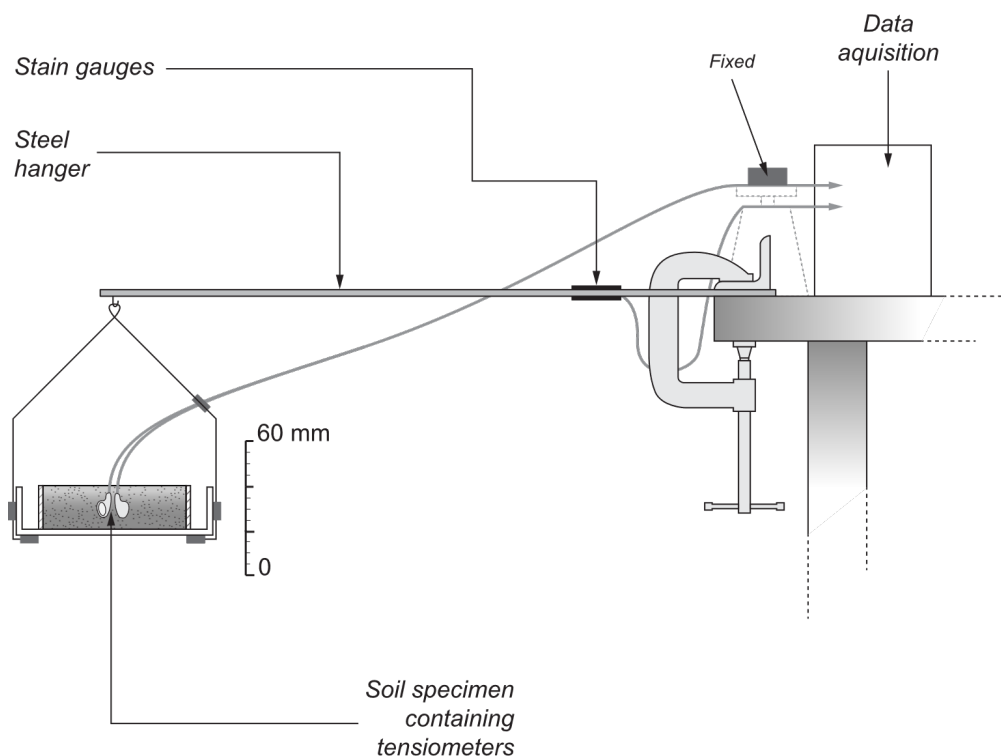


Figure 4-3 Test set-up on strain-gauged hangers

This first set-up, although crude, yielded satisfactory results. An accelerated record of the suction generated in three specimens of soil drying under floodlights could be combined with the record of the decreasing mass of the soil specimens with time to produce a gravimetric SWRC (Figure 4-4). However, the measurement sensitivity of the strain-gauged hanger was

low. The set-up was also susceptible to air currents, temperature changes and vibrations in the laboratory.

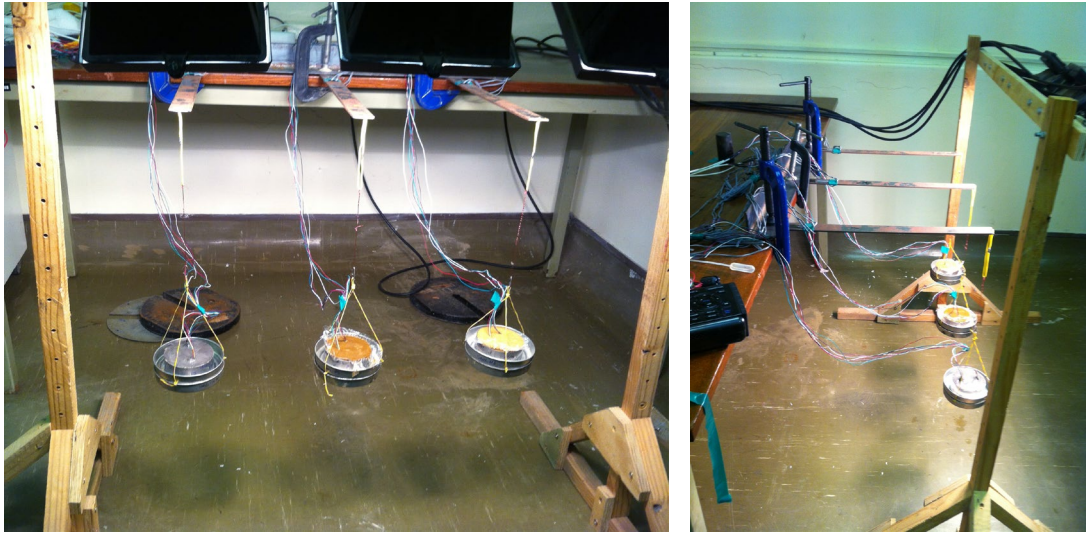


Figure 4-4 Complete continuous drying test set-up on strain-gauged hangers

4.2.2 Continuous drying with laboratory balance and environmental enclosure set-up

The experimental set-up was then graduated to the use of a high precision digital laboratory balance with data recording capabilities as described below.

4.2.2.1 Test set-up

The test was performed in an enclosed chamber constructed from wood with extruded polystyrene foam insulating the walls of the enclosure. The purpose of the enclosure was to regulate the temperature and humidity of the test environment. The front of the enclosure was also fitted with a transparent acrylic panel to allow for viewing. A camera was used to monitor the dimensional change of the specimen. The camera was mounted on the roof of the enclosure over a viewing port. The specimen's diameter could be monitored from above, while a precisely angled mirror gave a view of the specimen's height. A light inside the enclosure helped to illuminate the specimen. A heat source, in the form of an incandescent light bulb, was used to increase the temperature in the enclosure. A small diameter cooling fan from a personal computer was fitted to the roof of the enclosure over a ventilation hole. The fan was used to extract humid, hot air from the environment and help regulate the temperature inside the enclosure. A thermistor was used to monitor the temperature in the enclosure. The test set-up is shown in Figure 4-5 and Figure 4-6 with more detail shown in Figure 4-7 and Figure 4-8.

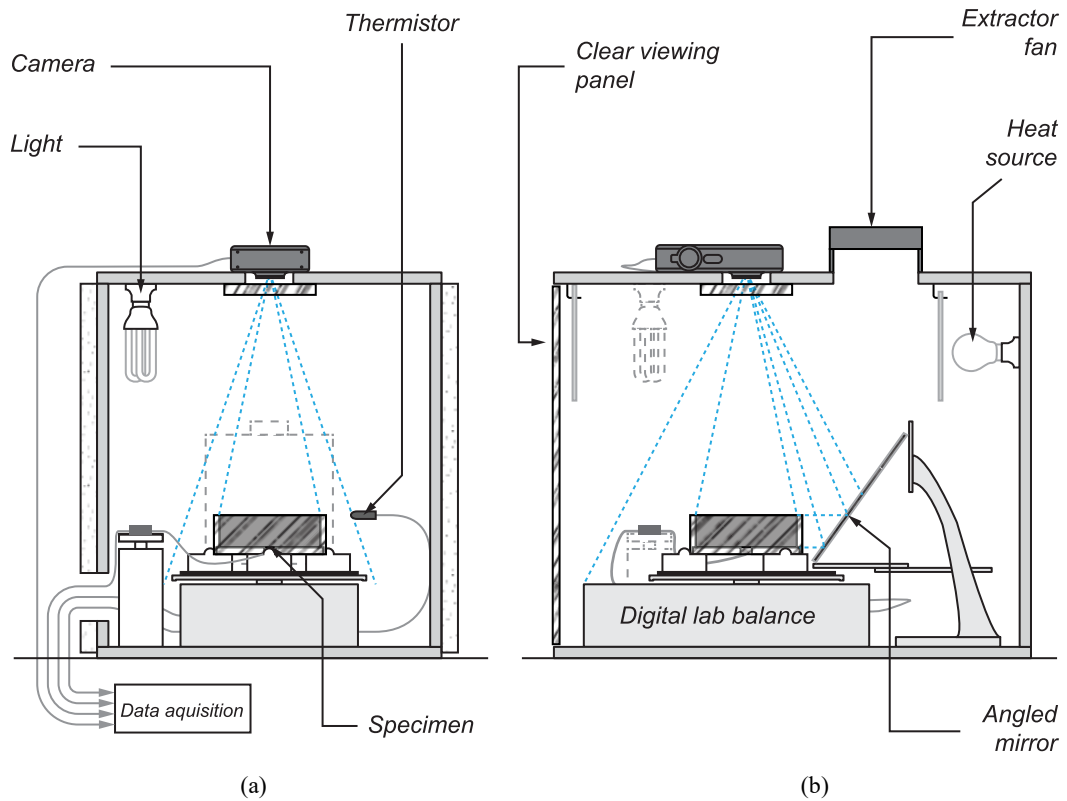


Figure 4-5 Continuous drying test set-up diagram: (a) front section view; (b) side section view

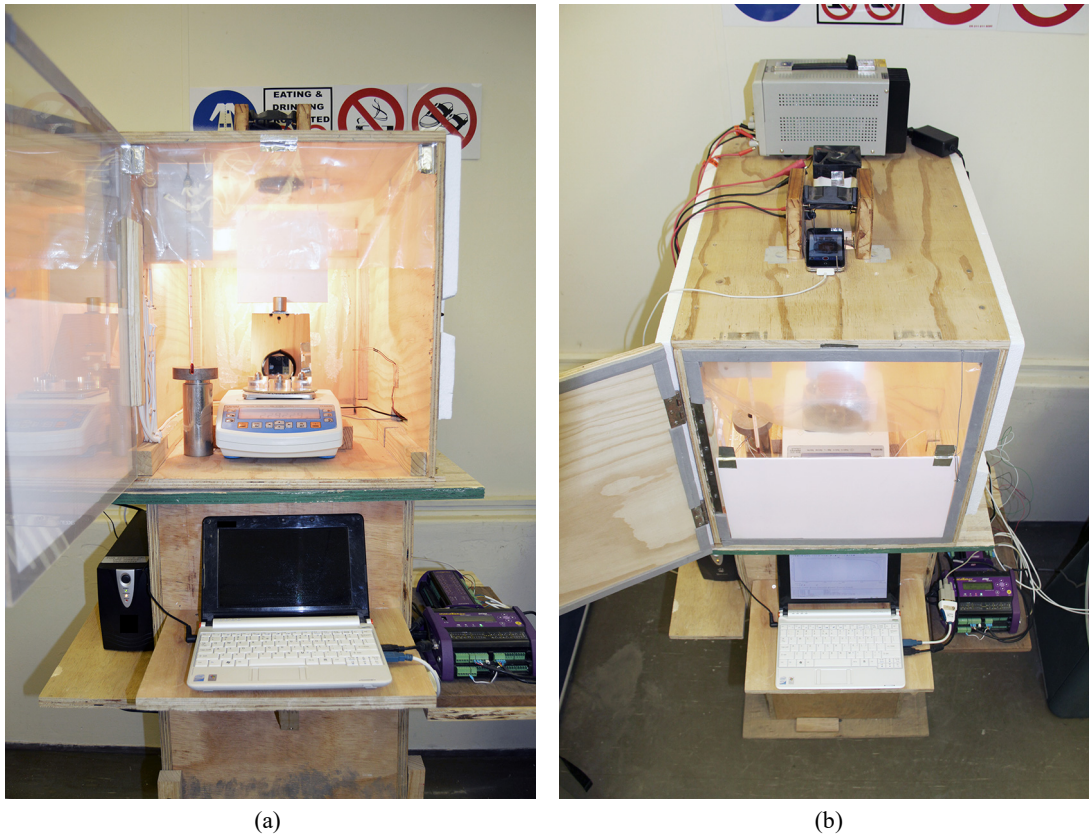


Figure 4-6 Continuous drying test set-up inside environmental enclosure: (a) prior to test; (b) during test

The test set-up (shown in Figure 4-7 and Figure 4-8) consisted of a *Radwag P600.R2* precision laboratory balance (S/N: 411643/3), a clear acrylic specimen container with a removable bottom, placed on a centring pedestal, and two tensiometers embedded in an initially saturated soil specimen.

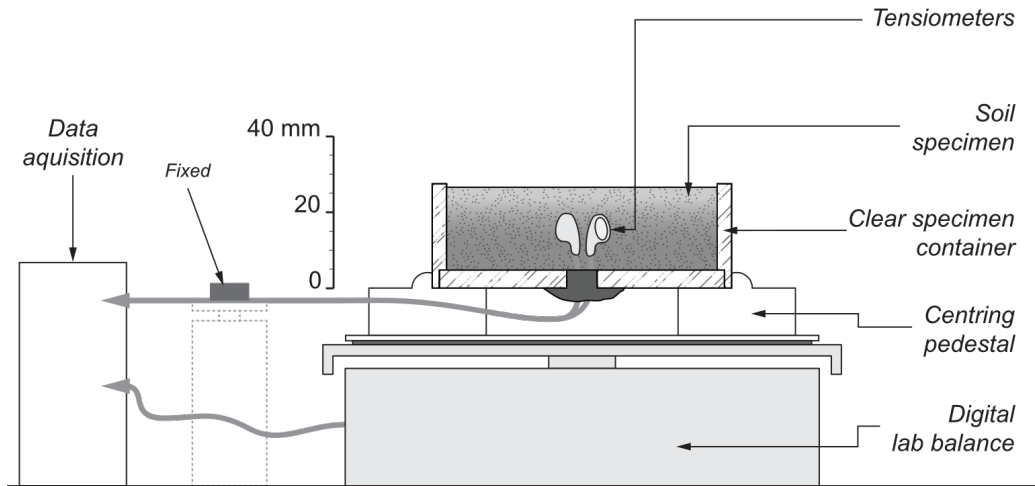


Figure 4-7 Essential continuous drying test set-up



Figure 4-8 Continuous drying test set-up during testing

4.2.2.2 Equipment

The equipment used for the continuous drying test is listed and described below.

- A transparent specimen container was used to hold the specimen being tested. The specimen container consisted of a clear outer ring in which a bottom plate was press-fit into place. The dimensions of the specimen container were 23.3 mm in height and 71.6 mm in diameter. The bottom had a centrally located hole, large enough for the head of a tensiometer to be inserted through (Figure 4-9). The tensiometers were inserted from the bottom of the specimen to limit boundary effects and cracking of the specimen due to the presence of the signal cables. This also allowed the camera an unobstructed view of the specimen from above.
- As with Toker (2002), the experimental set-up necessitated the need for thin cable connections to the tensiometers, such as the configuration in Figure 3-1. The cables could induce instability in the mass readings due to its own mass and relaxation with time.
- A centring pedestal was used to centre the specimen on the laboratory balance and raise it slightly, allowing the cables of the tensiometers to protrude from the bottom of the specimen container (Figure 4-7 and Figure 4-9). The cables were fixed to a small pedestal to the side of the balance to limit instability in the mass readings.
- Petroleum-based modelling clay was used as a sealing putty to seal the hole in the bottom plate around the tensiometer cables.
- A very light application of petroleum jelly was used to coat the inner surfaces of the specimen container. This helped to prevent the specimen from sticking to the specimen container or inducing cracks from forming in the specimen as it shrank during drying.
- A palette knife was used to place and smooth the specimen in the specimen container.
- A digital calliper was used to measure the dimensions of the specimen before, during and after the test.

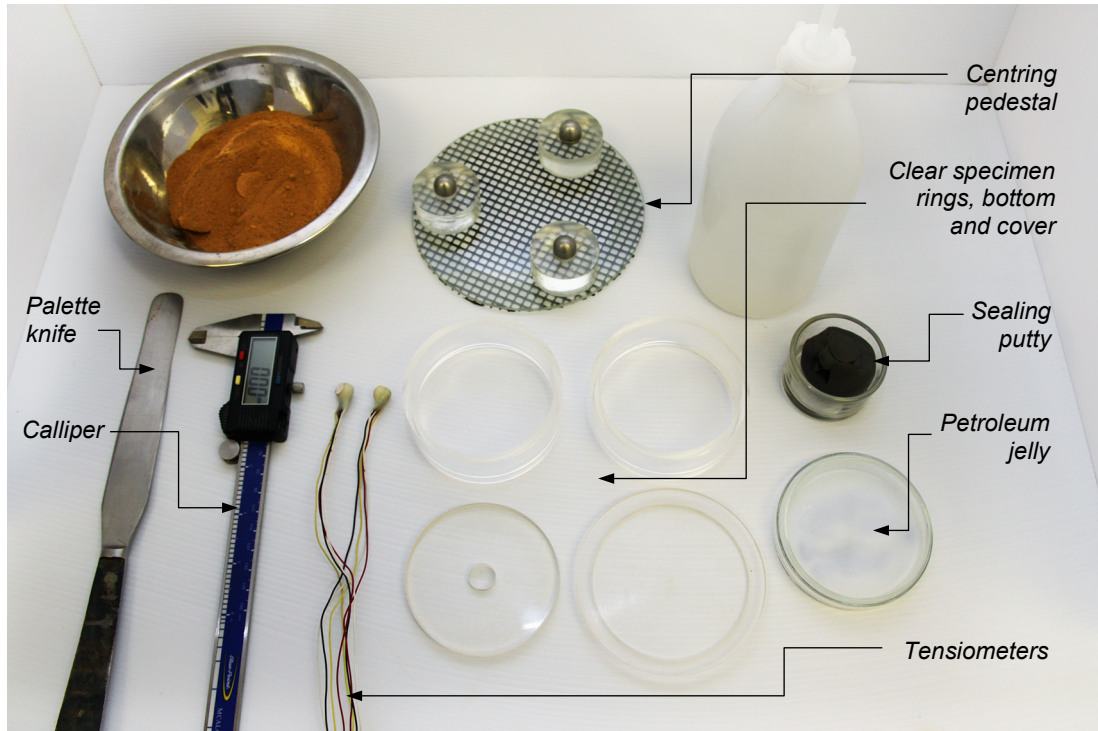


Figure 4-9 Equipment for placement of soil specimen

4.2.2.3 Test set-up preparation

The procedure for setting up the continuous drying test is listed below:

1. The heat source and ventilation fan were turned on to allow the environmental enclosure to reach thermal equilibrium (Figure 4-6 (a) and (b)).
2. The temperature inside the environmental enclosure was monitored through the data acquisition system.
3. When the enclosure had reached a stable temperature, the digital laboratory balance reading was zeroed.
4. A very light coating of petroleum jelly was applied to the inner surfaces of the specimen container.
5. Each of the components of the set-up was then weighed and their masses recorded.

4.2.2.4 Specimen preparation

The procedure for setting up the continuous drying test continues with specimen preparation, as is listed below:

6. The sample was first sieved to a uniform consistency and oven-dried at 60 °C.
7. The specimen was then prepared by mixing the sample soil with freshly prepared de-aired water to a uniform slurry-like consistency. The slurry-like consistency ensured

uniformity between specimens for comparison purposes and reduced the risk of the specimens cracking during drying. Alternatively, the specimen was prepared at a known gravimetric water content.

8. Entrained and entrapped air bubbles created during mixing were removed by placing the specimen in a vacuum desiccator connected to a vacuum pump for a few minutes (Figure 4-10). This ensured that almost all of the air could be removed from the specimen so that the volume of the soil could accurately be determined.



Figure 4-10 Equipment for mixing of soil specimen

9. Two tensiometers were placed inside the specimen container through the bottom plate (Figure 4-11 (a)).
10. Petroleum-based modelling clay was used to seal the hole around the tensiometer cables in the bottom of the bottom plate.
11. A firmly adhering aluminium flashing tape was used to fix the cables to the bottom of the specimen container (Figure 4-11 (b)).
12. Throughout the process, the tensiometer response was monitored in case brief exposure to the air would induce premature desaturation resulting in cavitation. The faces of the tensiometers were, therefore, continually wetted with de-aired water to prevent premature cavitation.

13. The prepared soil specimen was then placed into the specimen container, making sure to cover the ceramic faces of the tensiometers and prevent them from drying out (Figure 4-11 (c)).
14. The top of the specimen was then levelled and smoothed to the top of the specimen container.
15. The specimen was placed on the centring pedestal, and a small amount free water was added to the top surface of the specimen with a pipette and covered to prevent moisture loss (Figure 4-11 (d)).

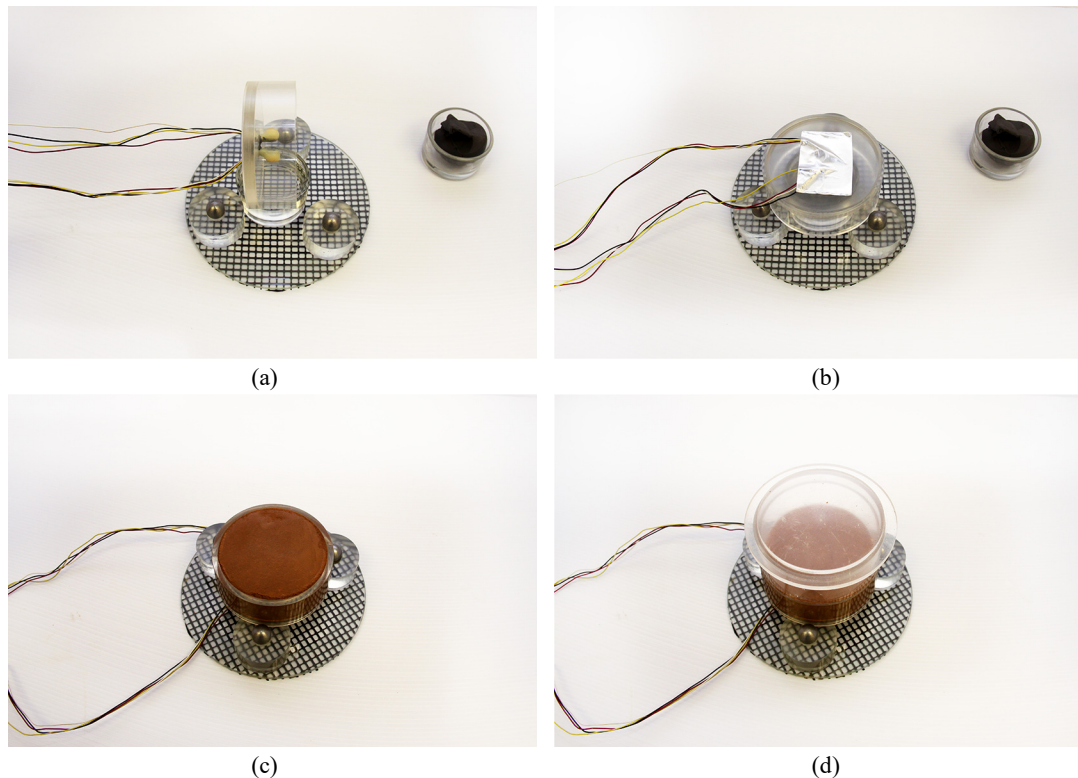


Figure 4-11 Test specimen placement: (a) placement of tensiometers; (b) sealing cables into specimen container; (c) placement of saturated soil; (d) addition of free water and cover

4.2.2.5 Continuous drying test procedure

When the specimen has been prepared, the test could proceed using the steps listed below:

16. The specimen, along with the centring pedestal and specimen container cover, was then placed on the laboratory balance.
17. Any spilt water droplets on the balance platform or the sides of the specimen container were soaked up with paper towelling.
18. The cables of the tensiometers were supported on a stand and under a small weight next to the laboratory balance and routed to the data acquisition system through a hole in the side of the enclosure.
19. The door of the enclosure was then closed.

20. While keeping the specimen covered and with sufficient free water, the specimen and test equipment was allowed to reach the ambient temperature inside the enclosure. This step allowed any temperature effects of the tensiometers to be mitigated and also allowed the tensiometer cables to reach their full slack (Figure 4-12).
21. From the time the specimen was placed on the balance, data acquisition was started. This included the recording of the tensiometer output, mass readings, enclosure temperature, and time-lapse photography of the specimen dimensions.
22. When both the tensiometer output and mass readings had stabilised (indicating that the test set-up had reached thermal equilibrium) the test was started.
23. The door of the enclosure was very briefly opened to remove the cover from the specimen.
24. The specimen was then allowed to dry naturally in the enclosure.
25. When both tensiometers had reached their maximum suction measurement, and cavitation had occurred, or the specimen had been dried to near-zero water content, the test was concluded.



Figure 4-12 Continuous drying test set-up in the enclosure

4.2.2.6 Disassembly of test equipment and post-processing specimen

After the test had been concluded, the equipment could be disassembled, and the final measurements could be made as follows:

26. The specimen was removed from the environmental enclosure (Figure 4-13 (a)).
27. First, the aluminium flashing tape and sealing putty were removed and collected in a petri dish for weighing (Figure 4-13 (b)).
28. The specimen was then carefully removed from the specimen container (Figure 4-13 (b)).
29. The outer dimensions of the specimen were recorded using the digital calliper. Four equally spaced measurements of the specimen height and diameter were taken (Figure 4-13 (c)).
30. The tensiometers were then removed from the specimen. Care was taken to collect the entire specimen for weighing (Figure 4-13 (d)).
31. The specimen container was left uncleaned and collected for weighing with the petroleum jelly coating and small amounts of the specimen that remained on the surface. The slight error in measurement of the specimen mass and ultimately the final water content of the specimen was considered to be negligibly small compared to the specimen dimensions used.

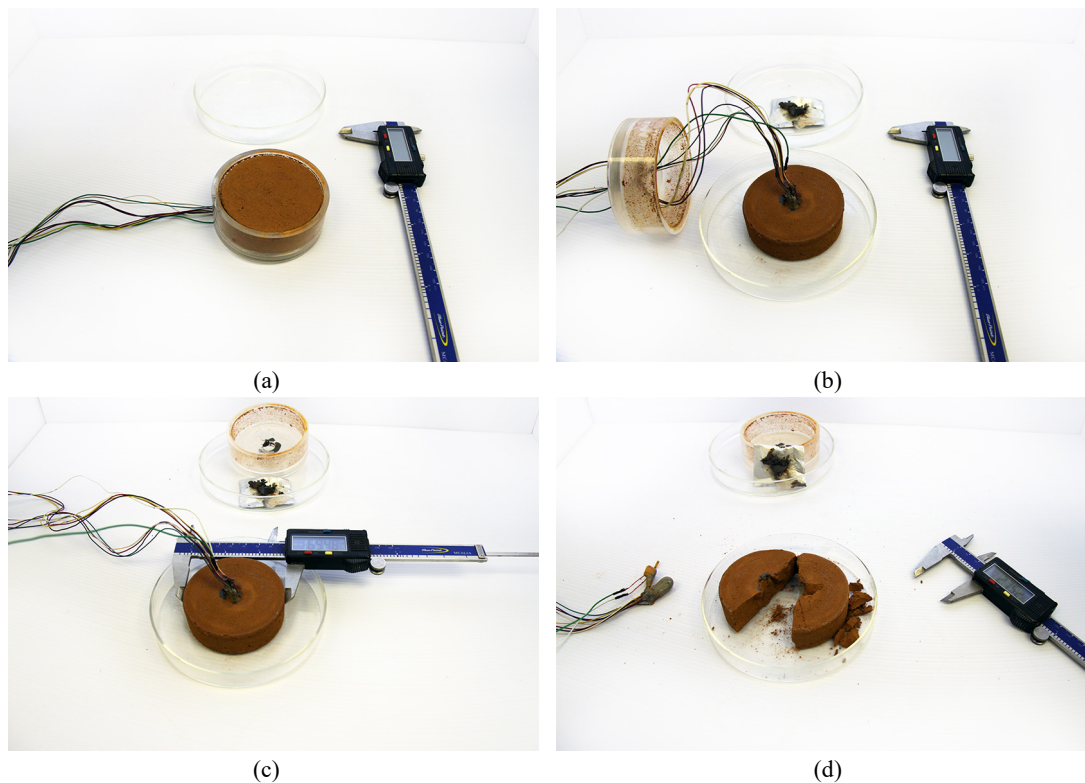


Figure 4-13 Processing of specimen after test:(a) specimen removed from balance; (b) removal of specimen container; (c) determination of specimen dimensions; (d) removal of tensiometers

4.2.2.7 Data processing

Figure 8-1 in Appendix A shows a data processing flow-chart used to convert the various data collected into SWRCs and together with Equations 8.1 and 8.2, the shrinkage curves for volume change soils.

4.3 COMPARISON OF RESULTS

The resulting suction measurements from the continuous drying procedures described above were compared with the filter paper method as described below. A series of suction measurements for each sample was used to construct SWRCs in the conventional method and could then be compared to the SWRCs determined from the tensiometer readings.

4.3.1 The filter paper method

As discussed in Section 2.3.1.1, the filter paper method has proven to be a reliable way to verify the results of comparatively new tensiometer studies. The ASTM D6836-02 standard method (ASTM, 2002) describes the method for the determination of SWRCs for desorption (drying). Although the standard omits the filter paper method, it is considered as a valid method of indirectly evaluating matric and total suction in ASTM D5298-03 (ASTM, 2003).

The filter paper used in this study was *Whatman* No. 42 ashless filter paper (Figure 4-14). The Greacen *et al.* (1987) piecewise-defined calibration curve was used to determine the suctions of each sample at different water contents. The calibration function in an adapted form from the current standard (ASTM, 2003) is given in Equation 2.9 (Section 2.3.1.1).



Figure 4-14 *Whatman* No. 42 filter paper

Test procedure

The test procedure used to determine filter paper suctions was slightly modified from the standard method. The procedure and modifications are described by steps 1 – 10 below:

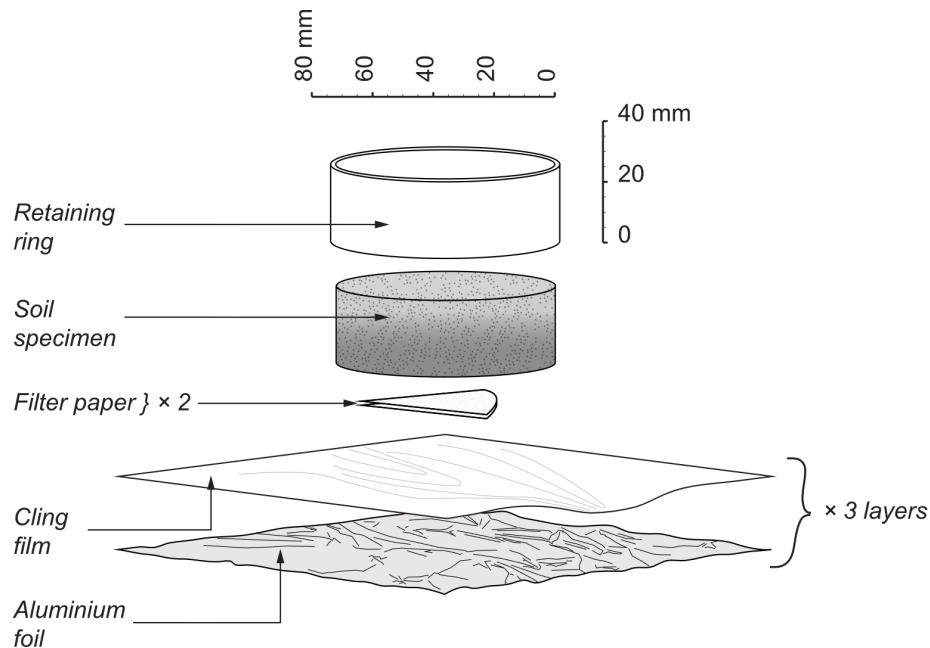


Figure 4-15 Filter paper specimen

1. The sample was first sieved to a uniform consistency and oven-dried at 60 °C.
2. Specimens were then prepared by mixing a specific mass of the sample soil with freshly prepared de-aired water to a series of known gravimetric water contents and targeted dry densities.
3. Wedges of filter paper were cut to fit inside the retaining rings.
4. The specimens were placed in retaining rings with two wedges of filter paper in contact with the soil and wrapped with multiple layers of cling film and aluminium foil to prevent moisture loss. Since only the matric suction component was of interest to the study, the contact filter paper method was used. Therefore, there was no need to enclose each specimen in a sealed container with separation of the filter paper and soil (Figure 4-15).
5. The filter paper was placed underneath the specimen rather than inside it and kept in contact with the soil by the weight of the specimen and the layers of cling film and aluminium foil. The procedure followed departed from the standard test procedure (ASTM, 2003). This change was made in order for the volume of the specimen to be more easily determined by keeping the specimen intact and contained in the retaining ring of known dimensions. The volume of the specimen was required to calculate the void ratio, and ultimately, the degree of saturation.

6. The specimens and filter paper were left to equilibrate for a minimum of one week, but for improved accuracy three weeks were allowed.
7. The specimens were then unwrapped one at a time, and the wet mass of each of the filter paper wedges was measured in quick succession using the *Mettler B5* precision single pan balance with a resolution of 0.0001 g (Figure 4-16).
8. The wet mass of the specimen was measured using the *Radwag P600.R2* precision laboratory balance before unwrapping the next specimen to prevent moisture loss during measurement.
9. After all the specimens have been weighed, the specimens and filter paper wedges were dried in an oven at 60 °C for 24 hours.
10. The dry masses of the specimens and filter paper wedges, the retaining rings and sample tins were then measured to determine the water contents after drying (Figure 4-17).



Figure 4-16 *Mettler B5* single-pan precision balance



Figure 4-17 Filter paper specimens after oven-drying

Discussion

Additional specimens were prepared with two filter papers on the bottom and two filter papers on the top of the specimen to evaluate whether filter papers placed on the bottom will absorb more water owing to the effects of gravity. It was found that a slight bias towards lower suction values was obtained from the filter paper placed on the bottom of the specimen, but only for specimens that were prepared above a degree of saturation of about 0.9 (very ‘wet’ specimens) and left to equilibrate for only one week. Results from specimens prepared at degrees of saturation of lower than 0.9 did not differ significantly. The error with these specimens showed a significant degree of scattering from the expected results rather than a bias towards lower suctions.

Conversely, no significant difference in measured suction was observed between specimens left to equilibrate for longer than the recommended one week. The time allowed for moisture transfer from soil to filter paper to reach equilibrium ultimately was thus extended from the recommended one week to three weeks for improved accuracy.

5 EXPERIMENTAL RESULTS AND DISCUSSION

This following chapter presents a discussion of the results obtained from the procedures for determining SWRCs for five different soil samples using the continuous drying method described in Section 4.2.2 and the tensiometer described in Chapter 3.

First, the results and SWRCs determined using the tensiometer for the granular soil samples are presented and discussed. These results are then compared to SWRCs derived from the filter paper method. Secondly, a similar set of results for the fine-grained soil samples with the addition of the measured shrinkage curves are presented and discussed. Lastly, the chapter concludes with general findings on the use of the tensiometer and the methods for determining SWRCs employed in the study.

5.1 SOIL-WATER RETENTION CURVES OF GRANULAR SOILS

The second primary focus of the study was the determination of SWRCs for granular (non-volume change) soils using the tensiometer developed in Chapter 3 and the experimental procedures outlined in Chapter 4. This section will discuss the results of these experimental procedures and offer a comparison to the results from the conventional filter paper method.

5.1.1 Testing program for granular soils

In total, five tests on two different granular samples were performed using the continuous drying and tensiometer method. The material properties for these samples are contained in Section 4.1. All the specimens were tested from an initially “over-saturated” slurry and allowed to dry in the enclosure as described in Section 4.2.2. A set of filter paper measurements were also taken for each sample on specimens prepared at a specified density as described in Section 4.3.1. The tests were performed at the specified specimen densities and are identified as listed below:

- Sample FS001: Fine sand
 - ‘FS001 Test #1’, $\rho_d = 1.65 \text{ g/cm}^3$
 - ‘FS001 Test #2’, $\rho_d = 1.71 \text{ g/cm}^3$
 - Filter paper suctions, $\rho_d = 1.58 \text{ g/cm}^3$
- Sample GT001: Gold mine tailings
 - ‘GT001 Test #1’, $\rho_d = 1.63 \text{ g/cm}^3$
 - ‘GT001 Test #2’, $\rho_d = 1.66 \text{ g/cm}^3$
 - ‘GT001 Test #3’, $\rho_d = 1.64 \text{ g/cm}^3$
 - Filter paper suctions, $\rho_d = 1.57 \text{ g/cm}^3$

5.1.2 Sample FS001: Fine sand – tensiometer method

Figure 5-1 (a) and (b) show the record of tensiometer response over time in Test #1 and Test #2 of sample FS001, respectively. Two tensiometers were inserted into each specimen, labelled T1 and T2 for Test #1, and T3 and T4 for Test #2. As in Sections 3.3.1 – 3.3.2, the sensor type and AEV of the ceramic filter are also indicated.

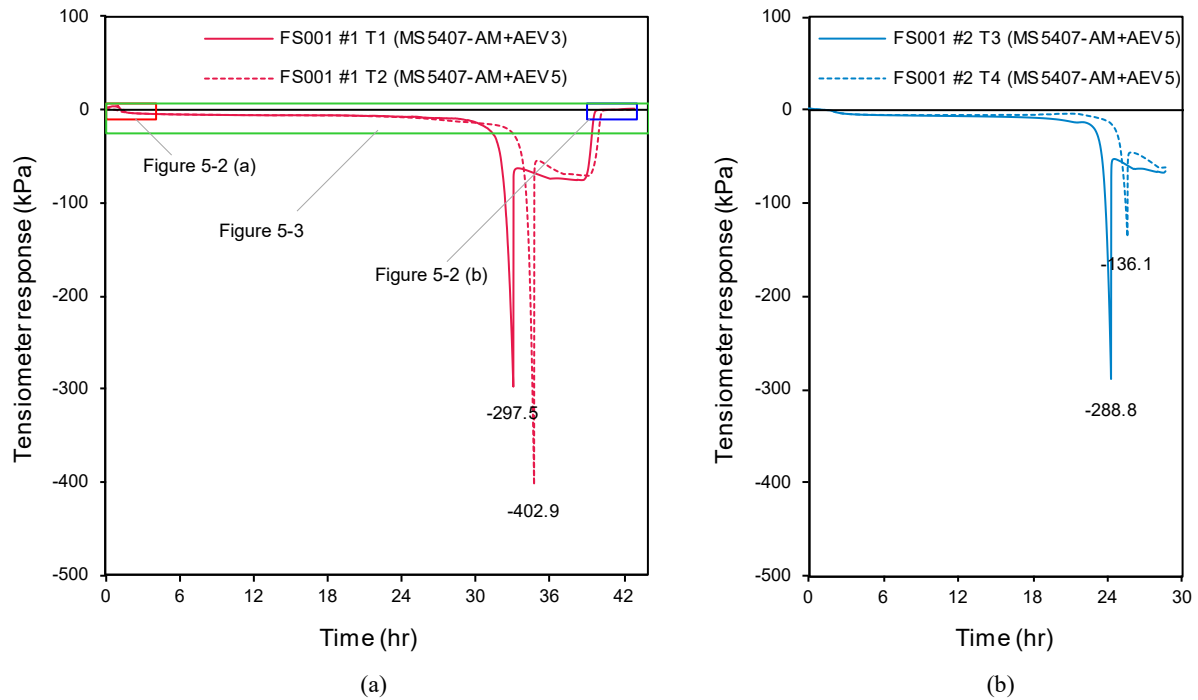


Figure 5-1 Tensiometer desaturation in sample FS001: (a) Test #1; (b) Test #2

Ensuring a consistent and accurate reading of the zero-pressure offset was required to interpret the SWRC at high water contents and low suction values, particularly for granular soils that typically generate very low suctions for most of the water content range. A closer look at the start and end of Test #1 shows how the tensiometer response was interpreted to confirm the zero-pressure offset in two ways. In Figure 5-2 (a) a small positive pore-water pressure is shown to dissipate linearly over time, consistent with the evaporation of free water on the surface of the specimen, between the evaporation of free water and where the slope of the tensiometer response increases is the zero-pressure offset. Beyond this point, a small negative pore-water pressure was generated while the specimen remained saturated up until the air-entry pressure of the specimen. Beyond the air-entry pressure, the specimen started to desaturate. After some time, the tensiometer would lose its hydraulic link with the pore water and experience air-entry or rapidly desaturate up until cavitation, as shown in Figure 5-1 (a) and (b). After cavitation, the tensiometer response would reflect the local vapour pressure for a period while a stable vapour or air bubble exists in the tensiometer reservoir. Further desaturation of the tensiometer

system occurred until the tensiometer response returned to the local atmospheric pressure, interpreted as the zero-pressure offset, as shown in Figure 5-2 (b).

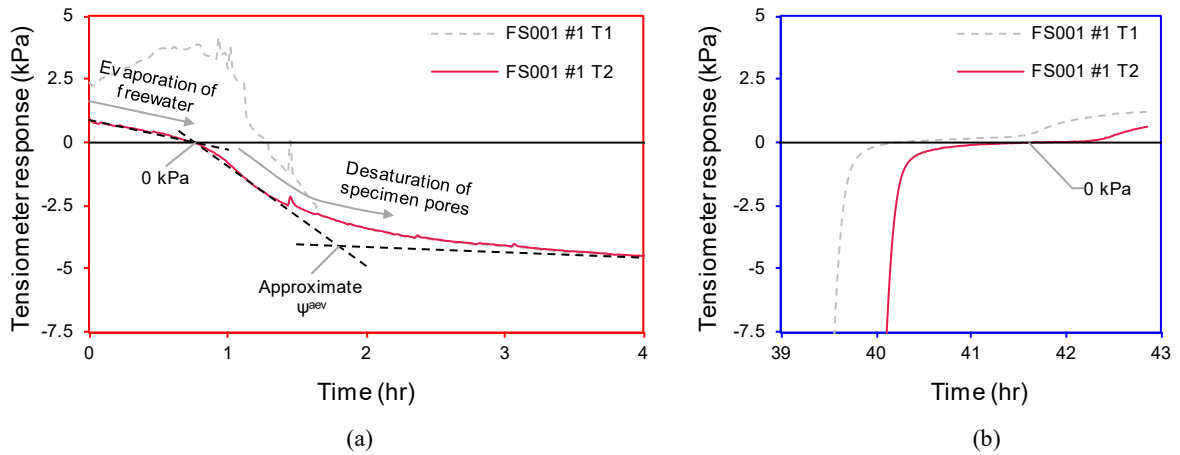


Figure 5-2 Zero-pressure offset confirmation: (a) at start of desaturation; (b) after cavitation; for Test #1

As just stated, at some point during the test, the tensiometer would lose its hydraulic link with the pore water. From this point onwards, the measurement system was no longer in equilibrium with the pore water in the specimen, and the tensiometer response would reflect desaturation of the tensiometer filter rather than the matric suction being developed. Figure 5-3 shows where filter desaturation of each tensiometer in the specimen was determined for Test #1. For tensiometer T1 it appears that low saturation or contamination of the water reservoir led to the expansion of nucleated air bubbles after -6.0 kPa. This is also supported by the erratic response of tensiometer T1 at the start of the test suggesting the presence of a pre-existing air bubble in the measurement system. Tensiometer T2, however, was able to keep good hydraulic contact with the pore water up to a pressure of about -12.7 kPa. After this point, the tensiometer would desaturate further until cavitation occurred, as shown in Figure 5-1 (a).

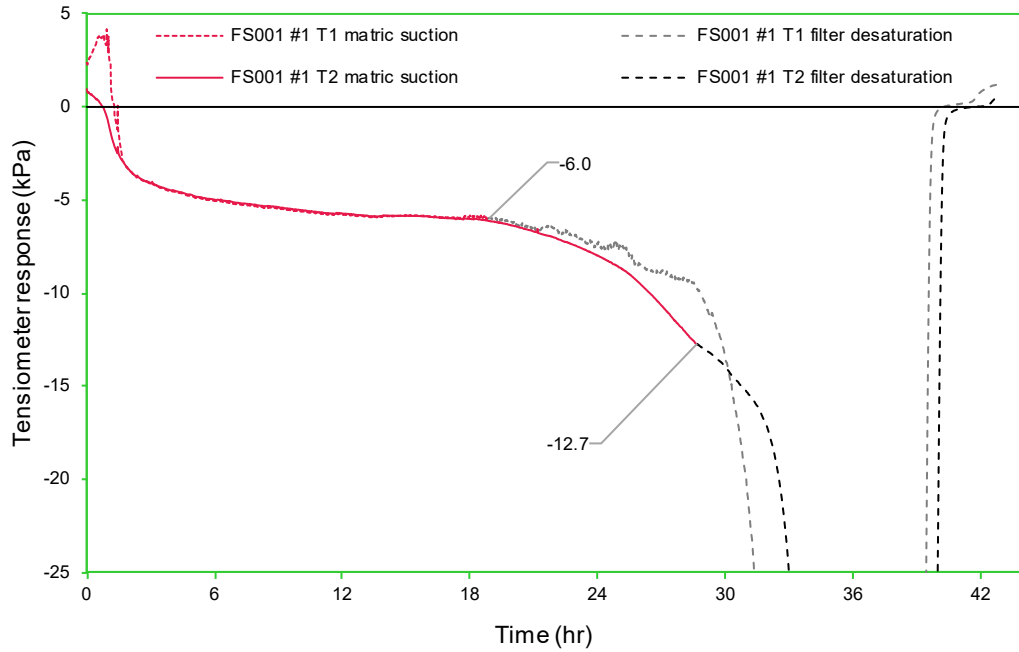


Figure 5-3 Matrix suction vs filter desaturation for Test #1

With the zero-pressure offset and the extent of matric suction measurement correctly determined, the negative tensiometer response could be converted to matric suction used to construct the SWRC.

Figure 5-4 (a) and (b) show the water content and temperature records of each specimen as they desaturated in the environmental enclosure. The average enclosure temperature for Test #1 was 33.3 °C and 40.3 °C for Test #2. The increased temperature affected the rate of evaporation, as is evidenced by the slope of the water content line. The water content and matric suction records could be combined to construct the SWRCs for each test.

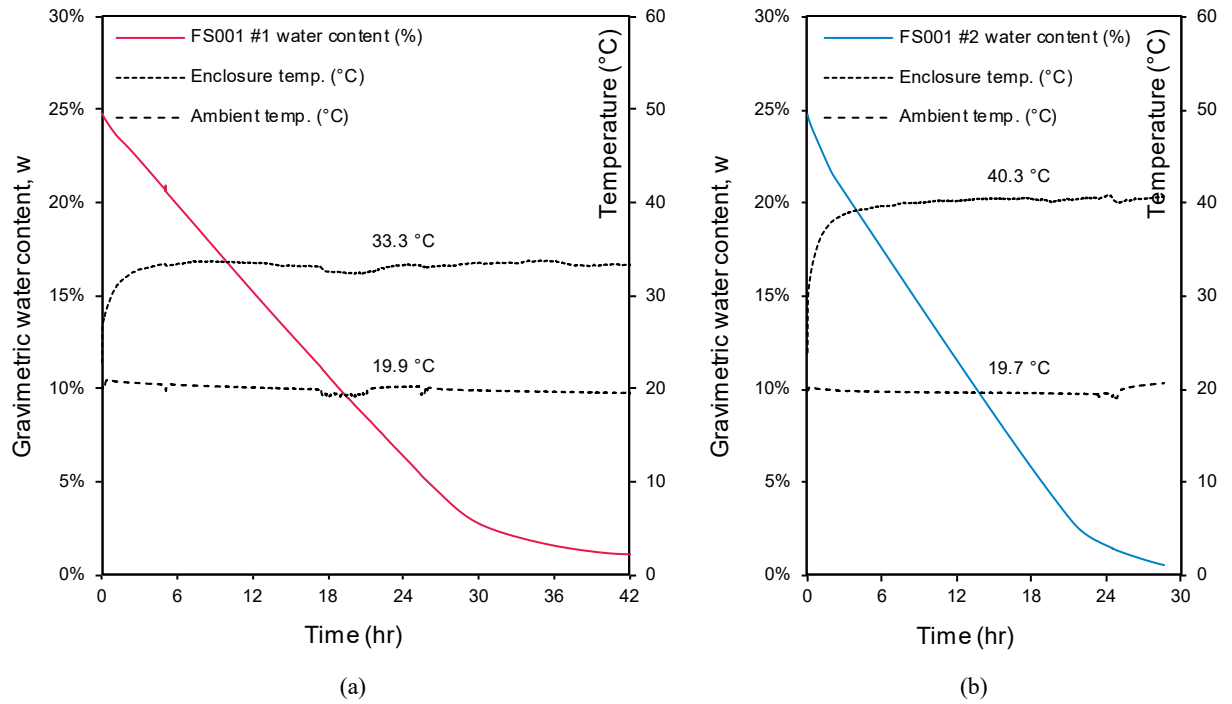
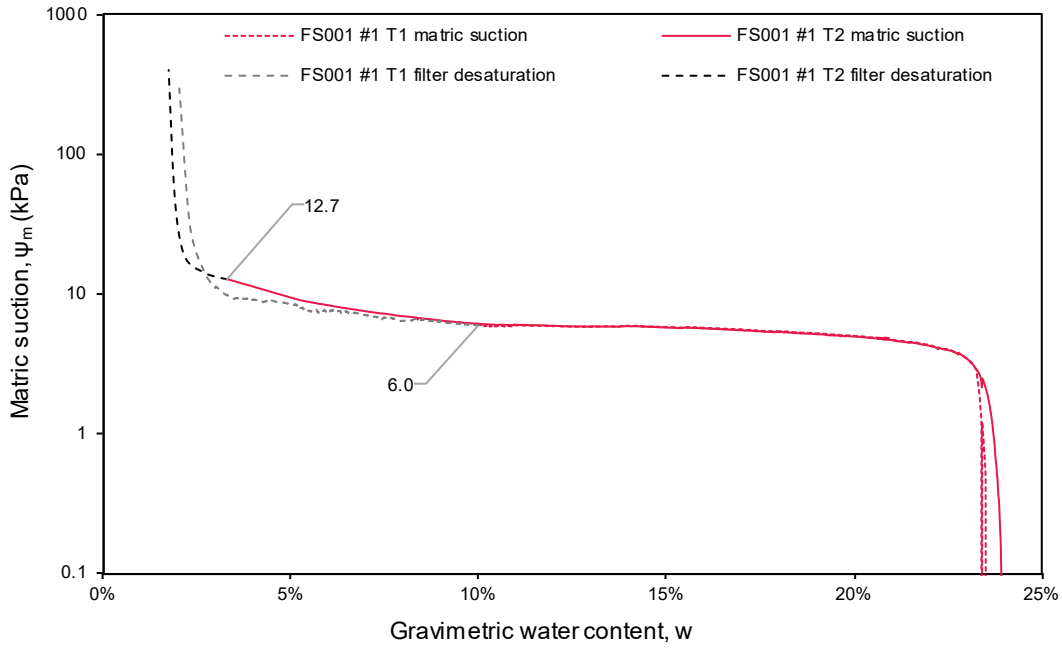
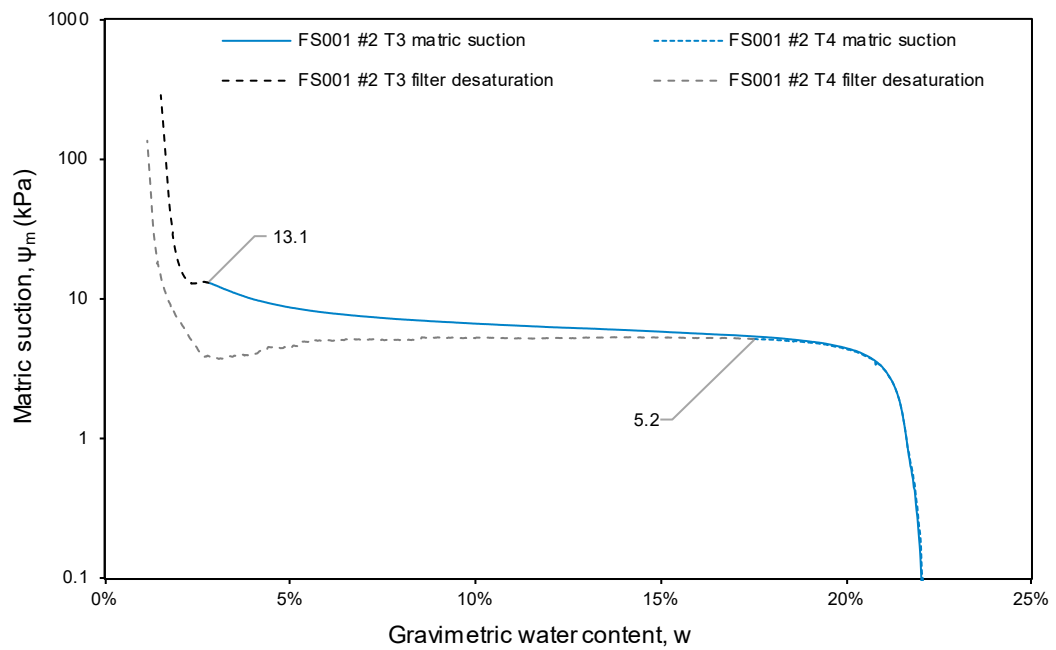


Figure 5-4 Evaporation of pore water in sample FS001: (a) Test #1; (b) Test #2

The resulting gravimetric water content SWRCs (ψ_{m-w}) of Test #1 and Test #2 are shown in Figure 5-5 (a) and Figure 5-5 (b) respectively. Due to the low matric suctions generated in the sample over most of the water content range, the scale of the vertical axis has been limited to 1000 kPa to reveal more of the shape of the SWRCs.



(a)



(b)

Figure 5-5 Tensiometer SWRCs (ψ_m-w) for sample FS001: (a) Test #1; (b) Test #2

The initial density of a soil is one of the most significant contributors to the form of the SWRC (Mercer *et al.*, 2019). This feature is evident from the starting point of each of the SWRCs. The specimen in Test #1 was prepared by mixing the sample with enough de-aired water to form a uniform slurry and then placed in the specimen container. The resulting dry density of the specimen was 1.65 g/cm^3 with a theoretical saturated water content of 23.4 %. Similarly, the specimen in Test #2 was prepared in the same way and had a dry density of 1.71 g/cm^3 and

theoretical saturated water content of 21.3 %. The SWRCs for granular soils are typically normalised with respect to the water content parameter to eliminate the effect of the initial density and thus, the resulting saturated water content, and enable direct comparison of different SWRCs on the same scale (Mercer *et al.*, 2019). The degree of saturation (S) is easily determined for soils of constant volume such as the fine sand sample. Figure 5-6 shows the normalised, degree of saturation SWRCs (ψ_m - S) for sample FS001. When comparing the two specimen results, it is shown that the tensiometer method delivered consistent SWRCs for matric suctions between 0 and 13 kPa.

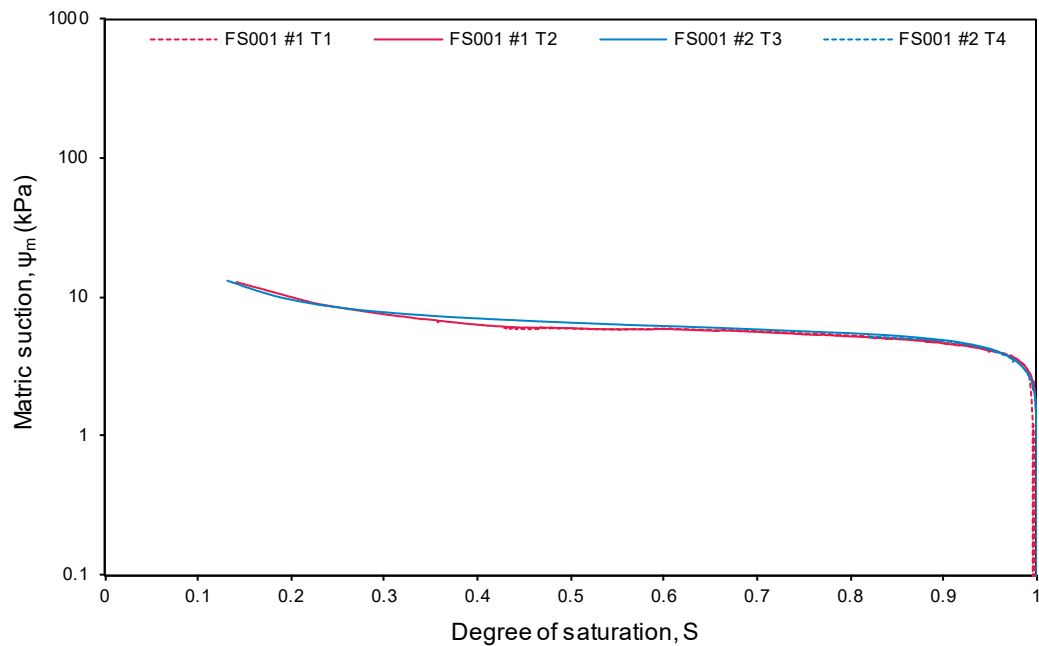


Figure 5-6 Tensiometer SWRCs (ψ_m - S) for sample FS001: Test #1 and Test #2

5.1.3 Sample GT001: Gold mine tailings – tensiometer method

When it had been established that the tensiometer could measure consistent suctions in different specimens of the fine sand sample, the experimental procedures were repeated on the gold mine tailings sample. Since the tensiometer response in the fine sand sample appeared to, at some point, reflect desaturation of the ceramic filter rather than equilibrated suctions, the effect of the specimen dimensions were investigated while testing the tailings. The specimen dimensions for each test were:

- Test #1: 18.5 mm in height and 116.8 mm in diameter,
- Test #2: 50.6 mm in height and 77.2 mm in diameter, and
- Test #3: 25.5 mm in height and 73.5 mm in diameter.

Figure 5-7 shows the tensiometer response over time during Test #1, Test #2, and Test #3 of sample GT001. Significantly higher negative pore-water pressures were measured in the largest specimen at -629.1 kPa; however, only for one of the tensiometers and no specific correlation between the measurable pressure and the specimen dimensions were found. Each pair of tensiometers registered the same suction up to air entry of one of the tensiometers. This suggests that the location of the tensiometers inside the sample does not affect the results. The results suggest that for the tensiometer method in granular soils, maintaining a good hydraulic link between the tensiometer and the pore water is critical, and methods to improve this link should be investigated.

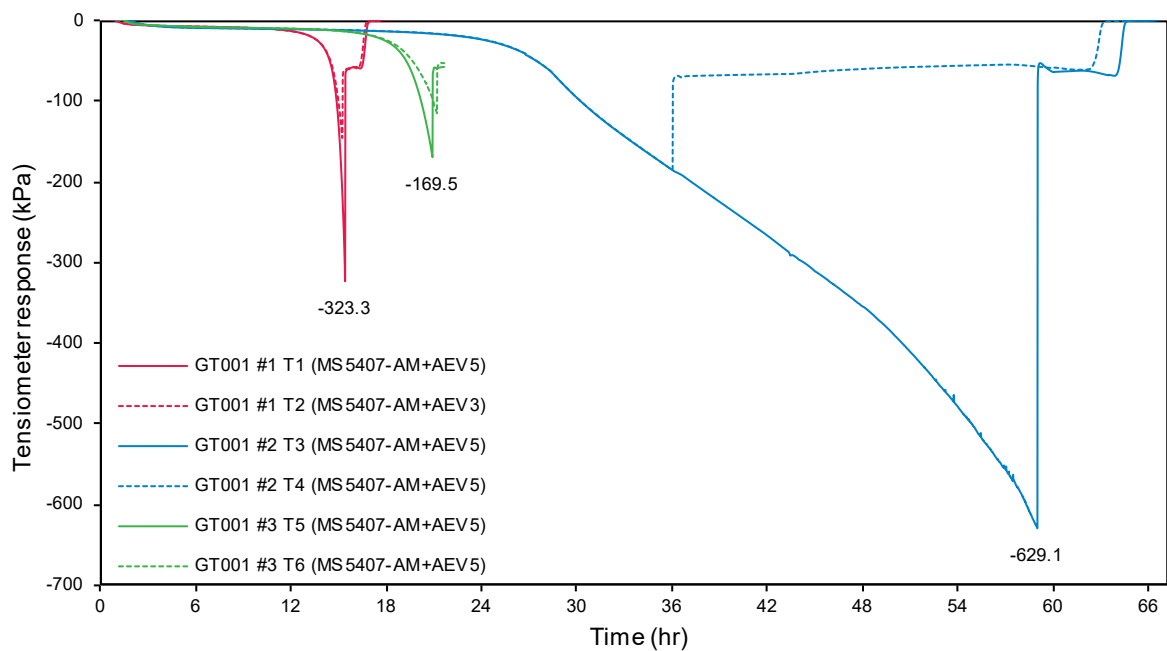


Figure 5-7 Tensiometer desaturation in sample GT001: Test #1, Test #2, and Test #3

Figure 5-8 shows the records of the water content of each specimen as they desaturated in the environmental enclosure. Only the temperatures for Test #3 are shown. The average enclosure temperature was observed to remain around 40 °C. In contrast to the tests on sample FS001, the rate of evaporation remained constant, but the specimen dimensions in each test affected the duration of each test.

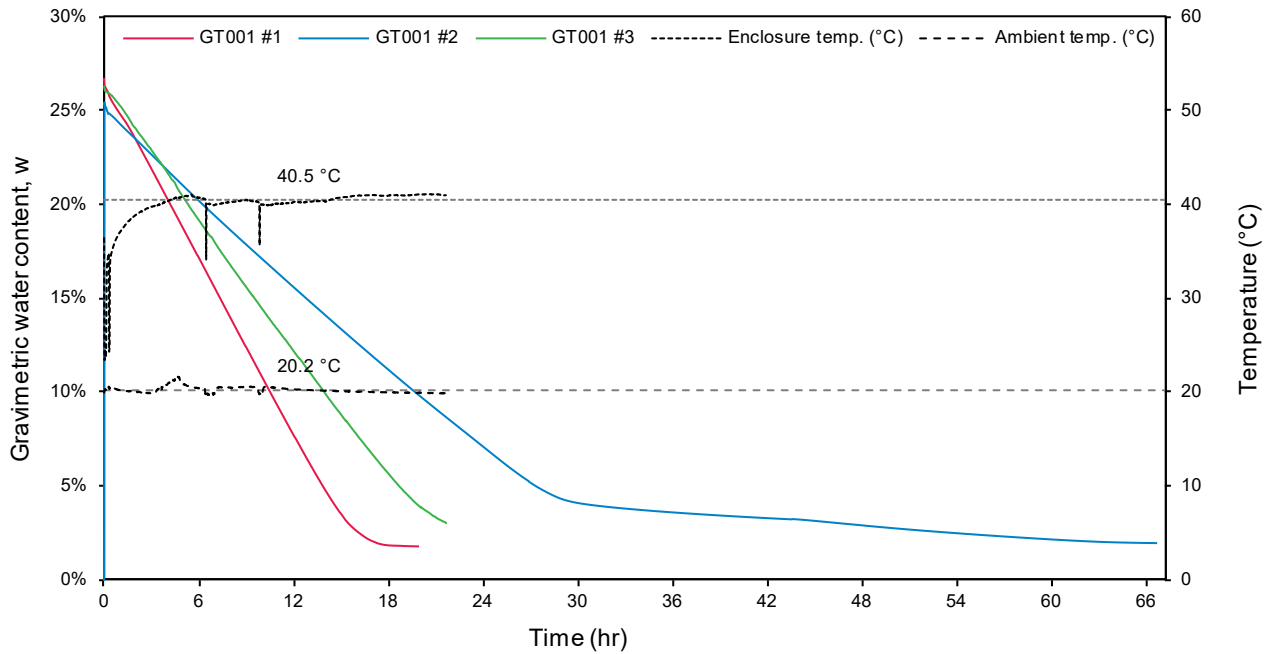


Figure 5-8 Evaporation of pore water in sample GT001: Test #1, Test #2, and Test #3

The gravimetric water content SWRCs (ψ_{m-w}) of Test #1, Test #2 and Test #3 were determined as before and are shown in Figure 5-9. The scale of the vertical axis has again been limited to 1000 kPa.

The specimens of sample GT001 were prepared by mixing the sample with de-aired water to form a uniform slurry with a water content of around 30 %. The soil was placed in the specimen container and would naturally settle out, releasing excess free water, and compacting to a dry density of 1.63 – 1.66 g/cm³ while remaining saturated. This is similar to how mine tailings is deposited on the surface of a TSF. The resulting dry densities of the specimens were then 1.63, 1.66, and 1.64 g/cm³ with saturated water contents of 24.2 %, 22.9 %, and 24.6 % for Test #1, Test #2 and Test #3 respectively. The slightly higher average density of the specimen in Test #2 is owed to the taller specimen height.

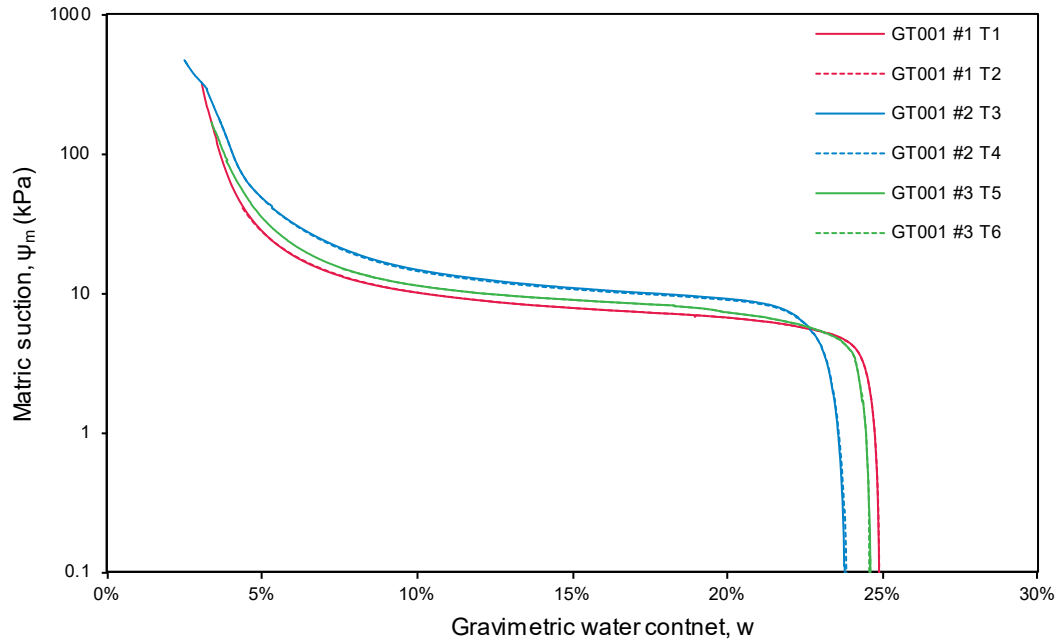


Figure 5-9 Tensiometer SWRCs (ψ_m-w) for sample GT001: Test #1, Test #2, and Test #3

As with the fine sand sample, the results can be normalised by the degree of saturation SWRCs (ψ_m-S) for sample GT001 and can be compared on the same scale as shown in Figure 5-10.

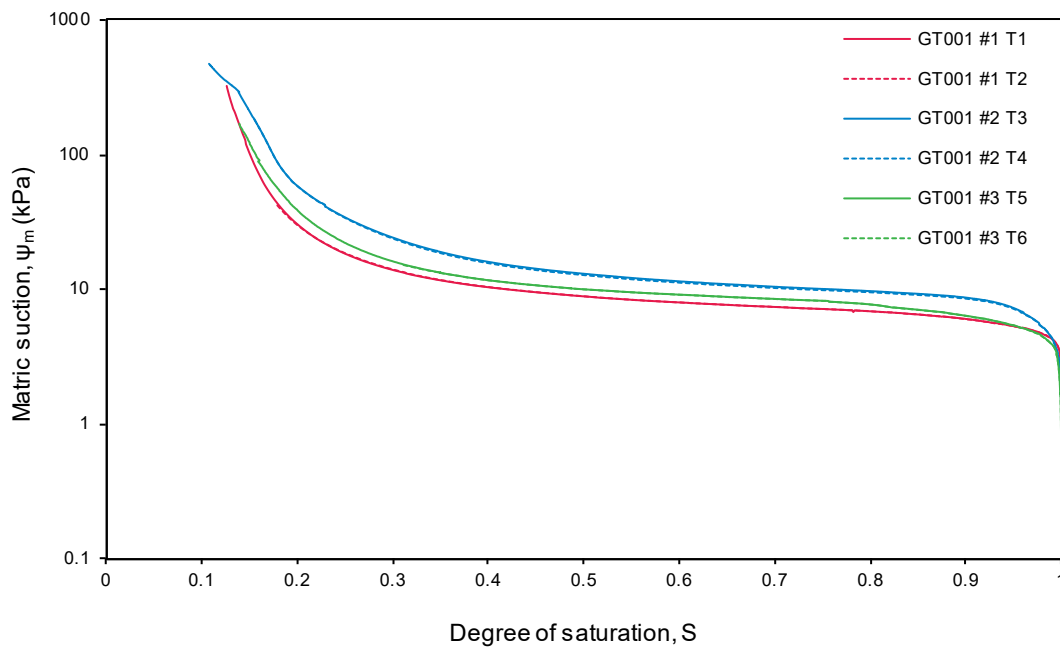


Figure 5-10 Tensiometer SWRCs (ψ_m-S) for sample GT001: Test #1, Test #2, and Test #3

When comparing the three specimen results, it is shown that the tensiometer method delivered consistent SWRCs for matric suctions between 0 and 320 kPa, particularly for the shorter specimens, Test #1 and Test #3. The SWRC for the taller specimen, Test #2, appeared to be

slightly shifted towards the higher water content range, which might be due to an uneven distribution of pore water throughout the taller sample. This uneven distribution should only affect the capillary regime, however. Higher values of suction were expected for the denser specimen, which also explains the slight disparity between the SWRCs.

5.2 COMPARISON OF THE TENSIO METER AND FILTER PAPER METHODS FOR DETERMINING SWRCs OF GRANULAR SOILS

The SWRCs determined from continuous drying with tensiometer suction measurements and the SWRCs determined by conventional discrete filter paper measurements for the two granular soil samples are compared in this section.

5.2.1 Granular soils - filter paper method

The procedure used for the filter paper method is described in Section 4.3.1. Two sets of 10 filter paper measurements were taken for the two granular soil samples. The specimens were prepared to target a range of degrees of saturation by mixing the oven-dried samples with varying amounts of water and compacting the specimens into small retaining rings. Preparing the specimens in this way had the advantage of accelerating the process over that of discrete drying of single or multiple specimens. The disadvantage of this method was that the specimens could not be compacted to the same density that was achieved from the drying form a slurry, and thus not simulating the same drying process.

It was found that preparing specimens at very high degrees of saturation ($S > 0.75$) was not feasible for the contact filter paper method using the procedure described. Therefore, the water contents of these specimens were lowered until the specimen consistency allowed it to be adequately contained in the retaining ring.

The specimens were allowed to equilibrate for three weeks, rather than the recommended one week for greater consistency and later comparison with the tensiometer measurements. Figure 5-11 (a) and (b) show the measured filter paper suctions for samples FS001 and GT001, respectively. A low degree of scattering is observed, owing to the extended equilibration time and consistency of the filter paper mass measurements.

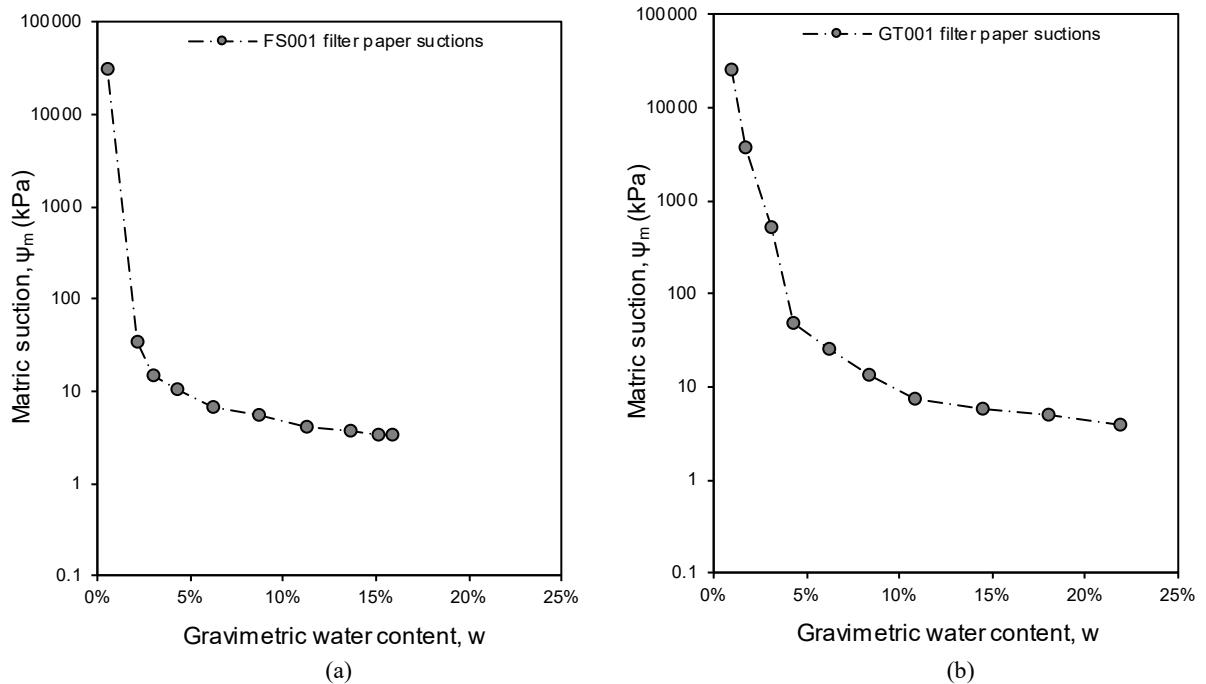


Figure 5-11 Filter paper suctions for granular soil samples: (a) FS001; (b) GT001

Curve-fitting

A curve-fit through the data points of the filter paper measurements was constructed to complete the SWRCs. The Fredlund & Xing (1994) best-fit gravimetric water content SWRC and its shape correction factor are described by Equation 2.5 and Equation 2.6 in Section 0. The curve-fit requires an estimation of the saturated water content (w_s) and residual suction (ψ_r) as inputs.

The saturated water content for each sample was determined from the average void ratio (e) related to the density (ρ_d) of the individual soil specimens used to determine the filter paper suctions. The volume-mass relationship is derived from the fundamental Equation 5.1:

$$S \cdot e = G_s \cdot w \tag{5.1}$$

Thus, for a degree of saturation of $S = 1$, the saturated water content is given by $w_s = e/G_s$.

A graphical construction was used to determine an initial estimate of the residual suction, as shown in Figure 5-12 for sample FS001 and Figure 5-14 for sample GT001. An initial estimate of the air-entry value (ψ_{aev}) of each sample is also determined in this way.

A spreadsheet solver was used to determine the three curve fitting parameters, a_f , m_f , and n_f that would produce the best fit curve through the data points using a least-squares error

approach. An initial curve-fit was generated using parameters determined from the graphical construction.

Since each set of filter paper measurements is generally sparse, an estimation of the residual suction may prove difficult from the limited set of data points. Therefore, the initial curve-fit was used to refine the estimation of the residual suction from further graphical construction. Regions on the curve were defined where tangent lines could be constructed in such a way that the intersection of these lines could be used to determine a refined estimation of the residual suction. By iteratively solving for the curve-fitting parameters and residual suction yielding the lowest error between the measured and predicted data using the spreadsheet solver, a very close curve-fit could be determined. Figure 5-13 and Figure 5-15 show the result of the refinement and the final best-fit SWRCs for samples FS001 and GT001. Table 5-1 summarises the features of the final SWRCs for each sample determined from the filter paper method.

Table 5-1 Filter paper SWRC properties and curve-fitting parameters

Sample FS001	Sample GT001
SWRC properties	
$w_s = 26.4 \%$	$w_s = 26.4 \%$
$\psi_{aev} = 2.7 \text{ kPa}$	$\psi_{aev} = 2.9 \text{ kPa}$
$w_r = 1.9 \%$	$w_r = 3.0 \%$
$\psi_r = 10.8 \text{ kPa}$	$\psi_r = 32.6 \text{ kPa}$
Curve-fitting parameters	
$a_f = 2.979$	$a_f = 3.724$
$n_f = 12.457$	$n_f = 5.001$
$m_f = 0.643$	$m_f = 0.605$

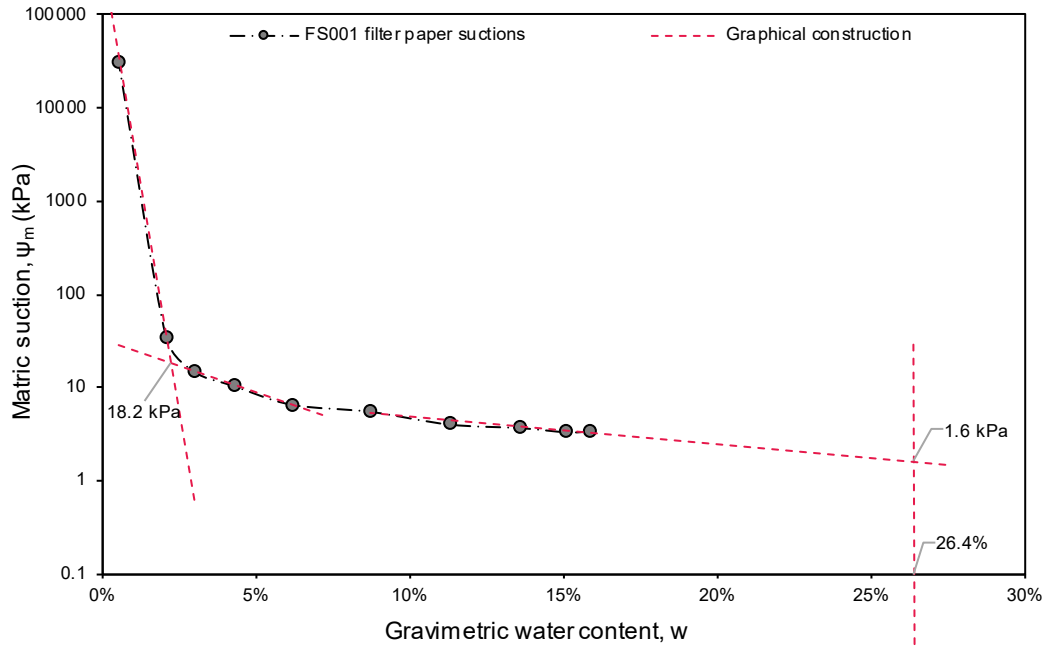


Figure 5-12 Initial graphical construction of SWRC (ψ_m-w) for sample FS001

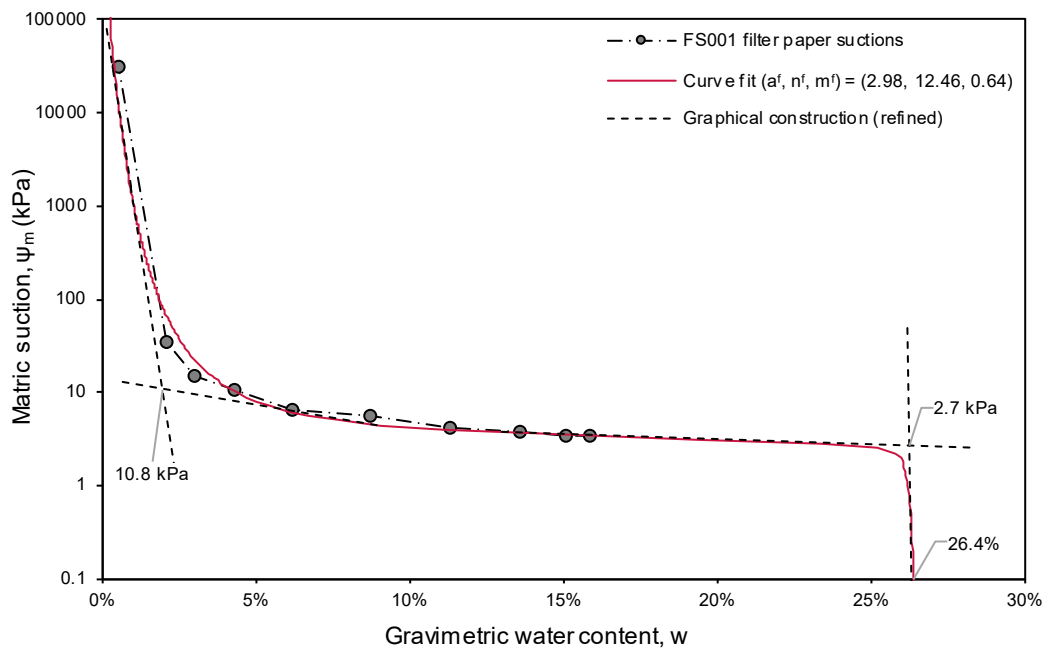


Figure 5-13 Final SWRC curve fit (ψ_m-w) for sample FS001

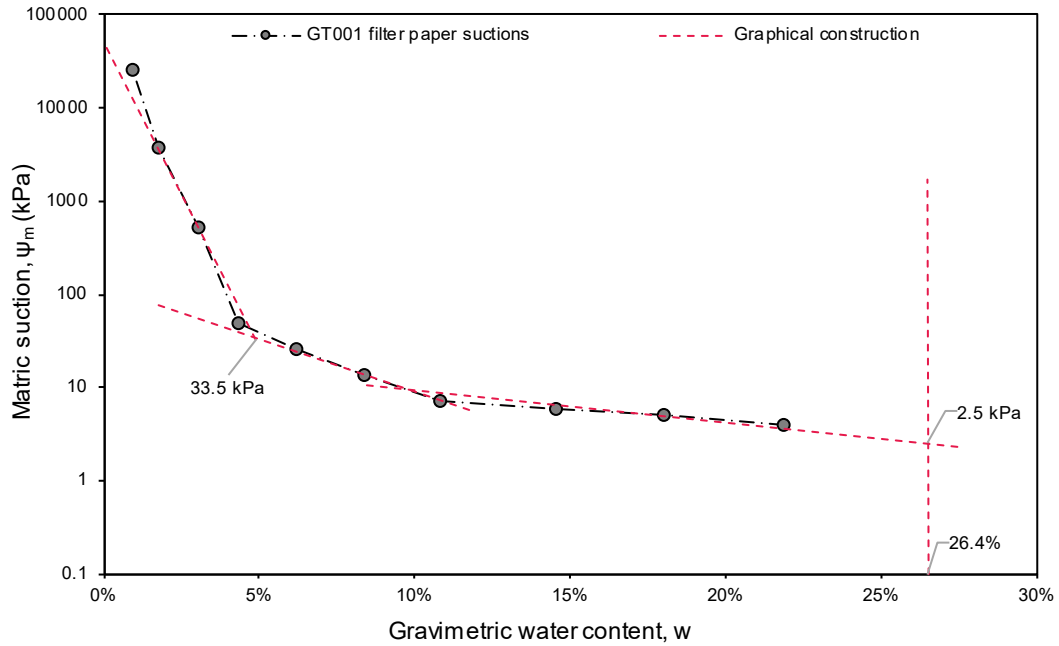


Figure 5-14 Initial graphical construction of SWRC (ψ_m-w) for sample GT001

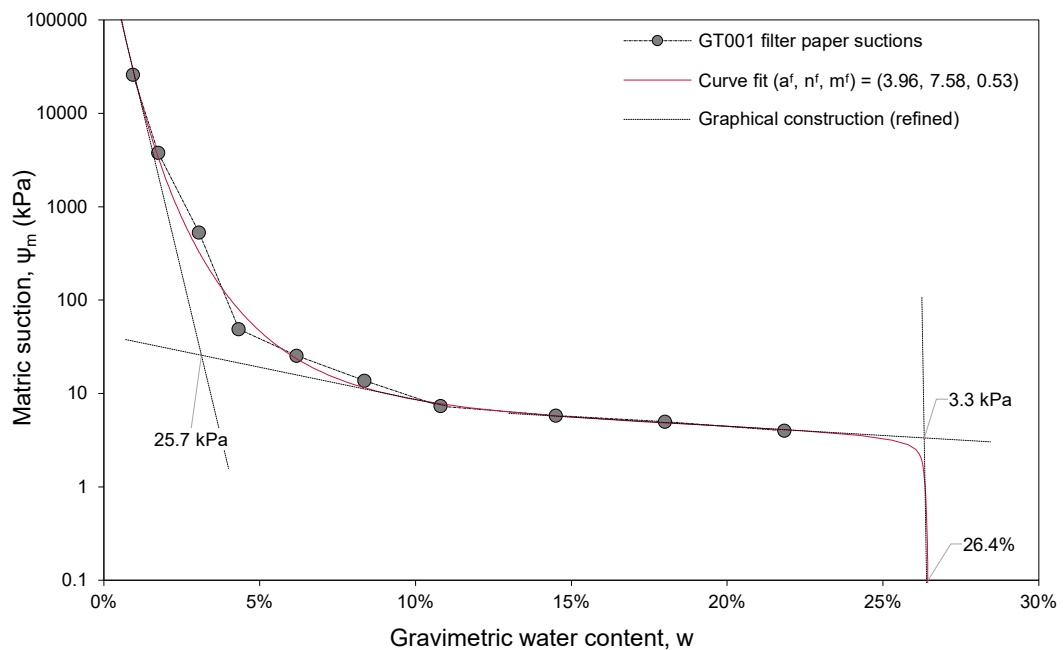


Figure 5-15 Final SWRC curve fit (ψ_m-w) for sample GT001

5.2.2 Sample FS001: Fine sand – tensiometer vs filter paper methods

Figure 5-16 compares the gravimetric water content SWRCs (ψ_m-w) determined by the filter paper and tensiometer methods for sample FS001. The ultimate magnitude of suctions measured using the tensiometer was limited to around 14.2 kPa, after which the tensiometer response is believed to reflect desaturation of the filter element rather than equilibrated suctions in the soil. This is likely due to the filter losing a continuous hydraulic link to the pore water at

the end of the capillary regime. The relatively large average pore size of the fine sand is thought to allow direct contact between the filter and the pore air in the adsorbed film regime, where after the filter starts to desaturate rapidly instead of equilibrating to the pore-water pressure. Nevertheless, a good agreement between the methods is found. For water contents above 5 %, the tensiometer method tends to measure higher values of suction, and for water contents below 5 %, the tensiometer method tends to measure lower values of suctions when compared to the filter paper method. It is important to note that the SWRCs determined from the tensiometer method are primary drying curves (PDCs). Due to the method in which the specimens were prepared, the SWRC determined from the filter paper method represent a scanning curve between the PDCs and the primary wetting curve (PWCs). Hysteresis between the curves is expected and can be seen from the offset between the SWRCs. The average offset between the methods is shown in Figure 5-16.

Since each specimen was prepared at different densities, it would be appropriate to compare the normalised SWRCs (ψ_m-S) as in Figure 5-17. Again, good agreement between the methods is found for the limited range of suctions measured using the tensiometer. There is also very little difference between the SWRCs determined from the two specimens of the same sample using the tensiometer, even when tested at different rates of evaporation. Although the magnitude of suctions was limited, the tensiometer measurement fully showcases the beginning of the PDCs. The filter paper method appears to serve as a valid method for extending the SWRC into the range of suctions that are beyond the capacity of the tensiometer.

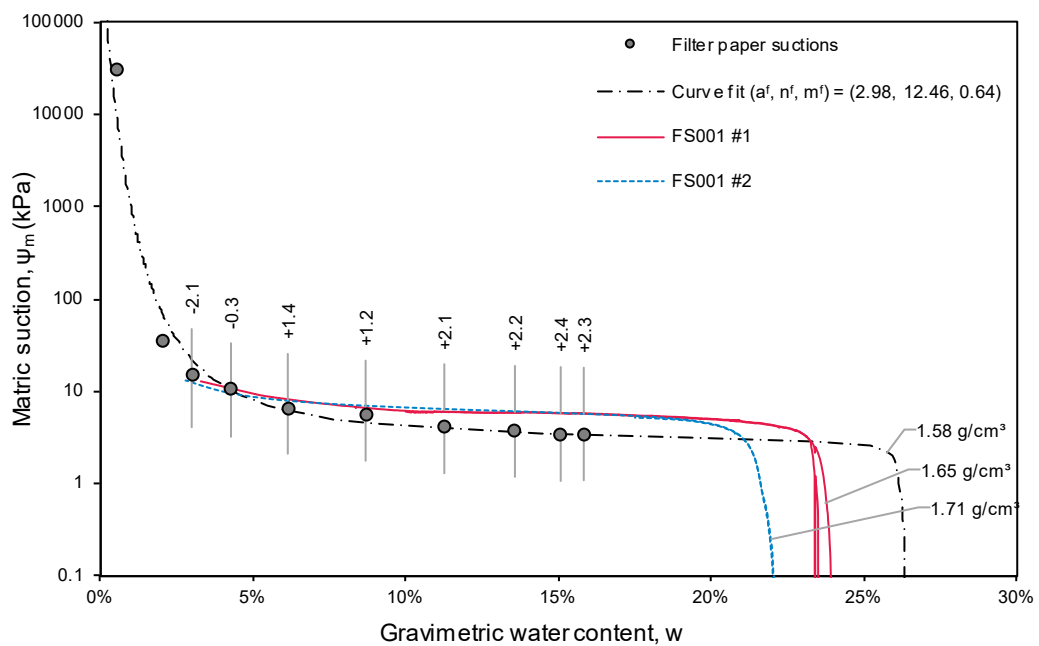


Figure 5-16 Tensiometer vs filter paper SWRCs (ψ_m-w) for sample FS001

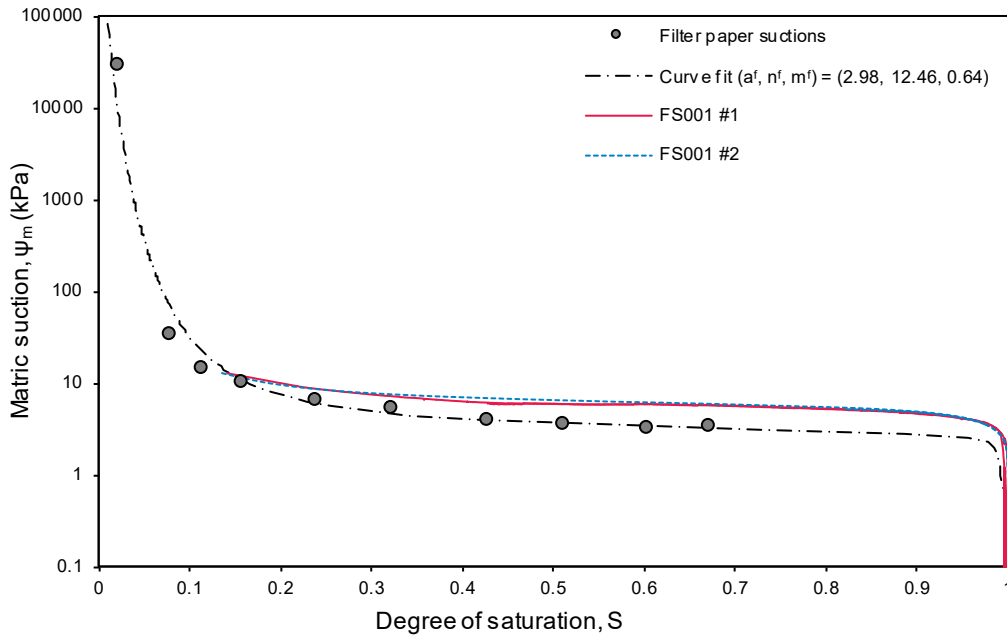


Figure 5-17 Tensiometer vs filter paper SWRCs (ψ_m -S) for sample FS001

5.2.3 Sample GT001: Gold mine tailings – tensiometer vs filter paper methods

Figure 5-18 compares the gravimetric water content SWRCs (ψ_m -w) and Figure 5-19 the degree of saturation SWRCs (ψ_m -S) determined by the two methods for sample GT001. The ultimate magnitude of suctions measured using the tensiometer for each test was between 150 and 630 kPa. In contrast to the fine sand sample, the finer particles and smaller average pore size of the gold mine tailings is believed to allow better contact between the ceramic of the tensiometer and the pore water of the soil allowing a higher suction measurement to be achieved before desaturation of the filter element initiates or cavitation occurs. Excellent agreement between the methods is found, with the tensiometer generally measuring slightly higher values of suctions than that of the filter paper method. Again, it is noted that hysteresis between the two methods is expected, with the tensiometer method determining PDCs and the filter paper method determining a scanning curve between the PDCs and the PWCs.

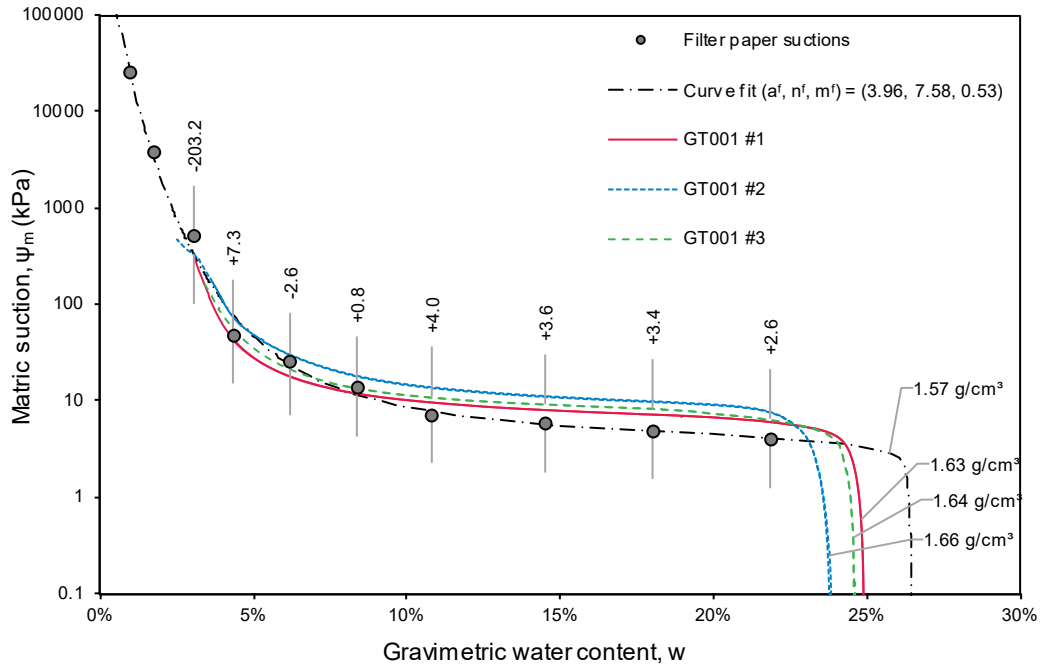


Figure 5-18 Tensiometer vs filter paper SWRCs (ψ_m-w) for sample GT001

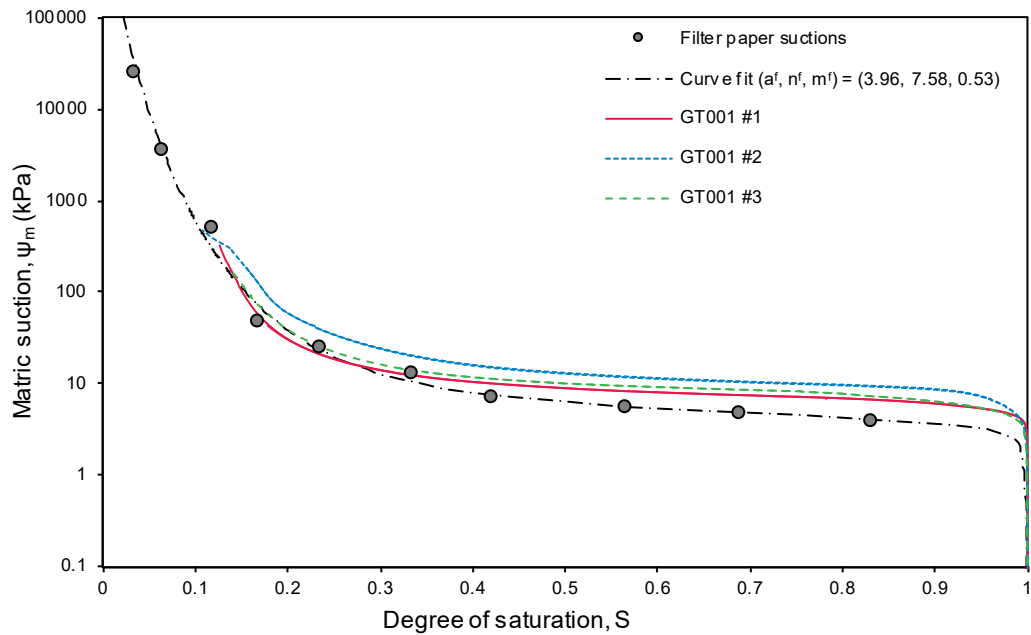


Figure 5-19 Tensiometer vs filter paper SWRCs (ψ_m-S) for sample GT001

5.3 SOIL-WATER RETENTION CURVES OF FINE-GRAINED SOILS UNDERGOING VOLUME CHANGE

After SWRCs were successfully determined for granular soils in Section 5.1, the study was expanded to investigate the use of the tensiometer developed in Chapter 3 and the experimental

procedures outlined in Chapter 4 for fine-grained soils that undergo a change in volume (shrinkage) during drying. This section discusses the results of these experimental procedures and again offers a comparison to the results from the filter paper method.

5.3.1 Testing program for fine-grained soils

In total, ten additional tests on three different fine-grained soil samples were performed using the continuous drying and tensiometer method. The material properties for these samples are contained in Section 4.1. The specimens were tested from initially saturated slurries of different densities to obtain PDCs. A set of filter paper measurements were also taken for each sample on specimens prepared at a specified density. The tests were performed at the specified initial specimen density, and ultimately reaching the final density as listed below:

- Sample TP148: Clayey sand
 - ‘TP148 Test #1’, $\rho_d = 1.31 - 1.63 \text{ g/cm}^3$
 - ‘TP148 Test #2’, $\rho_d = 1.54 - 1.70 \text{ g/cm}^3$
 - ‘TP148 Test #3’, $\rho_d = 1.50 - 1.65 \text{ g/cm}^3$
 - Filter paper suctions, $\rho_d = 1.55 \text{ g/cm}^3$
- Sample TP149: Lean clay
 - ‘TP149 Test #1’, $\rho_d = 1.09 - 1.61 \text{ g/cm}^3$
 - ‘TP149 Test #2’, $\rho_d = 1.18 - 1.58 \text{ g/cm}^3$
 - ‘TP149 Test #3’, $\rho_d = 1.15 - 1.59 \text{ g/cm}^3$
 - Filter paper suctions, $\rho_d = 1.59 \text{ g/cm}^3$
- Sample TP016: Clay
 - ‘TP016 Test #1’, $\rho_d = 0.95 - 1.91 \text{ g/cm}^3$
 - ‘TP016 Test #2’, $\rho_d = 0.97 - 1.93 \text{ g/cm}^3$
 - ‘TP016 Test #3’, $\rho_d = 1.02 - 1.89 \text{ g/cm}^3$
 - Filter paper suctions, $\rho_d = 1.35 \text{ g/cm}^3$
 - ‘TP016 Test #4’, $\rho_d = 1.34 - 1.50 \text{ g/cm}^3$ (using strain-gauged hangers)

5.3.2 Sample TP148: Clayey sand – tensiometer method

Figure 5-20 shows the record of tensiometer response over time in Test #1, Test #2 and Test #3 of sample TP148, respectively. As with the tests on granular soils, two tensiometers were inserted into each specimen, labelled T1 and T2 for Test #1, T3 and T4 for Test #2, and T5 and T6 for Test #3. The higher 15 bar AEV tensiometers were started to be used at this point. The sensor type and AEV of the ceramic filter are indicated. As with the granular soils tested, each pair of tensiometers registered nearly identical suctions up to air entry of one of the

tensiometers. This suggests that the location of the tensiometers inside the specimen does not affect the results for clayey soils either. However, this may only apply to samples with the specimen dimensions and aspect ratio of 23.3 mm in height and 71.6 mm in diameter.

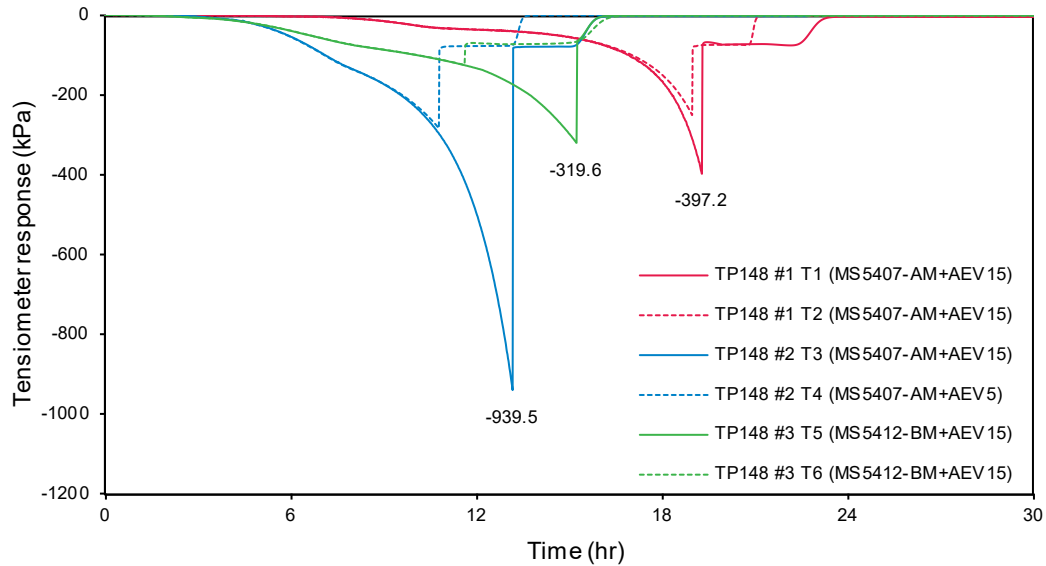


Figure 5-20 Tensiometer desaturation in sample TP148: Test #1, Test #2, and Test #3

The specimen for Test #1 was prepared by mixing the sample with an excess amount of de-aired water to form a uniform slurry with an initial water content of around 40 % to obtain the primary drying curve (PDC) and primary shrinkage curve (PSC) for the sample. The specimens for Test #2 and Test #3 were prepared at higher densities, the effect of which can be seen in the starting point of the gravimetric water content SWRCs (ψ_m-w) in Figure 5-21. The saturated water content, approximate air entry pressure and corresponding water content, and the ultimate value of measured suction for each specimen are indicated.

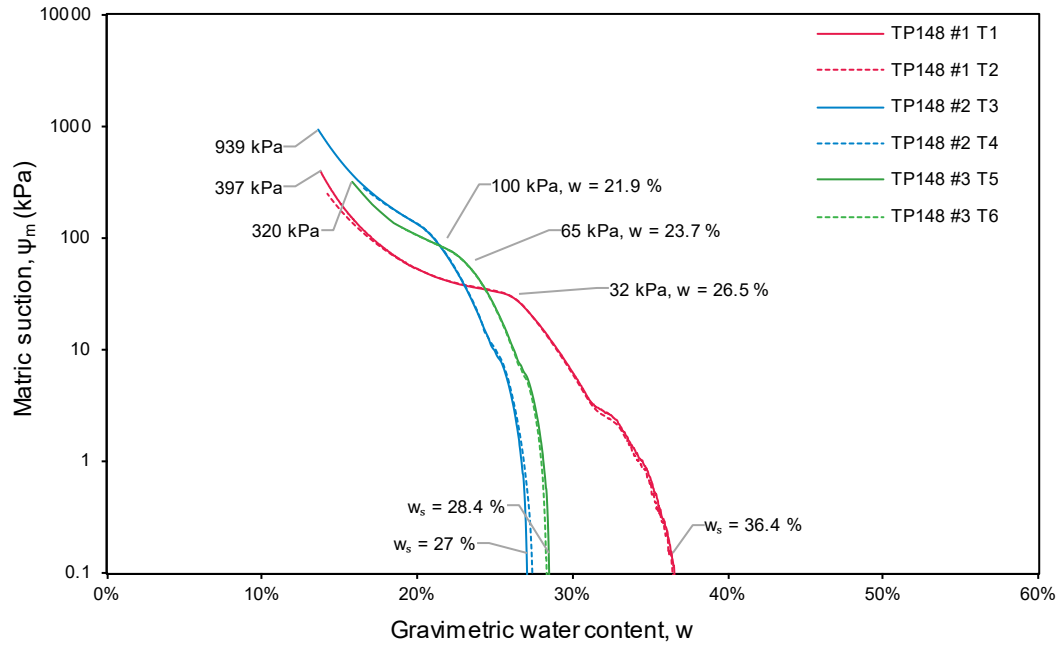


Figure 5-21 Tensiometer SWRCs (ψ_m-w) for sample TP148: Test #1, Test #2, and Test #3

Three direct measurements of the sample dimensions were taken at different stages of drying. The first measurement was made at the start of each test, then when the specimens were taken off the balance, and again after oven drying. The sample dimensions in between these points were determined from images obtained from the overhead camera. Processing of this data was discussed in Section A.3.2. The specimen dimensions were then used to determine the shrinkage curves ($e-w$) for each specimen as given in Equation 2.7. A fitting parameter (c_{sh}) was determined for each curve using a least-squares error approach and a spreadsheet solver. The shrinkage curves are shown in Figure 5-22, and their fitting parameters are summarised in Table 5-2.

Table 5-2 Shrinkage curve-fitting parameters for sample TP148

	TP148 #1	TP148 #2	TP148 #3
Minimum void ratio	$a_{sh} = 0.6233$	$a_{sh} = 0.5595$	$a_{sh} = 0.6048$
Slope of saturation line	$b_{sh} = 0.2352$	$b_{sh} = 0.2112$	$b_{sh} = 0.2283$
Curvature fitting parameter	$c_{sh} = 8.113$	$c_{sh} = 9.923$	$c_{sh} = 9.587$

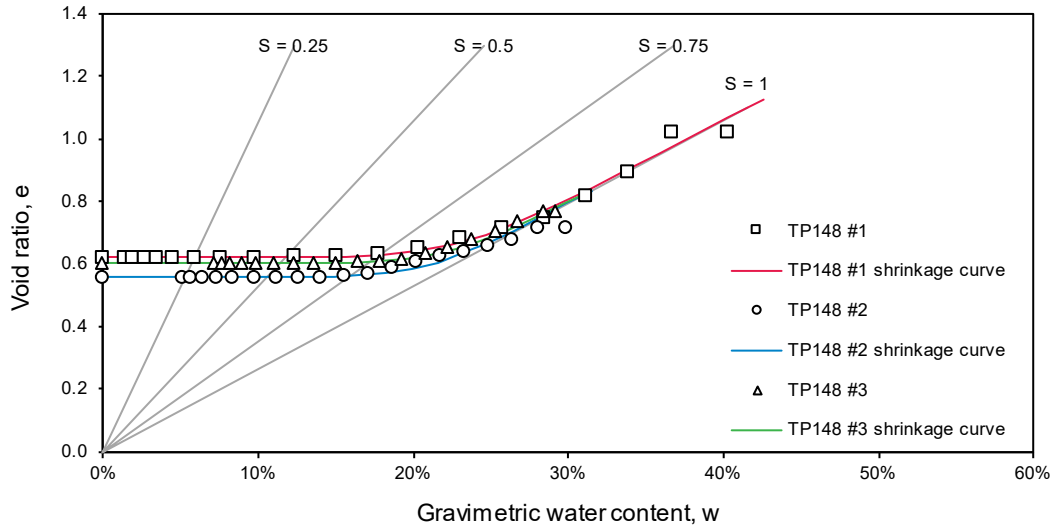


Figure 5-22 Shrinkage curves ($e-w$) for sample TP148: Test #1, Test #2, and Test #3

By combining the gravimetric water content SWRCs with the continuous shrinkage curves, the normalised degree of saturation SWRCs (ψ_m-S) can be determined and directly compared as in Figure 5-23. When comparing the three specimen results, the effect of volume change on the shape of the SWRC becomes evident. The approximate air-entry pressure and the corresponding void ratio at which air entry occurred are shown for each specimen. As the initial density of the specimens increased, the air entry pressure, overall density and values of suctions measured increased as well.

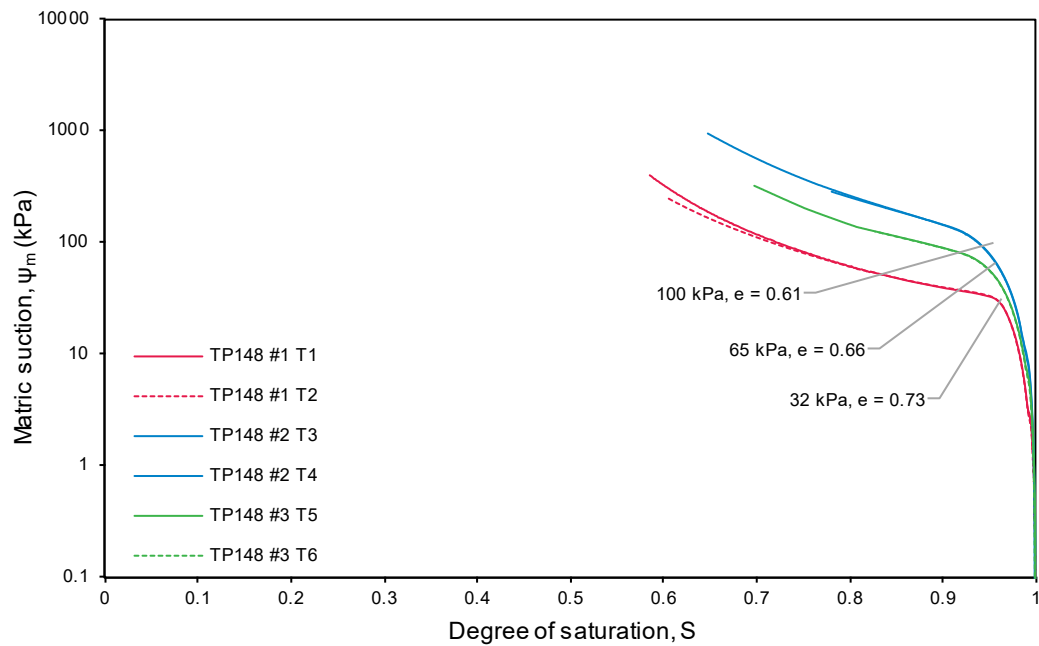


Figure 5-23 Tensiometer SWRCs (ψ_m-S) for sample TP148: Test #1, Test #2, and Test #3

5.3.3 Sample TP149: Lean clay – tensiometer method

Figure 5-24 shows the record of tensiometer response over time in Test #1, Test #2 and Test #3 of sample TP149, respectively. The sensor type and AEV of the ceramic filter of each tensiometer are indicated. Significantly higher suctions were measured using the 15 bar AEV tensiometers after having gained experience in the proper saturation procedure and testing method. However, the point at which cavitation or air-entry would occur remained variable. For Test #2, the 5 bar AEV tensiometers cavitated around the cavitation pressure early in the test. One tensiometer measured suctions in excess of 1000 kPa for Test #1 and Test #2, while the other tensiometer cavitated at a lower suction. The plasticity of the sample meant that each specimen underwent considerable shrinkage. It is thought the presence of the tensiometers in the specimen would induce cracking which exposed the filter surfaces of some of the tensiometers to the air and breaking hydraulic contact with the pore water.

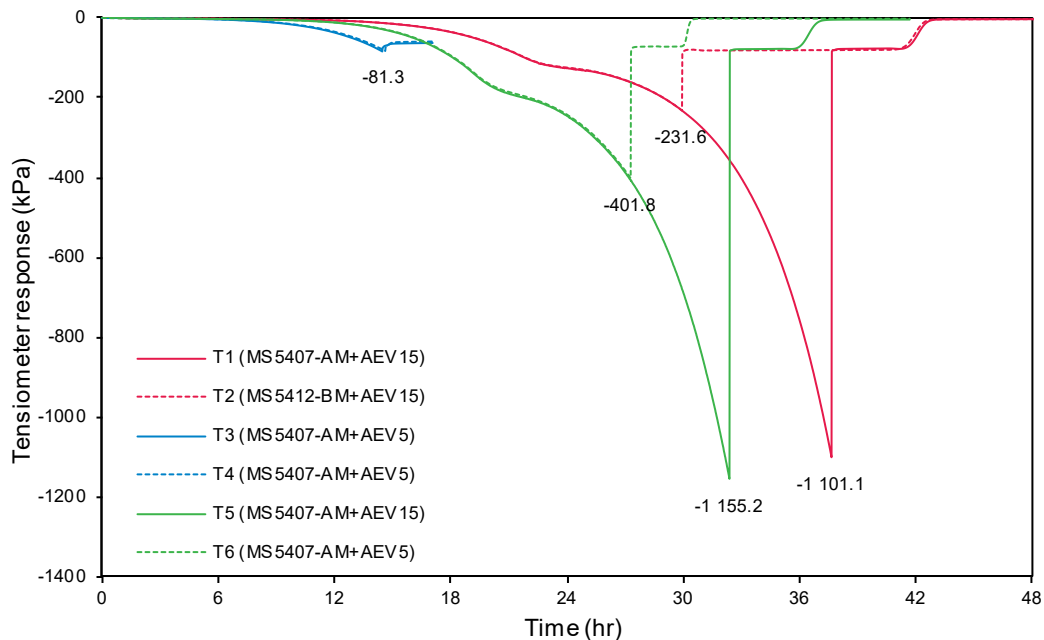


Figure 5-24 Tensiometer desaturation in sample TP149: Test #1, Test #2, and Test #3

The specimens for each test were prepared by mixing the sample with an excess amount of de-aired water to form a uniform slurry to obtain the primary drying curve (PDC) and primary shrinkage curve (PSC) for the sample. The initial density for each of the specimens varied slightly. The dry densities for each specimen were 1.09 g/cm³, 1.18 g/cm³, and 1.15 g/cm³ with saturated water contents of 54.2 %, 47.4 %, and 49.6 % for Test #1, Test #2 and Test #3 respectively.

The gravimetric water content SWRCs (ψ_m-w) for sample TP149 are shown in Figure 5-25. The saturated water content, approximate air entry pressure and corresponding water content and the ultimate value measured suction for each specimen are indicated.

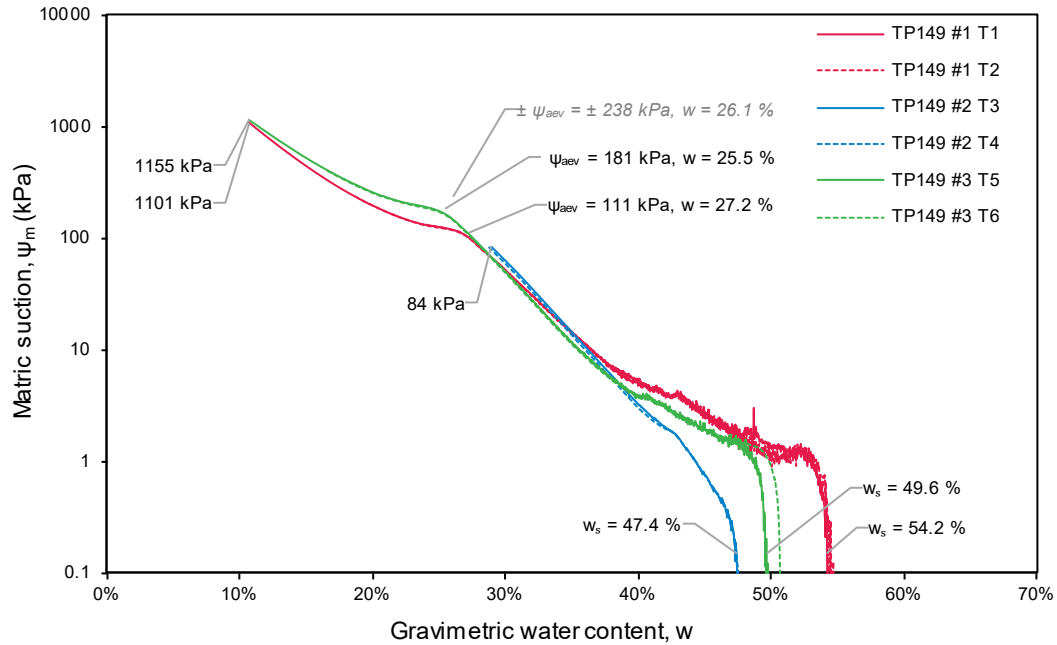


Figure 5-25 Tensiometer SWRCs (ψ_m-w) for sample TP149: Test #1, Test #2, and Test #3

The shrinkage curves ($e-w$) for sample TP149 are shown in Figure 5-22 with their fitting parameters are summarised in Table 5-3. All three specimens started off on the saturation line and only started to desaturate at a water content of around 26 %. As with the previous sample, a higher initial density would cause a specimen to shrink more and reach a higher final density. The air entry pressure, overall density, and values of suctions measured increased with an increase in initial density as well.

Table 5-3 Shrinkage curve-fitting parameters for sample TP149

	TP149 #1	TP149 #2	TP149 #3
Minimum void ratio	$a_{sh} = 0.6501$	$a_{sh} = 0.6737$	$a_{sh} = 0.6636$
Slope of saturation line	$b_{sh} = 0.2454$	$b_{sh} = 0.2543$	$b_{sh} = 0.2505$
Curvature fitting parameter	$c_{sh} = 6.790$	$c_{sh} = 10.934$	$c_{sh} = 10.064$

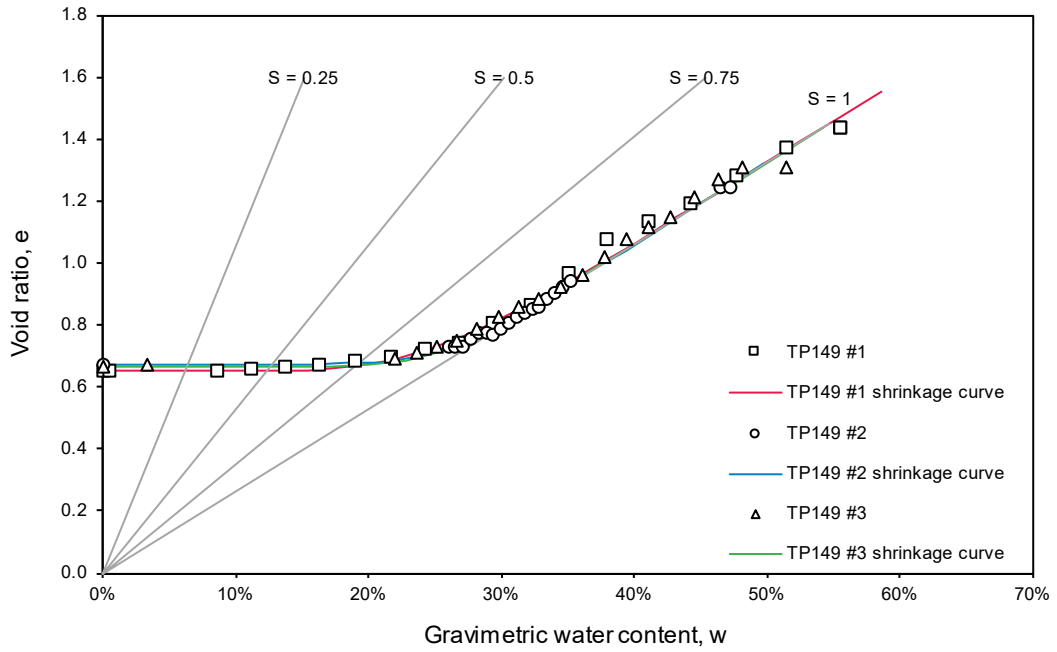


Figure 5-26 Shrinkage curves ($e-w$) for sample TP149: Test #1, Test #2, and Test #3

By combining the gravimetric water content SWRCs with the continuous shrinkage curves, the normalised degree of saturation SWRCs (ψ_m-S) can be determined and directly compared as before. Figure 5-23 depicts the degree of saturation SWRCs.

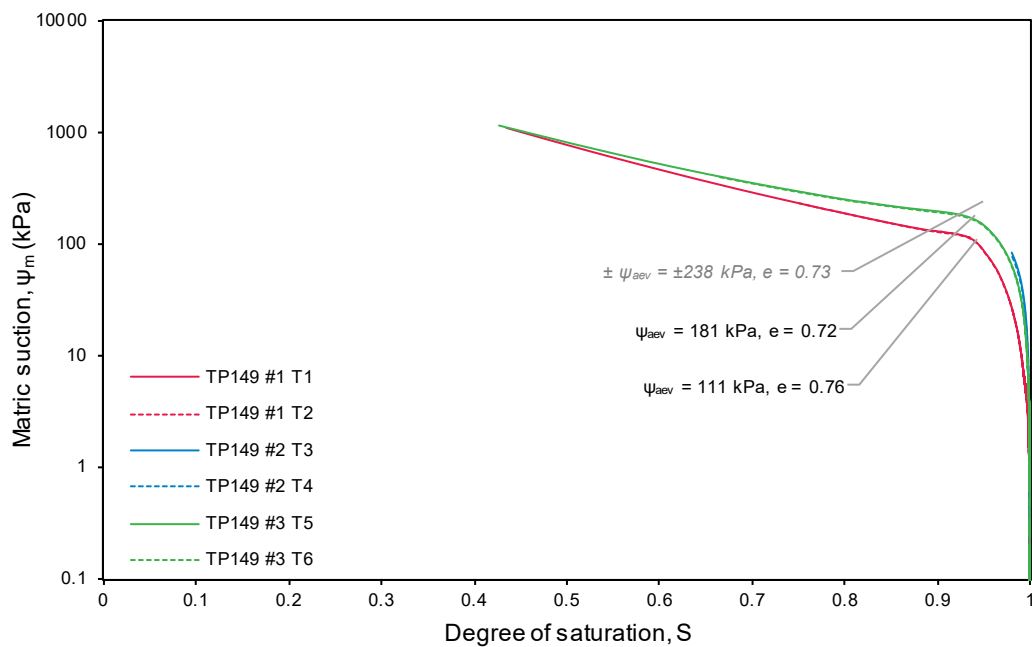


Figure 5-27 Tensiometer SWRCs (ψ_m-S) for sample TP149: Test #1, Test #2, and Test #3

5.3.4 Sample TP016: Clay – tensiometer method

Figure 5-28 shows the record of tensiometer response over time in Test #1, Test #2 and Test #3 of sample T016, respectively. The sensor type and AEV of the ceramic filter of each tensiometer are indicated. Due to the high plasticity of the sample, extreme shrinkage took place, particularly at the surface of the specimens where cracking would initiate. These cracks would propagate towards the tensiometers breaking the hydraulic contact with the pore water and causing early cavitation. Nevertheless, reasonably high suctions were recorded before cavitation occurred.

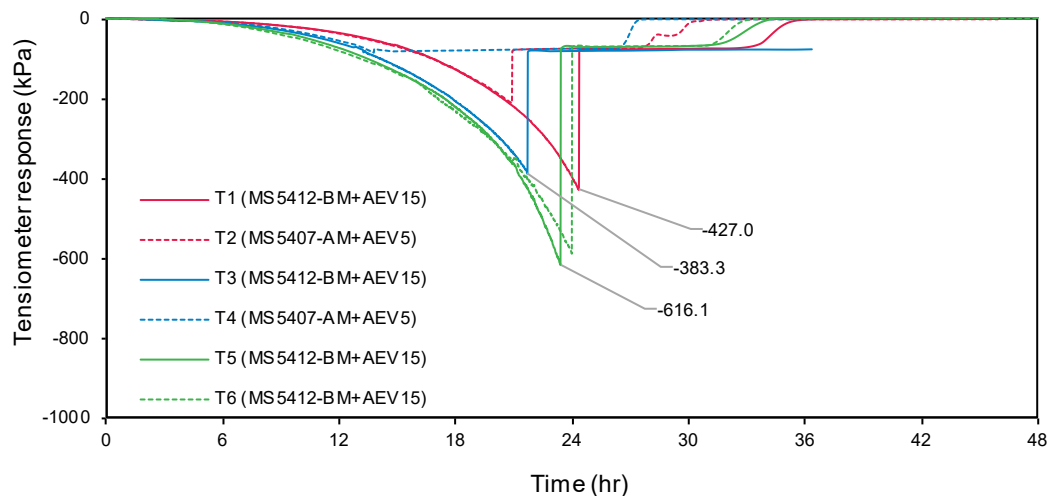


Figure 5-28 Tensiometer desaturation in sample TP016: Test #1, Test #2, and Test #3

The specimens for each test were prepared by crushing the desiccated sample into a fine powder and mixing it with an excess amount of de-aired water to form a uniform slurry. The specimens were also repeatedly placed in the vacuum desiccator to extract air bubbles that were trapped during the mixing process. As before, the primary drying curve (PDC) and primary shrinkage curve (PSC) for the sample could be determined in this way. Even so, slight differences in the mass of solid particles between specimens varied the initial densities slightly, although all three specimens started on the saturation line. The dry densities for each specimen were 0.95 g/cm^3 , 0.97 g/cm^3 , and 1.02 g/cm^3 with saturated water contents of 64.5 %, 62.5 %, and 58.2 % for Test #1, Test #2 and Test #3 respectively.

The gravimetric water content SWRCs (ψ_m-w) for sample TP016 are shown in Figure 5-29. The saturated water content and the ultimate value of measured suction for each specimen are indicated. Due to the high suctions generated in the highly plastic sample, cavitation occurred before the air entry pressure could be reached. Thus the approximate air entry pressures of the specimens thought to occur around a water content of 20 % as interpreted from the shrinkage curves ($e-w$) in Figure 5-30, could not be determined from the tensiometer data. The fitting

parameters for the shrinkage curves are summarised in Table 5-4 Shrinkage curve-fitting parameters for sample TP016.

Table 5-4 Shrinkage curve-fitting parameters for sample TP016

	TP016 #1	TP016 #2	TP016 #3
Minimum void ratio	$a_{sh} = 0.3458$	$a_{sh} = 0.3283$	$a_{sh} = 0.3576$
Slope of saturation line	$b_{sh} = 0.1348$	$b_{sh} = 0.1279$	$b_{sh} = 0.1393$
Curvature fitting parameter	$c_{sh} = 3.360$	$c_{sh} = 3.763$	$c_{sh} = 3.253$

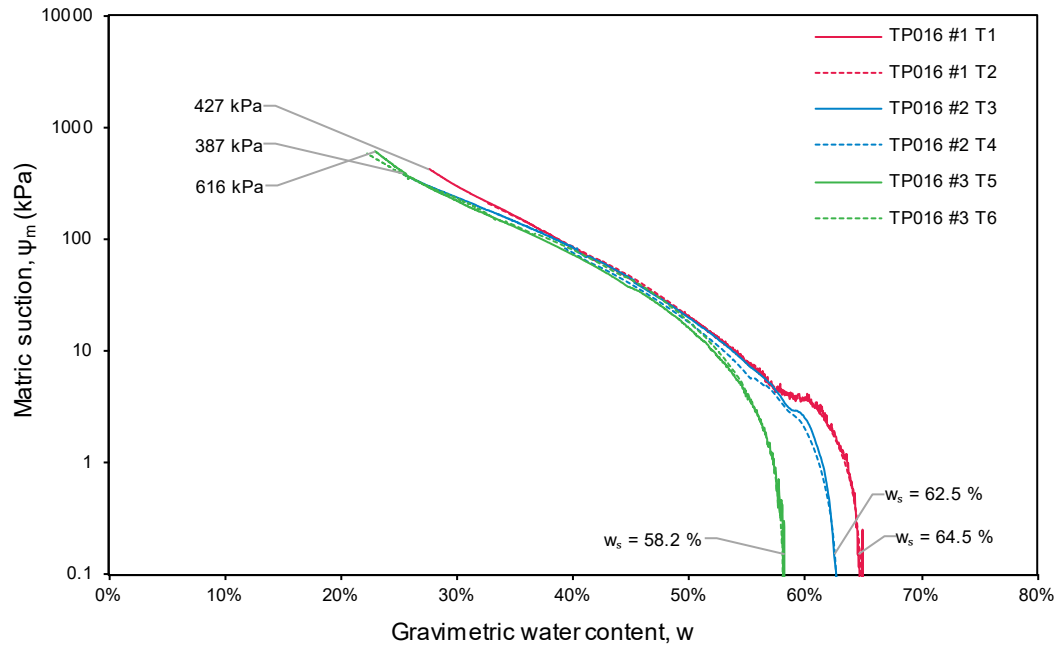


Figure 5-29 Tensiometer SWRCs (ψ_m-w) for sample TP016: Test #1, Test #2, and Test #3

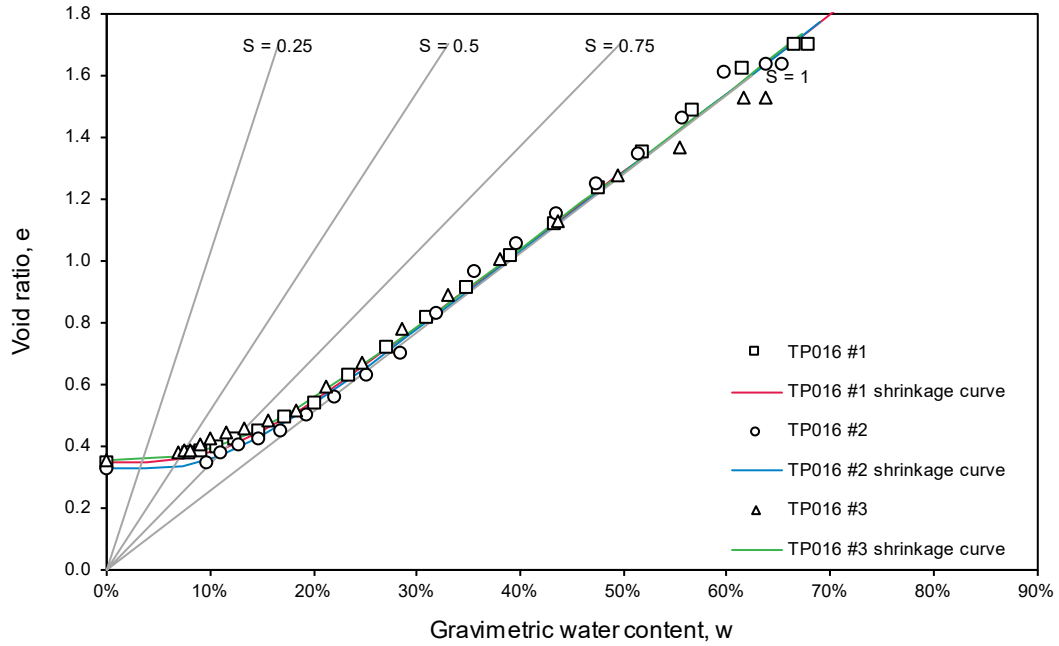


Figure 5-30 Shrinkage curves ($e-w$) for sample TP016: Test #1, Test #2, and Test #3

By combining the gravimetric water content SWRCs with the continuous shrinkage curves, the normalised degree of saturation SWRCs (ψ_m-S) can be determined and directly compared as before. Figure 5-31 depicts the degree of saturation SWRCs. Very little of the shape of the SWRCs were recorded due to the high suctions generated and the limited range of suction measurement prior to cavitation occurring.

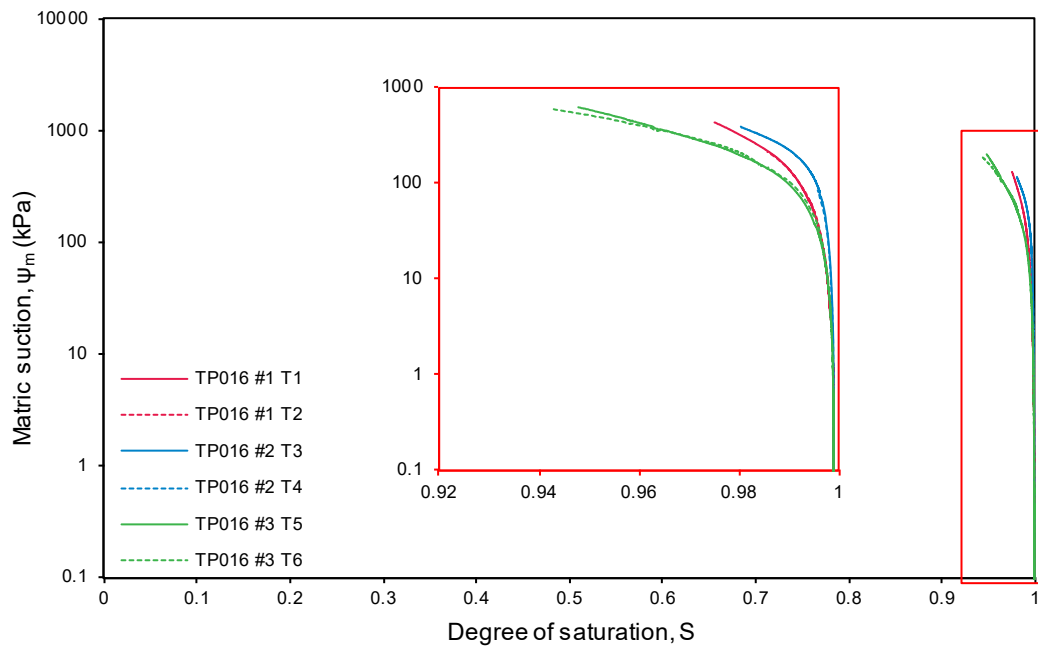


Figure 5-31 Tensiometer SWRCs (ψ_m-S) for sample TP016: Test #1, Test #2, and Test #3

5.4 COMPARISON OF THE TENSIOMETER AND FILTER PAPER METHODS FOR DETERMINING SWRCs OF FINE-GRAINED SOILS

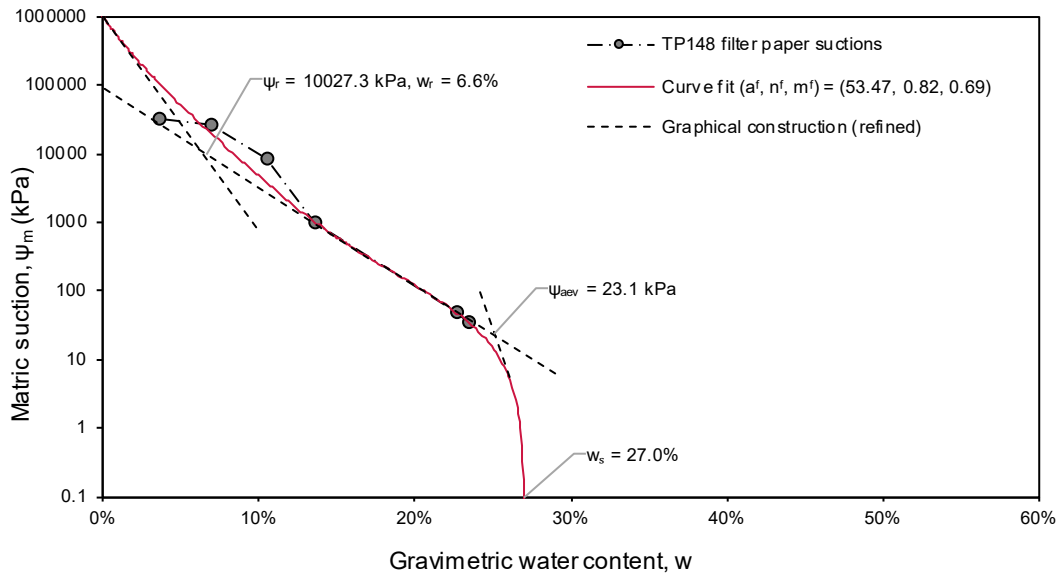
The SWRCs determined from continuous drying with tensiometer suction measurements and the SWRCs determined by conventional discrete filter paper measurements for the three fine-grained soil samples are compared in this section.

5.4.1 Fine-grained soils – filter paper method

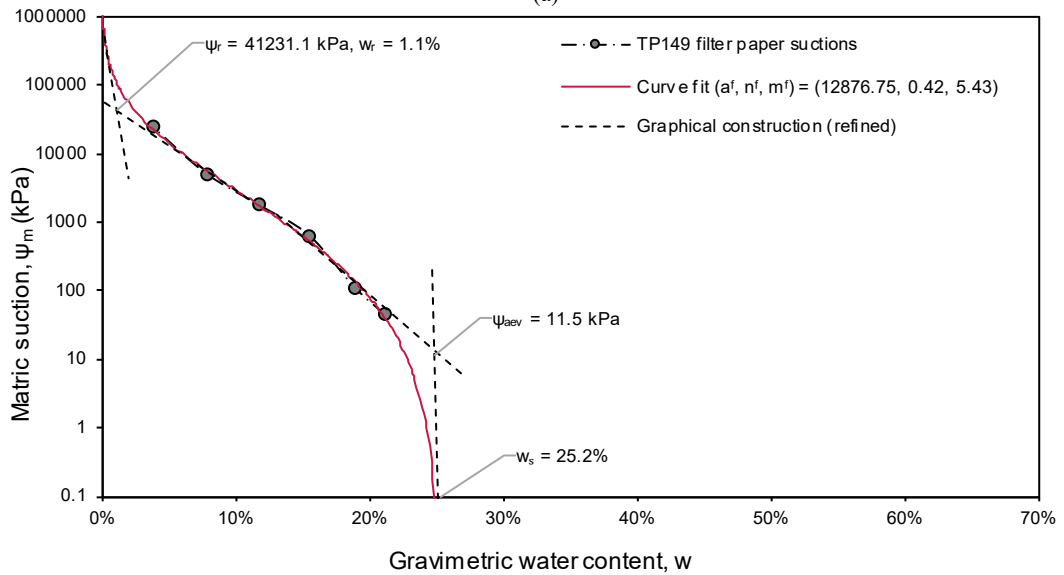
As with the granular soil samples, the specimens of the fine-grained soils were prepared to target a range of degrees of saturation by mixing the oven-dried samples with varying amounts of water and compacting the specimens into small retaining rings. The target density for sample TP148 was chosen as the average dry density at which the specimens were tested, taking into consideration the shrinkage of the sample, at 1.55 g/cm^3 . No amount of compacting would result in the same high density that the highly plastic samples would reach by shrinkage. Therefore, the target density for samples TP149 and TP016 was the maximum that could be achieved in the retaining rings at low degrees of saturation at 1.59 g/cm^3 and 1.35 g/cm^3 , respectively.

The specimens of the fine-grained soils were allowed to equilibrate for the one week as recommended in ASTM D5298 (2003), rather than the extended three weeks that was allowed for the granular soils tested in this study. Generally, more scattering was observed in the measurements at low water contents. This made the construction of the SWRCs slightly more challenging since some judgement was required for selecting the residual water content (ψ_r) for the curve-fitting routines, particularly for sample TP148.

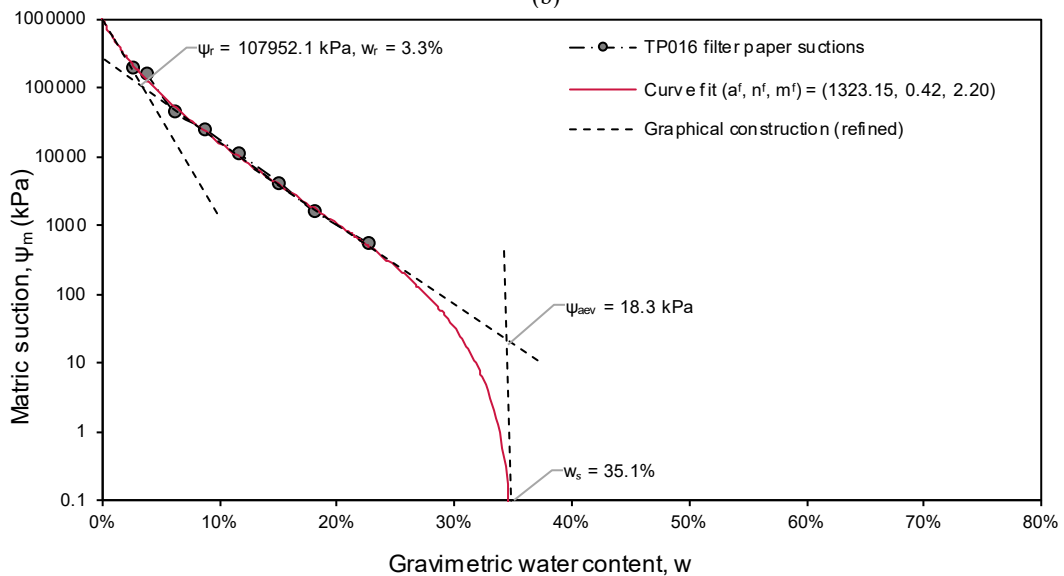
Figure 5-32 (a), (b) and (c) show the measured filter paper suctions and the refined gravimetric water content SWRC (ψ_m-w) curve-fits for samples TP148, TP149, and TP016, respectively.



(a)



(b)



(c)

Figure 5-32 Final SWRC curve fits (ψ_m-w) for fine-grained soil samples: (a) TP148; (b) TP149; (c) TP016

5.4.2 Sample TP148: Clayey sand – tensiometer vs filter paper methods

Figure 5-33 compares the gravimetric water content SWRCs (ψ_m-w) and Figure 5-34 the normalised degree of saturation SWRCs (ψ_m-S) determined by the filter paper and tensiometer methods for sample TP149. The filter paper measurements were taken from specimens prepared at an average dry density of 1.55 g/cm^3 , close to that of Test #2 at 1.54 g/cm^3 . Excellent agreement was found between the methods up to around 1000 kPa. When comparing the continuous SWRC determined by the tensiometer method and the SWRC from the filter paper method, some nuance in the form of the SWRC was lost by the curve-fitting for the specimen dried from an oversaturated slurry. A closer agreement could be expected for compacted or confined specimens.

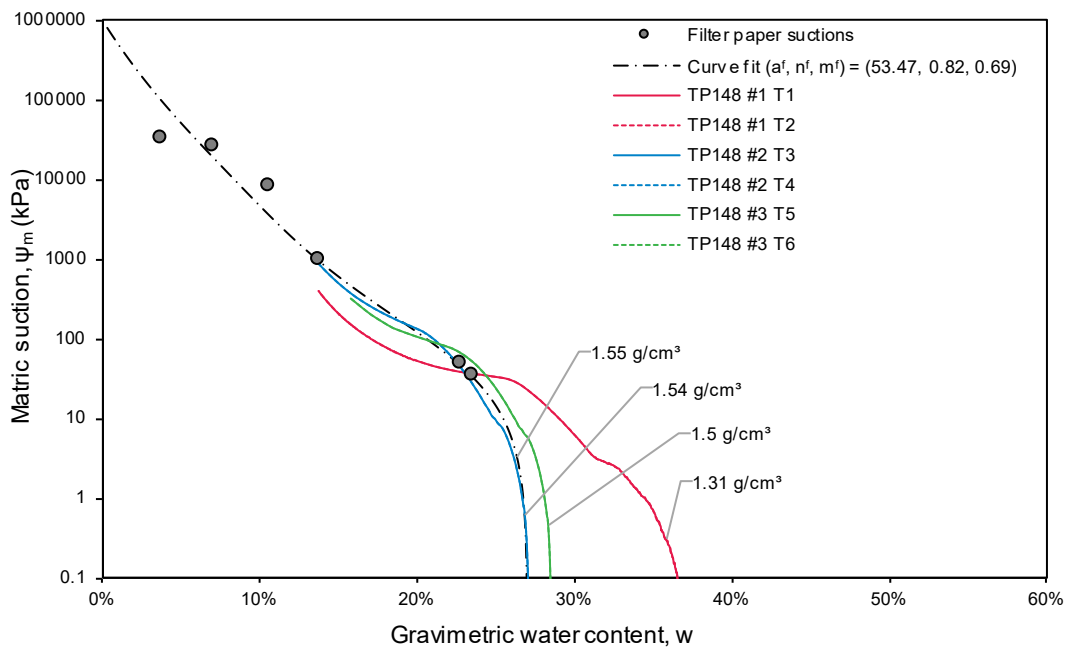


Figure 5-33 Tensiometer vs filter paper SWRCs (ψ_m-w) for sample TP148

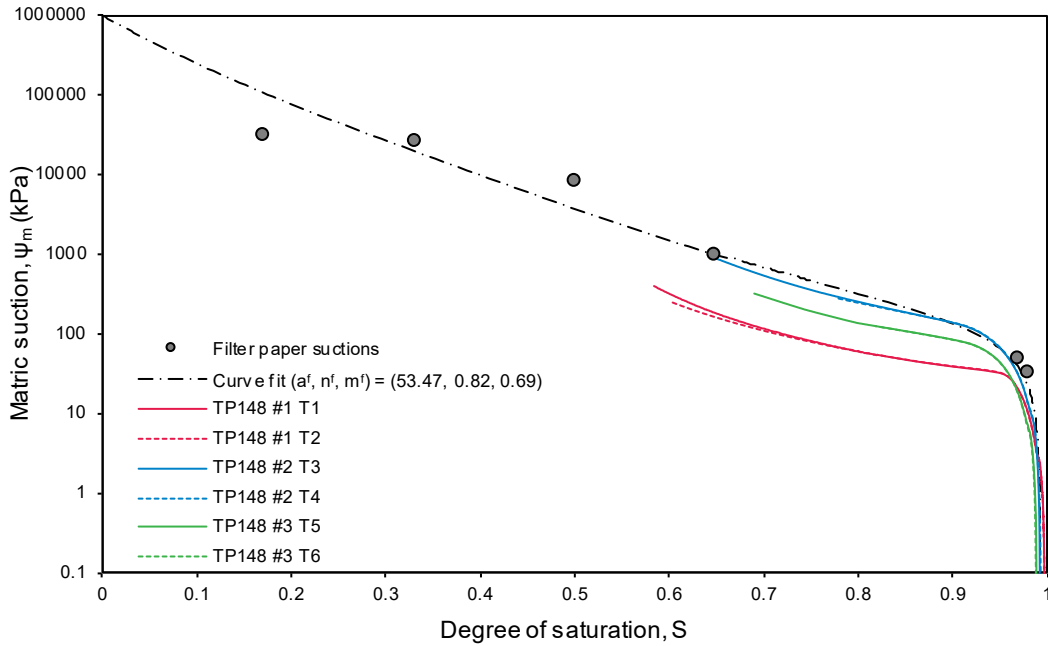


Figure 5-34 Tensiometer vs filter paper SWRCs (ψ_m - S) for sample TP148

5.4.3 Sample TP149: Lean clay – tensiometer vs filter paper methods

Figure 5-35 and Figure 5-36 compare the gravimetric water content SWRCs (ψ_m - w), and normalised degree of saturation SWRCs (ψ_m - S) determined by the filter paper and tensiometer methods for sample TP149, respectively. The filter paper measurements were taken from specimens prepared at an average dry density of 1.59 g/cm^3 , the highest that could be achieved in the retaining rings by compaction. Since the specimens for each method were prepared and tested differently, no direct comparison could be made. However, it appears that the tensiometer measurements tended towards the suctions measured by the filter paper method at very low water contents, and had the capacity of the tensiometer been higher the SWRCs would be close. The discrepancy in the SWRCs between the methods stems firstly from the difference in density at each water content due to the volumetric shrinkage of the specimens during continuous drying and the compacted density of the filter paper specimens. The second source of discrepancy stems from the hysteresis between PDCs determined from the tensiometer method and the scanning wetting curve determined from the filter paper method, which is expected to be between the PDCs and the PWCs (as was shown in Sections 5.2.2 and 5.2.3 for granular soils).

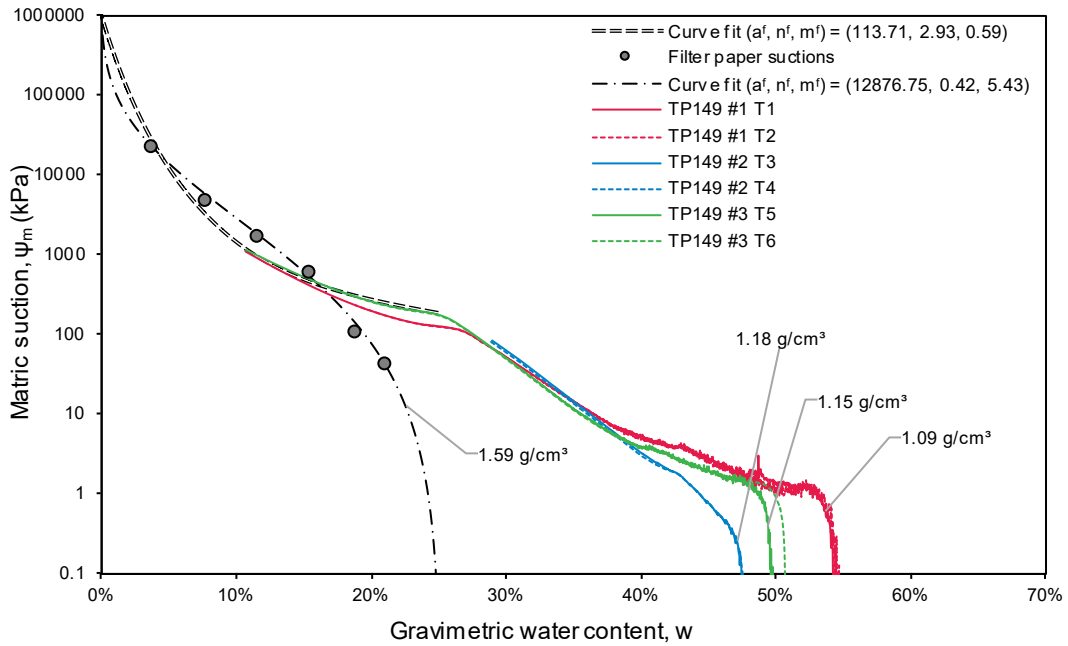


Figure 5-35 Tensiometer vs filter paper SWRCs (ψ_m-w) for sample TP149

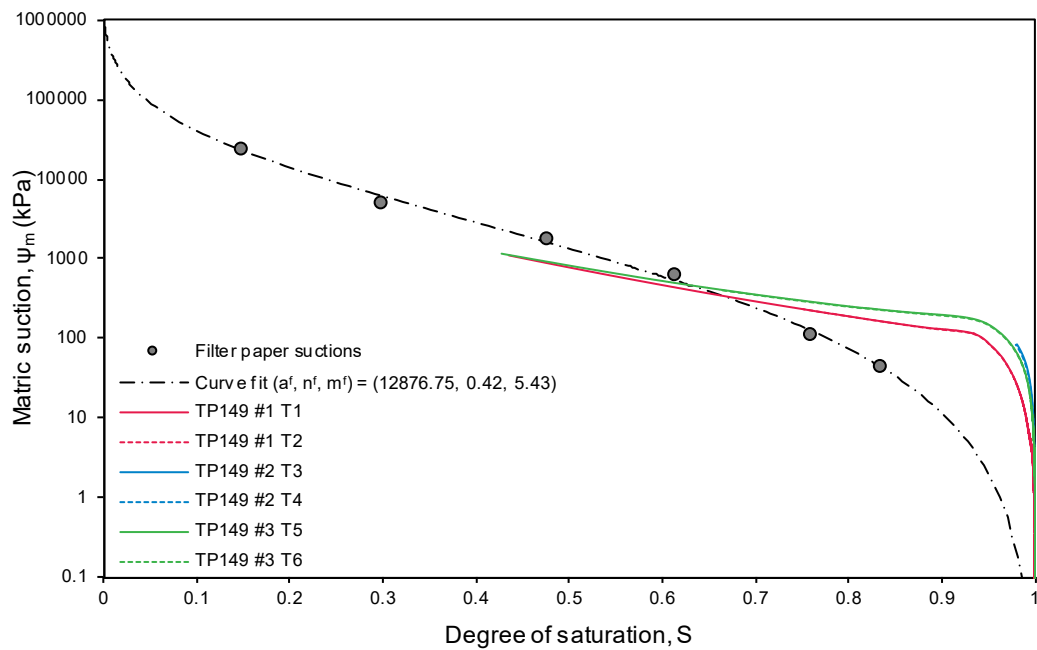


Figure 5-36 Tensiometer vs filter paper SWRCs (ψ_m-S) for sample TP149

5.4.4 Sample TP016: Clay – tensiometer vs filter paper methods

Figure 5-37 compares the gravimetric water content SWRCs (ψ_m-w) determined by the filter paper and tensiometer methods for sample TP016. The filter paper measurements were taken from specimens prepared at an average dry density of 1.35 g/cm^3 , whereas the tensiometer suctions were determined from the clay undergoing shrinkage during drying from around

1.00 g/cm³ to 1.87 g/cm³. As with the lean clay sample, a direct comparison could not be made, particularly at the higher water content range. Again, it appeared that the suctions measured by the tensiometer method tended towards that of the filter paper method at low water contents, beyond the capacity of the tensiometer.

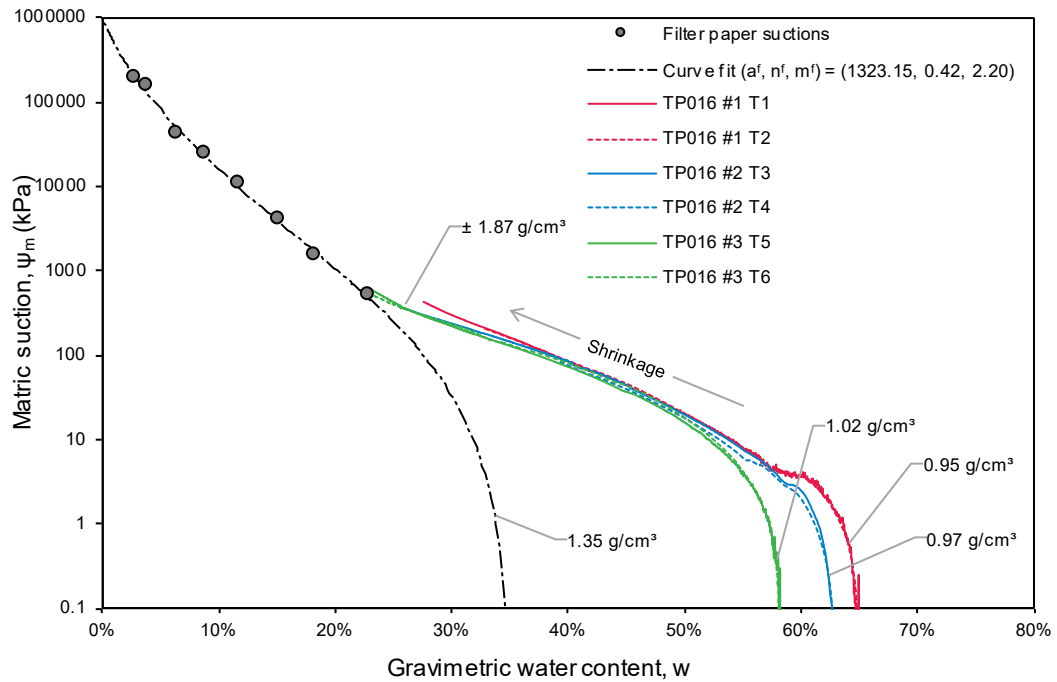


Figure 5-37 Tensiometer vs filter paper SWRCs (ψ_m-w) for sample TP016

A final test was performed on the clay sample (Test #4) using the tensiometer method and the strain-gauged hangers described in Section 4.2.1. This was done to verify the curve fit of the SWRC determined from the filter paper measurements from an initially compacted specimen. Figure 5-38 shows that, as with the granular soils and clayey sand samples, close agreement between the methods could be obtained. A curve fit for the SWRC determined from the initially slurried specimen in Test #3 combined with the filter paper measurements was attempted based on the assumption that the two methods would provide similar results at low water contents. The result is shown in Figure 5-38 and in Figure 5-39. By translating the filter paper suctions and curve fit on the degree of saturation axis using the specimen's shrinkage curve and the fundamental relationships of a soil's volumetric and saturation states (Equation 5.1), a reasonable estimation of the normalised degree of saturation SWRCs (ψ_m-S) could be made.

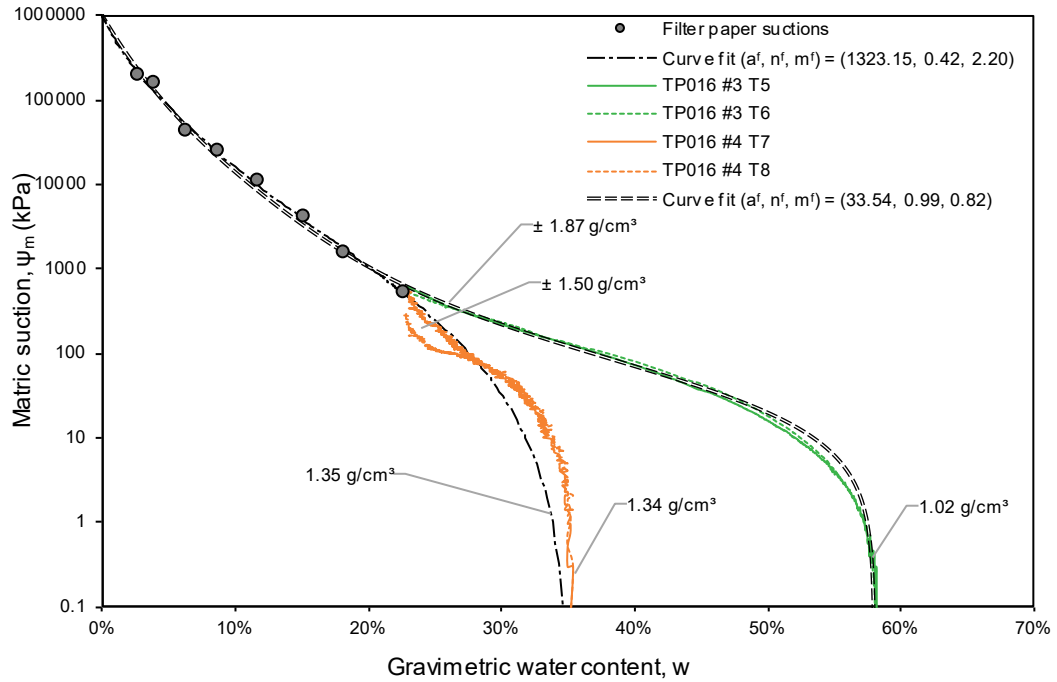


Figure 5-38 Compacted vs initially slurried SWRCs (ψ_m-w) for sample TP016

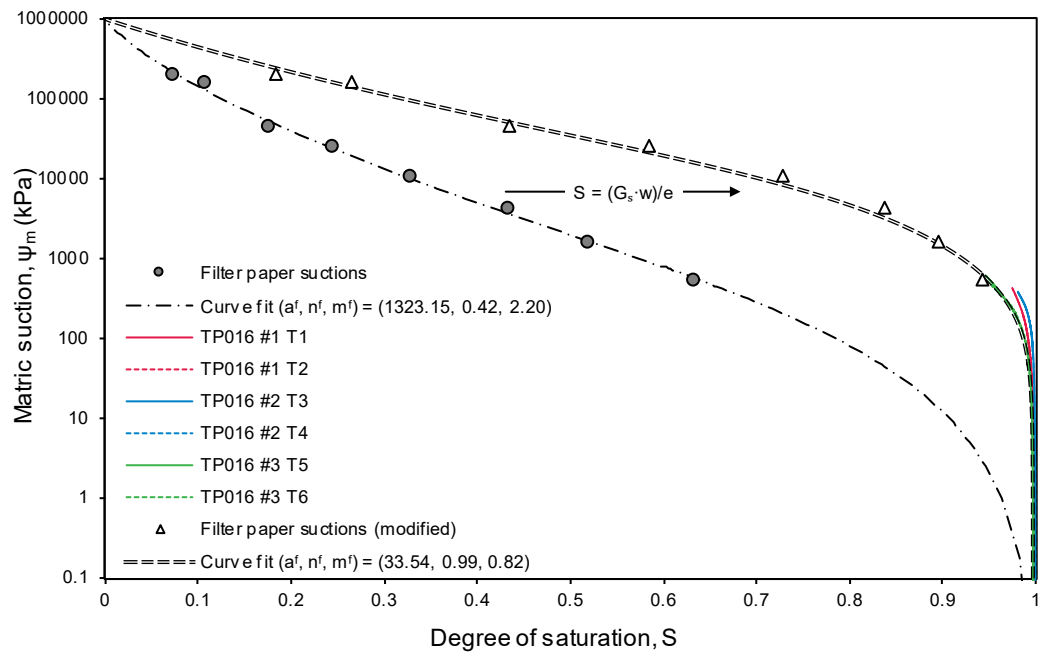


Figure 5-39 Tensiometer vs filter paper SWRCs (ψ_m-S) for sample TP016

6 CONCLUSIONS

In this section, the main conclusions reached based on the results obtained will be conveyed. The conclusions will focus on the objectives of the report, as outlined in Section 1.2. Subsequently, recommendations will be given to assist in future research relating to the project topic.

6.1 CONCLUSIONS

The following conclusions could be drawn from the research presented in this study:

- A new tensiometer made out of low-cost elements was presented in this study, with a focus on the reliable measurement of suctions between 0 – 1000 kPa, offering excellent resolution and sensitivity at a low cost.
- The tensiometer was able to measure suctions up to 1150 kPa. Although higher suctions can be measured with other indirect methods, the direct measurement of soil suctions in the 0 – 1000 kPa range is of great interest and has the potential for the use in unsaturated soil testing scenarios where extreme desaturation is infeasible such as centrifuge modelling. The added strength of a soil gained from suction pressures has been determined to peak at relatively lower water contents, where after the added strength gain diminishes as the water content reduces. The direct measurement of soil suctions in the 0 – 1000 kPa range can also enable further studies into the SWRC and strength gain function interdependency.
- The tensiometer used a piezoresistive silicon sensing element, rather than a more common strain-gauged diaphragm-type sensor to register pressures. Direct negative pressure calibration through the isotropic consolidation of a clay specimen and the extrapolation of positive pressure calibration was found to be identical, and thus the tensiometer design was determined to be suitable for the direct measurement of suction pressures.
- The tensiometer was used in the continuous drying method to determine the SWRCs for five different soils, including granular soils of negligible volume change and fine-grained clayey soils of significant volume change.
- The method tested soil specimens of negligible volume change under zero confinement pressure. This condition is directly applicable to studies on the strength gain and loss of materials such as mine tailings that undergo wetting and drying cycles during deposition.

- The method for determining SWRCs described in this study is a laboratory method used on reconstituted samples. However, compacted specimens were also tested successfully, and therefore the potential exists for the SWRCs of undisturbed samples to be tested by this method as well.
- A novel way of determining the specimen volume during testing was presented. A series of images of the specimen during the test could be used to determine the volume change relative to known direct measurements of the specimen dimensions before and after the test. This information could be used to determine the shrinkage curves of fine-grained clayey soils undergoing shrinkage to produce the degree of saturation SWRC.
- For the typical specimen dimensions (23.3 mm in height and 71.6 mm in diameter) and aspect ratio (approximately 1:3), the location of the tensiometers did not affect the results since nearly identical suctions were registered by each of the two tensiometers in each test for both granular and clayey soils. This suggests that direct contact suction measurement would be feasible and may improve the accuracy of specimen volume determination.
- The filter paper method was used to verify the tensiometer suction measurement with good agreement. Although the tensiometer method proposed cannot be used to replace the conventional method for the entire range of suctions, the filter paper method served as a valuable extension to the tensiometer method to validate and supplement the results beyond the capacity of the tensiometer to obtain a full SWRC.

6.2 RECOMMENDATIONS

Recommendations for future work related to this study include the following:

Tensiometer improvements:

- Future developments are related to the improvement of the tensiometer durability, measurement capacity and reliability. The handling and preparation of the delicate filter ceramic should be investigated. The epoxy coating should be replaced with a more durable machined housing. The gel layer covering the sensing element present in the pressure sensor seemed to accumulate contaminants over time and result in cavitation more readily. This protection layer should be removed from future prototypes.
- Since the pressure sensor was found to be slightly temperature-sensitive, the design of the tensiometer can be altered to include a small thermistor in the body of the device for in-situ temperature monitoring. This change would not add significant complexity to the device and only require two additional thin cable connections.

- The new tensiometer should be tested for its applicability in long term monitoring of suctions in-situ in, for example, tailings dams. Information into the suction gain and loss during deposition of tailings, seasonal changes and precipitation may provide invaluable insight into the suction induced strength, which may improve or optimise the design and safety of these structures.
- The tensiometer saturation procedures outlined in this study proved to be successful. However, other methods of applying high pre-pressurisation pressures outside of the laboratory environment should be considered. A portable saturation device may be considered and will prove to be very useful for testing the new tensiometer in-situ.

Determination of soil-water retention curves using the tensiometer method.

- Improved measurement of the specimen dimension changes during testing should be investigated, evaluating techniques like photogrammetry, LASER measurement or other non-contact dimensional measurement methods (as in White *et al.* (2003) or Le *et al.* (2016)).
- The over-saturated slurry consistency of the specimens tested in this study and the embedment of the tensiometer inside the specimens themselves ensured that good contact between the tensiometer filter and the soil pores could be maintained. It was, however, found that a degree of cracking could occur, breaking that contact and making the accurate determination of the specimen volume a challenge. Direct contact measurement of suctions with the tensiometer should be investigated to mitigate these issues.
- Temperature and humidity control during SWRC measurement were not addressed in this study. The rate of evaporation, and thus, the rate of suction development appeared to affect the maximum measurable value of suction by the tensiometer. This should be considered in future experiments where a humidity and temperature-controlled environment might yield more consistent results.

7 REFERENCES

- Archer, A. 2014. *Using Small-Strain Stiffness To Predict the Settlement of Shallow Foundation on Sand*. MEng Dissertation. University of Pretoria.
- ASTM 2002. *ASTM D6836-02: Standard Test Methods for Determination of the Soil Water Characteristic Curve for Desorption Using Hanging Column, Pressure Extractor, Chilled Mirror Hygrometer, or Centrifuge*. West Conshohocken, PA, United States: ASTM International.
- ASTM 2003. *ASTM D5298-03: Standard Test Method for Measurement of Soil Potential (Suction) Using Filter Paper*. West Conshohocken, PA, United States: ASTM International.
- ASTM 2011. *ASTM D4767-11: Standard Test Method for Consolidated Undrained Triaxial Compression Test for Cohesive Soils*. West Conshohocken, PA, United States: ASTM International.
- ASTM 2017a. *ASTM D2487-17: Standard Practice for Classification of Soils for Engineering Purposes (Unified Soil Classification System)*. West Conshohocken, PA, United States: ASTM International.
- ASTM 2017b. *ASTM D4318-17: Standard Test Methods for Liquid Limit, Plastic Limit, and Plasticity Index of Soils*. West Conshohocken, PA, United States: ASTM International.
- Beddoe, R.A., Rowe, R.K. & Take, W.A. 2010. Development of suction measurement techniques to quantify the water retention behaviour of GCLs. *Geosynthetics International* 17(5): 301-312.
- Bicalho, K.V. *et al.* 2010. Evaluation of filter paper calibrations for laboratory estimating of soil suctions. In Buzzi, O., Fityus, S. & Sheng, D. (eds.) *Unsaturated Soils: Theoretical and Numerical Advances in Unsaturated Soil Mechanics - Proceedings of the 4th Asia Pacific Conference on Unsaturated Soils.*, 2010 Taylor & Francis Group: 215-220.
- Bocking, K.A. & Fredlund, D.G. 1979. Use of the Osmotic Tensiometer to Measure Negative Pore Water Pressure. *Geotechnical Testing Journal* 2(1): 3-10.
- Bulut, R. & Leong, E.C. 2008. Indirect measurement of suction. *Geotechnical and Geological Engineering* 26(6): 21-32.

- Chandler, R.J., Crilly, M.S. & Montgomery-Smith, G. 1992. A Low-Cost Method of Assessing Clay Desiccation for Low-Rise Buildings. *Proceedings of the Institution of Civil Engineers - Civil Engineering* 92(2): 82-89.
- Chen, R., Liu, J., Li, J.H. & Ng, C.W.W. 2015. An Integrated High-Capacity Tensiometer for Measuring Water Retention Curves Continuously. *Soil Science Society of America Journal* 79(3): 943-947.
- Chiu, C.F. *et al.* 2005. Lessons learnt from suction monitoring during centrifuge modeling. In Tarantino, A., Romero, E. & Cui, Y.J. (eds.) *Proceedings of the International Symposium on Advanced Experimental Unsaturated Soil Mechanics*. Trento, Italy, 2005 CRC Press: 27-29.
- Cook, D.L. & Fredlund, D.G. 1998. TDR matric suction measurements. In *Proceedings of the International Conference on Unsaturated Soils*. Beijing, China, 1998: 338-343.
- Cui, Y.J., Tang, A.M., Mantho, A.T. & De Laure, E. 2008. Monitoring field soil suction using a miniature tensiometer. *Geotechnical Testing Journal* 31(1): 95-100.
- Fawcett, R.G. & Collins-George, N. 1967. A filter paper method for determining the moisture characteristics of soil. *Australian Journal of Experimental Agriculture and Animal Husbandry* 7: 162-167.
- Fredlund, D.G. 2006. Unsaturated Soil Mechanics in Engineering Practice. *Journal of Geotechnical and Geoenvironmental Engineering* 132(3): 286-321.
- Fredlund, D.G. & Houston, S.L. 2013. Interpretation of soil-water characteristic curves when volume change occurs as soil suction is changed. In B. Caicedo (ed.) *Advances in Unsaturated Soils*. London: Taylor & Francis Group. 15-31.
- Fredlund, D.G. & Morgenstern, N.R. 1977. Stress State Variables for Unsaturated Soils. *Journal of the Geotechnical Engineering Division* 103(5): 447-466.
- Fredlund, D.G. & Rahardjo, H. 1993. *Soil Mechanics for Unsaturated Soils*. New York: Wiley.
- Fredlund, D.G., Rahardjo, H. & Fredlund, M.D. 2012. *Unsaturated Soil Mechanics in Engineering Practice*. Hoboken, New Jersey: John Wiley & Sons, Inc.
- Fredlund, D.G., Rahardjo, H., Leong, E.C. & Ng, C.W.W. 2001. Suggestions and recommendations for the interpretation of soil-water characteristic curves. In *Proceedings of the 14th Southeast Asian Geotechnical Conference*. Hong Kong, 2001: 503-508.

- Fredlund, D.G., Shuai, F., Yazdani, J. & Feng, M. 1998. Recent developments of a sensor for the in situ measurement of matric suction. In *Proceedings of the 51st Canadian Geotechnical Conference*. Edmonton, Alberta, 1998: 81-86.
- Fredlund, M.D., Wilson, G.W. & Fredlund, D.G. 1997. Prediction of the soil-water characteristic curve from grain-size distribution. In *Proceedings of the 3rd Brazilian Symposium on Unsaturated Soils*. Rio de Janeiro, 1997: 13-24.
- Fredlund, M.D., Wilson, G.W. & Fredlund, D.G. 2002. Representation and estimation of the shrinkage curve. In Jucá, J.F.T., de Campos, T.M.P. & Marinho, F.A.M. (eds.) *Proceedings of the 3rd International Conference on Unsaturated Soils (UNSAT 2002)*. Recife, Brazil, 2002 Swets & Zeitlinger: 145-149.
- Fredlund, D.G. & Xing, A. 1994. Equations for the soil-water characteristic curve. *Canadian Geotechnical Journal* 31(3): 521-532.
- Gardener, R. 1937. A method of measuring the capillary tension of soil moisture over a wide moisture range. *Journal of Soil Science* 43(4): 277-283.
- Germaine, J.T. & Germaine, A.V. 2009. *Geotechnical Laboratory Measurements for Engineers*. Hoboken, New Jersey, United States of America: John Wiley & Sons, Inc.
- Greacen, E.L., Walker, G.R. & Cook, P.G. 1987. Evaluation of the Filter Paper Method for Measuring Soil Water Suction. In Logan, U.T. (ed.) *International Conference on Measurement of Soil and Plant Water Status*. Glen Osmond, Australia, 1987: 162-167.
- Guan, Y. & Fredlund, D.G. 1997. Use of the tensile strength of water for the direct measurement of high soil suction. *Canadian Geotechnical Journal* 34: 604-614.
- Guan, Y., Fredlund, D.G. & Gan, J.K.-M. 1998. Behaviour of water subjected to high tensile stress. In *Proceedings of the 2nd International Conference on Unsaturated Soils (UNSAT 1998)*. Beijing, China, 1998: 356-361.
- Hamblin, A.P. 1981. Filter-paper method for routine measurement of field water potential. *Journal of Hydrology* 53: 355-360.
- International Organization for Standardization 2002. *ISO 14688-1:2002 Geotechnical investigation and testing - Identification and classification of soil - Part 1: Identification and description*. Standard. International Organization for Standardization.
- Jacobsz, S.W. 2018. Low cost tensiometers for geotechnical applications. In McNamara, A. *et al.* (eds.) *Proceedings of the 9th International Conference on Physical Modelling in*

- Geotechnics (ICPMG 2018)*. London, United Kingdom, 2018 Taylor Francis Group: 305-310.
- Jacobsz, S.W. 2019. TUKS tensiometer measures to -1.7 Mega Pascal. *SAICE Civil Engineering*, January/February. 24-26.
- Krahn, J. & Fredlund, D.G. 1972. On total, matric and osmotic suction. *Soil Science* 144(5): 339-347.
- Le, B.T., Nadimi, S., Goodey, R.J. & Taylor, R.N. 2016. System to measure three-dimensional movements in physical models. *Géotechnique Letters* (6): 1-7.
- Leong, E.C., He, L. & Rahardjo, H. 2002. Factors Affecting the Filter Paper Method for Total and Matric Suction Measurements. *Geotechnical Testing Journal* 25(3): 322-332.
- Lourenço, S.D.N. *et al.* 2011. A new procedure for the determination of soil-water retention curves by continuous drying using high-suction tensiometers. *Canadian Geotechnical Journal* 48(2): 327-335.
- Lourenço, S.D.N., Gallipoli, D., Toll, D.G. & Evans, F.D. 2006. Development of a commercial tensiometer for triaxial testing of unsaturated soils. In *Proceedings of the 4th International Conference on Unsaturated Soils (UNSAT 2006)*. Phoenix, USA, 2006 ASCE Geotechnical: 1875-1886.
- Lourenço, S.D.N. *et al.* 2008. Calibrations of a high-suction tensiometer. *Géotechnique* 58(8): 659–668.
- Lourenço, S.D.N. *et al.* 2010. Calibrations of a high-suction tensiometer: Discussion. *Géotechnique* 60(3): 233-234.
- Lu, N. & Likos, W.J. 2004. *Unsaturated Soil Mechanics*. Hoboken: Wiley.
- Malaya, C. & Sreedeeep, S. 2012. Critical review on the parameters influencing soil-water characteristic curve. *Journal of Irrigation and Drainage Engineering* 138(1): 55-63.
- Marinho, F.A.M. & Chandler, R.J. 1995. Cavitation and the Direct Measurement of Soil. In *Proceedings of the 1st International Conference on Unsaturated Soils (UNSAT 1995)*. Paris, France, 1995: 623–630.
- Marinho, F.A.M. & Oliveira, O.M. 2006. The filter paper method revised. *ASTM geotechnical testing journal* 29(3): 250-258.

- Marinho, F.A.M., Take, W.A. & Tarantino, A. 2008. Measurement of Matric Suction Using Tensiometric and Axis Translation Techniques. *Geotechnical and Geological Engineering* 26: 615-631.
- Measurement Specialties 2012. *MS54XX Miniature SMD Pressure Sensor*. [Electronic document] Available at: <http://www.meas-spec.com/downloads/MS54XX.pdf> [Accessed 12 May 2013].
- Meilani, I., Rahardjo, H., Leong, E.C. & Fredlund, D.G. 2002. Mini suction probe for matric suction measurements. *Canadian Geotechnical Journal* 39(6): 1427-1432.
- Mendes, J. & Buzzi, O. 2013. New insight into cavitation mechanisms in high-capacity tensiometers based off on high-speed photography. *Canadian Geotechnical Journal* 50: 550-556.
- Mercer, K., Rahardjo, H. & Satyanaga, A. 2019. *Unsaturated Soils Guidelines - Volume 1: Soil-Water Characteristic Curves for Materials Classified According to the Unified Soil Classification System*. Crawley, Australia: Australian Centre for Geomechanics.
- Muñoz-Castelblanco, J.A., Pereira, J.M., Delage, P. & Cui, Y.J. 2012. The water retention properties of a natural unsaturated loess from northern France. *Géotechnique* 62(2): 95-106.
- Ng, C.W.W. & Menzies, B. 2007. *Advanced Unsaturated Soil Mechanics and Engineering*. New York: Taylor & Francis.
- Peck, A.J. & Rabbige, R.M. 1969. Design and performance of an osmotic tensiometer for the measuring of capillary potential. *Soil Science Society of America Proceedings* 33(2): 196-202.
- Pedrotti, M., Tarantino, A. & Boeck, F. 2014. Experience gained from the conditioning of high-capacity tensiometers. In Khalili, N., Russell, A. & Koshghalb, A. (eds.) *6th International Conference on Unsaturated Soils*. London, 2014 Taylor & Francis Group: 1651-1657.
- Pham, H.Q., Fredlund, D.G. & Barbour, S.L. 2001. Evaluation of physically based hysteresis models soil-water characteristic curve. In *International Conference on Management of the Land and Water Resources*. Hanoi, Vietnam, 2001: 41-48.
- Qingtian, L.I. & Standing, J. 2014. Experimental set-up for determining soil water retention curves for granular soils during drying. *Acta Geologica Sinica (English Edition)* 88(6): 1875-1883.

- Ridley, A.M. & Burland, J.B. 1993. A new instrument for the measurement of soil moisture suction. *Géotechnique* 43(2): 321-324.
- Ridley, A.M. & Burland, J.B. 1994. A new instrument for the measurement of soil moisture suction (Discussion). *Géotechnique* 44(3): 551-556.
- Ridley, A.M. & Burland, J.B. 1995. A pore pressure probe for the in situ measurement of soil suction. In *Proceedings of the Conference on Advances in Site Investigation Practice*. London, 1995: 510-520.
- Ridley, A.M. & Wray, W.K. 1995. Suction measurement: a review of current theory and practices. In Alonso, E.E. & Delage, P. (eds.) *Proceedings of the 1st International Conference on Unsaturated Soils (UNSAT 95)*. Paris, France, 1995 Balkema: 1293-1322.
- Sillers, W.S. 1997. *The mathematical representation of the soil-water characteristic curve*. MSc Thesis. University of Saskatchewan.
- Soilmoisture Equipment Corporation 2000. *1/4" (7.11 mm) Thick Ceramic Plates (0604 SERIES)*. [Online] Available at: <http://www.soilmoisture.com/1/4-inch-Thick-Ceramic-Plates-0604-SERIES/> [Accessed 24 February 2016].
- Standing, J.R. 2012. The Development of Unsaturated Soil Mechanics at Imperial College, London. *Geotechnical Engineering Journal of the SEAGS & AGSSEA* 43(1): 59-75.
- Suits, L., Sheahan, T., Marinho, F. & Gomes, J.d.S. 2012. The Effect of Contact on the Filter Paper Method for Measuring Soil Suction. *Geotechnical Testing Journal* 35(1): 172-181.
- Take, W.A. & Bolton, M.D. 2002. A new device for the measurement of negative pore water pressures in centrifuge models. In *International Conference on Physical Modelling in Geotechnics*. St John's, Newfoundland, 2002: 89-94.
- Take, W.A. & Bolton, M.D. 2003. Tensiometer saturation and the reliable measurement of soil suction. *Géotechnique* 53(2): 159-172.
- Tang, A.M., Cui, Y.J. & Qian, L.X. 2010. Calibration of the osmotic technique of controlling suction with respect to temperature using a miniature tensiometer (Technical Note). *Canadian Geotechnical Journal* 47(3): 359-365.
- Tarantino, A. & Mongiovì, L. 2001. Experimental procedures and cavitation mechanisms in tensiometer measurements. *Geotechnical and Geological Engineering* 19(3): 189-210.

- Tarantino, A. & Mongiovì, L. 2003. Calibration of tensiometer for direct measurement of matric suction. *Géotechnique* 53(1): 137-141.
- TE Connectivity 2018. *Miniature mV Output Pressure Sensor*. [Electronic Document] Available at: <https://www.te.com/usa-en/product-CAT-BLPS0028.html> [Accessed 23 September 2019].
- Toker, N.K. 2002. *Improvements and Reliability of MIT Tensiometers and Studies on Soil Moisture Characteristic Curves*. MSc Dissertation. Massachusetts Institute of Technology.
- Toker, N.K., Germaine, J.T., Sjoblom, K.J. & Culligan, P.J. 2004. A new technique for rapid measurement of continuous soil moisture characteristic curves. *Géotechnique* 54(3): 179-186.
- Toll, D.G. 2012. The behaviour of unsaturated soils. In B.B.K. Huat, D.G. Toll & A. Prasad (eds.) *Handbook of Tropical Residual Soils Engineering*. London, United Kingdom: Taylor & Francis.
- Toll, D.G., Lourenço, S.D.N. & Mendes, J. 2013. Advances in suction measurements. *Engineering Geology* 165(Special Issue: Research and Applications in Unsaturated Soil Mechanics): 29–37.
- Van Genuchten, M.T. 1980. A closed-form equation for predicting the hydraulic conductivity of unsaturated soils. *Soil Science Society of America Journal* 44: 892-898.
- Van Heerden, J.H.F. 2002. *Direct Measurement of Pore Fluid Suction in Gold Mine Tailings*. MEng Dissertation. University of Pretoria.
- Vanapalli, S.K., Sillers, W.S. & Fredlund, M.D. 1998. The meaning and relevance of residual state to unsaturated soils. In *Proceedings of the 51st Canadian Geotechnical Conference*. Edmonton, Alberta, 1998: 1-8.
- White, D.J., Take, W.A. & Bolton, M.D. 2003. Soil deformation measurement using particle image velocimetry (PIV) and photogrammetry. *Géotechnique* 53(7): 619-631.
- Yang, H., Rahardjo, H., Leong, E.-C. & Fredlund, D.G. 2004. Factors affecting drying and wetting soil-water characteristic curves of sandy soils. *Canadian Geotechnical Journal* 41(5): 908-920.
- Young, R.F. 1989. *Cavitation*. London: McGraw-Hill.

8 APPENDICES

APPENDIX A: DETAILED PROCEDURES

A.1 Detailed saturation procedure

This section, which follows from Section 3.2.2, the procedures for tensiometer saturation, including initial saturation and pre-pressurisation, are outlined in detail below.

A.1.1 Initial saturation

The oven-drying procedure for initial saturation of the tensiometers was:

1. The tensiometers were dried in an oven at 60 °C for a period sufficient to evaporate all traces of water from the water reservoir and filter element. For tensiometers previously dried and stored in a container of desiccant, 1 hour was appropriate. For tensiometers that had recently been removed from a sample, four or more hours were allowed.
2. The tensiometers were then transferred to a small container of desiccant while the saturation set-up was being prepared.

Assuming all pressure and flow control valves were closed, the saturation and calibration set-up was then prepared:

3. The deaerator was filled with clean water (opening valves in order 1.4, 1.2, then 1.1).
4. When the deaerator was full to the specified maximum level, the deaerator cell was isolated (closing valves in order 1.1, 1.2, and 1.4).
5. The water was de-aired for at least 20 minutes (opening valves 2.1 and 2.3, then turning on the vacuum pump and agitator).
6. When the water had been sufficiently de-aired, the vacuum was released (turning off the agitator, and closing valve 2.1, then opening 1.4).
7. The air-water interface was filled (opening valves in order 1.3, 3.4, then 3.3).
8. Excess air in the interface was let out (opening valve 4.1 until some water came out, then closing the valve).
9. The water supply lines were flushed with de-aired water (disconnecting the line at 5.3 and draining water through the line, then reconnecting the line).

Initial saturation by the application of a high vacuum could then continue:

10. The tensiometers were placed in the dry saturation cell.
11. The cell was then evacuated for at least 20 minutes (opening valves 5.1 and 2.2).

A.1.2 Saturation (pre-pressurisation)

The procedure for saturating the tensiometers, assuming all flow and pressure control valves were closed, and the tensiometers had been sealed into the cell and evacuated (continuing from step 11 above) was:

12. The cell was slowly filled with de-aired water from the bottom (opening valve 3.2, then partially opening valve 5.3). The flow was controlled to prevent excessive bubbles from forming, and a small weight inside the cell was used to prevent a sudden rush of water splashing onto the surface of the tensiometers.
13. When the level of water had risen above the level of the tensiometers, the vacuum was released (closing valve 5.1, then turning off the vacuum pump).
14. Excess air in the cell was let out through the air release valve on the cell top.
15. The cell pressure was raised to an arbitrarily selected 25 kPa (closing valve 3.4, opening valves 3.5, 3.6, 3.8 and 5.5, then regulating the pressure with regulator 3.7 and test gauge 3.1).
16. The water reservoirs and filter elements were then filled with de-aired water by allowing the pressure to equilibrate under the applied pressure for approximately 1 hour or until the response of the tensiometers, as monitored through the data acquisition system, showed a sharp increase to a constant, stable value.
17. The cell was pressurised for a period sufficient to saturate the tensiometers (slowly increasing the cell pressure with regulator 3.7 and test gauge 3.1).
18. If high pressure was required to saturate the tensiometers, the high-pressure controller was used (matching the cell pressure on test gauge 3.1, closing valve 5.3, opening valve 5.4, and then increasing the cell pressure with the controller).

Steps 6 – 9 could be performed concurrently with steps 10 and 11 to expedite the saturation process.

A.2 Detailed calibration procedure

This section, which follows from Section 3.2.3, describes the procedures for verifying tensiometer saturation and performing calibration outlined in detail below.

A.2.1 Response time

The electrical response of the tensiometers was monitored through the data acquisition system in real-time to assess whether the level of saturation was adequate. Figure 3-16 shows how the level of saturation was interpreted from the response time of a tensiometer.

19. A rapid change in cell pressure was applied (using regulator 3.7) and the time required for the response of the tensiometers to reach a constant, stable value was monitored.
20. If the response time was longer than about 5 seconds, the level of saturation was determined to be inadequate. In this case, the cell would be pressurised for a further period, or a higher saturation pressure would be applied as in steps 17 and 18. Longer response times were allowed for higher AEV ceramics.
21. If the response time was shorter than about 5 seconds or close to immediate, the level of saturation was determined to be adequate, and the calibration procedure could follow.

A.2.2 Calibration

The procedure for calibrating the saturated tensiometers, assuming that the cell was pressurised (continuing from step 21 above), was:

22. The tensiometer response to applied pressure was recorded through the data acquisition system.
23. The applied pressure was cycled up and down in known increments, typically 100 kPa, (with regulator 3.7 and test gauge 3.1 or the high-pressure controller), ensuring that at each increment of applied pressure the response of the tensiometers reached a constant, stable value (Figure 3-17). A typical set of three up and down positive pressure cycles was used to generate a calibration curve the tensiometer. The positive pressure calibration curve was then linearly extrapolated into the negative pressure range, i.e. suction range. The validity of this extrapolation was tested and is discussed in Section 3.3.1).

A.3 Data processing

A.3.1 Data processing and calculations

The flow-chart in Figure 8-1 describes all the necessary data collection and conversions used in the processing of the experimental method proposed in this study.

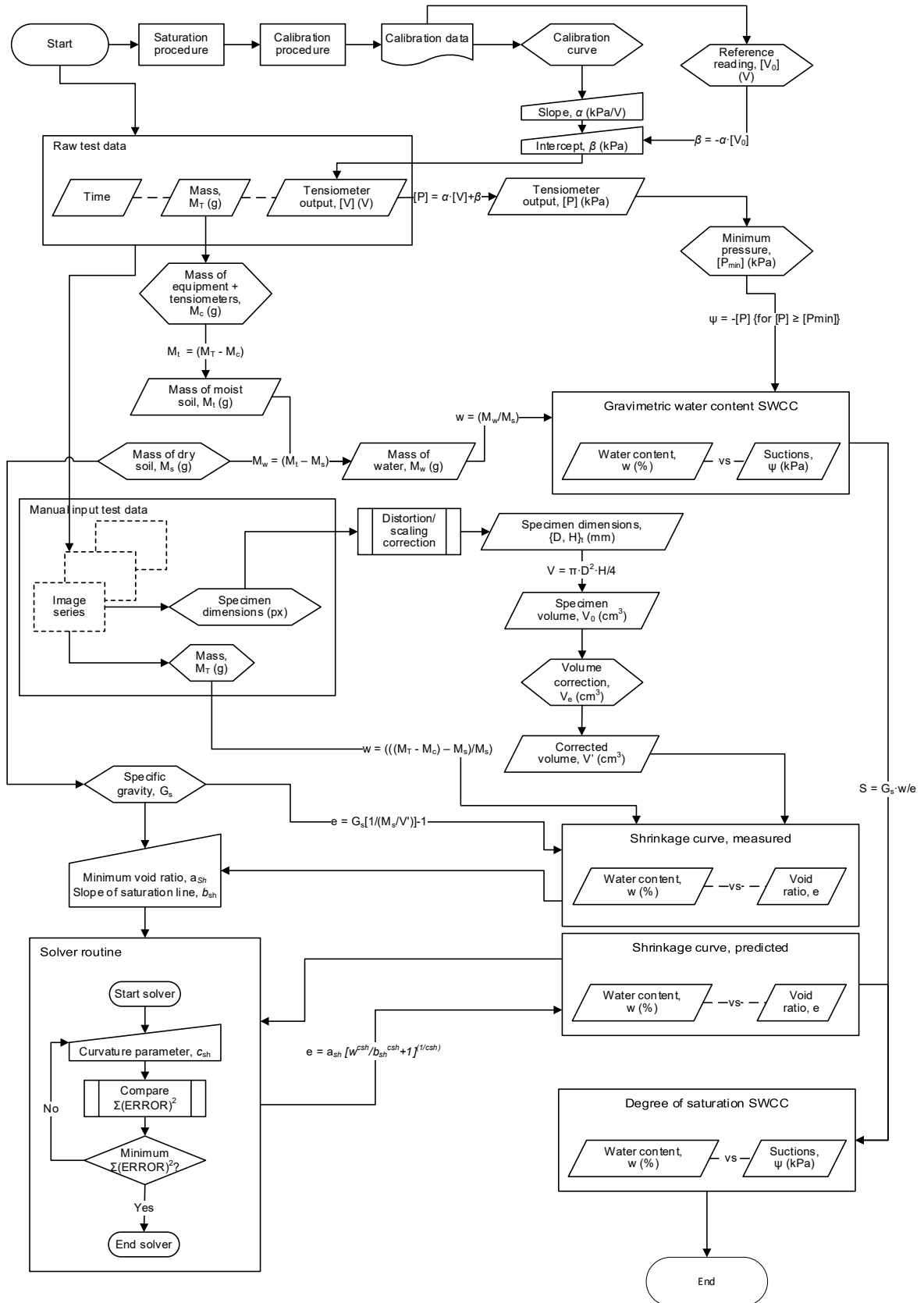


Figure 8-1 Data processing flow chart

A.3.2 Volume determination

The equations used to process the observed shrinkage of the samples into dimensional data are given in Equations 8.1 and 8.2.

$$d_{mm,i} = \left(\frac{d_{px,i}}{d_{px,1}} \right) \left(\frac{h_{px,i} - h_{px,2}}{h_{px,1} - h_{px,2}} \right) d_{mm,1} + \left(\frac{d_{px,i}}{d_{px,2}} \right) \left(\frac{h_{px,i} - h_{px,1}}{h_{px,2} - h_{px,1}} \right) d_{mm,2} \quad 8.1$$

$$h_{mm,i} = \left(\frac{h_{px,i}}{h_{px,1}} \right) \left(\frac{d_{px,i} - d_{px,2}}{d_{px,1} - d_{px,2}} \right) h_{mm,1} + \left(\frac{h_{px,i}}{h_{px,2}} \right) \left(\frac{d_{px,i} - d_{px,1}}{d_{px,2} - d_{px,1}} \right) h_{mm,2} \quad 8.2$$

where:

$h_{mm,1}$ = average measured height of specimen placed on balance (mm), and

$h_{mm,2}$ = average measured height of specimen taken off balance (mm).

$h_{mm,i}$ = corrected height (mm),

$h_{px,1}$ = average observed height of the first image (pixels),

$h_{px,2}$ = average observed height of the last image (pixels),

$h_{px,i}$ = average observed height (pixels),

$d_{mm,1}$ = average measured diameter of specimen placed on balance (mm),

$d_{mm,2}$ = average measured diameter of specimen taken off balance (mm),

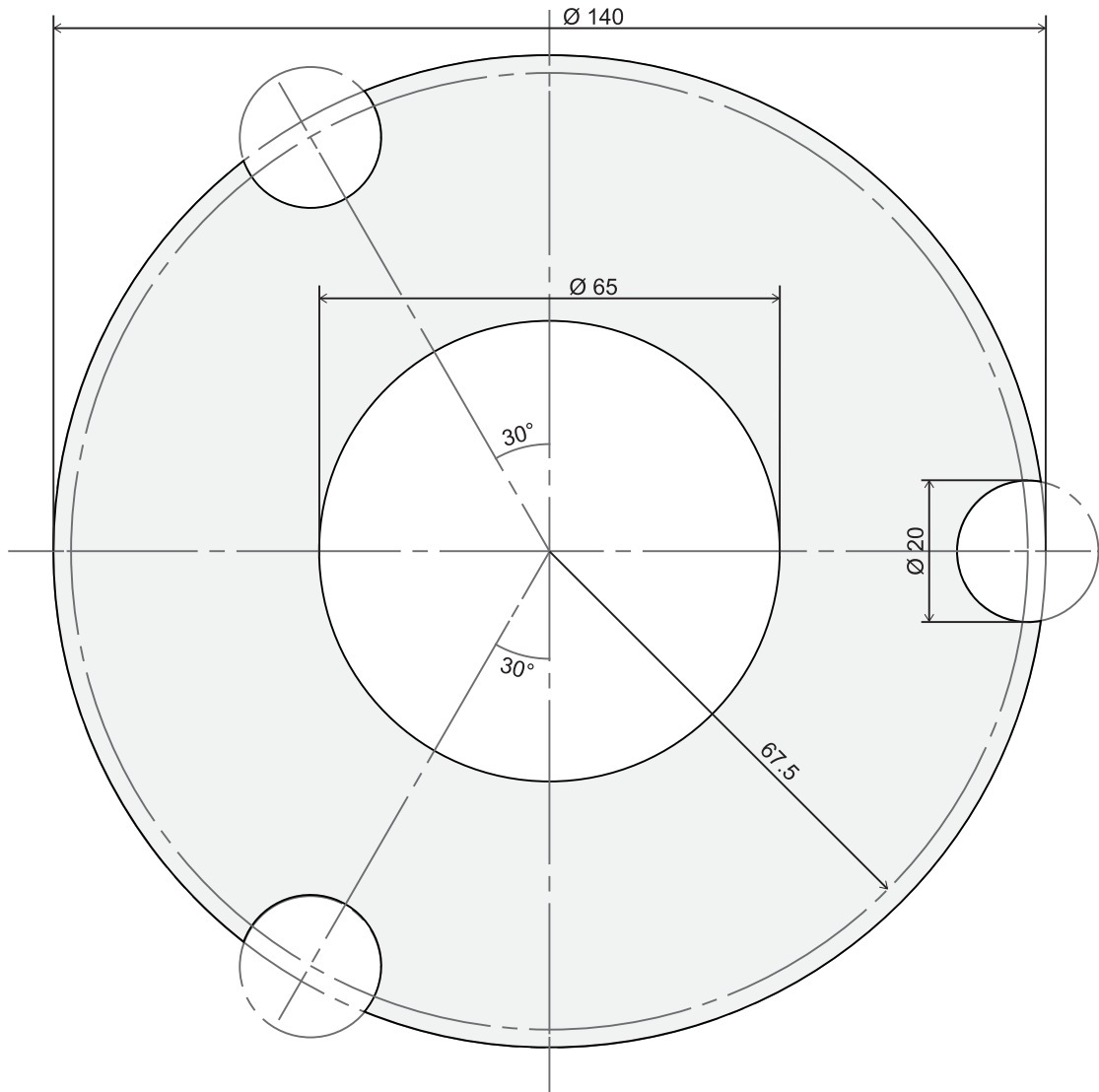
$d_{mm,i}$ = corrected diameter (mm),

$d_{px,1}$ = average observed diameter of the first image (pixels),

$d_{px,2}$ = average observed diameter of the last image (pixels),

$d_{px,i}$ = average observed diameter (pixels),

APPENDIX B: ADDITIONAL FIGURES



Scale 1:1
(All dimensions in mm)

Figure 8-2 Latex membrane seal dimensions

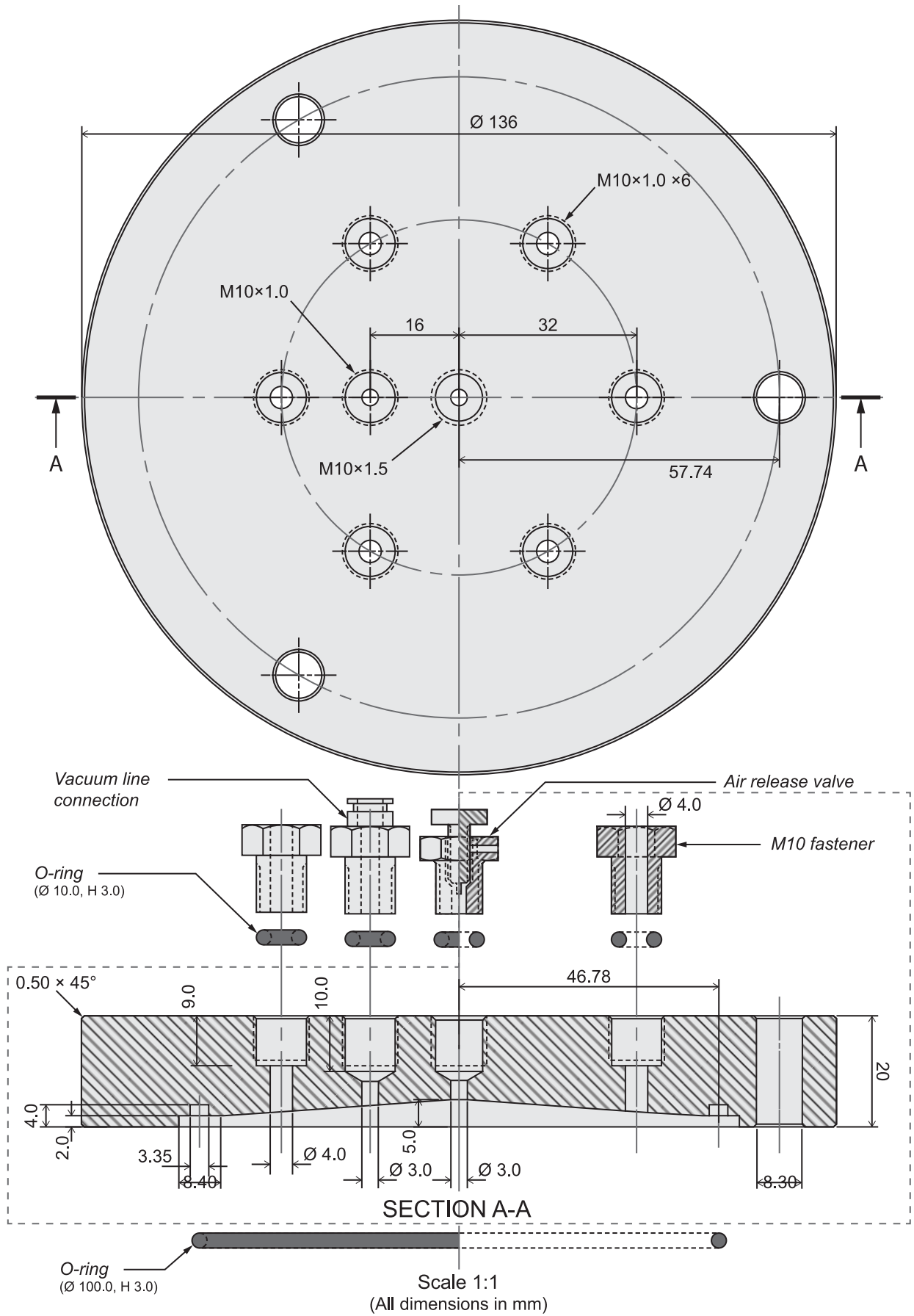


Figure 8-3 Custom triaxial cell top dimensions

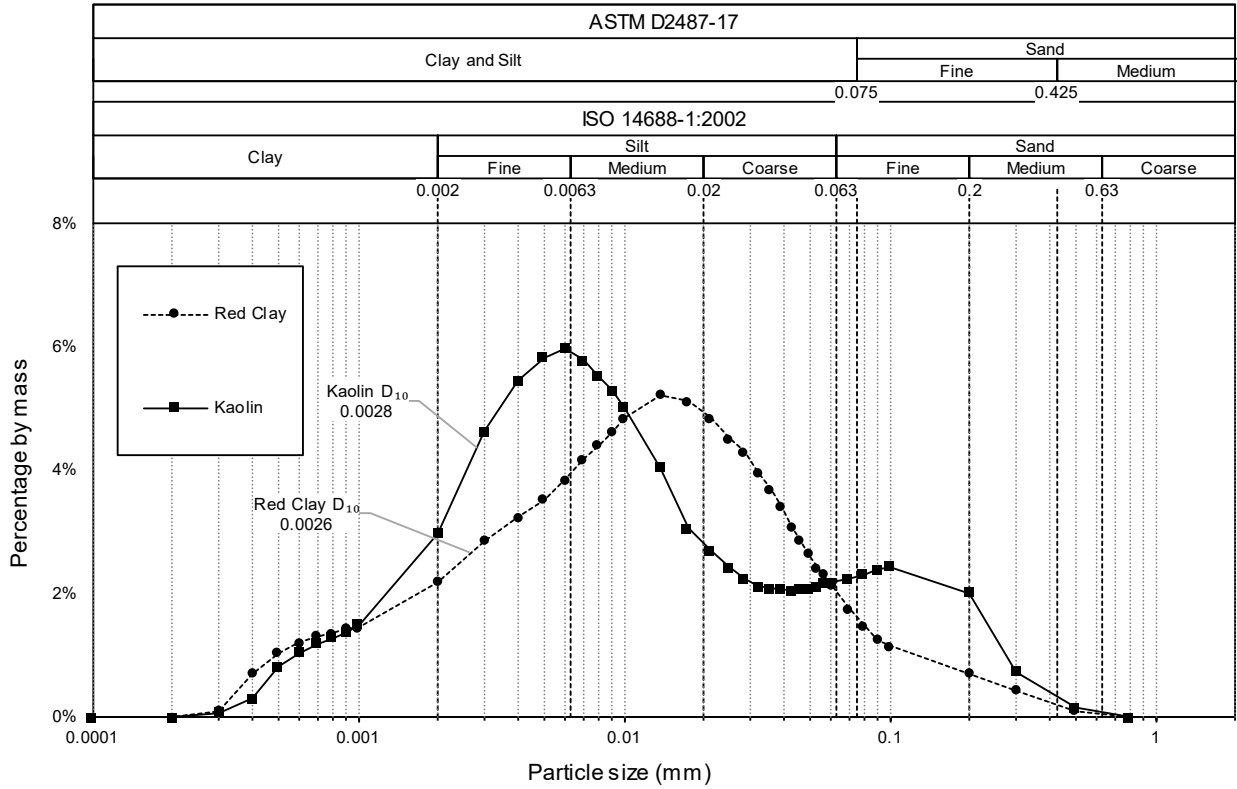


Figure 8-4 Additional particle size distributions

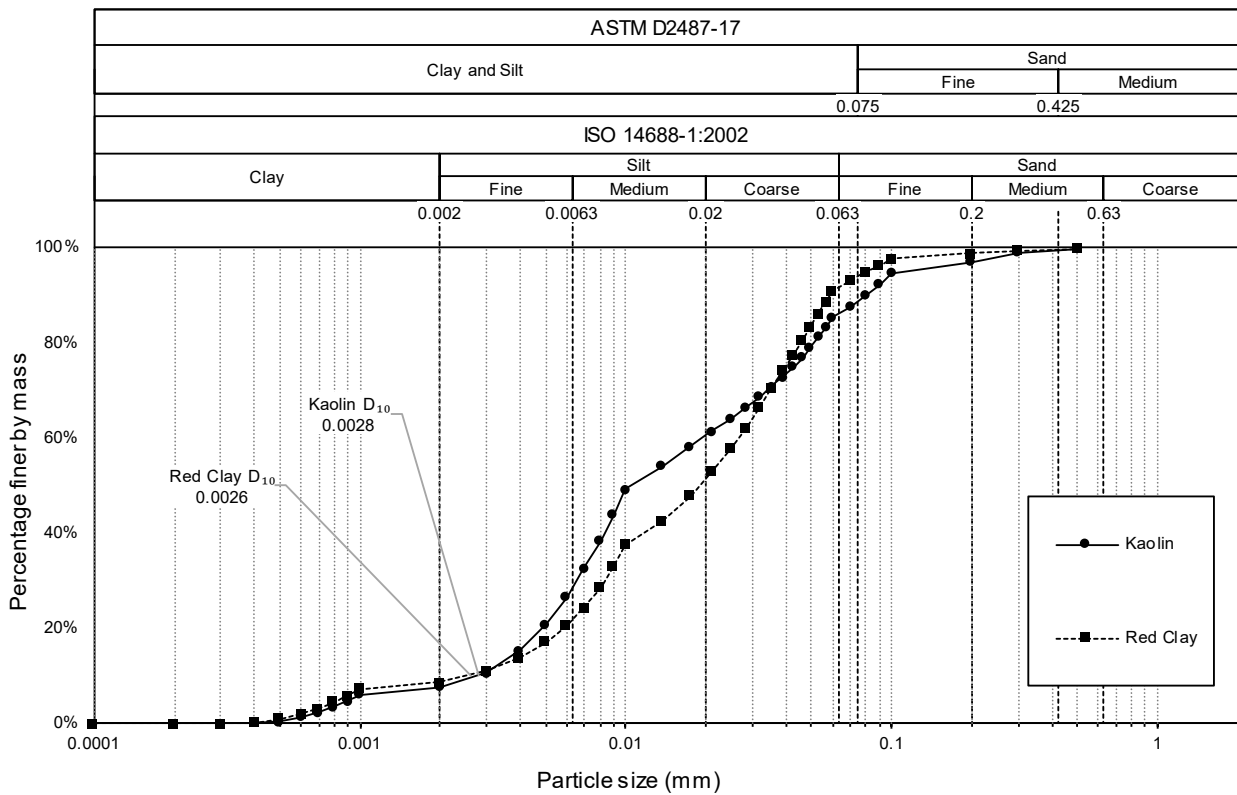
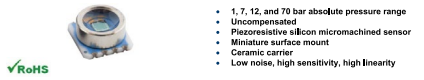


Figure 8-5 Additional cumulative particle size distributions

APPENDIX C: TECHNICAL DATA



DESCRIPTION

The MS54XX SMD pressure sensor series is designed for pressure sensor systems with highest demands on resolution and accuracy. The device consists of a silicon micromachined pressure sensor die mounted on a 6.2 x 6.4 mm ceramic carrier. The MS54XX can be delivered in a high sensitivity version giving a maximal output voltage or in a high linearity version. Both versions provide an output voltage directly proportional to the applied pressure.

Carrier	Full scale pressure	High Sensitivity Versions			High Linearity Versions		
		Product code	Full scale span	Linearity	Product code	Full scale span	Linearity
Ceramic	1 bar	MS5401-AM	240 mV	±0.20 % FS	MS5401-BM	150 mV	±0.05 % FS
	7 bar	MS5407-AM	392 mV	±0.20 % FS	MS5407-BM	150 mV	±0.05 % FS
	70 bar	MS5470-AM	310 mV	±0.25 % FS	MS5470-BM	150 mV	±0.05 % FS

FEATURES

- Low cost SMD package
- Small size
- High reliability, low drift
- 40 °C to +125 °C operation range
- Gel protection against humidity and water

APPLICATIONS

- Brake systems
- High resolution altimeters, variometers
- Barometers
- Engine management
- Waterproof watches and diving computers

PIN CONFIGURATION

VERSION WITH CERAMIC CARRIER AND METAL CAP



PIN DESCRIPTION

Pin Name	Pin No.	Function
OUT-	1	Negative output voltage of Wheatstone bridge
GND	2	Ground
VS+	3	Supply voltage of Wheatstone bridge
OUT+	4	Positive output voltage of Wheatstone bridge

ABSOLUTE MAXIMUM RATINGS

Parameter	Symbol	Conditions	Min	Max	Unit
Supply voltage	VS+	Ta = 25 °C	-	20	V
Storage temperature	Ts		-40	+125	°C
Overpressure MS5401-AM			-	5	bar
MS5401-BM (1)		Ta = 25 °C	-	10	bar
MS5407-AM			-	30	bar
MS5412-BM			-	180	bar

NOTES

- The MS5401-BM is qualified referring to ISO Standard 2281 and can withstand an absolute pressure of 11 bar in salt water or 100 m water respectively.
- The MS5407-AM is qualified referring to ISO Standard 2281 and can withstand an absolute pressure of 21 bar in salt water or 200 m water specifically.

ELECTRICAL CHARACTERISTICS

HIGH SENSITIVITY VERSIONS

Parameter	Min	Typ	Max	Unit	Notes	
						(Vs+ = 5 V, Ta = 25 °C)
MS5401-AM	Operating pressure range	0	-	1	bar	
	Full-scale span (FS)	190	240	290	mV	
	Sensitivity	190	240	290	mV/bar	
MS5407-AM	Operating pressure range	0	-	7	bar	1, 6
	Full-scale span (FS)	322	392	462	mV	
	Sensitivity	46	96	66	mV/bar	
MS5470-AM	Operating pressure range	0	-	70	bar	1, 6
	Full-scale span (FS)	250	310	370	mV	
	Sensitivity	3.6	4.4	5.3	mV/bar	
All Ranges	Operating temperature range	-40	-	+125	°C	
	Zero pressure offset	-40	-	40	mV	
	Pressure hysteresis	-	-	±0.20	% FS	2, 6
All Ranges	Temperature hysteresis	-	-	0.3	% FS	3, 6
	Repeatability	-	-	±0.20	% FS	4, 5
	Bridge resistance	3.0	3.4	3.8	kΩ	
All Ranges	Temperature coefficient of resistance	+2400	2900	+3300	ppm/°C	5, 6
	Temperature coefficient of span	-1500	-1900	-2300	ppm/°C	5, 6
	Temperature coefficient of offset	-80	-	+80	µV/°C	5, 6

NOTES

- Deviation at one half full-scale pressure from the least squares best line fit over pressure range.
- Maximum difference of output voltage after 1 pressure cycle at any pressure within the operating pressure range.
- Maximum difference in offset after one thermal cycle from -40°C to +125°C.
- Same as 2) after 10 pressure cycles.
- Slope of the end-point straight line from 25°C to 60°C.
- Not 100% tested.

ELECTRICAL CHARACTERISTICS (CONT.)

HIGH LINEARITY VERSIONS

Parameter	Min	Typ	Max	Unit	Notes	
						(Vs+ = 5 V, Ta = 25 °C)
MS5401-BM	Operating pressure range	0	-	1	bar	6
	Full-scale span (FS)	120	150	180	mV	
	Sensitivity	120	150	180	mV/bar	
MS5412-BM	Operating pressure range	0	-	12	bar	8
	Full-scale span (FS)	120	150	180	mV	
	Sensitivity	10	12.4	15	mV/bar	
All Ranges	Operating temperature range	-40	-	+125	°C	
	Zero pressure offset	-40	-	40	mV	
	Pressure hysteresis	-	-	±0.20	% FS	2, 6
All Ranges	Temperature hysteresis	-	-	0.3	% FS	3, 6
	Repeatability	-	-	±0.20	% FS	4, 5, 7
	Bridge resistance	3.0	3.4	3.8	kΩ	
All Ranges	Temperature coefficient of resistance	+2400	2900	+3300	ppm/°C	5, 6
	Temperature coefficient of span	-1500	-1900	-2300	ppm/°C	5, 6
	Temperature coefficient of offset	-80	-	+80	µV/°C	5, 6

NOTES

- Deviation at one half full-scale pressure from the least squares best line fit over pressure range.
- Maximum difference of output voltage after 1 pressure cycle at any pressure within the operating pressure range.
- Maximum difference in offset after one thermal cycle from -40°C to +125°C.
- Same as 2) after 10 pressure cycles.
- Slope of the end-point straight line from 25°C to 60°C.
- Not 100% tested.
- MS5412-BM - Max. 0.3% FS
- This sensor family is optimized for the linearity; it is suitable for applications with higher pressure where the linearity requirement is less critical.

APPLICATION INFORMATION

GENERAL

The MS54XX is a miniaturized absolute pressure sensor series which has been designed as a surface mount device (SMD). Its main advantages are the high performance of the semiconductor sensor and a design which makes it suitable for applications requiring small dimensions and cost efficiency.

The sensor element of the MS54XX consists of a micromachined silicon membrane with borosilicate glass wafer-bonded under vacuum to the back side for reference pressure. Implanted resistors make use of the piezoresistive effect to sense pressure applied to the membrane. The sensor is mounted using a special process allowing best offset stability making the device suitable for direct PCB assembly.

Typical applications for this miniaturized pressure sensor series MS54XX are altitude measurements and the measurement of atmospheric reference pressure in medical and industrial equipment as well as in automotive and household applications, consumer electronics and pneumatics.

Full Scale Pressure	High Sensitivity Versions (MS54XXAX)	High Linearity Versions (MS54XXBX)
1 bar	Variometer, Altimeter, Barometer	High End Altimeter, Medical Instrumentation
7 bar	Divers Watch, Tire Pressure, Electronic Scale	High End Electronic Scale
12 bar	Engine Control, Diving Computer	Pneumatic Brake, Diving Computer
70 bar	Engine Control, Diving Computer	Pneumatic Brake, Diving Computer

HUMIDITY, WATER PROTECTION

MS54XX-AM WITH METAL CAP

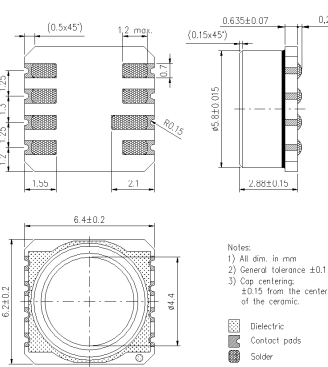
The MS54XX-AM / -BMXBA has an anticorrosive and antimagnetic metallic protection cap filled with silicone gel for enhanced protection against humidity. The properties of this gel ensure function of the sensor even when in direct water contact. This feature can be useful for waterproof watches or other applications, where direct water contact cannot be avoided. Nevertheless the user should avoid drying of hard materials like for example salt particles on the silicone gel surface. In this case it is advisable to rinse with clean water afterwards. Special care has to be taken not to mechanically damage the gel. Damaged gel may lead to air entrapment and consequently to unstable sensor signal, especially if the damage is close to the sensor surface. The metal cap is fabricated of special anticorrosive alloy in order to avoid any galvanic effects within the end product. The MS5401-BM is qualified referring to the ISO Standard 2281 and can withstand a pressure of 11 bar in salt water. The concentration of the sea water used for the qualification is 41 g of sea salt per 1 liter of DI water. The MS5407-BM satisfies salt-water testing with a pressure capability of 21 bar. For underwater operations as specified in ISO Standard 2281 it is important to seal the sensor with a rubber O-ring around the metal cap. Any salt water reaching the contact side (ceramic and pads) of the sensor could lead to permanent damage. Especially for "water-resistant 100 m" watches and for diving computers, it is recommended to provide a stable mechanical pusher from the backside of the sensor; otherwise the overpressure may push the sensor backwards and even deform the electronic board on which the sensor is mounted.

LIGHT SENSITIVITY

The MS54XX is sensitive to sunlight (visible and near-infrared spectrum). This is due to the strong photo effect of silicon. As the effect is reversible there will be no damage, but the user has to take care that in the final product the sensor cannot be exposed to direct light during operation as it affects the measurement. This can be achieved for instance by placing mechanical parts with holes in such that light cannot pass.

PACKAGE OUTLINES

CERAMIC CARRIER AND METAL CAP

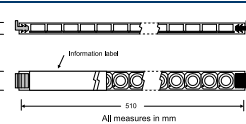


Device package outlines of MS54XXAM and MS54XXBM (M = anticorrosive and antimagnetic stainless steel cap)

PACKING

The MS54XX is packed in 51 cm (20-inch) anastatic plastic tubes with rubber end-plugs of different colors: one green and one black. The dot on the carrier next to Pin 1 is facing the green end-plug. Each tube contains 80 sensors. The tubes are marked "MITSUBISHI" and have an information label. See the drawings below for more details.

PACKING TUBE OUTLINES



ORDERING INFORMATION

Product code	Product	Art. No.	Package	Delivery Form
MS5401-AM	Miniature pressure sensor 1 bar, High sensitivity	325401001-00	Ceramic carrier	Tube
		325401000-50	Ceramic carrier, without transparent gel	Tube
MS5407-AM	Miniature pressure sensor 7 bar, High sensitivity	325407000-00	Ceramic carrier	Tube
		325407000-50	Ceramic carrier, without transparent gel	Tube
MS5470-AM	Miniature pressure sensor 70 bar, High sensitivity	325407000-00	Ceramic carrier	Tube
		325407000-50	Ceramic carrier, without transparent gel	Tube
MS5412-BM	Pressure sensor 12 bar, High Linearity	325412000-00	Ceramic carrier	Tube
MS5470-AM	Miniature pressure sensor 70 bar, High sensitivity	325470000-00	Ceramic carrier	Tube
		325470000-50	Ceramic carrier	Tube

AX = high sensitivity
BX = high linearity
XM = anticorrosive and antimagnetic metallic cap

FACTORY CONTACT

NORTH AMERICA	EUROPE	ASIA
Measurement Specialties 42198 Northport Loop West Fremont, CA 94538 Tel: +1 800 787 1888 Fax: +1 510 488 5718 e-mail: pjs.camer.drv@meas-spec.com Website: www.meas-spec.com	MEAS Switzerland Sàrl Ch. Chappolette-Péris 11 CH-2022 Bevilacqua Tel: +41 32 847 9550 Fax: +41 32 847 9569 e-mail: sales.eu@meas-spec.com Website: www.meas-spec.com	Measurement Specialties (China), Ltd. No. 26 Langshang Road Shenzhen High-Tech Park (North) Nanshan District, Shenzhen, 518057 China Tel: +86 755 3330 5088 Fax: +86 755 3330 5099 e-mail: pjs.asia@meas-spec.com Website: www.meas-spec.com

The information in this sheet has been carefully reviewed and is believed to be accurate; however, no responsibility is assumed for inaccuracies. This information does not convey to the purchaser of such devices any license under the patent rights to the manufacturer. Measurement Specialties, Inc. reserves the right to make changes without further notice to any product herein. Measurement Specialties, Inc. does not warrant, represent or guarantee the reliability or stability of its products in particular systems. We does Measurement Specialties, Inc. assume any liability arising out of the application or use of any product or circuit and specifically disclaims any and all liability, including without limitation consequential or incidental damages. Typical parameters can vary in different applications. All operating parameters must be validated for each customer application by customer's technical experts. Measurement Specialties, Inc. does not convey any license under its patent rights nor the rights of others.

Figure 8-6 MS54XX Miniature SMD Pressure Sensor (Measurement Specialties, 2012), (TE Connectivity, 2018)

